

THE UNIVERSITY OF HULL

**MEMBRANE PERMEATION FROM SOLUTIONS, PARTICLE  
DISPERSIONS AND PARTICLE-STABILISED EMULSIONS**

being a Thesis submitted for the Degree of Doctor of Philosophy  
in the University of Hull

by

Andrew James Johnson  
MChem (University of Hull)

March 2013

## **ACKNOWLEDGEMENTS**

First and foremost, I would like to thank my academic supervisors, Prof. Bernard P. Binks and Prof. Paul D.I. Fletcher, for their consistently excellent supervision and guidance. I am sincerely grateful to have worked with you both.

I also thank the Engineering and Physical Sciences Research Council (EPSRC) and GlaxoSmithKline (Barnard Castle, UK) for financial support in sponsoring this project. My industrial supervisor, Dr. Russell P. Elliott, has always offered great encouragement and enthusiasm, and for this I thank him.

I am grateful to all members of the Surfactant & Colloid Group, both past and present, for their support and friendship.

Finally, I would like to thank my family for their support and encouragement throughout this time. I especially thank my father (Joseph Johnson), my mother (Glenda A. Johnson), my elder brother (Christopher J. Johnson) and my younger brother (Joseph A. Johnson), for their patience and unconditional support. I truly feel failure is not possible with you all by my side.

## PUBLICATIONS, PATENTS AND PRESENTATIONS

The work contained within this thesis has given rise to the following publications, patents and presentations:

1. B.P. Binks, P.D.I. Fletcher, A.J. Johnson and R.P. Elliott, 'Membrane permeation of testosterone from either solutions, particle dispersions, or particle-stabilised emulsions', *Langmuir*, **28**, 2510, (2012).
2. B.P. Binks, P.D.I. Fletcher, A.J. Johnson and R.P. Elliott, 'How membrane permeation is affected by donor delivery solvent', *Phys. Chem. Chem. Phys.*, **14**, 15525, (2012).
3. B.P. Binks, A.J. Johnson and J.A. Rodrigues, 'Inversion of 'dry water' to aqueous foam on addition of surfactant', *Soft Matter*, **6**, 126, (2010).
4. Patent: 'Non-aqueous solid stabilized emulsions' *US Pat.*, 61/767,880, 2013. (Inventors: B.P. Binks, R.P. Elliott, P.D.I. Fletcher, A.J. Johnson and M.A. Thompson).
5. Award winning oral presentation: 'A kinetic approach to modelling the membrane permeation of pharmaceutically active ingredients from various topical formulation types', University of Hull Research Colloquia, 9<sup>th</sup> July 2012, Hull, UK.
6. Oral presentation: 'Particle-stabilised emulsions as new pharmaceutical vehicles', GlaxoSmithKline Learning Forum, 18<sup>th</sup> July 2011, Barnard Castle, UK.
7. Poster presentation: 'Membrane permeation of testosterone from either solutions, particle dispersions or particle-stabilised emulsions', University of Hull Research Colloquia, 11<sup>th</sup> July 2011, Hull, UK. (Authors: B.P. Binks, P.D.I. Fletcher, A.J. Johnson and R.P. Elliott).
8. Poster presentation: 'How membrane permeation is affected by the donor delivery solvent', Stratum Corneum VII conference, 10-11<sup>th</sup> September 2012, Cardiff, UK. (Authors: B.P. Binks, P.D.I. Fletcher, A.J. Johnson and R.P. Elliott).

## ABSTRACT

This thesis is primarily concerned with understanding how the rate and extent of membrane permeation of a drug is affected by switching the donor delivery vehicle for different permeants and membranes. The project is funded by an industrial Collaborative Awards in Science and Engineering (CASE) award with an additional sponsorship by GlaxoSmithKline (GSK). The interest of GSK in this research is in the understanding of how the various types of topical formulation available, such as solutions, ointments, dispersions and emulsions, influence the characteristics of drug transport across a membrane.

The rate and extent of membrane permeation from various types of topical formulation is experimentally investigated through the use of a developed automated method which is shown to be accurate and highly reproducible. The developed method incorporates stirred donor and re-circulating receiver compartments and continuous monitoring of the permeant concentration in the receiver phase. In a theoretical model based on rate-limiting membrane diffusion, an explicit set of equations are derived showing how the permeation extent and rate depend mainly on the membrane-donor and membrane-receiver partition coefficients of the permeant. The permeation of drug molecules from simple, single phase donor solutions are first investigated. The experimental permeation results for systems containing all possible combinations of hydrophilic or hydrophobic donor solvent, permeant and polymer membrane are measured using the developed method and are then compared to the calculated theoretical results. A quantitative comparison of model and experimental results from the widely-differing permeation systems successfully enables the systematic elucidation of all possible donor solvent effects in membrane permeation. For the experimental conditions used here, most of the permeation systems are in agreement with the model, demonstrating that the model assumptions are valid. In these cases, the dominant donor solvent effects arise from changes in the relative affinities of the permeant for the donor and receiver solvents and the membrane and are quantitatively predicted using the separately measured partition coefficients. It is also shown how additional donor solvent effects can arise when switching the donor solvent causes one or more of the model assumptions to be invalid. These effects include a change in rate-limiting step, permeant solution non-ideality and others.

The development of a new type of formulation is investigated whereby the preparation of waterless, particle-stabilised emulsions is reported upon. The prepared emulsions incorporate a non-aqueous polar liquid phase, an immiscible oil phase and are stabilised by solid nanoparticles. Variation of the incorporated oil, polar liquid and particle hydrophobicity allow for the preparation of stable emulsions containing a wide range of liquids of both oil-in-polar liquid and polar liquid-in-oil emulsion types. The prepared formulations show great potential as vehicles for use in drug delivery in the pharmaceutical industry. These waterless emulsions provide several advantages such as high emulsion stability, aesthetic textures for topical application, aesthetic appearances (including the preparation of transparent emulsions through matching of the refractive index of the liquid phases) and the capability of containing very high hydrophobic drug concentrations dissolved within due to the absence of an aqueous liquid phase.

The permeation of a drug molecule from more complex multiphase donor formulations, such as particle dispersions and particle stabilised emulsions, is also investigated. The delivery of a permeant across a synthetic membrane from both conventional oil-water and the developed waterless emulsions is discussed. The same experimental technique as that used to investigate the membrane permeation from single phase donor solutions is employed and a comparison of the experimental results to those calculated using the derived theoretical model is given. The theoretical model is adapted to account for the additional partitioning of the permeant between the multiple phases present in these more complex donor formulations, but maintains the same set of underlying assumptions and fundamental principles of diffusion. The model successfully accounts for the experimental observations and reveals information regarding the mechanism of drug delivery from particle-stabilised emulsions. It is conclusively illustrated that permeant delivery from particle-stabilised emulsions occurs via partitioning of the drug between the dispersed and continuous emulsion phases prior to partitioning to the membrane exclusively from the emulsion continuous phase (i.e. dispersed emulsion droplet adhesion onto the surface of the membrane does not occur). Through analysis of the derived theoretical model, the extent and rate of membrane permeation of a permeant are correctly predicted to be independent of the emulsion type (i.e. oil-in-water or water-in-oil) and emulsion dispersed volume fraction for a given emulsion composition.

# MEMBRANE PERMEATION FROM SOLUTIONS, PARTICLE DISPERSIONS AND PARTICLE-STABILISED EMULSIONS

## CONTENTS

<b>CHAPTER 1 - INTRODUCTION</b> .....	13
<b>1.1 Industrial relevance of current research</b> .....	13
<b>1.2 Diffusion</b> .....	14
<i>1.2.1 Fick's laws of diffusion</i> .....	15
<i>1.2.2 Diffusion through an isotropic membrane: an introduction to diffusion lag times and the steady state approximation</i> .....	16
<b>1.3 Solvation and solute partitioning</b> .....	18
<i>1.3.1 Solvation</i> .....	18
<i>1.3.2 Solute partition coefficients and causes of non-ideal behaviour</i> .....	21
<b>1.4 Emulsions</b> .....	23
<i>1.4.1 Surfactant-stabilised emulsions</i> .....	24
<i>1.4.2 Particle-stabilised emulsions</i> .....	26
<i>1.4.3 Emulsion stability</i> .....	31
<b>1.5 Current opinions in membrane permeation studies and topical formulation design</b> .....	34
<b>1.6 Presentation of thesis</b> .....	35
<b>1.7 References</b> .....	37
<b>CHAPTER 2 - EXPERIMENTAL</b> .....	43
<b>2.1 Materials</b> .....	43
<i>2.1.1 Solvents</i> .....	43
<i>2.1.2 Permeants</i> .....	46
<i>2.1.3 Membranes</i> .....	46
<i>2.1.4 Oils and polyols</i> .....	48
<i>2.1.5 Fumed silica particles</i> .....	49

2.1.6	<i>Other materials</i> .....	52
<b>2.2</b>	<b>Methods</b> .....	53
2.2.1	<i>Calibration of UV-vis spectrophotometer for the determination of permeant concentration within a liquid solvent</i> .....	53
2.2.2	<i>Permeant in solvent solubility measurements</i> .....	53
2.2.3	<i>Measurement of solvent/solvent and solvent/membrane equilibrium permeant partition coefficients</i> .....	54
2.2.4	<i>Membrane permeation measurements</i> .....	55
2.2.5	<i>Preparation of fumed silica particle dispersions</i> .....	58
2.2.6	<i>Preparation of particle-stabilised emulsions</i> .....	58
2.2.7	<i>Characterisation of particle-stabilised emulsions</i> .....	59
<b>2.3</b>	<b>References</b> .....	61
<b>CHAPTER 3 – MEMBRANE PERMEATION FROM DONOR SOLUTIONS ..</b>		<b>62</b>
<b>3.1</b>	<b>Introduction</b> .....	<b>62</b>
<b>3.2</b>	<b>Theoretical modelling of membrane permeation from donor solutions .</b>	<b>63</b>
3.2.1	<i>Theoretical model assumptions</i> .....	64
3.2.2	<i>Derivation of the theoretical model for membrane permeation into the closed-loop, fixed volume receiver compartment</i> .....	64
3.2.3	<i>Predicting the rate and extent of membrane permeation from donor solutions</i> .....	67
3.2.4	<i>Comparing the theoretical model with experimental permeation results</i>	70
3.2.5	<i>Deviations from the model assumptions</i> .....	92
<b>3.3</b>	<b>Membrane permeation studies influenced by undesired solvent-membrane interactions</b> .....	<b>99</b>
<b>3.4</b>	<b>Membrane permeation studies influenced by mutually miscible, dissimilar donor and receiver solvents</b> .....	<b>108</b>
<b>3.5</b>	<b>Theoretical modelling of membrane permeation from donor solutions into open, variable-volume receiver solutions</b> .....	<b>123</b>

3.5.1	<i>Adapting the theoretical model to account for membrane permeation into open, variable-volume receiver solutions .....</i>	124
3.5.2	<i>Comparing the theoretical model with experimental results for membrane permeation into an open, variable-volume receiver configuration .....</i>	126
<b>3.6</b>	<b>Conclusions .....</b>	<b>130</b>
<b>3.7</b>	<b>References .....</b>	<b>132</b>
<b>CHAPTER 4 – PREPARATION AND PROPERTIES OF WATERLESS, PARTICLE-STABILISED EMULSIONS.....</b>		<b>134</b>
<b>4.1</b>	<b>Introduction .....</b>	<b>134</b>
<b>4.2</b>	<b>Preparation and properties of waterless, particle-stabilised emulsions incorporating paraffin liquid oil and various diol polar phases.....</b>	<b>135</b>
4.2.1	<i>A theoretical method for predicting the particle hydrophobicity required to induce transitional phase inversion of particle-stabilised emulsions.....</i>	137
4.2.2	<i>Waterless, particle-stabilised emulsions of paraffin liquid and either butane-1,2-diol or pentane-1,5-diol.....</i>	141
<b>4.3</b>	<b>Preparation and properties of waterless, particle-stabilised emulsions incorporating propane-1,2-diol polar phases and various oil phases.....</b>	<b>145</b>
4.3.1	<i>Gelling of oil-continuous waterless emulsions around the point of transitional phase inversion.....</i>	148
4.3.2	<i>Preparation and properties of transparent waterless, particle-stabilised emulsions incorporating paraffin liquid oil and various polyol polar phases ...</i>	152
<b>4.4</b>	<b>Preparation of waterless emulsions stabilised by precipitated calcium carbonate particles .....</b>	<b>156</b>
<b>4.5</b>	<b>Conclusions .....</b>	<b>157</b>
<b>4.6</b>	<b>References .....</b>	<b>158</b>
<b>CHAPTER 5 – MEMBRANE PERMEATION FROM DONOR PARTICLE DISPERSIONS AND PARTICLE-STABILISED EMULSIONS .....</b>		<b>160</b>
<b>5.1</b>	<b>Introduction .....</b>	<b>160</b>



<b>5.2 Adapting the unified theoretical model to account for donor particle dispersions and particle-stabilised emulsions.....</b>	<b>161</b>
5.2.1 <i>Derivation of the adapted theoretical model to account for donor particle dispersions and particle-stabilised emulsions .....</i>	<i>163</i>
5.2.2 <i>Predicting the extent and rate of membrane permeation from donor particle-stabilised emulsions.....</i>	<i>167</i>
<b>5.3 Measuring the membrane permeation of permeants from donor particle dispersions.....</b>	<b>173</b>
<b>5.4 Measuring the membrane permeation of permeants from donor particle-stabilised emulsions.....</b>	<b>179</b>
5.4.1 <i>Justifying the mechanism of permeant release from donor particle-stabilised emulsions .....</i>	<i>179</i>
5.4.2 <i>Membrane permeation from waterless particle-stabilised emulsions of squalane and PG .....</i>	<i>180</i>
5.4.3 <i>Membrane permeation of testosterone from a conventional oil-water emulsion of IPM and water .....</i>	<i>186</i>
<b>5.5 Conclusions .....</b>	<b>190</b>
<b>5.6 References .....</b>	<b>192</b>
<b>CHAPTER 6 – A SUMMARY OF CONCLUSIONS AND FUTURE WORK...</b>	<b>193</b>
<b>6.1 Conclusions .....</b>	<b>193</b>
<b>6.2 Future work .....</b>	<b>195</b>
<b>6.3 References .....</b>	<b>197</b>
<b>APPENDIX .....</b>	<b>198</b>

## LIST OF SYMBOLS AND ABBREVIATIONS

DCDMS	dichlorodimethylsilane
IPM	isopropyl myristate
PBS	phosphate-buffered saline solution
PDMS	polydimethylsiloxane
PEG	polyethylene glycol
PG	propane-1,2-diol (also called propylene glycol)
SEM	scanning electron microscope
TEM	transmission electron microscope
UV-vis	ultraviolet-visible
$A$	surface area of membrane
$C_{\text{cont}}$	concentration of permeating species per total volume of the donor emulsion continuous phase
$C_{\text{don}}$	overall concentration of permeating species per total volume of the donor compartment
$C_{\text{don},0}$	initial overall concentration of permeating species per total volume of the donor compartment
$C_{\text{don},\infty}$	overall concentration of permeating species per total volume of the donor compartment at infinite time
$C_{\text{drop}}$	concentration of permeating species per total volume of the donor emulsion drops
$C_{\text{mem}}$	overall concentration of permeating species in the membrane
$C_{\text{mem},d}$	concentration of permeating species at donor-side surface of membrane
$C_{\text{mem},r}$	concentration of permeating species at receiver-side surface of membrane
$C_{\text{rec}}$	concentration of permeating species in the receiver compartment
$C_{\text{rec},0}$	initial concentration of permeating species in the receiver compartment

$C_{\text{rec},\infty}$	concentration of permeating species in the receiver compartment at infinite time
$D$	diffusion coefficient of the permeating species within the membrane
$F$	volumetric flow rate in the receiver compartment
$K_{\text{a-b}}$	equilibrium partition coefficient of the permeant species between immiscible phases a and b ( $=C_{\text{a}}/C_{\text{b}}$ )
$K_{\text{don-rec}}$	equilibrium partition coefficient of the permeant species between the donor phase and the receiver phase ( $C_{\text{don}}/C_{\text{rec}}$ )
$K_{\text{drop-cont}}$	equilibrium partition coefficient of the permeating species between the drop and continuous phases of the donor emulsion ( $=C_{\text{drop}}/C_{\text{cont}}$ )
$K_{\text{mem-cont}}$	equilibrium partition coefficient of the permeating species between the membrane and the donor emulsion continuous phase ( $=C_{\text{mem,d}}/C_{\text{cont}}$ )
$K_{\text{mem-don}}$	equilibrium partition coefficient of the permeant species between the membrane and the donor phase ( $C_{\text{mem}}/C_{\text{don}}$ )
$K_{\text{mem-rec}}$	equilibrium partition coefficient of the permeant species between the membrane and the receiver phase ( $C_{\text{mem}}/C_{\text{rec}}$ )
$k$	first-order permeability rate coefficient for closed-loop receiver compartments
$k_{\text{o}}$	first-order permeability rate coefficient for open receiver compartments
$k_{\text{p}}$	permeability coefficient
$L$	time taken to establish the steady-state, linear concentration gradient of permeant across the membrane (“lag time”)
$m_{\text{p}}$	mass of particles in the donor compartment
$n_{\text{t}}$	total number of moles of permeating species
$t$	time
$t_{1/2}$	half-life
$V_{\text{don}}$	volume of donor compartment
$V_{\text{mem}}$	volume of membrane

$V_{\text{rec}}$	volume of receiving compartment
$X$	total thickness of the membrane
$x$	perpendicular distance coordinate within the membrane
$\theta$	three-phase contact angle
$\phi_{\text{drop}}$	emulsion dispersed phase volume fraction
$\Gamma$	moles of species adsorbed to the particle surface per mass of particles
$\Gamma_{\text{max}}$	maximum moles of species adsorbed to the particle surfaces per mass of particles

## **CHAPTER 1**

### **INTRODUCTION**

#### **1.1 Industrial relevance of current research**

This research project was funded by an industrial CASE (Collaborative Awards in Science and Engineering) award provided by the Engineering and Physical Sciences Research Council (EPSRC) in collaboration with GlaxoSmithKline (GSK), Barnard Castle, UK. Industrial CASE awards provide funding for Ph.D. studentships whereby businesses take the lead in arranging projects with an academic partner of their choice. The aim of these awards is to provide Ph.D. students with a first-rate, challenging research-training experience, within the context of a mutually beneficial research collaboration between academic and partner organisations.

GSK is one of the world's leading research based pharmaceutical companies, and is the fourth largest with regards to revenue. GSK has therapeutic areas including respiratory, gastro-intestinal/metabolic, central nervous system, vaccines and anti-infectives. In addition, the company has a consumer healthcare section which produces some of the world leading nutritional drinks and counter medicines. They also formulate and manufacture a wide range of pharmaceutical creams for consumer and therapeutic uses. The area of creams and ointments within GSK is growing with the acquisition of a leading dermatological pharmaceutical company, Stiefel, in July 2009.

The interest of GSK in this Ph.D. studentship is in the understanding of the mechanisms and underlying principles determining the drug delivery characteristics of the various different types of topical formulations produced in the pharmaceutical industry (i.e. solutions, ointments, emulsions, etc.). With an understanding of how and why a given type of topical formulation produces the observed drug delivery characteristics, the development of future formulations can be conducted such that the desired extent and rate of drug delivery can be pursued. Hence, whether the application requires a rapid, short-term release of a drug or a delayed, consistent release of a drug, the required formulation design can be correctly proposed prior to trial productions. In addition, a further interest of GSK in this Ph.D. studentship is in the development of a new type of topical formulation for the delivery of an active drug across the skin barrier. Both the development and drug delivery characteristics of this new formulation

design are explained within, and hence, an insight into the potential advantages that such a formulation can offer to the pharmaceutical industry is given.

This chapter introduces the fundamental subjects which are most relevant to this research. The primary topic of concern is the phenomenon of molecular diffusion and therefore a brief introduction to the theory and elemental concepts of diffusion is firstly given. The topic of solvation is then discussed whereby the dissolution of a permeant within a solvent and the causes of non-ideal behaviour of a solution are explained. The later chapters of this research refer to the preparation of emulsion formulations and therefore, an introduction to the fundamental concepts of emulsion stabilisation by both surfactants and solid particles is given. The subsequent results chapters also offer more detailed introductions to these topics where it is more appropriate. Finally, a review of the current literature on membrane permeation and topical formulation design is described and a resultant summary of the work presented in this thesis, which aims to fulfil that which has not yet been disclosed, is portrayed.

## 1.2 Diffusion

Diffusion is the phenomenon by which matter is transported from one part of a system to another as a result of random molecular motions.<sup>1</sup> In a dilute solution of molecules, each solute molecule behaves independently of the others, which it seldom meets, but is constantly undergoing collisions with the surrounding solvent molecules. As a result of these collisions, a solute molecule moves sometimes towards a region of higher concentration, and sometimes towards a region of lower concentration, having no preferred direction of motion towards one or the other. The motion of a single molecule can be described in terms of the familiar ‘random walk’ picture which was first introduced by Pearson in 1905.<sup>2</sup> Whilst it is possible to calculate the mean-square distance travelled within a given time interval during a random walk, it is not possible to say in what direction a given molecule will move during that time.

This picture of random molecular motions, in which no molecule has a preferred direction of motion, has to be reconciled with the fact that a transfer of molecules from a region of higher to a region of lower concentration is nevertheless observed. To help explain this observation, consider the classical experiment whereby a tall cylindrical vessel has its lower volume filled with a coloured solution, such as an iodine solution,

and a column of clear water is carefully and slowly poured on top, so that no convection currents are created. Initially, the lower coloured iodine solution is separated from the upper clear water by a sharp, well-defined boundary. It is later found that the upper water solution becomes coloured, but gradually becomes transparent towards the top, while the lower volume becomes correspondingly less intensely coloured. Finally, after a sufficient time, the whole solution appears uniformly coloured throughout. There is evidently therefore, a transfer of iodine molecules from the lower volume to the upper volume, occurring in the absence of convection currents. The iodine is said to have diffused into the upper water volume. Now consider any horizontal section within the solution and two thin, equal elements of volume; one just below and one just above this section. Though it is not possible to say which direction any particular iodine molecule will move in a given time, it can be said that on the average, a definite fraction of iodine molecules in the lower element of volume will cross the section from below, and the same fraction of water molecules in the upper element will cross the section from above within a given time. Thus, simply because there are more iodine molecules in the lower element than in the upper one, there is a net transfer from the lower (more concentrated) to the upper (less concentrated) side of the section as a result of random molecular motions.<sup>1</sup>

### 1.2.1 *Fick's laws of diffusion*

The transfer of heat by conduction is also due to random molecular motions, and there is an obvious analogy between the two processes. This was recognised by Fick in 1855, when he first put diffusion on a quantitative basis by adopting the mathematical equation of heat conduction derived some years earlier by Fourier in 1822. The mathematical theory of diffusion in isotropic substances is therefore based on the hypothesis that the rate of transfer of a diffusing substance through unit area of a section, is proportional to the concentration gradient measured normal to that section.<sup>1</sup> This is Fick's first law and hence

$$J = -D \frac{\partial C}{\partial x} \quad (1.1)$$

where  $J$  is the rate of transfer per unit area of section,  $C$  is the concentration of the diffusing substance,  $x$  is the space coordinate measured normal to the section and  $D$  is

called the diffusion coefficient. The negative sign in equation 1.1 arises because diffusion occurs in the direction opposite to that of increasing concentration.<sup>1</sup>

It should be emphasised that the statement expressed mathematically by equation 1.1 is in general consistent only for an isotropic medium, whose structure and diffusion properties in the neighbourhood of any point are the same relative to all directions. Because of this symmetry, the flow of diffusing substance at any point is along the normal to the surface of constant concentration through the point. As described by Crank,<sup>1</sup> this need not be true in an anisotropic medium for which the diffusion properties depend on the direction in which they are measured.

As also illustrated by Crank,<sup>1</sup> Fick's second law can subsequently be derived from that of Fick's first law (equation 1.1) and is used to describe the rate of change of concentration of a diffusing substance at any given point in space. Fick's second law is given by

$$\frac{\partial C}{\partial t} = D \frac{\partial^2 C}{\partial x^2} \quad (1.2)$$

where  $t$  represents time. In the context of diffusion of a substance through an isotropic membrane, Fick's second law explains how the concentration of the diffusing species at any given depth  $x$ , changes with time.

### 1.2.2 *Diffusion through an isotropic membrane: an introduction to diffusion lag times and the steady state approximation*

Consider the case of diffusion through a plane sheet or isotropic membrane of thickness  $X$  and diffusion coefficient  $D$ , whose surfaces,  $x = 0$  and  $x = X$ , are maintained at constant concentrations  $C_1$  and  $C_2$  respectively. After a time, a steady state is reached in which the concentration remains constant at all depths of the sheet. Hence, Fick's second law (equation 1.2) in one dimension then reduces to

$$d^2C/dx^2 = 0 \quad (1.3)$$

provided the diffusion coefficient  $D$  is constant. Integration of equation 1.3 with respect to  $x$  gives

$$dC/dx = \text{constant} \quad (1.4)$$



and by further integration, on introducing the conditions at  $x = 0$  and  $x = X$ , equation 1.4 becomes

$$\frac{C - C_1}{C_2 - C_1} = \frac{x}{X} \quad (1.5)$$

Both equations 1.4 and 1.5 show that upon reaching this steady state, the concentration changes linearly from  $C_1$  to  $C_2$  through the sheet. Also, the rate of transfer of diffusing substance is the same across all sections of the membrane and is given by

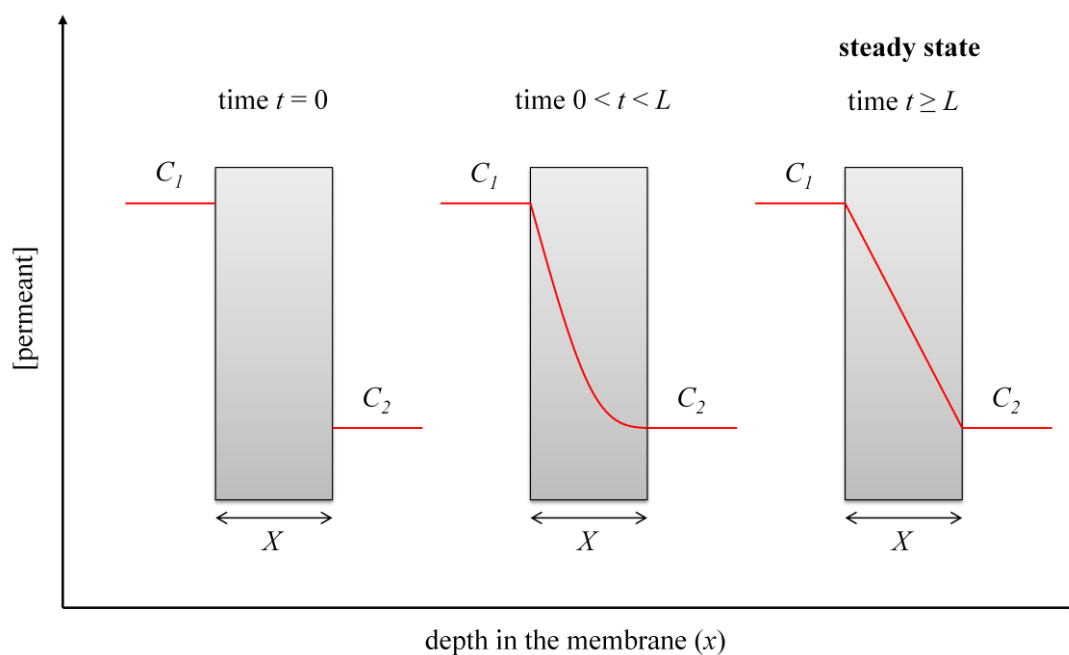
$$J = -DdC/dx = D(C_1 - C_2)/X \quad (1.6)$$

As illustrated by Frisch,<sup>3</sup> the time required to achieve this steady state linear concentration gradient across the membrane (so-called the lag time ( $L$ )) is derived in a complex manner and is dependent on the membrane thickness ( $X$ ) and the membrane diffusion coefficient of the permeant ( $D$ ) according to

$$L = \frac{X^2}{6D} \quad (1.7)$$

Figure 1.1 helps illustrate the concepts of membrane permeation lag times and steady state diffusion through a membrane, via the representation of permeant concentration across a cross-section of an isotropic membrane, during diffusion between constant permeant concentrations  $C_1$  and  $C_2$  at three different time intervals. Initially, at time  $t = 0$ , the constant permeant concentrations  $C_1$  and  $C_2$  are shown at each respective side of the membrane, but no permeant is present within the membrane. At time scales less than the lag time but greater than  $t = 0$  (i.e.  $0 < t < L$ ), the permeant concentration at depth  $x = 0$  is equal to that of  $C_1$  and gradually decreases with increasing depth  $x$  into the membrane. Here, the permeant concentration follows a non-linear profile across the membrane, in accordance with Fick's second law, until the value of  $C_2$  is reached, where  $x = X$ . Finally, at time scales greater than the lag time (i.e.  $t \geq L$ ) a linear permeant concentration gradient across the membrane is established and the system is described as been at steady state.

**Figure 1.1.** A schematic representation of the concentration profiles of a permeant diffusing across an isotropic membrane at three different time intervals. The permeant concentration profiles initially ( $t = 0$ ) (left), at time scales greater than  $t = 0$  but less than the lag time ( $0 < t < L$ ) (middle) and time scales greater than or equal to the lag time ( $t \geq L$ ) (right) are shown.



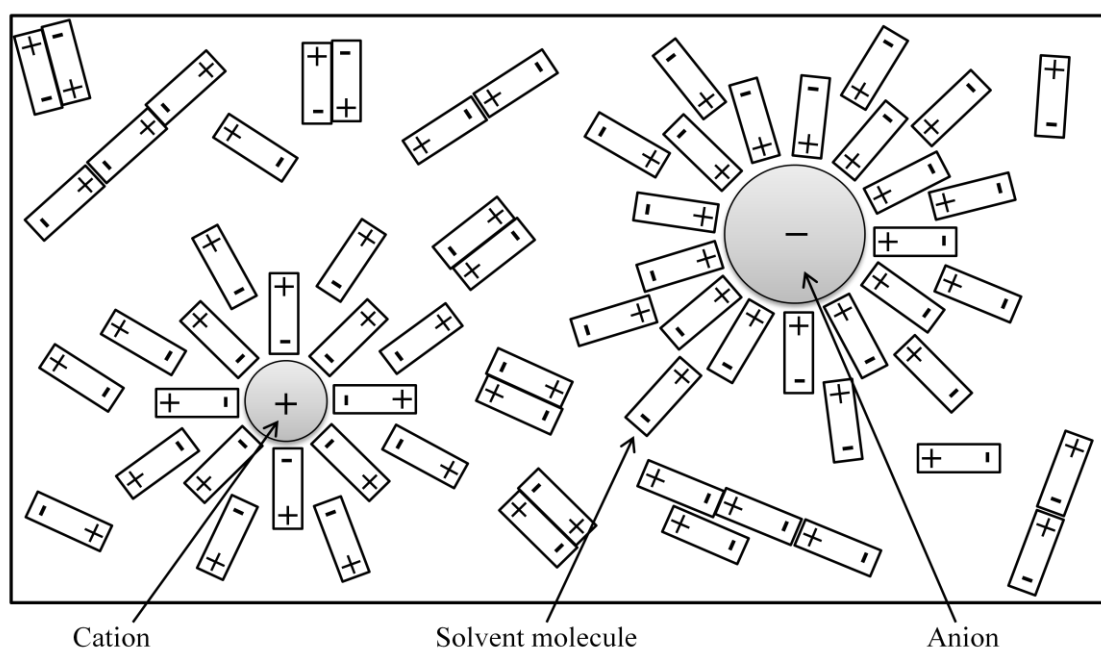
### 1.3 Solvation and solute partitioning

#### 1.3.1 Solvation

The topic of solvation is a large branch of chemistry and hence, only a brief introduction, relevant to the research presented here, is subsequently discussed. The term solvation refers to the surrounding of a dissolved molecule or ion by a shell of more or less tightly bound solvent molecules as a result of intermolecular forces between the solute and solvent.<sup>4</sup> The solvation energy can be described as the change in Gibbs energy when an ion or molecule is transferred from a vacuum (or the gas phase) into a solvent. The Gibbs energy of solvation,  $\Delta G_{solv}^{\circ}$ , a measure of the solvation ability of a particular solvent, is the result of a superimposition of four principal components of a different nature:<sup>5</sup>

- I. The cavitation energy associated with the hole that the dissolved molecule or ion produces in the solvent.
- II. The orientation energy corresponding to the phenomenon of partial orientation of the dipolar solvent molecules caused by the presence of the solvated molecule or ion (see Figure 1.2).
- III. The isotropic interaction energy corresponding to the unspecific intermolecular forces with a long range of activity (i.e. electrostatic, polarisation, and dispersion energy).
- IV. The anisotropic interaction energy resulting from the specific formation of hydrogen bonds or electron-pair donor/electron-pair acceptor bonds at well localized points in the dissolved molecules.

**Figure 1.2.** Solvation of ions in a solvent consisting of dipolar molecules. The charges of the dipolar molecules are partial charges  $\delta^+$  and  $\delta^-$ . Image redrawn from reference 6.



The dissolution of a substance requires that not only the interaction energy of the solute molecules (for crystals the lattice energy) be overcome but also the interaction energy between the solvent molecules themselves. This is compensated by the gain in Gibbs energy of solvation,  $\Delta G^\circ_{solv}$ . The standard molar Gibbs energy of solvation,  $\Delta G^\circ_{solv}$ , can be formulated as the difference between the Gibbs energy of solution,  $\Delta G^\circ_{soln}$ , and the crystal lattice energy,  $\Delta G^\circ_{latt}$ , such that

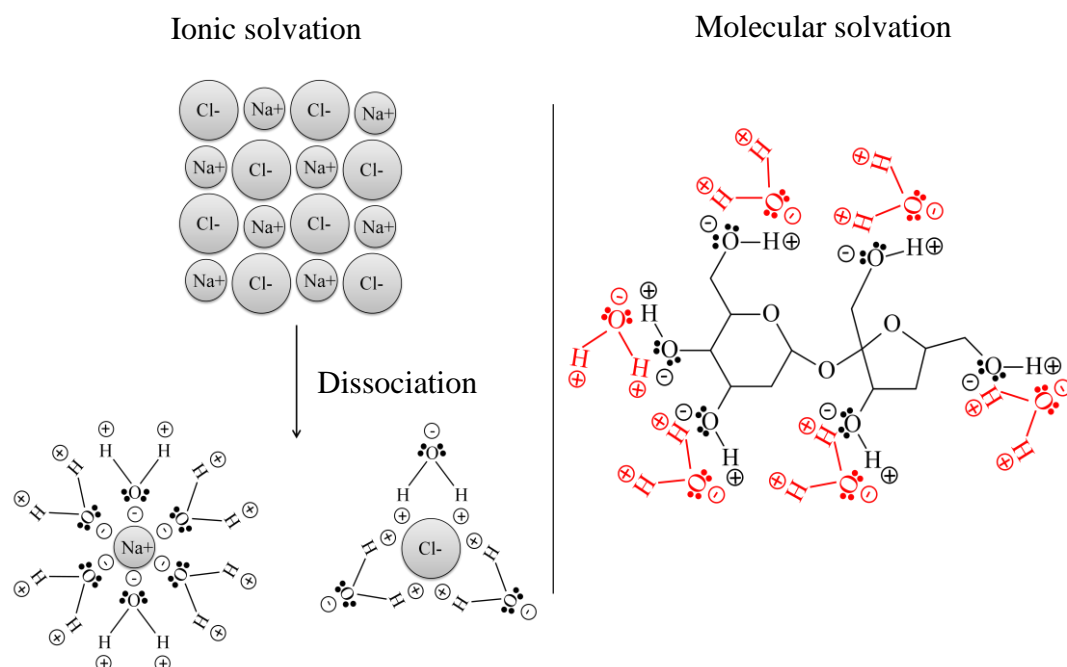
$$\Delta G^{\circ}_{solv} = \Delta G^{\circ}_{soln} - \Delta G^{\circ}_{latt} \quad (1.8)$$

Hence, if the liberated solvation energy is higher than the lattice energy, then the overall process of dissolution is exothermic and conversely, if the system uses energy, then the dissolution is endothermic.

Solvation can occur by either an ionic or a molecular process. Ionic solvation occurs when an ionic solute, for example sodium chloride (NaCl), dissociates into ions when mixed with a polar solvent. When water is used as the solvent, the process of solvation may be referred to as hydration. The hydration of NaCl, as shown in Figure 1.3 (left), occurs via the dissociation of NaCl into  $\text{Na}^+$  and  $\text{Cl}^-$  ions, which are then surrounded by water molecules orientated according to their partial charge. The electronegative oxygen atom of water molecules reside more closely to the  $\text{Na}^+$  ions, whilst the electropositive hydrogen atoms of other water molecules form a hydration layer around the  $\text{Cl}^-$  ions. The dissolution of such solutes is energetically favourable, in accordance with equation 1.8, for solute concentrations up to the solubility in the given solvent at a constant temperature.

Conversely, molecular solvation does not incorporate the loss of electrostatic interactions like that in the dissociation of ionic compounds. Consider the hydration of a sucrose molecule, as shown in Figure 1.3 (right). Upon dissolution of a polar solute molecule, such as sucrose, within a polar solvent, such as water, the solvent molecules again orientate around the solute molecules according to electrical charge. In the example of sucrose in water, the electronegative oxygen atom of a water molecule resides closely to the electropositive terminal hydrogen atom of a hydroxyl functional group on the sucrose molecule. The electropositive hydrogen atom of either the same or a different water molecule resides more closely to the electronegative hydroxyl oxygen atom of the sucrose molecule, forming an energetically favourable hydration layer around the molecule up to the point of solvent saturation.

**Figure 1.3.** Schematic representations of the mechanisms of ionic solvation of sodium chloride in water (left) and molecular solvation of sucrose in water (right). The charges of the dipolar water molecules and sucrose molecule are partial charges  $\delta^+$  and  $\delta^-$ .



The saturation of a solvent, by a solute, occurs because it is no longer energetically favourable for dissolution to occur in accordance with the four principle components previously listed, which determine the Gibbs energy of solvation of the system. The Gibbs energy of solvation of an oil solvent is also a result of a superposition of the same four principle components listed previously.

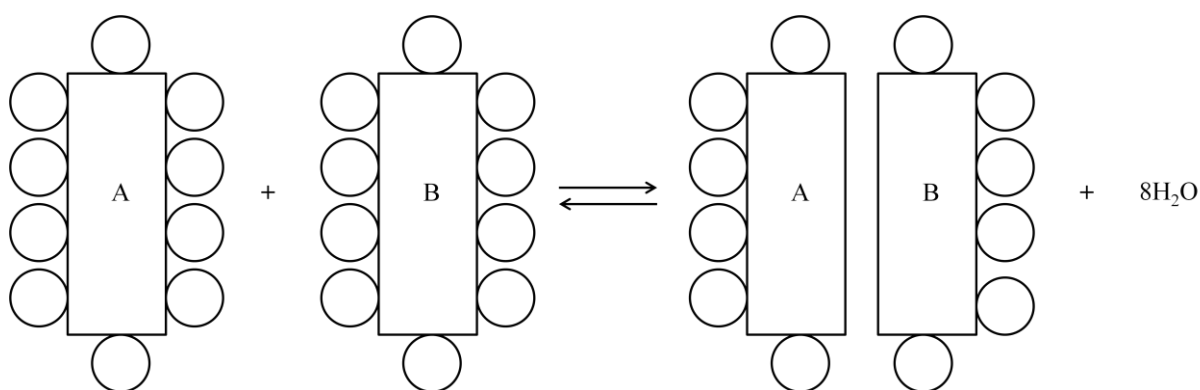
### 1.3.2 Solute partition coefficients and causes of non-ideal behaviour

When two immiscible solvents are contacted with each other, and one or both of these solvents contain a solute dissolved within, the solute(s) will transfer between the two solvents until an equilibrium distribution is reached for a given temperature. This equilibrium distribution of the solute is known as the partition coefficient of the solute between the two immiscible phases. The extent to which the solute partitions between the two phases is determined by how energetically favourable it is for the solute to reside in one solvent over the other, and therefore relates to the ratio of the standard molar Gibbs energies of the two immiscible solvents. The value of a solutes partition coefficient is therefore often assumed to equal the ratio of the solute solubilities within the two solvents. However, the ideality of many solute-in-solvent systems dramatically

changes with increasing solute concentration and hence the system partition coefficient is farthest from accurate at the points of solvent saturation.

Consider the extremely low solubility of hydrocarbons in water. Accordingly, the dissolution of a hydrocarbon in water is usually associated with an increase in the Gibbs energy  $G$  of the system ( $G > 0$ ). Since it is known experimentally that the dissolution of a hydrocarbon in water is exothermic ( $\Delta H < 0$ ) it follows from  $\Delta G = \Delta H - T\Delta S$  that the entropy of the system must decrease. This can be interpreted as a consequence of the highly ordered structure of the water molecules around the dissolved hydrocarbon molecules.<sup>4</sup> In other words, the water molecules are more tightly packed around the dissolved hydrocarbon than in pure water. This is called a structure increase. If aqueous solutions of two hydrocarbons are mixed, the two hydrocarbons may form an aggregate with simultaneous partial reconstruction of the original undisrupted water structure. This is shown in Figure 1.4.

**Figure 1.4.** The formation of a hydrophobic interaction between two hydrocarbon molecules A and B. The circles represent water molecules. Image redrawn from reference 7.



Due to the contact between A and B, fewer water molecules are now in direct contact with the hydrocarbon molecules. Thus, the ordering influence of the hydrophobic molecules will be diminished and the entropy increases ( $\Delta S > 0$ ). Although thermal energy is required for the destructuring of the hydration shells around A and B ( $\Delta H > 0$ ), the free energy diminishes upon aggregation ( $\Delta G < 0$ ). Therefore, it is energetically advantageous for apolar molecules, or apolar groups in otherwise polar molecules, when dissolved in water, to aggregate with expulsion of water molecules from their hydration shells. In order to minimise the unfavourable

solute/water interactions, the apolar solute molecules (or apolar groups) will interact preferentially, thus reducing the number of their water contacts.<sup>8</sup> The water molecules around an inert apolar solute have a higher coordination and are thus more ordered than in the bulk liquid, which is entropically unfavourable. The aggregation of apolar solutes, as shown in Figure 1.4, releases water molecules into the bulk water, which is entropically very favourable. Many solute molecules, including testosterone and caffeine, have been reported to undergo such aggregating behaviour via an attractive, non-covalent interaction between aromatic rings.<sup>9-11</sup> This interaction is often referred to as pi stacking.

The aggregation of solute molecules via interactions such as pi stacking causes an overall decrease in the activity of a solution. The reduction in the activity of a solution causes numerous non-ideal characteristics such as a loss of the linear relationship between photospectroscopic absorbance and concentration, as described by the Beer-Lambert law, or variations in a solutes partition coefficient with changing solute concentration as such aggregation adjusts a solutes affinity to the phases of which it is partitioning between. The true, concentration-independent value of a partition coefficient  $K_{a-b}$  is the equilibrium ratio of the solute activity in each phase ( $= a_a/a_b$ ). The activities are then equal to the product of the activity coefficient  $\gamma$  and the concentration as shown below.

$$K_{a-b} = \frac{a_a}{a_b} = \frac{\gamma_a C_a}{\gamma_b C_b} \quad (1.9)$$

Hence, in general, an apparent partition coefficient value (taken to equal the ratio of solute concentrations between two equilibrated immiscible solutions) will only equal the true value in the limit of low concentrations when the solute in both solution phases behaves ideally, which is when the activity coefficients reduce to unity.

#### 1.4 Emulsions

An emulsion may be defined as an opaque heterogeneous system of two immiscible liquid phases (for example, oil and water) where one of the phases is dispersed in the other as drops of a microscopic size (diameter  $> 1 \mu\text{m}$ ). Although emulsion drops are larger than the range specified for colloidal dispersions (diameter  $< 1 \mu\text{m}$ ),<sup>12</sup> their behaviour and characteristics are typically colloidal in nature, and thus, they can be

described as colloids. Simple emulsions exist as two types, one where oil drops are dispersed in water, which are termed oil-in-water (o/w) emulsions, and the other where water drops are dispersed in oil, termed water-in-oil (w/o) emulsions. Multiple emulsions are relatively more complex and a scope for dispersed droplets within droplets is observed. Water-in-oil-in-water (w/o/w) and oil-in-water-in-oil (o/w/o) emulsion compositions are hereby observed in multiple emulsions.<sup>13</sup>

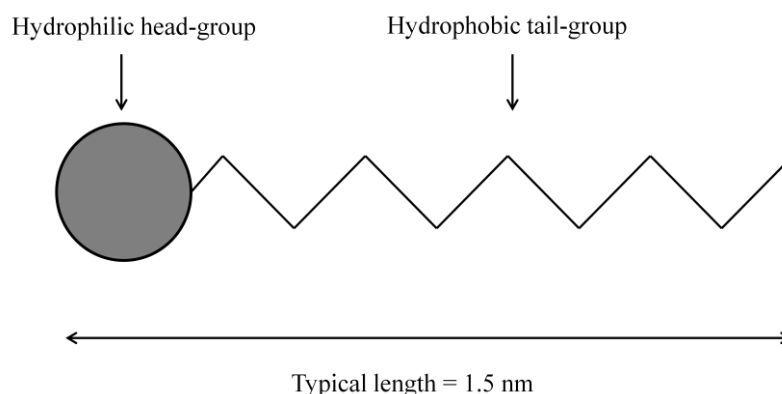
#### 1.4.1 *Surfactant-stabilised emulsions*

The research presented in the subsequent chapters is primarily concerned with the preparation of particle-stabilised emulsions, and so only a brief introduction to emulsions stabilised by surfactants is given.

The mixing of two immiscible liquids results in the formation of an unstable emulsion, which typically undergoes complete separation into the bulk phases within seconds. In order to produce a stable emulsion a third component is required. This third component is an emulsifier or a surface-active agent (commonly referred to as a surfactant) and is added to the emulsion mixture to lower the energetically unfavourable interfacial tension between the two immiscible phases by adsorbing at the oil-water interface.<sup>14</sup> The emulsifier adsorbs at the interface, creating a film around the dispersed drops which, as well as lowering the interfacial tension between the two immiscible phases, also prevents coalescence of the drops.<sup>12</sup> This important characteristic is a result of their amphiphilic nature. Surfactant molecules possess two parts, a hydrophilic head-group and a hydrophobic tail, as shown in Figure 1.5. When adsorbed at an oil-water interface the hydrophilic head-group is situated in the water phase, and the hydrophobic tail group is situated in the oil phase, so that the surfactant molecule bridges the interface.



**Figure 1.5.** Schematic representation of a single-tailed surfactant molecule.



Bancroft proposed that the emulsion type (o/w or w/o) depends on the solubility of the surfactant.<sup>15</sup> The phase in which the emulsifier is most soluble tends to be the continuous phase of the resulting emulsion. Another way of predicting emulsion type based on the emulsifier was introduced by Griffin.<sup>16</sup> The hydrophile-lipophile balance (HLB) number is a quantitative measure of the balance between hydrophilic and hydrophobic moieties of a surfactant molecule. A hydrophilic surfactant has a high HLB number and is therefore predicted to stabilise o/w emulsions. Conversely, hydrophobic surfactants with low HLB numbers are predicted to stabilise w/o emulsions. The system HLB can be affected by several parameters, such as electrolyte concentration, temperature, oil type and chain length and co-surfactant concentration. This occurs as the geometry of the surfactant at the interface is modified,<sup>17</sup> and thus changes the curvature of the surfactant monolayer, which influences the preferred emulsion type.<sup>18</sup>

The free energy of emulsion formation from the bulk immiscible phases is given by:

$$\Delta G = \Delta A\gamma - T\Delta S \quad (1.10)$$

where  $\Delta A$  is the change in the interfacial area,  $\gamma$  is the interfacial tension, and  $\Delta S$  is the change in the entropy in the system at temperature  $T$ . If the interfacial tension is relatively large then the interfacial energy  $\Delta A\gamma$  is greater than the entropy contribution  $T\Delta S$ , and the free energy change  $\Delta G$  is positive. Emulsification is non-spontaneous and therefore work is required to break-up the two bulk phases, e.g. mechanical mixing. These emulsions are known as macroemulsions, as they generally consist of larger emulsion drops which are thermodynamically unstable. Microemulsions, unlike

macroemulsions, exhibit an ultralow interfacial tension. In such systems the change in interfacial energy  $\Delta A\gamma$  is smaller than the entropy contribution  $T\Delta S$ , and so the free energy change on emulsion formation is negative. Microemulsions are therefore formed spontaneously and are thermodynamically stable indefinitely.

#### 1.4.2 *Particle-stabilised emulsions*

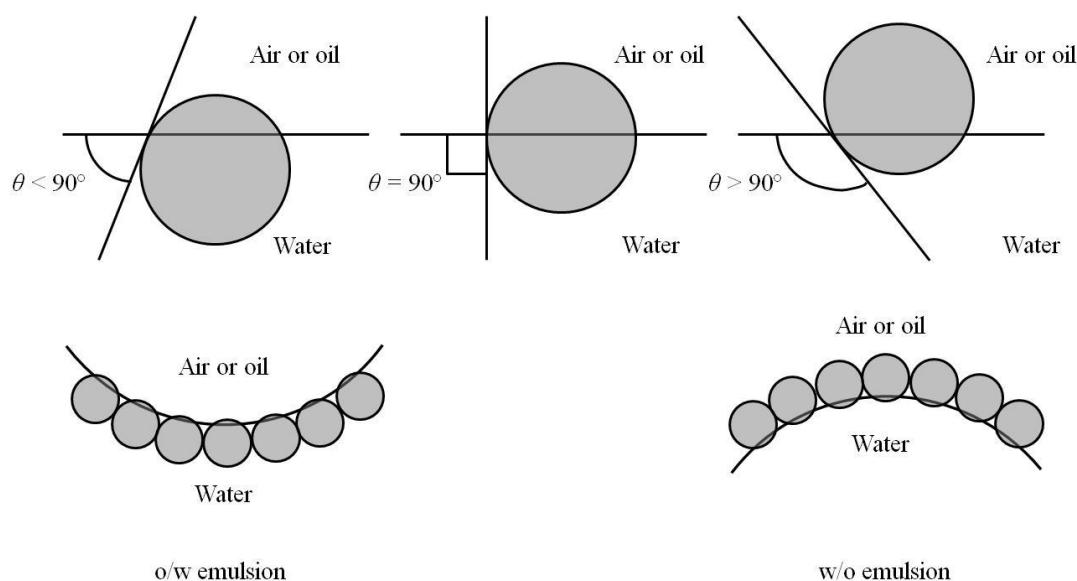
Unlike surfactant molecules, solid particles need not be amphiphilic in order to be considered surface active.<sup>19</sup> Colloidal particles that are partially wetted by both an aqueous and oil phase are capable of strongly adsorbing to oil-water interfaces. The driving force behind this adsorption is to remove an area of high interfacial tension that exists between the two fluid phases and replace this area with a lower interfacial tension between the two fluid phases and the solid particle.

Interest in particle-stabilised emulsions has seen a substantial surge in recent years since their discovery over 100 years ago.<sup>20,21</sup> Solid particles now represent an important class of emulsifying agents, highlighted by the publication of many recent reviews.<sup>22-29</sup> There are many examples of solid particles that have been shown to stabilise emulsions, such as silica,<sup>30-32</sup> clay,<sup>33,34</sup> carbon,<sup>35</sup> a variety of minerals,<sup>36-38</sup> as well as polymer latexes,<sup>39,40</sup> waxes<sup>41</sup> and microgels.<sup>42,43</sup>

The fact that finely divided solid particles can act as the sole stabiliser in emulsions has been known since the beginning of the last century. Pickering<sup>21</sup> conducted the first systematic study on particle-stabilised emulsions and hence they are often referred to as “Pickering emulsions.” However, four years previously, and cited by Pickering, Ramsden<sup>20</sup> described the formation of a membrane of solid particles enveloping both air bubbles in water (foams) and oil drops in water (emulsions). Finkle *et al.*<sup>44</sup> noted that bi-wettable particles resting at an interface between two immiscible liquids are likely to be wet more by one liquid than by the other, with the more poorly wetting liquid becoming the dispersed phase of the resultant emulsion upon homogenisation. They observed that more water-wet particles such as silica were renowned to stabilise o/w emulsions whilst oil-wet particles such as carbon black would preferentially stabilise w/o emulsions. The importance of the differing particle wettabilities, quantified by the three-phase contact angle  $\theta$ , recorded through the aqueous phase, which the particle made when resting at an oil-water interface, was noted. Furthermore, Schulman and Leja<sup>45</sup> showed the influence of the three-phase contact angle of solid

particles on the emulsion type and stability. For conditions such that the three-phase contact angle  $\theta$ , measured through the aqueous phase (see Figure 1.7), was slightly  $< 90^\circ$  particles stabilised o/w emulsions, but for particles with  $\theta > 90^\circ$  particles stabilised w/o emulsions. However, it was noted that if the emulsifying particles were too hydrophilic (low  $\theta$ ) or too hydrophobic (high  $\theta$ ) they tended to remain dispersed within the aqueous or oil phase respectively and thus acted as poor emulsion stabilisers. Figure 1.6 illustrates this influence of particle wettability and therefore the three-phase contact angle on the type of emulsion prepared.

**Figure 1.6.** (Upper) Position of a small spherical particle at a planar oil (or air)–water interface for a contact angle (measured through the aqueous phase) less than  $90^\circ$  (left), equal to  $90^\circ$  (centre) and greater than  $90^\circ$  (right). (Lower) Corresponding probable positioning of particles at a curved oil (or air)–water interface. For  $\theta < 90^\circ$ , particle-stabilised o/w emulsions form (left) and for  $\theta > 90^\circ$ , particle-stabilised w/o emulsions form (right). Image redrawn from reference 24.



As suggested by Figure 1.6, solid particles can also be used to stabilise both air-in-water foams and water-in-air dry powders.<sup>46</sup>

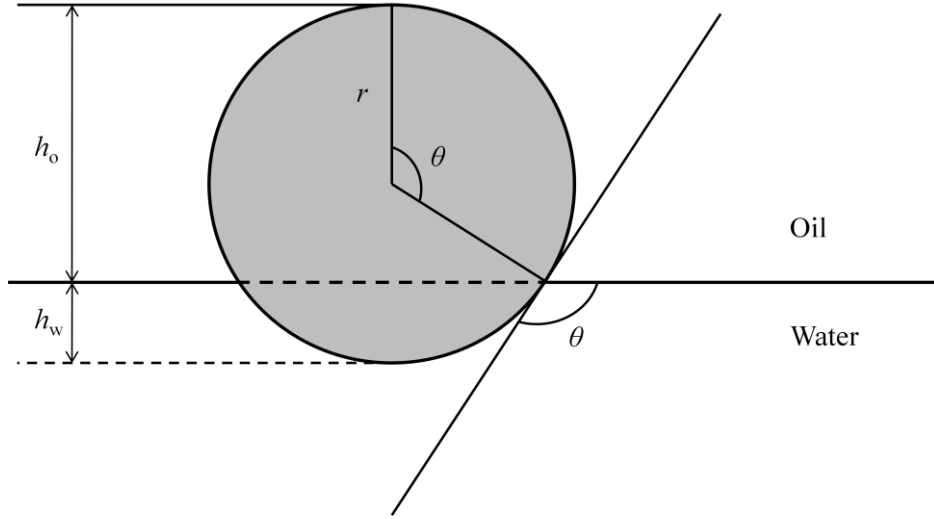
There are several mechanisms by which colloidal particles stabilise emulsions. Most often drop stability is attributed to steric hindrance provided by the formation of a dense film of particles at the oil-water interface, present as either a monolayer or multilayer.<sup>47,48</sup> This is usually the case in particle-stabilised emulsions, whereby droplet coalescence is prevented by two particle layers, one layer adsorbed on each

approaching droplet. Another mechanism for droplet stabilisation is the configuration of particle bridging between two emulsion drops. This has been directly observed between sparsely coated emulsion drops stabilised by slightly hydrophobic silica particles, which interestingly showed much denser packing within the bridging film through immersion capillary attraction.<sup>49</sup> For this configuration particles must have an interfacial position where the majority portion of the particle is in the continuous phase (i.e. a hydrophobic particle bridging a water-oil-water film), otherwise the emulsion drop interfaces would overlap resulting in coalescence. An additional particle configuration has been proposed by Vignati *et al.*<sup>50</sup> for the stabilisation of sparsely covered emulsion drops. It was suggested that particle re-distribution over the surface of droplets toward inter-drop contact areas may play a part in emulsion stabilisation. Furthermore, the formation of a 2-D network of aggregated particles across the interface can also explain the stability to coalescence of emulsion drops that are less than fully coated.<sup>51</sup> Finally, when an abundance of particles is present in the continuous phase, a 3-D network of particles can form.<sup>52,53</sup> The resulting increase in viscosity of the emulsion helps to stabilise the emulsion by preventing instabilities such as creaming, flocculation and coalescence of emulsion drops. These emulsion instabilities are explained later in this chapter.

#### 1.4.2.1 Energy of particle detachment from a liquid-liquid interface

The strength of attachment of a particle to the oil-water interface is related to the magnitude of the interfacial tension between the two liquid phases, as well as the position of the colloidal particle at the fluid interface, quantified by the three-phase contact angle  $\theta$  (see Figure 1.7).

**Figure 1.7.** Representation of a spherical solid particle in its equilibrium position at an oil-water interface. The effect of gravity is assumed to be negligible for small particles ( $< 5 \mu\text{m}$ ) so that the oil-water interface remains planar up until the contact line with the particle.<sup>19</sup>



For a single spherical particle of radius  $r$ , adsorbed at an oil-water interface at a contact angle  $\theta$  measured through the aqueous phase, the depth of immersion into water,  $h_w$ , equals  $r(1 + \cos \theta)$ . The surface area of the particle in contact with water,  $A_{sw}$ , is given by  $2\pi r h_w = 2\pi r^2(1 + \cos \theta)$ . The planar area of oil-water interface removed by the adsorption of the particle is therefore given by

$$A_{ow} = \pi r^2 \sin^2 \theta = \pi r^2 (1 - \cos^2 \theta) \quad (1.11)$$

The energy,  $E_{det}$ , required to detach the resting particle from the interface into the oil phase is given by

$$E_{det} = 2\pi r^2 (1 + \cos \theta)(\gamma_{so} - \gamma_{sw}) + \pi r^2 (1 - \cos^2 \theta) \gamma_{ow} \quad (1.12)$$

where  $\gamma$  refers to the appropriate interfacial tension and the subscripts s, o and w refer to the solid, oil and water respectively. The tensions are related to the contact angle through the Young equation, such that

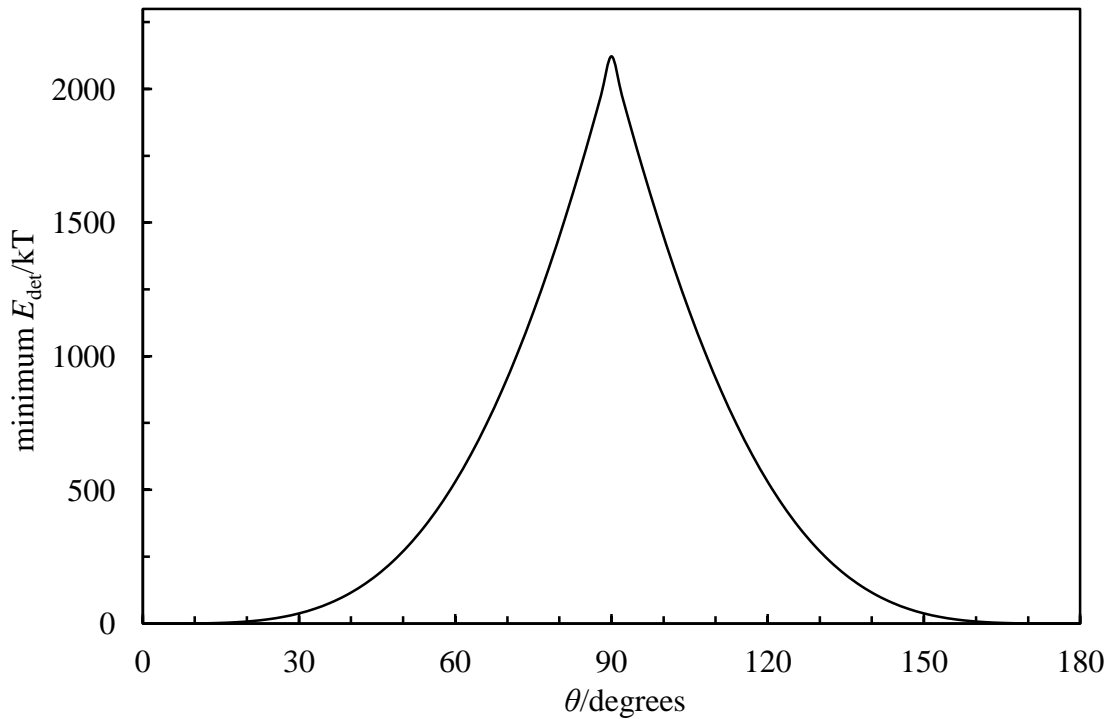
$$\gamma_{so} - \gamma_{sw} = \gamma_{ow} \cos \theta \quad (1.13)$$

Therefore equation 1.12 can be simplified to

$$E_{det} = \pi r^2 \gamma_{ow} (1 + \cos \theta)^2 \quad (1.14)$$

For the removal of the same particle from the interface into the water phase, the sign within the bracket of equation (1.14) becomes negative. From equation 1.14, the removal of a hydrophobic particle ( $\theta > 90^\circ$ ) into the oil phase requires less energy than removal of the same particle into the water phase, whereas the opposite is true for a hydrophilic ( $\theta < 90^\circ$ ) particle. The variation of the minimum energy of detachment with the contact angle  $\theta$  at fixed  $\gamma_{ow}$  and particle radius is shown in Figure 1.8.

**Figure 1.8.** Variation in minimum energy of detachment of a spherical particle of radius  $r = 10$  nm with contact angle  $\theta$  at the planar isopropyl myristate-water interface of interfacial tension  $\gamma_{ow} = 27.32$  mN m<sup>-1</sup> at 298 K.



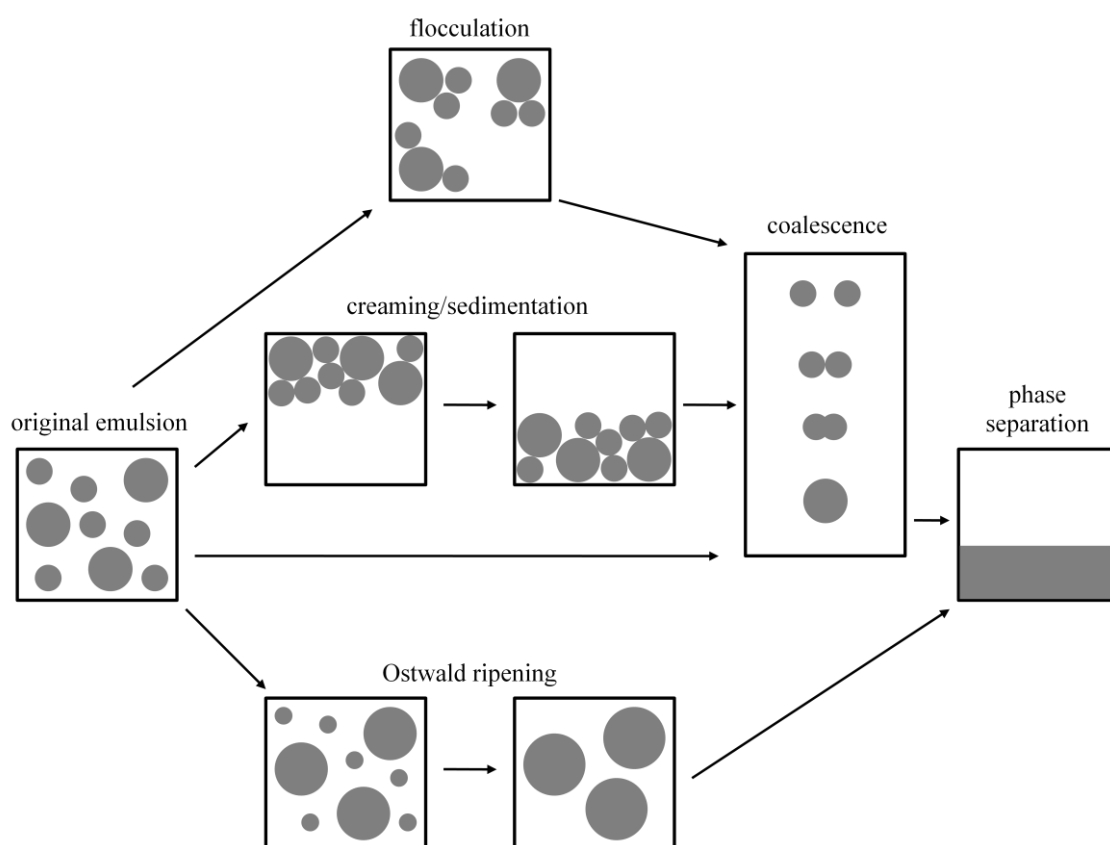
From Figure 1.8 it can be seen that particles are most strongly adsorbed at the oil-water interface when  $\theta = 90^\circ$ . Either side of  $90^\circ$ ,  $E_{det}$  falls rapidly such that for particles with  $\theta$  between  $0$  and  $20^\circ$ , or between  $160$  and  $180^\circ$ , the energy of detachment is only  $10$  kT or less. Hence particles that are too hydrophilic (low  $\theta$ ) or too hydrophobic (high  $\theta$ ) are easily removed from the interface and do not stabilise emulsions, as described previously. At values of  $\theta$  around  $90^\circ$ , the energy of particle detachment is typically orders of magnitude higher than the thermal energy. Solid particles of intermediate wettability can therefore be considered irreversibly adsorbed,<sup>19,54</sup> unlike surfactant molecules which are in rapid dynamic equilibrium with non-adsorbed surfactant.

Particle-stabilised emulsions therefore offer great potential to the pharmaceutical industry for the production of high stability topical formulations.

### 1.4.3 *Emulsion stability*

As macroemulsions are ultimately thermodynamically unstable, emulsion stability is a kinetic concept.<sup>55</sup> An emulsion is considered stable if it is resistant to physical changes over a certain time scale. Figure 1.9 shows the four main ways in which an emulsion can become unstable. These processes are called flocculation, creaming/sedimentation, coalescence and Ostwald ripening, and they can occur simultaneously or consecutively within an emulsion.

**Figure 1.9.** Schematic representation of the different types of physical instabilities exhibited by an emulsion. Redrawn from reference 22.



#### 1.4.3.1 Creaming/sedimentation

Creaming refers to the movement of drops of the dispersed phase under gravity or in a centrifuge to form a concentrated layer at the top of a sample, but with no

accompanying change in the drop size distribution. Typically this is observed in o/w emulsions, as the oil phase is usually less dense than the aqueous phase. Initially, a concentration gradient of drops develops in the vertical direction, often followed by the appearance of a distinct boundary between an upper cream layer and a lower depleted emulsion layer.<sup>55</sup> When the dispersed phase is more dense than the continuous phase, typically the case in w/o emulsions, the equivalent phenomenon is called sedimentation. Creaming or sedimentation represents a reversible type of emulsion instability in that gentle agitation is sufficient to restore uniform distribution of drops. In very dilute emulsions, the creaming speed  $v_s$  of an isolated, spherical drop of radius  $r$  moving through a fluid medium of density  $\rho_0$  and Newtonian shear viscosity  $\eta_0$  is given by an expression based on Stokes law<sup>56</sup> by

$$v_s = \frac{2r^2(\rho_0 - \rho)g}{9\eta_0} \quad (1.15)$$

where  $g$  is the acceleration due to gravity and  $\rho$  is the density of the dispersed phase. In the absence of significant emulsion drop interaction, this equation indicates that creaming or sedimentation can be retarded by reducing the size of the emulsion drops, increasing the viscosity of the continuous phase or by decreasing the density difference between the phases.

#### 1.4.3.2 Flocculation

Flocculation is the process in which emulsion drops aggregate, without rupture of the stabilising interfacial film.<sup>55</sup> Whether or not emulsion drops flocculate is determined by the free energy of interaction between the emulsion drops as a function of their separation. This is generally described by the Derjaguin and Landau, and Verwey and Overbeek (DLVO) theory which is not discussed here as it is not of primary relevance to the contents of this research. If the free interaction energy is appreciably negative at a certain separation, flocculation of the emulsion drops occurs. Like creaming this process can be reversible in that gentle agitation is often sufficient to restore the uniform distribution of drops. Stronger interdrop attractions however can also cause irreversible flocculation, where far greater energy input is required to re-disperse the emulsion drops. Flocculation usually results in enhanced creaming, as the effective radius of the flocs is larger than that of individual drops. On the other hand,



flocculation can also result in a gel-like network of emulsion drops, effectively arresting creaming. Like other colloids, emulsions are also susceptible to non-DLVO forces. Their stability can be enhanced by the use of polymeric surfactants imparting steric stabilisation of the emulsion drops against flocculation. The presence of excess emulsifier, as either micellar surfactant aggregates in surfactant-stabilised emulsions or nanoparticles in particle-stabilised emulsions, can also cause the flocculation of emulsion drops through depletion attraction.

#### 1.4.3.3 Coalescence

Coalescence is the process in which two or more emulsion drops fuse together to form a single larger emulsion droplet, and in doing so reduce their surface free energy. This process is irreversible and, if allowed to continue, ultimately results in complete phase separation of an emulsion into the two bulk liquid phases. For coalescence to occur, the forces between the emulsion drops must be such that the film of continuous phase separating them becomes sufficiently thin that film rupture becomes a likely possibility. A consequence of this is that interdrop coalescence will be enhanced in creamed or flocculated systems. Rupture of the separating films between emulsion drops is thought to occur through the presence of surface waves at the molecular scale. The Brownian motion of molecules in and near film surfaces may provide the activation energy required to produce a small hole in the thin film, which then propagates across the film resulting in coalescence. The presence of larger surface waves has been postulated by Vrij,<sup>57</sup> whose amplitude is greater at larger drop diameter. Overlap of these waves between emulsion drops creates local thin-spots in the liquid film, which promote hole formation and coalescence.

#### 1.4.3.4 Ostwald ripening

Ostwald ripening refers to the molecular diffusion of dispersed phase between emulsion drops of differing size. As such it is particularly apparent when the dispersed phase shows significant solubility in the continuous phase. According to the Kelvin equation,<sup>58</sup> the solubility of a substance in the form of spherical drops increases with increasing size by

$$c(r) = c(\infty) \exp\left(\frac{2\gamma V_m}{rRT}\right) \quad (1.16)$$

where  $c(r)$  is the continuous phase solubility of the dispersed phase within a drop of radius  $r$ ,  $c(\infty)$  is the solubility in a system with only a planar interface,  $\gamma$  is the interfacial tension,  $V_m$  is the molar volume of the dispersed phase,  $R$  is the gas constant and  $T$  is the temperature. As a consequence of its enhanced solubility, material contained within small emulsion drops tends to dissolve into the continuous phase and recondense onto larger emulsion drops. This process results in an increase in the average emulsion drop size without coalescence, which theoretically continues until all the drops are merged into one.<sup>55</sup>

### 1.5 Current opinions in membrane permeation studies and topical formulation design

The study of solute permeation across a membrane is important in many applications, including the retention of perfumes and flavours within food packaging, the exclusion of toxic chemicals by chemical safety suits, the control of pests and plant diseases using bioactive agrochemicals, cosmetics and the delivery of pharmaceutical actives across membrane barriers such as the skin. The permeating species may be contacted with the donor side of the membrane in a variety of formulation types (or “vehicles”) including, *inter alia*, solutions in either aqueous or low polarity organic solvents, or dissolved within multiphase, colloiddally microstructured systems, such as particle dispersions or emulsions which may be of either an oil-in-water or water-in-oil conformation.

There is an extensive literature on membrane permeation covering both biological membranes such as skin and synthetic, polymer membranes. Effects of donor solvent type, including both thermodynamic (reflecting the relative affinity of the permeant for the membrane) and kinetic effects (how the solvent type affects the diffusivity of the permeant in the membrane) have been investigated.<sup>59-64</sup> Donor vehicles have included not only single-solvent solutions but also permeants dissolved in mixed solvents<sup>65-70</sup> and more complex, multi-phase vehicles such as emulsions including oil-in-water, water-in-oil and multiple types stabilised by either surfactants, polymers or particles.<sup>71-79</sup> Overall, it is well established that the extent and rate of permeation for a particular permeating species and membrane system depends strongly on the nature of the type of formulation applied to the donor side of the membrane. As discussed in this research, donor solvent effects can arise from many possible causes which can depend on both

the nature of the specific system together with details of the experimental conditions (for example, the donor and receiver compartment stirring rates, volumes and membrane thicknesses) used in the permeation measurements. Despite numerous literature reports of donor solvent effects on permeation, many of the studies lack sufficient detailed information to enable unambiguous resolution of which effect or combination of effects may be operating in particular donor vehicle systems. An additional problem is that switching between the same polar and apolar donor solvents can affect permeation in dramatically different ways for systems with different permeating species or membranes. Hence, although many individual aspects of donor solvent effects on permeation have been reported, there remains a clear need to clarify (i) all the possible origins of such effects and how to discriminate between them and (ii) how donor solvent effects depend on the natures of the permeant and the membrane. The primary aim of the work discussed in this thesis is to address both of these points using a combination of theory and experiment.

The recent development in the understanding of particle behaviour at a fluid-fluid interface, and therefore the use of particles as emulsifiers, has allowed for the production of a wide range of novel formulations. Each of these novel formulations are potential vehicles for the delivery of active drugs to the skin and include formulation designs such as dry aqueous powders,<sup>46</sup> powdered oils,<sup>80</sup> liquid marbles<sup>81</sup> and powdered emulsions.<sup>82</sup> By further application of this developing knowledge, the secondary aim of the work discussed in this thesis concerns the production of waterless, particle-stabilised emulsions and the characteristics of drug delivery from these developed formulations. A thorough understanding of the mechanisms of drug delivery from such formulations subsequently allows for the exploitation of the potential benefits that they can provide to the pharmaceutical industry.

## **1.6 Presentation of thesis**

The initial aim of this work is to establish a reproducible method for accurately monitoring the membrane permeation of an active drug from various different types of topical formulation. Chapter 2 describes the experimental methods and apparatus used for these analyses, and discusses the materials and techniques used for the development of the various different topical formulations investigated.

Chapter 3 introduces the fundamental theoretical model which describes the predicted characteristics of drug delivery across an isotropic membrane from a donor solution. The derived model illustrates an intrinsic prediction for the theoretical rate and extent of membrane permeation for any given combination of donor solution type (i.e. aqueous or oil solvent), membrane wettability (i.e. hydrophilic or hydrophobic membrane) and permeant hydrophobicity (i.e. hydrophilic or hydrophobic permeant). A comparison between these predictions and data recorded experimentally, via the use of the methods described in Chapter 2, is then conducted and the model is shown to provide accurate predictions across an extensive magnitude of  $10^6$  units. All assumptions proposed for the derivation of the theoretical model are fully exploited and the additional solvent effects which can arise by rendering each assumption individually invalid is accordingly tested and understood.

Chapter 4 describes the development of a new class of formulation which is a potential vehicle for use in the delivery of an active drug across the skin barrier. The preparation and properties of waterless, particle-stabilised emulsions are investigated. Investigations into the formation of numerous different waterless, particle-stabilised emulsions are presented, and several interesting observations, such as the preparation of transparent emulsions, are analysed and understood.

The work described in Chapter 5 introduces a systematic modification to the intrinsic theoretical model derived in Chapter 3. This adapted model allows for the explanation and prediction of the rate and extent of drug delivery from colloiddally microstructured donor formulations, such as particle dispersions within a solvent or particle-stabilised emulsions of both oil-in-water and water-in-oil types. The delivery of an active drug across a membrane from both conventional oil-water and the developed waterless, particle-stabilised emulsions is experimentally investigated and compared to the theoretical values predicted by the adapted model. The mechanisms of drug delivery from such donor formulations are described and the theoretical model is again shown to correctly account for the experimental observations made.

Finally, a summary of the conclusions and suggestions for future work are described in Chapter 6.

## 1.7 References

1. J. Crank, *The Mathematics of Diffusion*, Oxford University Press, London, 1956.
2. K. Pearson, *Nature*, **72**, 294, (1905).
3. H.L. Frisch, *J. Phys. Chem.*, **62**, 401, (1958).
4. C. Reichardt, *Solvents and Solvent Effects in Organic Chemistry*, 3<sup>rd</sup> edn., Wiley-VCH, Weinheim, 2003.
5. R. Daudel, *Quantum Theory of Chemical Reactivity*, Reidel, Dordrecht, 1973.
6. K.L. Wolf, *Theoretische Chemie*, 4<sup>th</sup> ed., J.A. Barth, Leipzig, 1959.
7. B.R. Baker, *J. Chem. Educ.*, **44**, 610, (1967).
8. F. Franks, *Water – A Matrix of Life*, 2<sup>nd</sup> ed., Royal Society of Chemistry, Cambridge, 2000.
9. K. Ulanowska, J. Piosik, A. Gwizdek-Wisniewska and G. Wegrzyn, *Bioorganic Chem.*, **33**, 402, (2005).
10. G. Gattuso, G. Manfredi and S. Sammartano, *Fluid Phase Equilib.*, **308**, 47, (2011).
11. A.A. Rasool, A.A. Hussain and L.W. Ditter, *J. Pharm. Sci.*, **80**, 387, (1991).
12. D. Myers, *Surfaces, Interfaces and Colloids: Principles and Applications*, 2<sup>nd</sup> edn., Wiley-VCH, New York, 1999.
13. N. Garti, *Colloids Surf. A*, **123**, 233, (1997).
14. P. Walstra, *Encyclopaedia of Emulsion Technology*, vol. 4, Marcel Dekker, New York, 1996.
15. W.D. Bancroft, *J. Phys. Chem.*, **17**, 501, (1913).
16. W.C. Griffin, *J. Soc. Cosmet. Chem.*, **1**, 337, (1949).

17. R. Aveyard, B.P. Binks and P.D.I. Fletcher, *The Structure, Dynamics and Equilibrium Properties of Colloidal Systems*, eds. D.M. Bloor and E. Wyn-Jones, Kluwer, Dordrecht, 1990.
18. A. Graciaa, J. Lachaise, G. Marion and R.S. Schechter, *Langmuir*, **5**, 1315, (1989).
19. B.P. Binks and T.S. Horozov, (Eds.), in *Colloidal Particles at Liquid Interfaces*, Cambridge University Press, Cambridge, 2006, p.1.
20. W. Ramsden, *Proc. Roy. Soc.*, **72**, 156, (1903).
21. S.U. Pickering, *J. Chem. Soc.*, **91**, 2001, (1907).
22. R.J.G. Lopetinsky, J.H. Masliyah and Z. Xu, in *Colloidal Particles at Liquid Interfaces*, B.P. Binks and T.S. Horozov (Eds.), Cambridge University Press, Cambridge, 2006, p.186.
23. D.E. Tambe and M.M. Sharma, *Adv. Colloid Interface Sci.*, **52**, 1, (1994).
24. B.P. Binks, *Curr. Opinion Colloid Interface Sci.*, **7**, 21, (2002).
25. R. Aveyard, B.P. Binks and J.H. Clint, *Adv. Colloid Interface Sci.*, **100-102**, 503, (2003).
26. C. Zeng, H. Bissig and A.D. Dinsmore, *Solid State Commun.*, **139**, 546, (2006).
27. S. Tcholakova, N.D. Denkov and A. Lips, *Phys. Chem. Chem. Phys.*, **10**, 1608, (2008).
28. P.S. Clegg, *J. Phys: Condens. Matter*, **20**, 113101, (2008).
29. T.N. Hunter, R.J. Pugh, G.V. Franks and G.J. Jameson, *Adv. Colloid Interface Sci.*, **137**, 57, (2008).
30. P.S. Clegg, E.M. Herzig, A.B. Schofield, T.S. Horozov, B.P. Binks, M.E. Cates and W.C.K. Poon, *J. Phys: Condens. Matter*, **17**, S3433, (2005).
31. N. Yan, M.R. Gray and J.H. Masliyah, *Colloids Surf. A*, **193**, 97, (2001).

32. B. Braisch, K. Köhler, H.P. Schuchmann and B. Wolf, *Chem. Eng. Technol.*, **32**, 1107, (2009).
33. S. Abend, N. Bonnke, U. Gutschner and G. Lagaly, *Colloid Polym. Sci.*, **276**, 730, (1998).
34. B.P. Binks, J.H. Clint and C.P. Whitby, *Langmuir*, **21**, 5307, (2005).
35. B.P. Binks, Z.-G. Cui and P.D.I. Fletcher, *Langmuir*, **22**, 1664, (2006).
36. S. Stiller, H. Gers-Barlag, M. Lergenmueller, F. Pflücker, J. Schultz, K.P. Witten and R. Daniels, *Colloids Surf. A*, **232**, 261, (2004).
37. A. Menner, V. Ikem, M. Salgueiro, M.S.P. Shaffer and A. Bismarck, *Chem. Commun.*, **41**, 4274, (2007).
38. H. Liu, C. Wang, Q. Gao, X. Liu and Z. Tong, *Int. J. Pharm.*, **351**, 104, (2008).
39. B.P. Binks and J.A. Rodrigues, *Angew. Chem. Int. Ed.*, **44**, 441, (2005).
40. Z.Ao, Z. Yang, J. Wang, G. Zhang and T. Ngai, *Langmuir*, **25**, 2572, (2009).
41. B.P. Binks and A. Rocher, *J. Colloid Interface Sci.*, **335**, 94, (2009).
42. T. Ngai, S.H. Behrens and H. Auweter, *Chem. Commun.*, **3**, 331, (2005).
43. D. Dupin, S.P. Armes, C. Connan, P. Reeve and S.M. Baxter, *Langmuir*, **23**, 6903, (2007).
44. P. Finkle, H.D. Draper and J.H. Hildebrand, *J. Am. Chem. Soc.*, **45**, 2780, (1923).
45. J.H. Schulman and J. Leja, *Trans Faraday Soc.*, **50**, 598, (1954).
46. B.P. Binks, and R. Murakami, *Nature Mater.*, **5**, 865, (2006).
47. K. Golemanov, S. Tchloкова, P.A. Kralchevsky, K.P. Ananthapadmanabhan and A. Lips, *Langmuir*, **22**, 4968, (2006).
48. B.P. Binks and M. Kirkland, *Phys. Chem. Chem. Phys.*, **4**, 3727, (2002).
49. T.S. Horozov and B.P. Binks, *Angew. Chem. Int. Ed.*, **45**, 773, (2006).

50. E. Vignati, R. Piazza and T.P. Lockhart, *Langmuir*, **19**, 6650, (2003).
51. B.R. Midmore, *Colloids Surf. A*, **132**, 257, (1998).
52. J. Thieme, S. Abend and G. Lagaly, *Colloid Polym. Sci.*, **277**, 257, (1999).
53. T.S. Horozov, B.P. Binks and T. Gottschalk-Gaudig, *Phys. Chem. Chem. Phys.*, **9**, 6398, (2007).
54. S. Levine, B.D. Bowen and S.J. Partridge, *Colloids Surf.*, **38**, 325, (1989).
55. B.P. Binks, in *Modern Aspects of Emulsion Science*, B.P. Binks (Ed.), Royal Society of Chemistry, Cambridge, 1998, p. 1.
56. G.G. Stokes, *Philos. Mag.*, **1**, 337, (1851).
57. A. Vrij, *Disc. Faraday Soc.*, **42**, 23, (1966).
58. W. Thompson (Lord Kelvin), *Philos. Mag.*, **42**, 448, (1871).
59. A.C. Watkinson, H. Joubin, D.M. Green, K.R. Brain and J. Hadgraft, *Int. J. Pharm.*, **121**, 27, (1995).
60. S.E. Cross, W.J. Pugh, J. Hadgraft and M.S. Roberts, *Pharm. Res.*, **18**, 999, (2001).
61. P.C. Mills, *Veterinary Res. Commun.*, **31**, 227, (2007).
62. M. Dias, J. Hadgraft and M.E. Lane, *Int. J. Pharm.*, **340**, 65, (2007).
63. M. Dias, J. Hadgraft and M.E. Lane, *Int. J. Pharm.*, **336**, 108, (2007).
64. A. Fini, V. Bergamante, G.C. Ceschel, C. Ronchi and C.A.F. De Moraes, *AAPS Pharm. Sci. Tech.*, **9**, 762, (2008).
65. M.-L. Leichtnam, H. Rolland, P. Wuthrich and R.H. Guy, *J. Controlled Release*, **113**, 57, (2006).
66. W.J. McAuley, K.T. Mader, J. Tetteh, M.E. Lane and J. Hadgraft, *Eur. J. Pharm. Sci.*, **38**, 378, (2009).



67. W.J. McAuley, M.D. Lad, K.T. Mader, P. Santos, J. Tetteh, S.G. Kazarian, J. Hadgraft and M.E. Lane, *Eur. J. Pharm. Biopharm.*, **74**, 413, (2010).
68. G. Oliveira, A.E. Beezer, J. Hadgraft and M.E. Lane, *Int. J. Pharm.*, **393**, 61, (2010).
69. W.J. McAuley, G. Oliveira, D. Mohammed, A.E. Beezer, J. Hadgraft and M.E. Lane, *Int. J. Pharm.*, **396**, 134, (2010).
70. R.M. Watkinson, R.H. Guy, G. Oliveira, J. Hadgraft and M.E. Lane, *Skin Pharmacol. Physiol.*, **24**, 22, (2011).
71. P. Izquierdo, J.W. Wiechers, E. Escribano, M.J. Garcia-Celma, T.F. Tadros, J. Esquena, J.C. Dederen and C. Solans, *Skin Pharmacol. Physiol.*, **20**, 263, (2007).
72. K. Wiren, H. Frithiof, C. Sjoqvist and M. Loden, *Brit. J. Dermatol.*, **160**, 552, (2009).
73. A. Otto, J. du Plessis and J.W. Wiechers, *Int. J. Cosmetic Sci.*, **31**, 1, (2009).
74. S. Simovic and C.A. Prestidge, *Eur. J. Pharm. Biopharm.*, **67**, 39, (2007).
75. H. Sarhan, M.A. Ibrahim, M.A. Amin and A.K.F. Dyab, *Bull. Pharm. Sci.*, **31**, 155, (2008).
76. J. Frelichowska, M.A. Bolzinger, J. Pelletier, J.P. Valour and Y. Chevalier, *Int. J. Pharm.*, **371**, 56, (2009).
77. J. Frelichowska, M. A. Bolzinger J. P. Valour, H. Mouaziz, J. Pelletier and Y. Chevalier, *Int. J. Pharm.*, **368**, 7, (2009).
78. N. G. Eskandar, S. Simovic and C. A. Prestidge, *J. Pharm. Sci.*, **99**, 890, (2010).
79. S. Simovic, N.G. Eskander and C.A. Prestidge, *J. Drug Deliv. Sci. Technol.*, **21**, 123, (2011).
80. H. Adelman, B.P. Binks and R. Mezzenga, *Langmuir*, **28**, 1694, (2012).

81. B.P. Binks, A.N. Boa, M.A. Kibble, G. Mackenzie and A. Rocher, *Soft Matter*, **7**, 4017, (2011).
82. R. Murakami, H. Moriyama, M. Yamamoto, B.P. Binks and A. Rocher, *Adv. Mater.*, **24**, 767, (2012).

## CHAPTER 2

### EXPERIMENTAL

This chapter describes the materials and experimental methods used throughout this research.

#### 2.1 Materials

##### 2.1.1 *Solvents*

###### 2.1.1.1 Water

Water was purified by passing through an Elgastat Prima reverse osmosis unit followed by a Millipore Milli-Q reagent water system. Measurements of the resulting Milli-Q water surface tension using the du Noüy ring method were typically  $71.9 \text{ mN m}^{-1}$  at  $25^\circ\text{C}$ , which is in good agreement with the accepted literature value<sup>1</sup> for ultrapure water. The resistivity of the Milli-Q water was consistently around  $18 \text{ M}\Omega \text{ cm}$ .

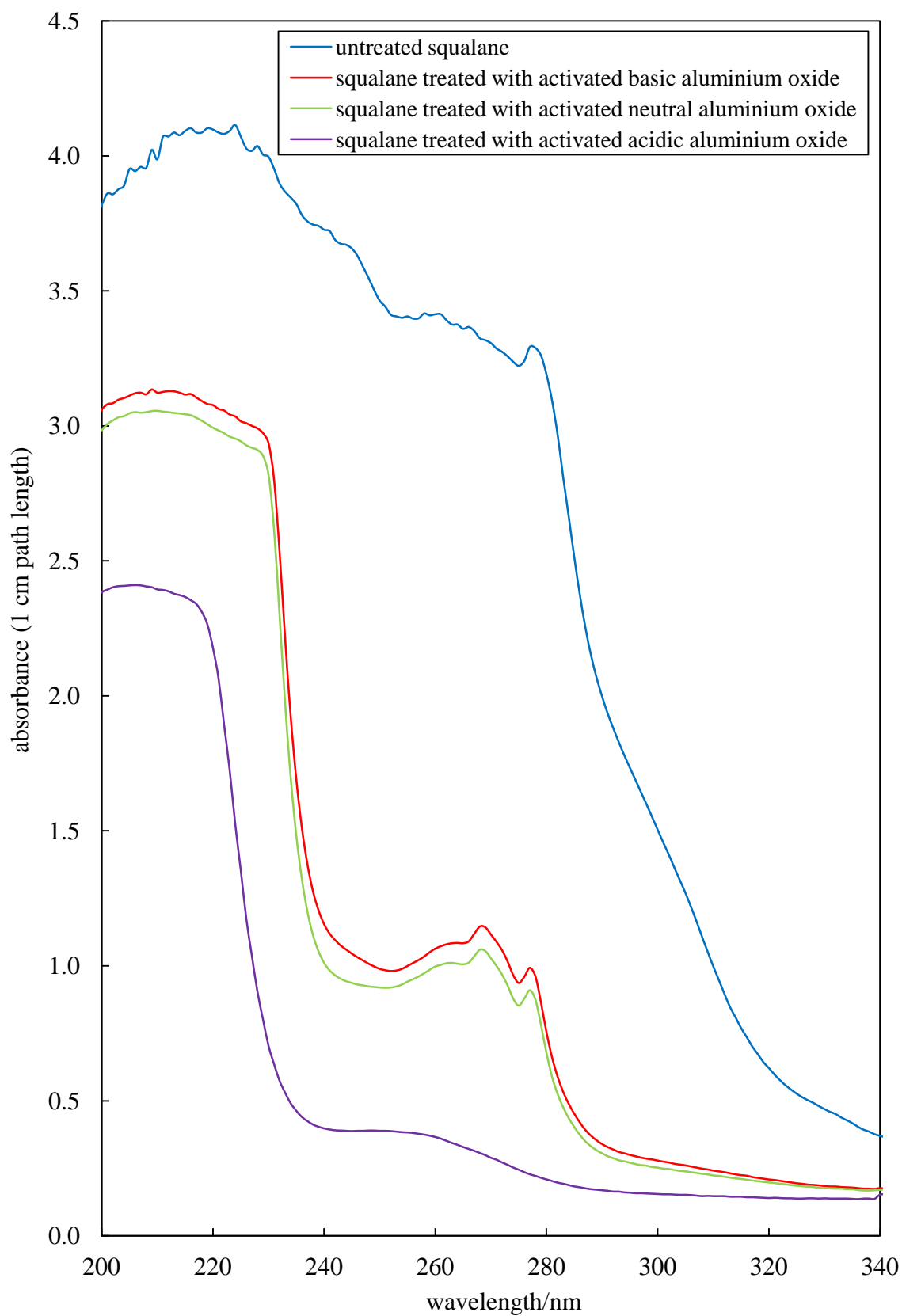
###### 2.1.1.2 Phosphate-buffered saline solution

Phosphate-buffered saline (PBS) solutions were prepared by dissolution of  $137 \text{ mM}$  NaCl,  $2.7 \text{ mM}$  KCl,  $10 \text{ mM}$   $\text{Na}_2\text{HPO}_4$  and  $2 \text{ mM}$   $\text{KH}_2\text{PO}_4$  in Milli-Q water. The produced PBS solutions had a pH of 7.3 at  $25^\circ\text{C}$ . All inorganic salts used to prepare the PBS solution were used as supplied (see Table 2.4).

###### 2.1.1.3 Squalane

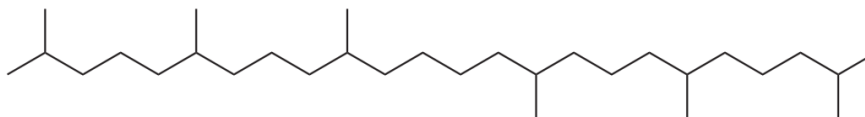
Squalane ( $> 99\%$  purity, Sigma-Aldrich) (chemical structure shown in Figure 2.2) was purified prior to use by column chromatography through activated acidic aluminium oxide. This was repeated numerous times in order to remove polar impurities. The purity of the squalane was analysed after passing through each column using ultraviolet-visible (UV-vis) spectrophotometry, until the optimum purity had been reached. The influence of purification by column chromatography, through various types of activated aluminium oxide, upon the UV absorption spectra of squalane is illustrated in Figure 2.1.

**Figure 2.1.** UV absorption spectra before (blue line) and after purification of 50 ml squalane, by column chromatography, through 50 g of basic (red), neutral (green) and acidic (purple) activated aluminium oxide.



The UV absorbance is shown to drastically reduce from approximately 3.5 absorbance units to less than 0.5 absorbance units across the wavelength of 240-280 nm, indicating the importance of this purification method.

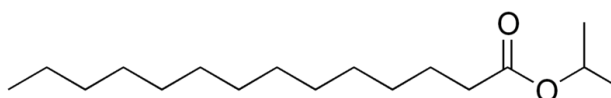
**Figure 2.2.** Chemical structure of squalane ( $C_{30}H_{62}$ ).



#### 2.1.1.4 Isopropyl myristate

Isopropyl myristate (IPM) (> 98% purity, Sigma-Aldrich) was purified prior to use by column chromatography through activated neutral aluminium oxide 3 times in order to remove polar impurities. The chemical structure of IPM is shown in Figure 2.3.

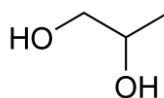
**Figure 2.3.** Chemical structure of IPM ( $C_{17}H_{34}O_2$ ).



#### 2.1.1.5 Propane-1,2-diol

Propane-1,2-diol (also called propylene glycol (PG)) ( $\geq 99.5\%$  purity, Sigma-Aldrich) was used as received. The chemical structure of PG is shown in Figure 2.4.

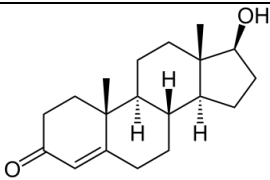
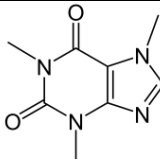
**Figure 2.4.** Chemical structure of PG ( $C_3H_8O_2$ ).



### 2.1.2 Permeants

Table 2.1 summarises the permeant molecules used in this research with their structures, suppliers and purities.

**Table 2.1.** Structure, supplier and purity of the permeants used in the membrane permeation studies.

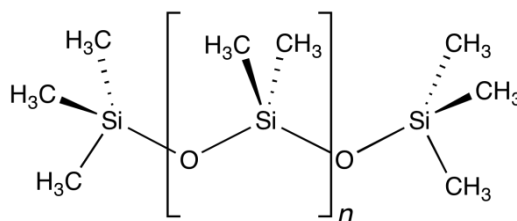
Permeant	Structure	Supplier	Purity/%
Testosterone		TCI Europa	98
Caffeine		Sigma-Aldrich	> 99

### 2.1.3 Membranes

#### 2.1.3.1 Polydimethylsiloxane

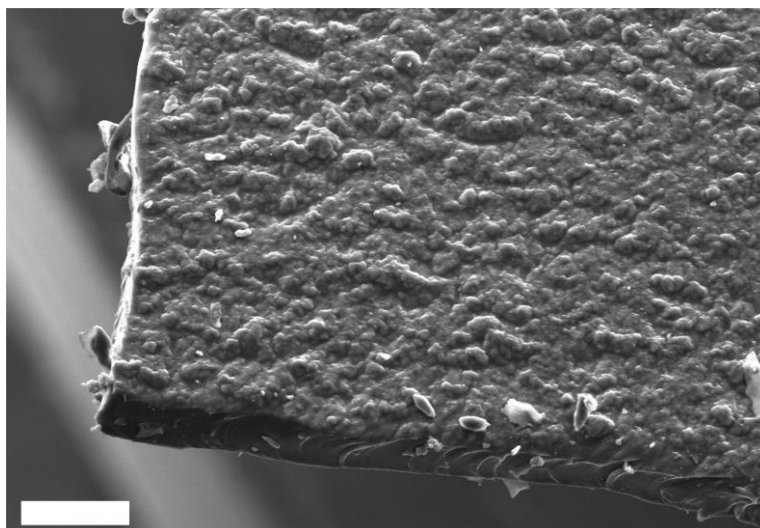
Polydimethylsiloxane (PDMS) elastomeric membranes (model 7-4107) were a gift from Dow Corning, Europe and had a mean thickness of  $81 \pm 15$   $\mu\text{m}$ . The membranes were pre-soaked in PBS for 24 hours before being cut to size with a clean, sharp scalpel prior to use. Following soaking experiments for 24 hours, it was found that the PDMS membrane did not swell significantly in either area or thickness when submersed in PBS, squalane or PG solvents. However, PDMS was shown to swell by approximately 20% in both area and thickness after 24 hours submersion in IPM, as discussed in Chapter 3. Figure 2.5 illustrates the chemical structure of PDMS.

**Figure 2.5.** Chemical structure of PDMS.



The advancing and receding three-phase contact angles (measured using a Krüss Drop Shape Analyser 10) on the PDMS membrane of water drops in air were  $117^\circ$  and  $92^\circ$  respectively, whilst IPM drops in air spread on the membrane surface (i.e. the equilibrium contact angle was  $< 3^\circ$ ) illustrating the hydrophobic nature of the membrane. Figure 2.6 shows a scanning electron microscope (SEM) image of the PDMS membrane coated with a 30 nm thick, thermally evaporated backing film of titanium, which acts as an electron beam heat sink to protect the membrane structure during analysis. Increased magnification resulted in damage to the structure of the membrane. The surface roughness and depth uniformity is illustrated.

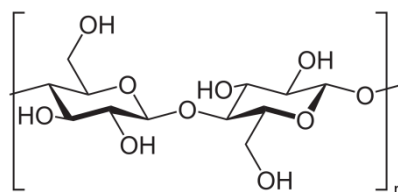
**Figure 2.6.** SEM image of a dry PDMS membrane coated with a 30 nm thick, thermally evaporated backing film of titanium. Scale bar = 100  $\mu\text{m}$ .



#### 2.1.3.2 Cellulose

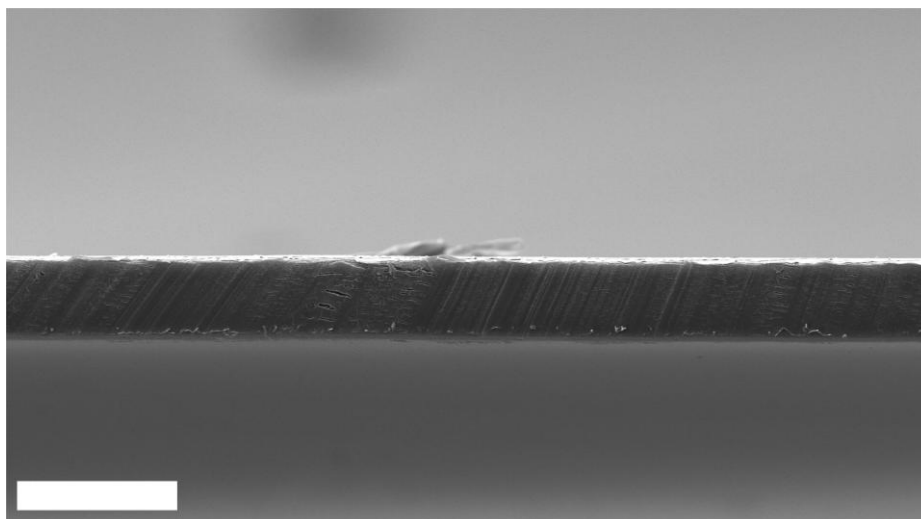
Cellulose membranes were dialysis membranes (12-14 kD molecular weight cut-off, Medicell International Ltd.) and had a dry membrane thickness of 23  $\mu\text{m}$ . The membranes were pre-soaked in PBS for 24 hours before being cut to size with a clean, sharp scalpel prior to use. Following soaking experiments for 24 hours, it was found that the cellulose membrane did not swell significantly in either area or thickness when submersed in squalane, IPM or PG solvents. However, submersing cellulose in PBS caused the membrane to swell in thickness from 23 to 48  $\mu\text{m}$  but produced no change in the membranes area. Figure 2.7 illustrates the chemical structure of a cellulose monomer unit.

**Figure 2.7.** Chemical structure of cellulose.



In an attempt to measure the three-phase contact angle of a water drop on the PBS soaked cellulose membrane, the droplet immediately spread across the surface producing an equilibrium contact angle of  $< 1^\circ$ . The advancing and receding three-phase contact angles of squalane drops in air on the PBS soaked cellulose membrane were  $31^\circ$  and  $27^\circ$  respectively, illustrating the hydrophilic nature of the membrane. Figure 2.8 shows an SEM image of a cross-section of a dry cellulose membrane which is also coated with a 30 nm thick, thermally evaporated backing film of titanium to protect the membrane. Increased magnification beyond that illustrated resulted in damage to the structure of the membrane. The surface smoothness and depth uniformity is illustrated.

**Figure 2.8.** SEM image of a cross-section of a dry cellulose membrane coated with a 30 nm thick, thermally evaporated backing film of titanium. Scale bar = 40  $\mu\text{m}$ .



#### 2.1.4 Oils and polyols

As will be seen in Chapter 4 several oils and polyols are used for the preparation of emulsions which do not serve as solvents in the membrane permeation studies. Table 2.2 summarises these liquids with their supplier and purity. All oils were purified prior



to use by column chromatography through activated neutral aluminium oxide 3 times in order to remove polar impurities. All polyols were used as received.

**Table 2.2.** Supplier and purity of the additional oils and polyols used in the preparation of emulsions.

Liquid	Supplier	Purity/%
Paraffin Liquid (grade 783LP)	Total	> 98
DC 200 PDMS oil (50 cSt)	Dow Corning	-
Miglyol 812 (a medium chain triglyceride)	Sasol (batch 110711)	-
Butane-1,2-diol	Sigma-Aldrich	≥ 98
Pentane-1,5-diol	Sigma-Aldrich	≥ 97
Propan-1-ol	BDH	≥ 99.5
Glycerol	Sigma-Aldrich	≥ 99
Polyethylene glycol (PEG 300) (molecular weight = 285-315 g mol <sup>-1</sup> )	Sigma-Aldrich	-

#### 2.1.5 Fumed silica particles

Fumed silica particles with different hydrophobicities were kindly provided by Wacker-Chemie in Burghausen, Germany. Raw silica particles were produced by hydrolysis of silicon tetrachloride in an oxygen-hydrogen flame at a high temperature.<sup>2</sup>



In the flame process at 1200°C, particles of SiO<sub>2</sub> collide and coalesce to give smooth and approximately spherical primary particles of 10-30 nm in diameter. These primary particles collide and may fuse at lower temperatures to form stable aggregates of 100 – 500 nm in diameter. Fumed silica particles are considered hydrophilic due to silanol groups on the particle surface<sup>3</sup> and possess a surface area of 200 m<sup>2</sup> g<sup>-1</sup>. Hydrophobic silica was prepared by reacting hydrophilic silica with dichlorodimethylsilane (DCDMS) in the presence of molar amounts of water, followed by drying at 300°C for 1 hour.<sup>4</sup> This reaction results in the formation of dimethylsiloxy

groups on the particle surface, which cover the silica surface like a monolayer, without significantly altering the particle diameter<sup>3</sup> (see Figure 2.9). Table 2.3 shows the codename and silanol content of all the silica particles used in this study. The silanol content on the silica surface was determined by acid-base titration with sodium hydroxide and relative contents of silanol groups after surface modification were determined by dividing the silanol content of the modified silica by that of the unmodified silica (100% SiOH). The content of silanol groups on particle surfaces decreases during silanisation, therefore the particle surface becomes more hydrophobic.<sup>5</sup> Further DCDMS-modification of silica particles to an extent below 14% SiOH is problematic due to steric hindrance between neighbouring silane groups.

**Figure 2.9.** Envisaged structure of a hydrophilic (100% SiOH) primary silica particle (left) and a hydrophobic DCDMS-modified primary silica particle (right).

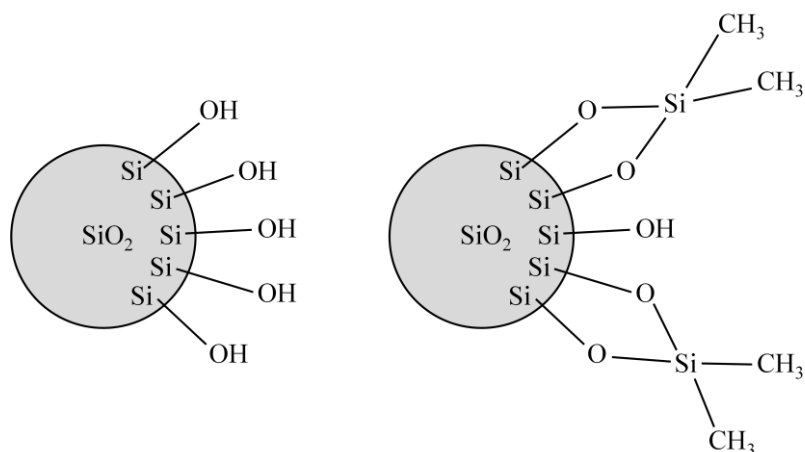
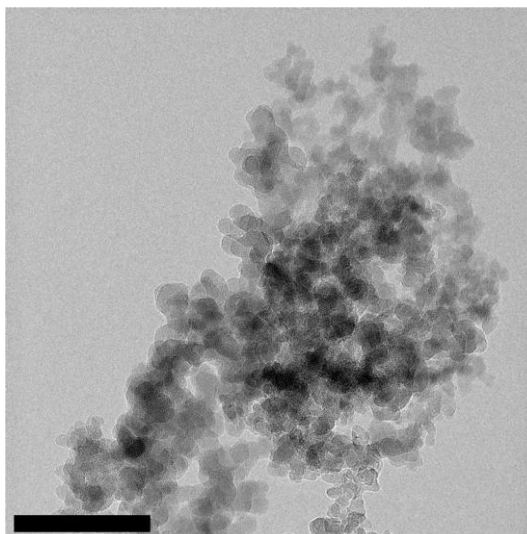


**Table 2.3.** Codename and silanol content of the fumed silica particles used in this study.

<b>Codename</b>	<b>% SiOH</b>
HDK N20	100
SLM 4330002/68-18	88
SLM 433002/160	87
SLM 433002-MM038/3a-d	80
SLM 433002-MM038/1a-d	75
SLM433002/135	71
SLM433002/150	67
SLM 433003-43/1	65
SLM 4330002/68-19	62
SLM433002-MM038/2a-d	61
SLM 433002/140-1a/b	58
SLM433002/239	53
HDK H30	47
SLM4330002/68-20	42
SLM 433002/121-2	37
SLM4330002/68-21	32
SLM 433002/121-1	25
HDK H18	20
SLM 433002/MM004	14

Figure 2.10 shows a transmission electron microscope (TEM) image of a dispersion of 20% SiOH silica particles arrested within a cured resin to prevent extensive particle aggregation. The observed aggregation of primary silica particles occurs due to the formation of hydrogen bonds between silanol groups at the particle surface.

**Figure 2.10.** TEM image of a dispersion of 20% SiOH silica particles arrested within a resin cured within 3 minutes of initially dispersing the particles. Scale bar = 100 nm.



#### 2.1.6 Other materials

Within specific sections of this work, materials other than those already detailed have been used. These materials along with their supplier and purity are listed in Table 2.4.

**Table 2.4.** Suppliers and purities of additional materials used within this study.

Material	Supplier	Purity
Sodium chloride	BDH	> 99.5%
Potassium chloride	BDH	> 99.5%
Disodium hydrogen orthophosphate	Fischer Scientific	> 99%
Potassium dihydrogen orthophosphate	BDH	> 99%
Activated aluminium oxide (basic, neutral and acidic)	Merck	> 99.5%
n-Decane	Sigma-Aldrich	99%
Calofort U (precipitated calcium carbonate)	Speciality Minerals Inc.	-
Calofort SV (precipitated calcium carbonate)	Speciality Minerals Inc.	-

## 2.2 Methods

### 2.2.1 *Calibration of UV-vis spectrophotometer for the determination of permeant concentration within a liquid solvent*

A Unicam UV3 UV-vis spectrophotometer thermostated at 32°C was used throughout this study to determine the permeant concentration in numerous different solvents. This analysis primarily required the production of an absorbance versus permeant concentration calibration graph for each combination of permeant/solvent. To produce these calibration graphs, a sub-saturated stock solution of known permeant concentration in the required solvent was first prepared and then analysed spectrophotometrically. The instrument was configured such that the background absorbance of both the cuvette and the chosen solvent were subtracted from the overall absorption spectra producing accurate and reproducible data corresponding to the absorbance from only the permeant under analysis. The absorption spectra of the prepared stock solution was initially analysed over an exhaustive wavelength range of 190-1100 nm to highlight which wavelength of light gave the largest absorbance signal per unit concentration (i.e. the  $\lambda_{\text{max}}$  wavelength was determined). The  $\lambda_{\text{max}}$  wavelengths required for the analysis of testosterone and caffeine varied slightly from solvent to solvent, as expected, but were typically 251 nm and 273 nm respectively. Aliquots of the prepared stock solution were then diluted to produce several more solutions of known, lower permeant concentration. Each of these dilutions were then analysed spectrophotometrically at the corresponding  $\lambda_{\text{max}}$  wavelength until the concentration of the permeant was lower than the detectable capabilities of the instrument. The recorded absorbance at the corresponding  $\lambda_{\text{max}}$  wavelength was then plotted against the known permeant concentration to produce the required calibration graphs. All absorbance versus permeant concentration calibration graphs used in this study are given in Appendix I. The analysis of these calibration graphs reveals information regarding the ideality of the permeant in solvent solutions, as discussed later.

### 2.2.2 *Permeant in solvent solubility measurements*

The solubilities of testosterone and caffeine in the respective solvents were measured at 32°C. To measure these parameters, an excess of the permeant was added to a known volume of a chosen solvent and the mixture was stirred for 48 hours at

32°C. The permeant-saturated supernatant liquid was then extracted from the mixture and diluted to be within the concentration range of the respective calibration graph. The analysis of the UV absorption spectra of the dilute supernatant then allowed, in conjunction with the applied dilution factor, for the accurate determination of the concentration of the permeant within the saturated solvent at 32°C.

### 2.2.3 *Measurement of solvent/solvent and solvent/membrane equilibrium permeant partition coefficients*

The equilibrium permeant partition coefficients between two immiscible liquids were measured by contacting a known volume (typically 5.0 ml) of solution of the required permeant concentration in the aqueous (for caffeine) or oil phase (for testosterone) with a known volume of the appropriate second phase. The mixture was then stirred at 1000 rpm at 32°C for either 1 or 2 weeks in a sealed glass vessel. Following this equilibration, the oil and aqueous layers were allowed to separate, samples of both phases were withdrawn and the equilibrium permeant concentration was determined by UV-vis spectrophotometry. Control measurements were made using samples with no permeant in order to correct the measured UV absorbance values for small (typically 10% or less) errors due to the presence of trace UV-absorbing impurities arising from the oil solvents. The concentration values enabled the calculation of the partition coefficient, equal to the ratio of equilibrium permeant concentrations in the two phases. All partition coefficients are denoted using the consistent nomenclature that  $K_{a-b} = C_a/C_b$ . It was found that either 1 or 2 weeks equilibration time yielded identical permeant partition coefficient values.

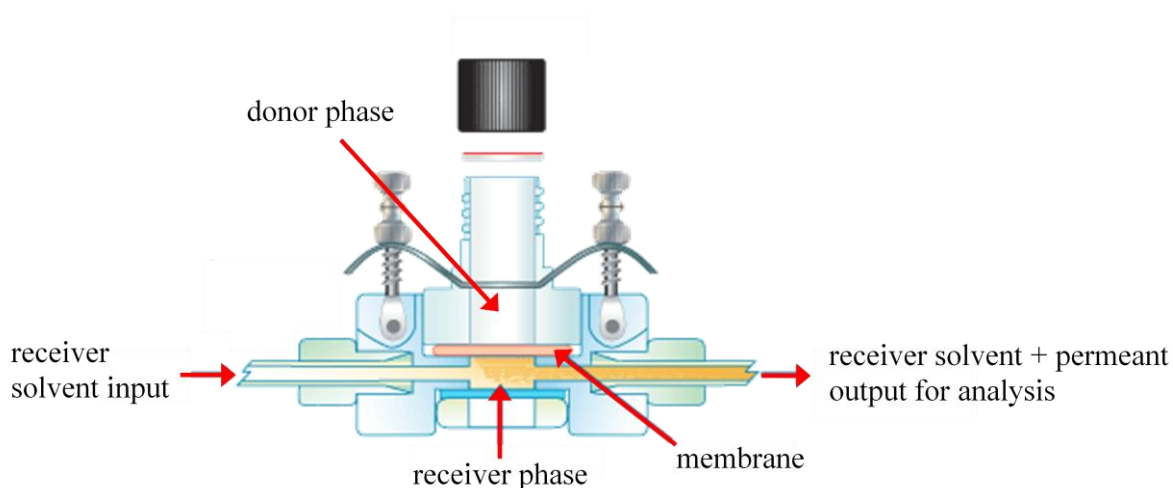
The equilibrium partition coefficients of the permeants between either aqueous or oil solutions and the two membranes (PDMS and cellulose) were measured by the equilibration of a known volume of permeant solution of known initial concentration with a known volume of the membrane at 32°C. Following equilibration, the equilibrium permeant concentration in the solution phase (decreased by loss of permeant to the membrane) was determined spectrophotometrically and the result was used to calculate the respective permeant partition coefficient. The value of the permeant partition coefficients measured in this way did not change with equilibration times varying from 1 day to 5 weeks. Each final value of the permeant partition coefficient was the mean of at least 5 independent measurements. Control

measurements with systems containing no permeant were again used to correct UV absorbance values for trace UV-absorbing impurities leached from the membranes. This correction was less than 5% in all cases.

#### 2.2.4 Membrane permeation measurements

The permeation of testosterone and caffeine from a donor compartment through PDMS and cellulose membranes to a flow-through receiver compartment was monitored via the use of an in-line permeation cell supplied by PermeGear, Inc. (model #1K001-15-VD). The schematic diagram of the cells cross-section, shown in Figure 2.11, illustrates the membrane trapped between the donor and receiver compartments. In performing a membrane permeation study, the donor compartment is filled with a topical formulation of known initial permeant concentration and the release of the permeant through the membrane to the receiver compartment is monitored. The cell has a circular membrane window of diameter 15 mm, exposed membrane area of 1.76 cm<sup>2</sup> and an upper, fixed volume (2.18 ml) donor compartment which is sealable with a screw-cap septum. The donor compartment of the permeation cell was magnetically stirred during the permeation experiments with a stirrer bar of dimensions 12.5 x 3.5 mm rotating at 5000 rpm (unless stated otherwise). The cell is constructed from chemically inert polychlorotrifluoroethylene (PCTFE) and was thermostated at 32°C to simulate the temperature of the surface of human skin.

**Figure 2.11.** Cross-section of the in-line permeation cell supplied by PermeGear Inc. used in the membrane permeation studies presented here. Image taken from the manufacturer's website.<sup>6</sup>



The receiver compartment of the permeation cell can be configured to incorporate either a closed-loop (fixed volume) or an open (variable volume) receiver configuration, as illustrated in Figure 2.12. In a closed-loop receiver configuration the receiver solvent volume is constant and is continuously pumped around a series of instruments, which analyse the change in permeant concentration within the receiver phase over time. In an open receiver configuration, the volume of the receiver solvent is variable because a continuous stream of fresh solvent flows from a reservoir supply beneath the membrane, through an analytical detector to determine the concentration of permeant present in the receiver phase and into a waste collection chamber. The total volume of the receiver phase in an open receiver configuration is therefore dependent on the extent of time the permeation experiment is conducted and the volumetric flow rate of the receiver phase. All permeation experiments incorporating a closed-loop receiver configuration were conducted with a receiver phase flow rate of  $3 \text{ ml min}^{-1}$  whereas permeation experiments incorporating an open receiver phase configuration were conducted at various different receiver phase flow rates as discussed in Chapter 3.

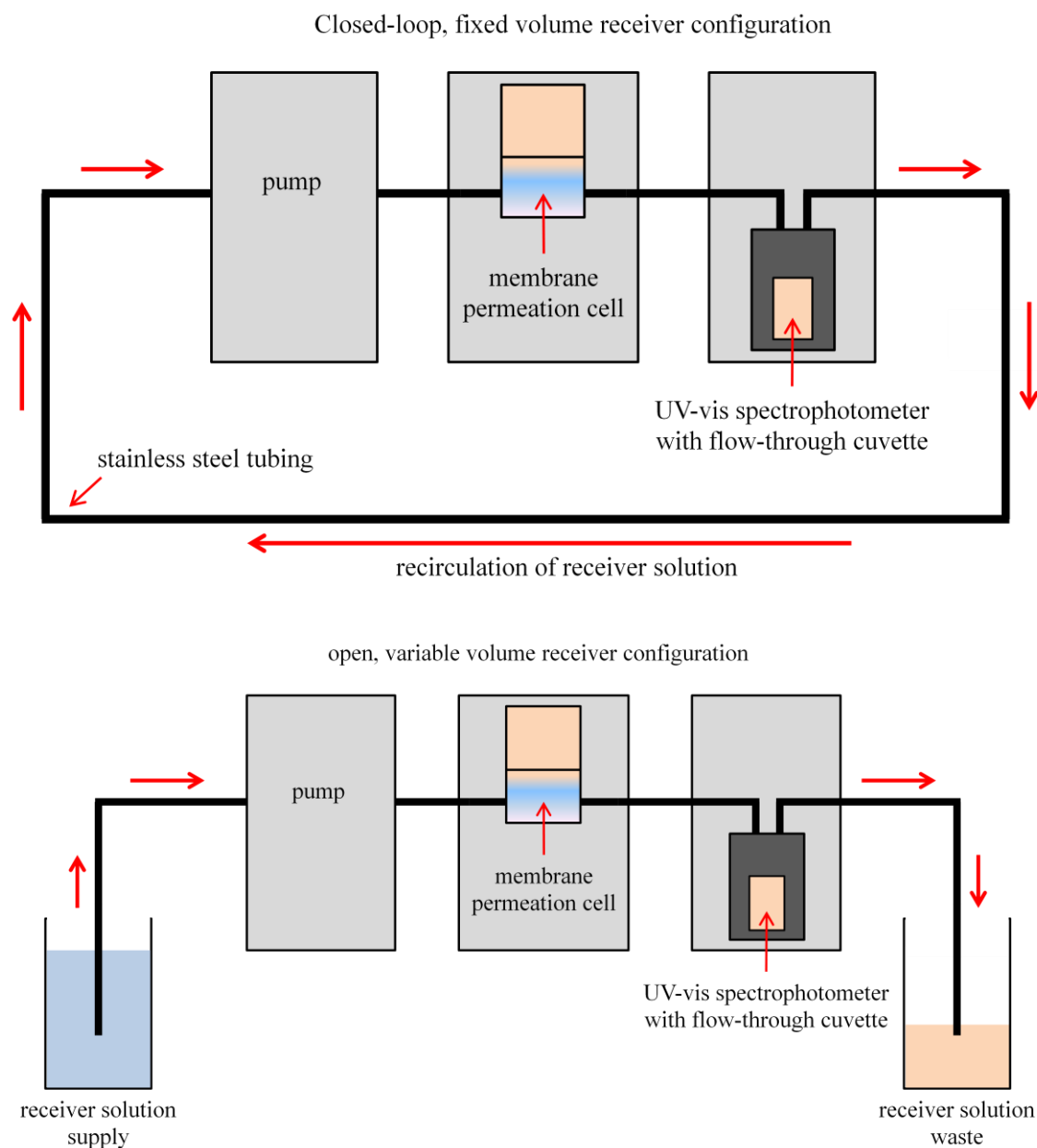
Pumping of the receiver compartment solution was achieved using a Spectra System P1500 Isocratic Liquid Chromatography Pump, capable of flow rates between  $0.01 - 10 \text{ ml min}^{-1}$ , which operates a dual sapphire piston mechanism to produce a pulse-free flow. The permeant concentration in the receiver compartment was monitored by pumping the receiver solution through a flow-through quartz cuvette ( $1 \text{ ml}$ , closed-loop receiver configuration or  $0.08 \text{ ml}$ , open receiver configuration internal solution volume) with a  $10 \text{ mm}$  path length mounted within the temperature controlled Unicam UV3 UV-vis Spectrophotometer also maintained at  $32^\circ\text{C}$ . The permeant concentration in the receiver phase was derived from the solution absorbance values measured at the corresponding  $\lambda_{\text{max}}$  wavelengths via reference to the calibration graphs. The receiver solution UV-absorbance values were captured automatically at  $20 \text{ second}$  intervals over permeation runs lasting up to  $80 \text{ hours}$ .

The flow circuit components were connected using  $0.762 \text{ mm}$  internal diameter stainless steel tubing plus push-fit, polytetrafluoroethylene (PTFE) tubing connections to the inlet and outlet of the UV-Vis flow-through cuvette. Tubing connection lengths were kept to a minimum and were insulated to optimise thermostating. For the open, variable volume receiver configuration, it was necessary to incorporate a  $75 \text{ psi}$  back pressure regulator between the pump and the permeation cell to ensure proper



operation of the pump valves. In addition, a coil of 0.762 mm internal diameter stainless steel tubing was added to the flow line exit into the receiver waste container in order to achieve a low back pressure within the permeation and UV-Vis cells and thereby minimise problems with gas bubble formation.

**Figure 2.12.** Schematic diagrams of the closed-loop, fixed volume (upper) and open, variable volume (lower) receiver phase flow configurations used in this study.



### 2.2.5 *Preparation of fumed silica particle dispersions*

Dispersions of silica particles were prepared using an ultrasonic processor Vibra-cell (Sonics & Materials). A known amount of particles was dispersed in either aqueous or oil solvent by operating the processor with a probe tip of diameter 3 mm at 20 kHz and up to 10 W for 2 minutes. The vessel containing the dispersion was kept cool during sonication by immersing it in an ice bath.

### 2.2.6 *Preparation of particle-stabilised emulsions*

Particle-stabilised emulsions were prepared via homogenisation of 5 ml of oil, 5 ml of polar phase and the required mass of fumed silica particles in glass vessels (diameter 25 mm, length 75 mm) thermostated at 25°C. Emulsions containing a required concentration of permeant were prepared via the dissolution of the required mass of permeant in the respective phase prior to emulsification (i.e. testosterone was dissolved in the oil phase and caffeine was dissolved in the polar liquid phase). For the purpose of emulsion characterisation, the polar phase was doped with 4 mM NaCl to increase the conductivity of the liquid. Emulsions were prepared using the powdered particle method. In this method, fumed silica particles were added as a powder on top of the most dense polar liquid phase followed by the least dense oil phase. This method removes the possibility that the initial location of the particles may influence the subsequent emulsion properties and so particles dictate the emulsion behaviour due solely to their inherent wettability. Emulsification was achieved with an IKA Ultra-Turrax homogeniser fitted with a dispersing head of diameter 18 mm operating at 13,000 rpm for 5 minutes.

### 2.2.7 *Characterisation of particle-stabilised emulsions*

#### 2.2.7.1 Drop test

The continuous phase of an emulsion was inferred by observing whether a drop of emulsion dispersed or remained when added to either the pure oil or pure water.<sup>7</sup> Water continuous emulsions would disperse in water and remain as drops in oil, whereas oil continuous emulsions would remain as drops in water but disperse in oil.

#### 2.2.7.2 Conductivity

A Jenway 4310 conductivity meter using Pt/Pt black electrodes was used to determine the conductivity of emulsions. Conductivity measurements were made immediately after emulsification. Low conductivity values indicated continuous emulsions whereas high conductivity values were associated with polar liquid continuous emulsions doped with 4 mM NaCl.<sup>7</sup>

#### 2.2.7.3 Optical microscopy

Emulsions were observed with optical microscopy using an Olympus BX51 microscope. The emulsion was observed raw or diluted in its continuous phase in a dimple cell microscope slide covered by a cover slip. Digital micrographs were taken with a 12-bit Olympus DP70 camera and edited using Adobe Photoshop CS3 to add a scale bar. The mean droplet diameter of an emulsion was calculated from at least fifty individual drops on digital micrographs taken within five minutes of emulsion preparation. Optical microscopy was also used to distinguish between simple oil-in-polar liquid or polar liquid-in-oil emulsions.

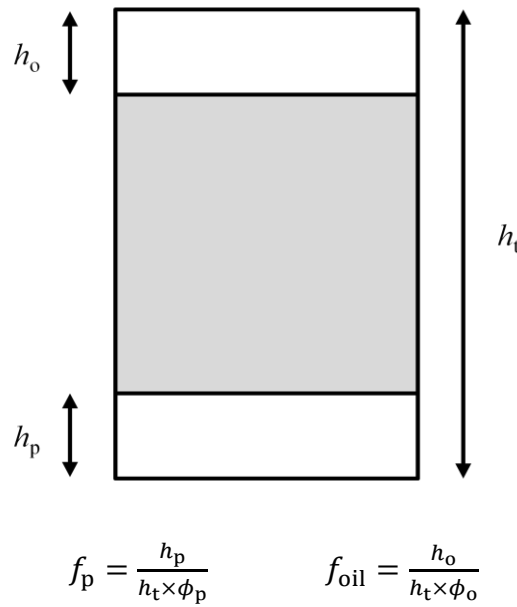
#### 2.2.7.4 Stability

Emulsions were stored at room temperature in the vessels used during homogenisation, these being foil lined screw-capped glass sample tubes of inner diameter 25 mm and length 75 mm. The stability of polar liquid continuous emulsions to creaming and coalescence was assessed by monitoring the change with time of the polar liquid-emulsion boundary and oil-emulsion interface, respectively. For oil continuous emulsions, the stability to sedimentation and coalescence was assessed by

monitoring the change with time of the oil-emulsion boundary and polar liquid-emulsion interface, respectively.

Figure 2.13 depicts how the fraction of polar liquid ( $f_p$ ) and oil ( $f_{oil}$ ) resolved from an emulsion are determined from the height of polar liquid resolved ( $h_p$ ), height of oil resolved ( $h_o$ ), initial volume fraction of polar liquid ( $\phi_p$ ) and oil ( $\phi_o$ ) and the total height of emulsion plus polar liquid and oil resolved ( $h_t$ ).

**Figure 2.13.** Determination of water and oil resolved from an emulsion.



### 2.3 References

1. CRC Handbook of Chemistry and Physics, CRC Press, Boca Raton, 89<sup>th</sup> Ed., 2008.
2. Wacker HDK Fumed Silica Product Information, Wacker-Chemie, (October 2000).
3. H. Barthel, *Colloids Surf. A.*, **101**, 217 (1995).
4. R.K. Iler, *The Chemistry of Silica*, John Wiley & Sons, New York, (1979).
5. B.P. Binks and J.H. Clint, *Langmuir*, **18**, 1270 (2002).
6. See, <http://www.permeagear.com/inline.htm> (checked for access on 16<sup>th</sup> January 2013).
7. I.D. Morrison and S. Ross, *Colloidal Dispersions: Suspensions, Emulsions and Foams*, Wiley-Interscience, New York, (2002).

## CHAPTER 3

### MEMBRANE PERMEATION FROM DONOR SOLUTIONS

#### 3.1 Introduction

The permeation of a species from a donor to a receiver compartment across a membrane is important in many applications. The primary interest here is in the delivery of pharmaceutical actives across membrane barriers such as the skin. The aim of the work presented in this chapter is to understand how changing the donor compartment solvent can affect both the rate and extent of membrane permeation of a chosen permeant to a receiver compartment containing an aqueous electrolyte solution. The results discussed within this chapter aim to explain (i) all possible origins of the observed donor solvent effects, (ii) how to resolve which donor solvent effect or effects may be operating in a particular system and (iii) how the donor solvent effects depend on the natures of both the permeating species and the membrane. The work discussed in this chapter addresses these points using a combination of theory and experiment.

The overall problem is tackled in several steps. Firstly, a theoretical model is developed based on the assumption that the rate-determining step of the overall mass transport of the permeant from donor to receiver compartments is diffusion across the membrane, i.e. that all other steps in the overall process, such as diffusion within the donor or receiver compartment solutions and entry or exit of the membrane are relatively fast. This theory enables quantitative prediction of how the donor solvent affects both the extent and rate of permeation for all combinations of permeant and membrane species for systems and conditions for which the set of model assumptions are valid. Secondly, the permeation kinetics are measured for all combinations of hydrophilic and hydrophobic donor solvents (aqueous solution and squalane), hydrophilic and hydrophobic permeants (caffeine and testosterone) and hydrophilic and hydrophobic membranes (cellulose and PDMS). Thirdly, using ancillary measurements of partition coefficients, the experimental permeation rate data are compared with the predictions of the theoretical model. The model comparisons enable distinction between experimental systems which obey the model assumptions and those which do not. In turn, this enables a rigorous resolution of which of the different possible donor solvent effects are operating in the different experimental systems.

### 3.2 Theoretical modelling of membrane permeation from donor solutions

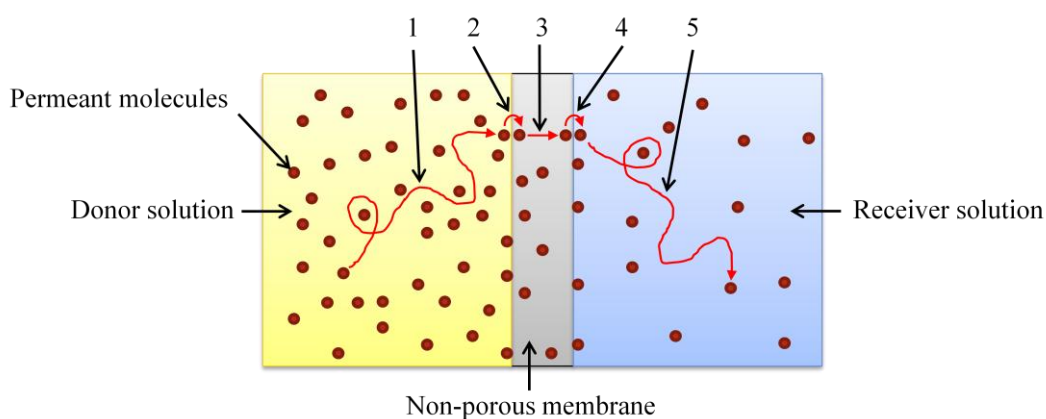
The derivation of a theoretical model to describe the transport of a permeant from a stirred donor solution, through a membrane to a recirculating receiver solution in the closed-loop experimental configuration as described in Chapter 2, firstly requires the proposition of assumptions. The validity or otherwise of these assumptions for particular experimental conditions must, of course, be questioned and tested for all comparisons with experiments.

The envisaged mechanism for the transport of a permeant from a donor solution, through a non-porous membrane, into a receiver solution is described by five key steps. These steps are:

1. Permeant diffusion from within the bulk donor solution to the membrane interface
2. Permeant partitioning from the donor solution to the outermost layer of the membrane
3. Permeant diffusion across the membrane
4. Permeant partitioning from the outermost layer of the membrane to the receiver solution
5. Permeant diffusion within the bulk receiver solution

Figure 3.1 schematically illustrates these five key steps.

**Figure 3.1.** A schematic representation of the five key steps describing the transport of a permeant from a donor solution, through a non-porous membrane, into a receiver solution.



### 3.2.1 *Theoretical model assumptions*

In order to establish a basic theoretical frame work, the following assumptions are made:

- I. The rate limiting step of the entire membrane permeation process is assumed to be diffusion of the permeating species across the membrane (i.e. step 3 in Figure 3.1). Hence, all other mass transfer and partitioning steps within the bulk donor and receiver compartments and transfer across the solution-membrane interfaces are relatively fast (i.e. steps 1,2,4 and 5 in Figure 3.1).
- II. The lag time required to establish a steady-state mass transfer rate is negligibly small compared with the overall timescale of the permeation.
- III. The diffusion of the permeant in the membrane follows Fick's Laws. Hence, it is assumed that the membrane is uniform and that the diffusion coefficient has a fixed value which is independent of the permeant concentration in the membrane.
- IV. Only the single permeant species under consideration permeates across the membrane, i.e. the donor and receiver compartment solvents do not cross the membrane. If solvent permeation was to simultaneously occur, then it would cause changes in the partition coefficients of the permeant to the membrane, as a function of time as the donor and receiver phase compositions change throughout.
- V. The theory is restricted to uncharged permeant species and it is assumed that the permeant solutions in the donor, receiver and membrane volumes behave ideally, i.e. that concentrations can be substituted for activities in equations for equilibrium partition coefficients.

### 3.2.2 *Derivation of the theoretical model for membrane permeation into the closed-loop, fixed volume receiver compartment*

For the experimental permeation measurements described in this chapter, a permeant solution of initial concentration  $C_{\text{don},0}$  is loaded into the donor compartment and the permeant concentration  $C_{\text{rec}}$  in the fixed-volume, recirculating receiver compartment is recorded over time, from its initial value of zero ( $C_{\text{rec},0}$ ) until the final, equilibrium value  $C_{\text{rec},\infty}$  is reached. To fit the experimental permeation runs, a theoretical expression is derived for the variation of  $C_{\text{rec}}$  with time  $t$  as follows. With



the first assumption listed previously, the local permeant concentrations in the membrane on the donor and receiver sides ( $C_{\text{mem,d}}$  and  $C_{\text{mem,r}}$  respectively) are maintained in local equilibrium with the concentrations  $C_{\text{don}}$  and  $C_{\text{rec}}$  and hence

$$C_{\text{mem,d}} = K_{\text{mem-don}} C_{\text{don}} \quad (3.1)$$

$$C_{\text{mem,r}} = K_{\text{mem-rec}} C_{\text{rec}} \quad (3.2)$$

For the purpose of this derivation, all partition coefficients are denoted using the consistent nomenclature that  $K_{\text{a-b}} = C_{\text{a}}/C_{\text{b}}$  where  $K_{\text{a-b}}$  is the partition coefficient of the permeant between phases a and b and  $C_{\text{a}}$  and  $C_{\text{b}}$  are the equilibrium permeant concentrations in phases a and b respectively. Hence,  $K_{\text{mem-don}}$  and  $K_{\text{mem-rec}}$  are the permeant partition coefficients between the membrane and the donor solution, and the membrane and the receiver solution respectively.

The ratio of donor and receiver concentrations ( $= C_{\text{don}}/C_{\text{rec}}$ ) is not maintained equal to the equilibrium permeant partition coefficient between the donor and receiver solutions ( $K_{\text{don-rec}}$ ) during a permeation run; the equilibrium value is only reached at long times when  $C_{\text{don}}$  and  $C_{\text{rec}}$  achieve their equilibrium values of  $C_{\text{don},\infty}$  and  $C_{\text{rec},\infty}$ .

For permeation times longer than the so-called “lag-time”, Fick’s second law predicts that a linear concentration gradient of permeant across the membrane is established and permeation under these conditions is denoted as “steady-state”. The steady-state permeant concentration gradient across the membrane ( $dC_{\text{mem}}/dx$ ) is therefore described by

$$\frac{dC_{\text{mem}}}{dx} = \frac{(C_{\text{mem,d}} - C_{\text{mem,r}})}{X} \quad (3.3)$$

where  $C_{\text{mem}}$  is the permeant concentration at depth  $x$  in the membrane and  $X$  is the total membrane thickness. The rate of change of permeant concentration in the receiver compartment ( $dC_{\text{rec}}/dt$ ) is related to the concentration gradient across the membrane according to Fick’s first law, such that

$$\frac{dC_{\text{rec}}}{dt} = \left( \frac{AD}{XV_{\text{rec}}} \right) (C_{\text{mem,d}} - C_{\text{mem,r}}) = \left( \frac{AD}{XV_{\text{rec}}} \right) (K_{\text{mem-don}} C_{\text{don}} - K_{\text{mem-rec}} C_{\text{rec}}) \quad (3.4)$$

where  $A$  is the surface area of the membrane exposed to the donor solution,  $D$  is the diffusion coefficient of the permeant in the membrane and  $V_{\text{rec}}$  is the volume of the receiver compartment. At any time during the permeation, the total amount of permeant in the whole system is distributed between the donor and receiver compartments and the membrane and consideration of the permeant mass balance therefore gives

$$C_{\text{don}} = \frac{(n_t - C_{\text{rec}} V_{\text{rec}} - C_{\text{mem}} V_{\text{mem}})}{V_{\text{don}}} \quad (3.5)$$

where  $n_t$  is the total number of moles of permeant,  $V_{\text{don}}$  and  $V_{\text{mem}}$  are the volumes of the donor compartment and the membrane and  $C_{\text{mem}}$  is the average concentration of permeant within the membrane. Under steady-state permeation conditions, the permeant concentration in the membrane varies linearly between  $C_{\text{mem,d}}$  and  $C_{\text{mem,r}}$  and hence  $C_{\text{mem}} = (C_{\text{mem,d}} + C_{\text{mem,r}})/2$ . Substituting for  $C_{\text{mem}}$  in equation 3.5, according to equations 3.1 and 3.2 gives, after some re-arrangement, the following expression for  $C_{\text{don}}$  in terms of  $C_{\text{rec}}$ .

$$C_{\text{don}} = \frac{n_t / V_{\text{don}}}{(1 + (K_{\text{mem-don}} V_{\text{mem}} / 2V_{\text{don}}))} - \frac{(V_{\text{rec}} / V_{\text{don}} + K_{\text{mem-rec}} V_{\text{mem}} / 2V_{\text{don}})}{(1 + (K_{\text{mem-don}} V_{\text{mem}} / 2V_{\text{don}}))} C_{\text{rec}} \quad (3.6)$$

Equation 3.6 can be expressed in the form  $C_{\text{don}} = Y - Z C_{\text{rec}}$  where  $Y$  is the first fraction term in equation 3.6 and  $Z$  is the multiplier term of  $C_{\text{rec}}$ . Substituting this expression for  $C_{\text{don}}$  into equation 3.4 yields

$$\frac{dC_{\text{rec}}}{dt} = \left\{ \frac{ADK_{\text{mem-don}}Y}{XV_{\text{rec}}} \right\} - \left\{ \frac{AD(K_{\text{mem-don}}Z + K_{\text{mem-rec}})}{XV_{\text{rec}}} \right\} C_{\text{rec}} \quad (3.7)$$

Integration of equation 3.7 gives

$$C_{\text{rec}} = C_{\text{rec},\infty} + (C_{\text{rec},0} - C_{\text{rec},\infty}) \exp(-kt) \quad (3.8)$$

where  $C_{\text{rec},0}$  and  $C_{\text{rec},\infty}$  are the initial and the equilibrium values of the permeant concentration in the receiver compartment respectively. From equation 3.8, it can be seen that  $C_{\text{rec}}$  is predicted to increase exponentially from  $C_{\text{rec},0}$  to  $C_{\text{rec},\infty}$  with a first-order permeation rate coefficient  $k$  (units:  $\text{s}^{-1}$ ). Experimental permeation plots of  $C_{\text{rec}}$

versus time are therefore fully characterised by two parameters:  $C_{\text{rec},\infty}$  and  $k$  which, in turn, are given by

$$C_{\text{rec},\infty} = \left\{ \frac{K_{\text{mem-don}} Y}{K_{\text{mem-don}} Z + K_{\text{mem-rec}}} \right\} \quad (3.9)$$

and

$$k = \left\{ \frac{AD(K_{\text{mem-don}} Z + K_{\text{mem-rec}})}{XV_{\text{rec}}} \right\} \quad (3.10)$$

The final equations reveal the key observable characteristics of experimental permeating systems for which the underpinning model assumptions are valid. These characteristics are:

- I. The variation of  $C_{\text{rec}}$  with time is predicted to follow an exponential curve.
- II. The value of the 1<sup>st</sup>-order permeation rate coefficient  $k$  is predicted to be independent of the initial permeant concentration in the donor compartment.
- III. The values of  $C_{\text{rec},\infty}$  and  $k$  are predicted to be independent of the donor stirring rate and the receiver compartment flow-through rate as long as these are sufficiently high to ensure that mass transport within either the donor or receiver compartments is not rate-determining, (i.e. the first assumption is justified).
- IV. The values of  $C_{\text{rec},\infty}$  and  $k$  are predicted to depend on the nature of the permeant, donor and receiver solvents and the membrane as expressed by the values of the membrane diffusion coefficient  $D$  and the two partition coefficients  $K_{\text{mem-don}}$  and  $K_{\text{mem-rec}}$ .
- V. The values of  $C_{\text{rec},\infty}$  and  $k$  are predicted to depend on the geometrical parameters of the permeation system, i.e.  $A$ ,  $V_{\text{don}}$ ,  $V_{\text{rec}}$  and  $V_{\text{mem}}$ .

### 3.2.3 Predicting the rate and extent of membrane permeation from donor solutions

Equations 3.8-3.10 enable the prediction of how the rate and extent of permeation from donor to receiver compartments depends on the chemical natures of the permeant, the donor and receiver solvents and the membrane. For the purposes of this prediction, in order to remove factors such as permeant concentration and the geometrical

parameters of the permeation system, let  $V_{\text{don}} = V_{\text{rec}}$  and  $V_{\text{mem}} = 0$ . The permeation rate coefficient is expressed as the dimensionless rate coefficient ( $kXV_{\text{rec}}/AD$ ) and the extent of permeation as the fraction of total permeant concentration which is extracted from the donor to the receiver compartment at equilibrium ( $C_{\text{rec},\infty}/C_{\text{don},0}$ ). The different combinations of hydrophilic/hydrophobic permeant, donor solvent and membrane can be represented in terms of hypothetical values of  $K_{\text{mem-don}}$  and  $K_{\text{mem-rec}}$  for each system as shown subsequently in Table 3.1. For this analysis, the partition coefficients have been taken to be either 40 (for a permeant partitioning from a low affinity environment to a high affinity environment, e.g. a hydrophobic permeant going from water to a hydrophobic membrane), 1 (for a permeant partitioning between two environments for which it has equal affinity, e.g. a hydrophilic permeant going from water to a hydrophilic membrane) or 1/40 (for partitioning from a high affinity environment to a low one, e.g. for a hydrophilic permeant going from water to a hydrophobic membrane). Using these hypothetical  $K$  values with equations 3.8-3.10 allows a simple means to visualise how the rate and extent of permeation are predicted to change with donor solvent for different permeant and membrane combinations. For the conditions set here ( $V_{\text{don}} = V_{\text{rec}}$  and  $V_{\text{mem}} = 0$ ), the factor  $Z$  reduces to 1, the factor  $Y$  reduces to  $C_{\text{don},0}$  and, from equation 3.9, the fraction of permeant extracted  $C_{\text{rec},\infty}/C_{\text{don},0}$  is equal to

$$\frac{C_{\text{rec},\infty}}{C_{\text{don},0}} = \left\{ \frac{K_{\text{mem-don}}}{K_{\text{mem-don}} + K_{\text{mem-rec}}} \right\} \quad (3.11)$$

Similarly, from equation 3.10, the dimensionless permeation rate coefficient reduces to

$$\frac{kXV_{\text{rec}}}{AD} = K_{\text{mem-don}} + K_{\text{mem-rec}} \quad (3.12)$$

**Table 3.1.** Calculated values of fraction of total permeant extracted from donor compartment and dimensionless permeation rate coefficient for hypothetical systems containing all combinations of hydrophilic and hydrophobic donor solvents, permeants and membranes. Values have been designated as “high” (colour coded red), “medium” (colour coded white) or “low” (colour coded yellow).

Donor solvent	Permeant	Membrane	$K_{\text{mem-don}}$	$K_{\text{mem-rec}}$	Fraction permeant extracted	Dimensionless permeation rate coefficient ( $kXV_{\text{rec}}/AD$ )
Water	Hydrophobic	Hydrophobic	High (40)	High (40)	Medium (0.5)	High (80)
Oil	Hydrophobic	Hydrophobic	Medium (1)	High (40)	Low (0.024)	High (41)
Water	Hydrophilic	Hydrophobic	Low (0.025)	Low (0.025)	Medium (0.5)	Low (0.05)
Oil	Hydrophilic	Hydrophobic	Medium (1)	Low (0.025)	High (0.98)	Medium (1)
Water	Hydrophobic	Hydrophilic	Medium (1)	Medium (1)	Medium (0.5)	Medium (2)
Oil	Hydrophobic	Hydrophilic	Low (0.025)	Medium (1)	Low (0.024)	Medium (1)
Water	Hydrophilic	Hydrophilic	Medium (1)	Medium (1)	Medium (0.5)	Medium (2)
Oil	Hydrophilic	Hydrophilic	High (40)	Medium (1)	High (0.98)	High (41)

As seen in Table 3.1, the calculated dimensionless permeation rate coefficients all lie within one of three ranges: high (41-80 for the  $K$  values taken here), medium (1-2) or low (0.05). The values of the equilibrium fraction of permeant extracted are similarly either high (0.98), medium (0.5) or low (0.024) depending on the ratio of  $K_{\text{mem-don}}$  and  $K_{\text{mem-rec}}$  which is equal to the overall partition coefficient  $K_{\text{rec-don}}$ .

Although the values of  $K_{\text{mem-don}}$  and  $K_{\text{mem-rec}}$  used here (either 40, 1 or 1/40) are, of course, only broadly representative of the relative hydrophilic/hydrophobic natures of different permeant, donor solvent and membrane systems, the comparison of Table 3.1 allows useful insight into how widely differing systems are expected to permeate. Some of the results summarised in Table 3.1 follow easily from intuitive considerations of the relative affinities of the permeant for the donor and receiver solvents and the membrane. However, a key general and less intuitive conclusion is that the permeation rate coefficient is proportional to the sum of the two partition coefficients ( $K_{\text{mem-don}} + K_{\text{mem-rec}}$ ), as seen in equation 3.12. It is this relationship which causes the permeation rate effects of switching between the same polar and apolar donor solvents to vary widely between different permeant/membrane combinations.

### 3.2.4 *Comparing the theoretical model with experimental permeation results*

The development of the theoretical framework based on the stated model assumptions enables the prediction and comparison of different, hypothetical system behaviours, as shown in Table 3.1. In the next step, it is determined (i) whether or not different real permeation systems obey the model predictions and (ii) how the rates and extents of permeation vary for widely differing systems. To this end, the permeation of systems containing all possible combinations of permeant (testosterone (hydrophobic) or caffeine (hydrophilic)), donor solvent (squalane (hydrophobic) or PBS (hydrophilic)) and membrane (PDMS (hydrophobic) or cellulose (hydrophilic)) have been investigated. For each system, the receiver phase was PBS. Analysis of the experimental permeation behaviour in terms of the model requires knowledge of the permeant partition coefficients relevant to each system as described subsequently.

#### 3.2.4.1 Permeant solubilities

Prior to describing the relevant permeant partition coefficients, the permeant solubilities in the respective phases are noted. At 32°C, the equilibrium solubilities of testosterone in water, PBS and squalane were measured to be 0.12, 0.098 and 0.81 mM respectively; the values for caffeine in water, PBS and squalane were 140, 122 and 0.48 mM respectively. Literature values for the solubilities of testosterone in water (0.11 mM at 31°C and 0.13 mM at 35°C) and of caffeine in water (133 mM at 30°C and 167 mM at 35°C) are in good agreement with these experimental values.<sup>1</sup>

### 3.2.4.2 Permeant partition coefficients

Fitting the plots of experimental measurements of  $C_{\text{rec}}$  as a function of time yields measured values of the rate coefficient  $k$  and  $C_{\text{rec},\infty}$ . Using equations 3.9 and 3.10 to interpret these values requires knowledge of the two partition coefficients  $K_{\text{mem-don}}$  and  $K_{\text{mem-rec}}$  for each different permeant/solvent/membrane system. Two aspects require some additional discussion here. Firstly, as explained in Chapter 2, the membrane/solvent partition coefficients are measured by equilibrating a permeant solution of known volume and initial concentration with a known membrane volume and deriving  $K$  from the measured depletion of permeant concentration from the solution to the membrane. However, this method is not accurate if the magnitude of  $K$  is such that there is no significant depletion of the permeant concentration in the solution by partitioning to the membrane. In these cases, the unknown value of  $K$  can be derived from measured values of two related partition coefficients. For example,  $K_{\text{PDMS-PBS}}$  for caffeine is not directly measureable since too small a fraction of the caffeine distributes to the membrane to produce a measureable depletion of caffeine in the PBS solution, even when the membrane:solution volume ratio is maximised. However, the value of  $K_{\text{PDMS-PBS}}$  can be calculated using measured values of  $K_{\text{PBS-squalane}}$  and  $K_{\text{PDMS-squalane}}$ , as shown below.

$$K_{\text{PDMS-PBS}} = \frac{C_{\text{PDMS}}}{C_{\text{PBS}}} = \frac{C_{\text{PDMS}}}{C_{\text{squalane}}} \frac{C_{\text{squalane}}}{C_{\text{PBS}}} = \frac{K_{\text{PDMS-squalane}}}{K_{\text{PBS-squalane}}} \quad (3.13)$$

Similar calculations are used to derive all partition coefficients which are not directly measureable. The second aspect to be considered is the effect of possible non-ideal solution behaviour on the partition coefficients. The true, concentration-independent value of a partition coefficient  $K_{\text{a-b}}$  is the equilibrium ratio of the solute activity in each phase ( $= a_{\text{a}}/a_{\text{b}}$ ). The activities are then equal to the product of the activity coefficient  $\gamma$  and the concentration as shown below.

$$K_{\text{a-b}} = \frac{a_{\text{a}}}{a_{\text{b}}} = \frac{\gamma_{\text{a}} C_{\text{a}}}{\gamma_{\text{b}} C_{\text{b}}} \quad (3.14)$$

Hence, in general, an apparent  $K$  value (taken to equal the ratio of concentrations) will only equal the true value in the limit of low concentrations when the solutions in both phases behave ideally, which is when the activity coefficients reduce to unity. For

finite concentrations, non-ideal behaviour in one or both of the phases is manifested as a concentration dependence of the apparent  $K$  value equal to the ratio of equilibrium concentrations. Because of the two aspects noted here, apparent  $K$  values (equal to the ratio of equilibrium concentrations) have been measured for solvent-solvent combinations to enable the derivation of values for membrane-solvent combinations which are not directly measureable. In addition, all  $K$  values have been measured for different permeant concentrations in order to assess possible non-ideality effects. Figures 3.2, 3.3 and 3.4 show plots of measured apparent  $K$  values versus the equilibrium concentration of the distributing species for all combinations of permeant, solvent and membrane used here. In each plot, the horizontal dashed line indicates the concentration range used in the membrane permeation measurements since we are interested in the value of  $K$  which corresponds to that concentration range. In Figure 3.2, it can be seen that  $K_{\text{PBS-squalane}}$  for both caffeine and testosterone are concentration-independent over the concentration range relevant to the membrane permeation measurements and hence average values over this concentration range are used in the permeation model calculations. Slight non-ideality deviations from these low-concentration-range average values are observed at higher concentrations which continue up to the highest possible concentrations, equal to the relevant permeant solubilities.

The  $K$  values derived from the solubility ratios (marked by the vertical dashed lines) are in line with the trends of the plots. It is noted here that the use of  $K$  values derived from solubility ratios is not recommended since such values refer to the highest achievable concentrations and therefore are likely to be subject to errors due to non-ideal behaviour.

Figure 3.3 shows plots for four different permeant/membrane/solvent systems for which apparent  $K$  values do not show significant variation with concentration, relative to the reasonably large experimental uncertainties. In these cases, the average concentration-independent values of  $K$  used in the analysis of the permeation runs are indicated by the vertical axis positions of the horizontal dashed lines for each system. Finally, Figure 3.4 shows the plot for caffeine distributing between the cellulose membrane and PBS where it can be seen that  $K$  varies significantly with caffeine concentration over the relevant concentration range.



**Figure 3.2.** Variation of the measured  $K_{\text{PBS-squalane}}$  partition coefficient at 32°C with equilibrium permeant concentration in PBS for testosterone (filled diamonds) and caffeine (open triangles). The horizontal dashed lines indicate the permeant concentration range used in the respective permeation experiments and the corresponding average value of  $K_{\text{PBS-squalane}}$  over this experimental permeant concentration range. The vertical dashed lines indicate the solubility values of the permeant for which  $K_{\text{PBS-squalane}}$  was taken to be the ratio of solvent solubilities.

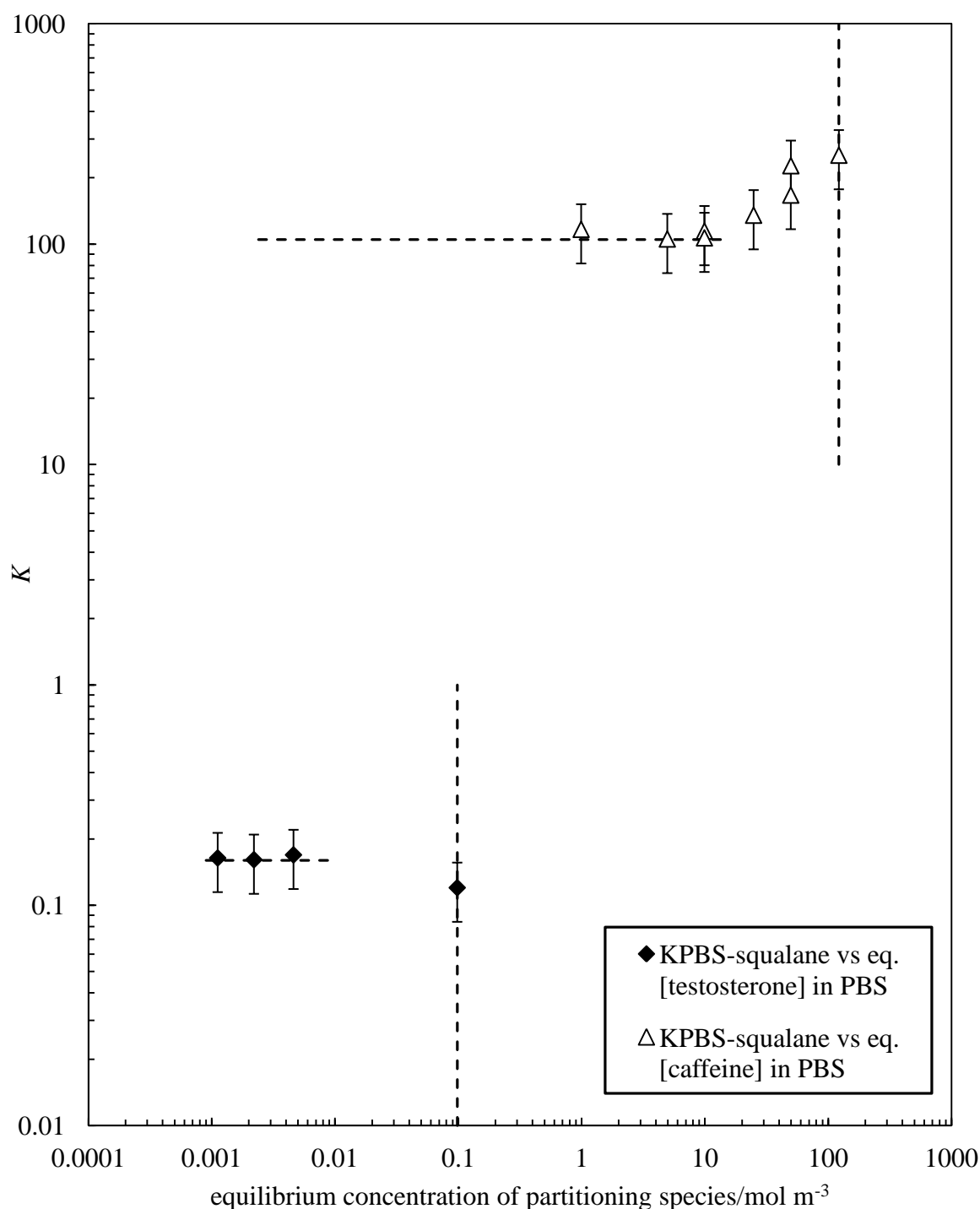


**Figure 3.3.** Variation of the measured  $K_{\text{membrane-liquid}}$  partition coefficients at 32°C with liquid phase permeant concentration. The system details are indicated in the key and the horizontal dashed lines indicate the permeant concentration range used in the respective permeation experiments and the corresponding average value of  $K_{\text{membrane-liquid}}$  over this experimental permeant concentration range.

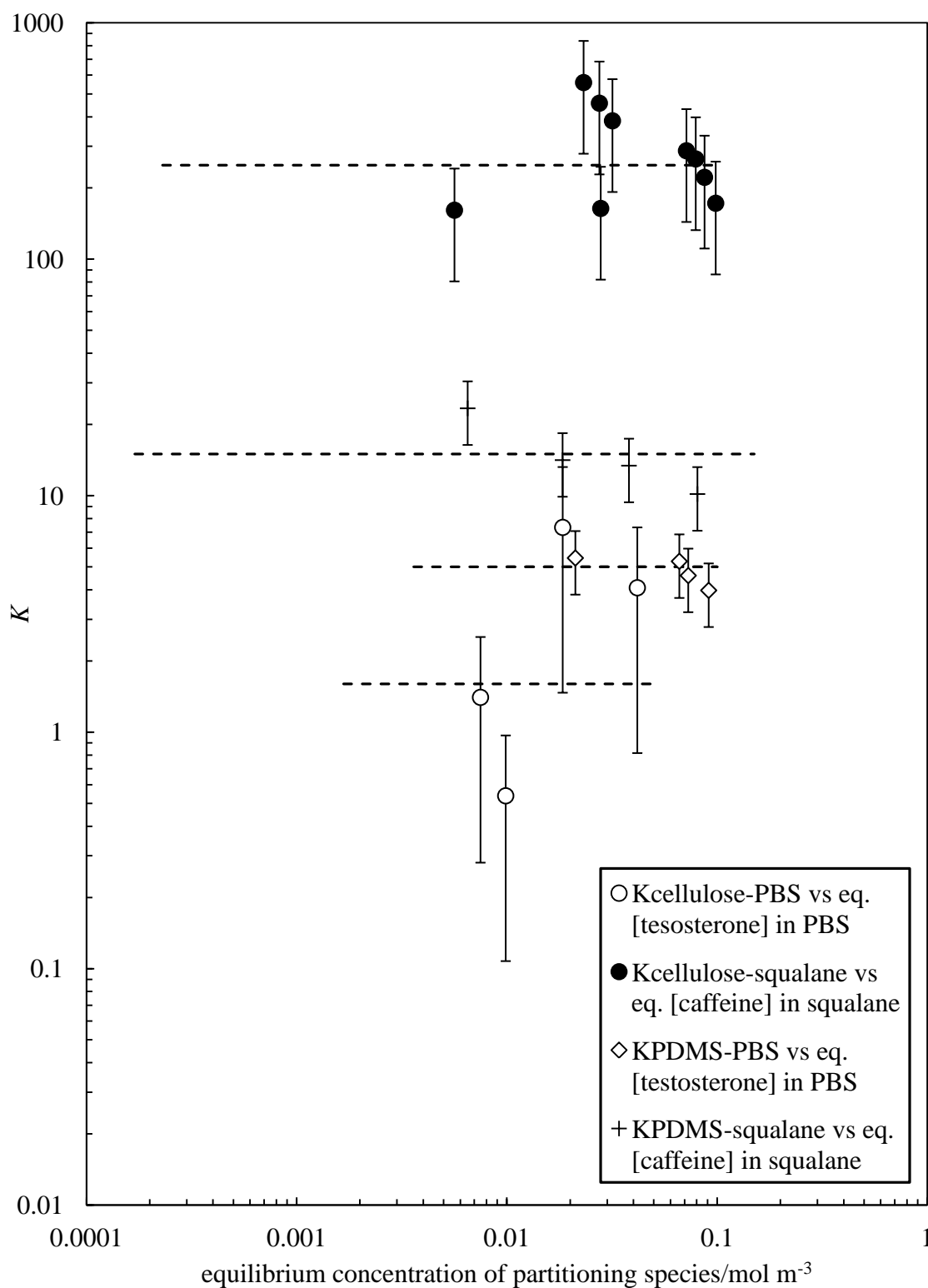
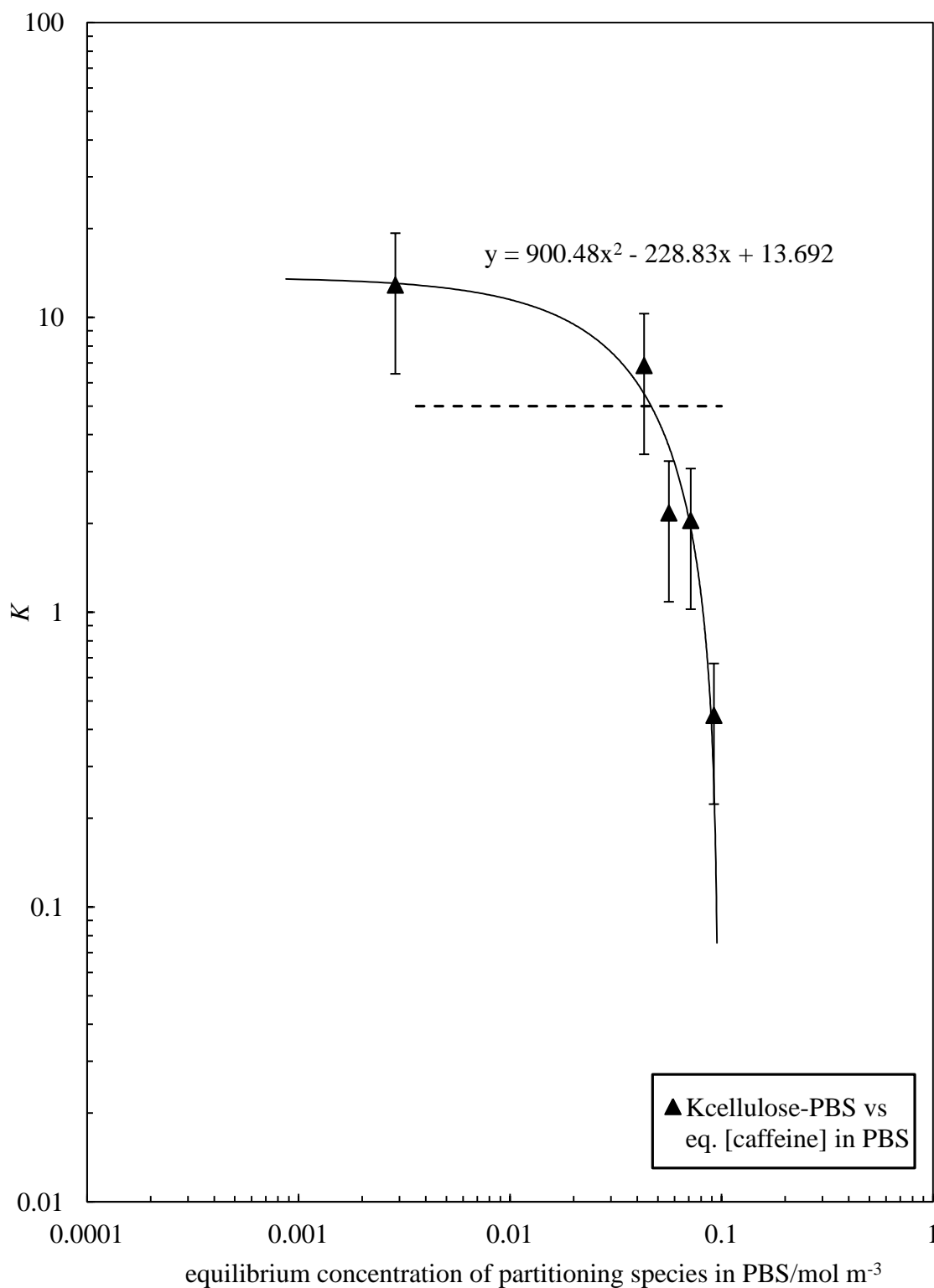


**Figure 3.4.** Variation of caffeine's  $K_{\text{cellulose-PBS}}$  measured partition coefficient at 32°C with equilibrium caffeine concentration in PBS. The horizontal dashed line indicates the caffeine concentration range used in the respective permeation experiments. The plot illustrates that caffeine's  $K_{\text{cellulose-PBS}}$  partition coefficient is concentration dependent over the relevant concentration range used for this system.



The final values of all partition coefficients used in the analysis of the membrane permeation measurements described subsequently are summarised in Table 3.2. For the table cells, where the entry is denoted as “concentration dependent”, the value of  $K$  appropriate to the average concentration for each individual permeation rate run has been estimated using the fitting equation corresponding to the solid line shown in Figure 3.4. The values of the permeant diffusion coefficients  $D$  and the permeation lag time  $L$  are next discussed.

**Table 3.2.** Equilibrium partition coefficients and permeant diffusion coefficients through the membranes ( $D$ ) used to obtain the calculated values of  $C_{\text{rec},\infty}$  and  $k$  for all the measured combinations of hydrophilic and hydrophobic donor solvents, permeants and membranes at 32°C. Estimated lag times  $L$  are also shown.

Donor solvent	Permeant	Membrane	$K_{\text{mem-don}}$	$K_{\text{mem-rec}}$	$K_{\text{rec-don}}$	$D / \text{m}^2 \text{s}^{-1}$	$L / \text{s}$
PBS	Testosterone (Hydrophobic)	PDMS (Hydrophobic)	5±2	5±2	1	9.3 x 10 <sup>-12a</sup>	118 <sup>c</sup>
squalane	Testosterone (Hydrophobic)	PDMS (Hydrophobic)	0.8 <sup>b</sup>	5±2	0.16±0.05		
PBS	Caffeine (Hydrophilic)	PDMS (Hydrophobic)	0.14 <sup>b</sup>	0.14 <sup>b</sup>	1	1.6 x 10 <sup>-12a</sup>	683 <sup>c</sup>
squalane	Caffeine (Hydrophilic)	PDMS (Hydrophobic)	15±5	0.14 <sup>b</sup>	105±30		
PBS	Testosterone (Hydrophobic)	Cellulose (Hydrophilic)	1.6±1.3	1.6±1.3	1	16 x 10 <sup>-12a</sup>	24 <sup>c</sup>
squalane	Testosterone (Hydrophobic)	Cellulose (Hydrophilic)	0.26 <sup>b</sup>	1.6±1.3	0.16±0.05		
PBS	Caffeine (Hydrophilic)	Cellulose (Hydrophilic)	Conc. dep.	Conc. dep.	1	3.0 x 10 <sup>-12a</sup>	128 <sup>c</sup>
squalane	Caffeine (Hydrophilic)	Cellulose (Hydrophilic)	250±130	Conc. dep.	105±30		

<sup>a</sup> Obtained by fitting measured rates.

<sup>b</sup> Derived from measured  $K$  values.

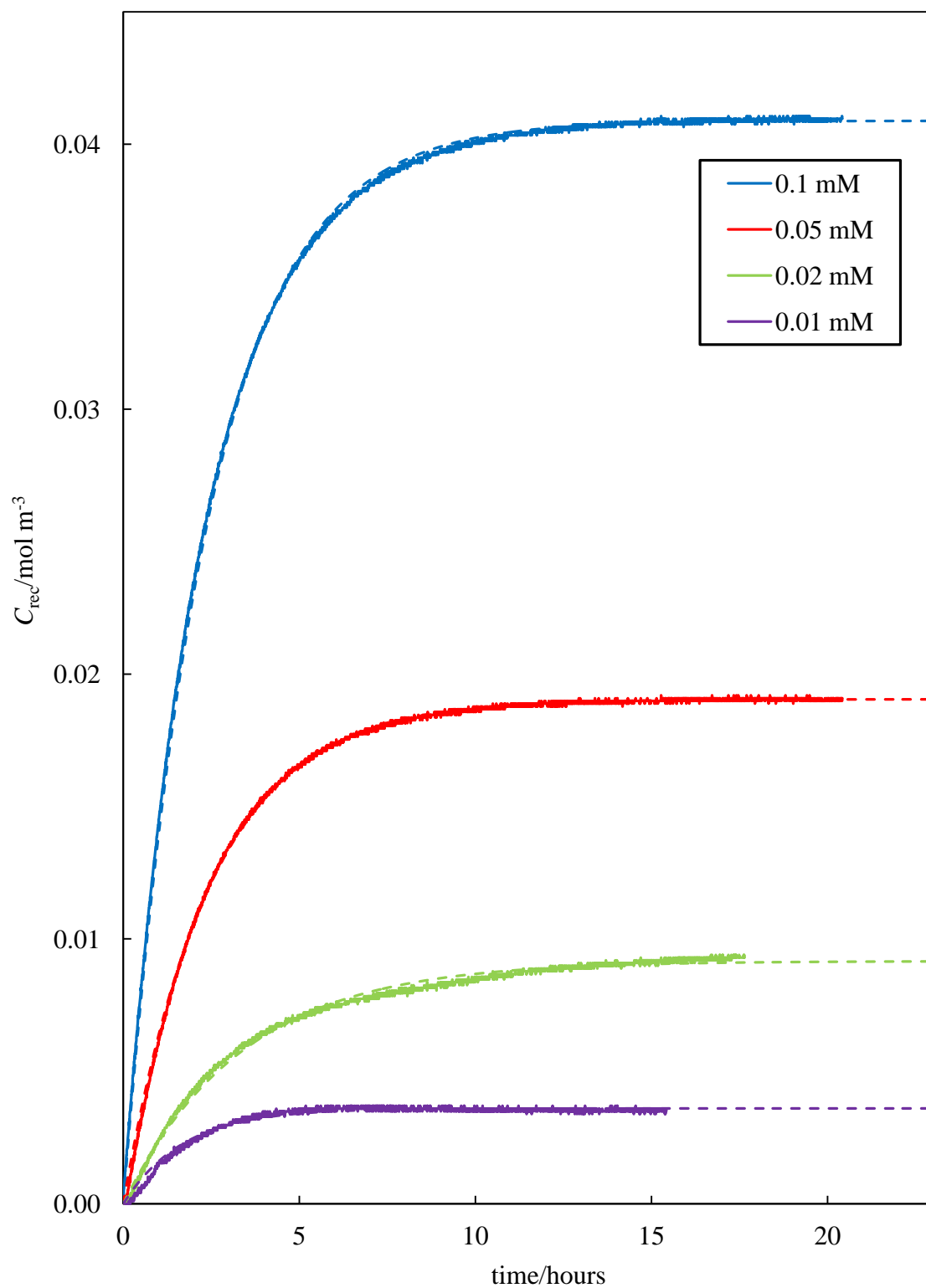
<sup>c</sup> Lag times estimated using equation 3.15.

#### 3.2.4.3 Membrane permeation measurements and their analysis

Figure 3.5 shows examples of measured plots of  $C_{\text{rec}}$  versus time for caffeine permeating from a PBS donor phase with different initial concentrations of caffeine through a cellulose membrane to a PBS receiver phase. The observed behaviour of this system is accurately described by the theoretical model expressed through equations 3.8-3.10. In particular, the measured curves are accurately exponential as expected from equation 3.8; the rate coefficient  $k$  is virtually identical for all different initial donor phase concentrations (illustrated by the permeation curve half-lives) and  $C_{\text{rec},\infty}$  scales with the initial donor phase concentration, as predicted previously. Hence it is concluded that the set of assumptions underpinning the model are valid for this system under the experimental permeation conditions used here.

In ensuring that the first model assumption is valid (i.e. the rate determining step of the entire membrane permeation process is permeant diffusion across the membrane) it is required that both the donor phase stirring rate and receiver phase flow rate are sufficient such that mass transfer of the permeant to and from the membrane is relatively instantaneous. Complementary studies were therefore performed which conclusively illustrated that the chosen experimental conditions (donor phase stirring rate = 5000 rpm and receiver phase flow rate = 3 ml min<sup>-1</sup>) are above the required threshold to justify and validate this assumption.

**Figure 3.5.** Measured variation of receiver compartment permeant concentration  $C_{\text{rec}}$  with time (solid lines) for caffeine in PBS permeating through a cellulose membrane at 32°C. The initial donor compartment concentrations of caffeine are shown in descending order in the key; the dashed lines correspond to the best-fit to the exponential function predicted by the theoretical model (equation 3.8).



One of the model assumptions leading to the prediction of exponential concentration plots is that the permeation occurs under so-called steady-state conditions, when the linear concentration gradient of permeant across the membrane is fully established. As described in Chapter 1, the time required to establish this steady-state (the so-called lag-time  $L$ ), is given by the approximate expression below.

$$L \approx \frac{X^2}{6D} \quad (3.15)$$

For the systems investigated here, the membrane thickness  $X$  ranges from 48 to 80  $\mu\text{m}$  and (as discussed later) the values of permeant diffusion coefficient in the membrane  $D$  range from  $1.6 \times 10^{-12} \text{ m}^2 \text{ s}^{-1}$  to  $16 \times 10^{-12} \text{ m}^2 \text{ s}^{-1}$ . The values of  $L$ , estimated using equation 3.15, for all the different systems measured here are listed in Table 3.2 and lie in the range from 24 to 683 s. All values of  $L$  are small relative to the timescales of the experimental permeation runs which are typically 5 to 50 hours and so all the permeation runs occur under steady-state conditions for all but the first few minutes or so. Hence, for most of the systems, the plots of  $C_{\text{rec}}$  versus time are exponential in shape and do not show an obvious lag phase at short times. The estimated lag times are similar in magnitude to the experimental uncertainty in estimating time zero for permeation (approximately  $\pm 2$  minutes), corresponding to the time required to load and seal the donor compartment of the permeation cell and initiate membrane permeation data collection with the proposed experimental methods. Lag time effects are discussed in more detail in section 3.2.5.2.

From the theoretical discussion of permeation rates for the hypothetical permeant, donor solvent and membrane combinations summarised in Table 3.1, it is seen that the slowest permeation is predicted to occur for a combination of hydrophilic permeant from a water donor phase through a hydrophobic membrane. Of the different experimental systems measured here, this very slow permeation case is realised for caffeine (hydrophilic) permeating through a PDMS (hydrophobic) membrane from a PBS (aqueous) donor phase as predicted. Figure 3.6 shows experimental plots of  $C_{\text{rec}}$  versus time for different initial concentrations of caffeine in the PBS donor phase having permeated through a PDMS membrane. It can be seen that the permeation rate is so slow that the full exponential curves are not observed over the 15 hour timescales of the runs. The measured plots correspond to the permeation of only a small fraction of the total caffeine present and are approximately linear. The gradients of the lines correspond to the initial steady-state permeation rates which, according to the theoretical model, are predicted to scale with initial donor phase concentration with the constant of proportionality equal to the permeation rate coefficient  $k$ . The linear scaling of initial steady-state permeation rate with initial permeant concentration is shown in Figure 3.7 and hence, the gradient of this linear plot is equal to the 1<sup>st</sup>-order permeation rate coefficient  $k$ .



**Figure 3.6.** Measured initial rate of change of receiver compartment permeant concentration  $C_{\text{rec}}$  with time for caffeine permeating through PDMS from PBS donor solutions at 32°C. The initial donor compartment concentrations of caffeine (in descending order) are shown in the key.

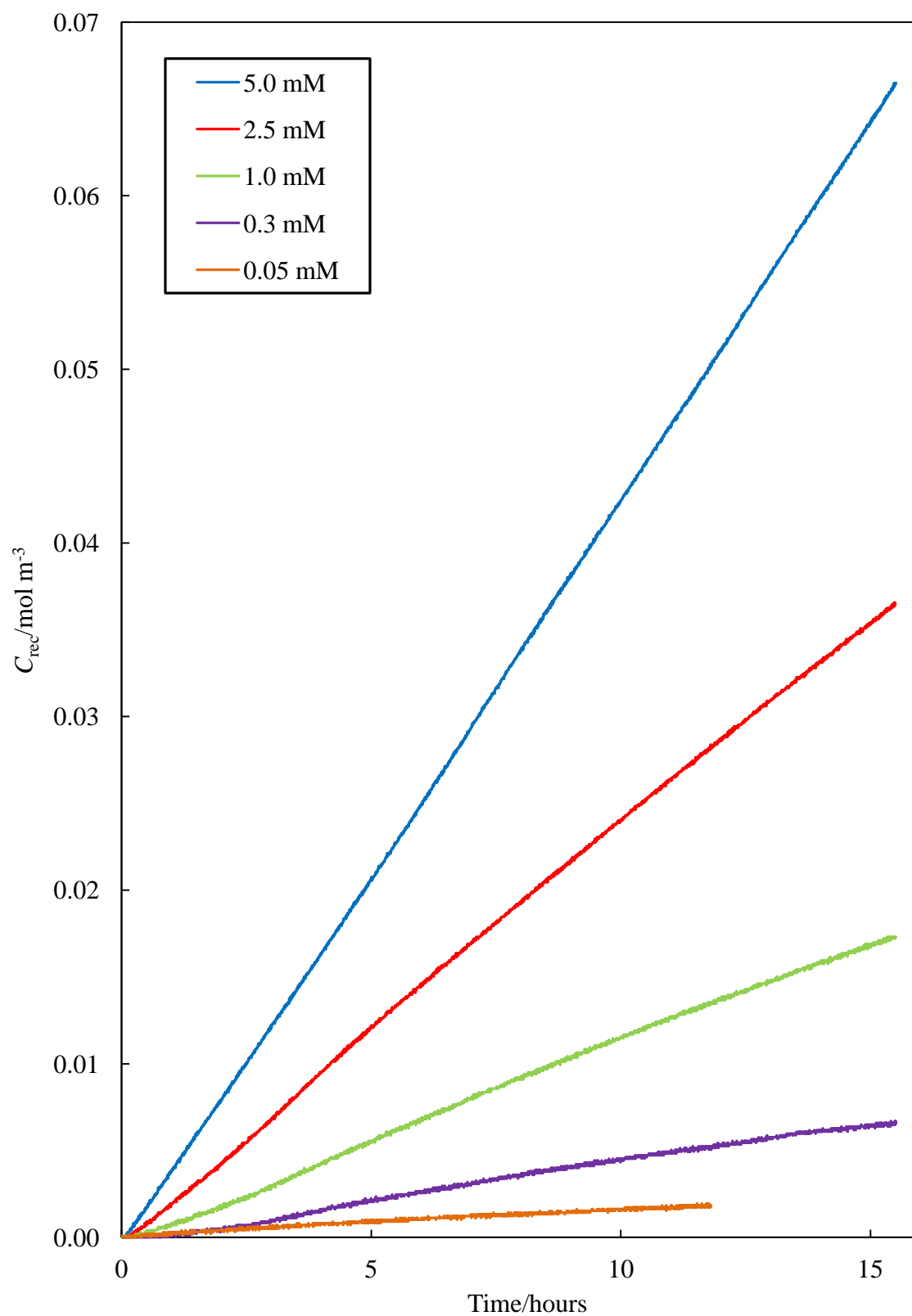
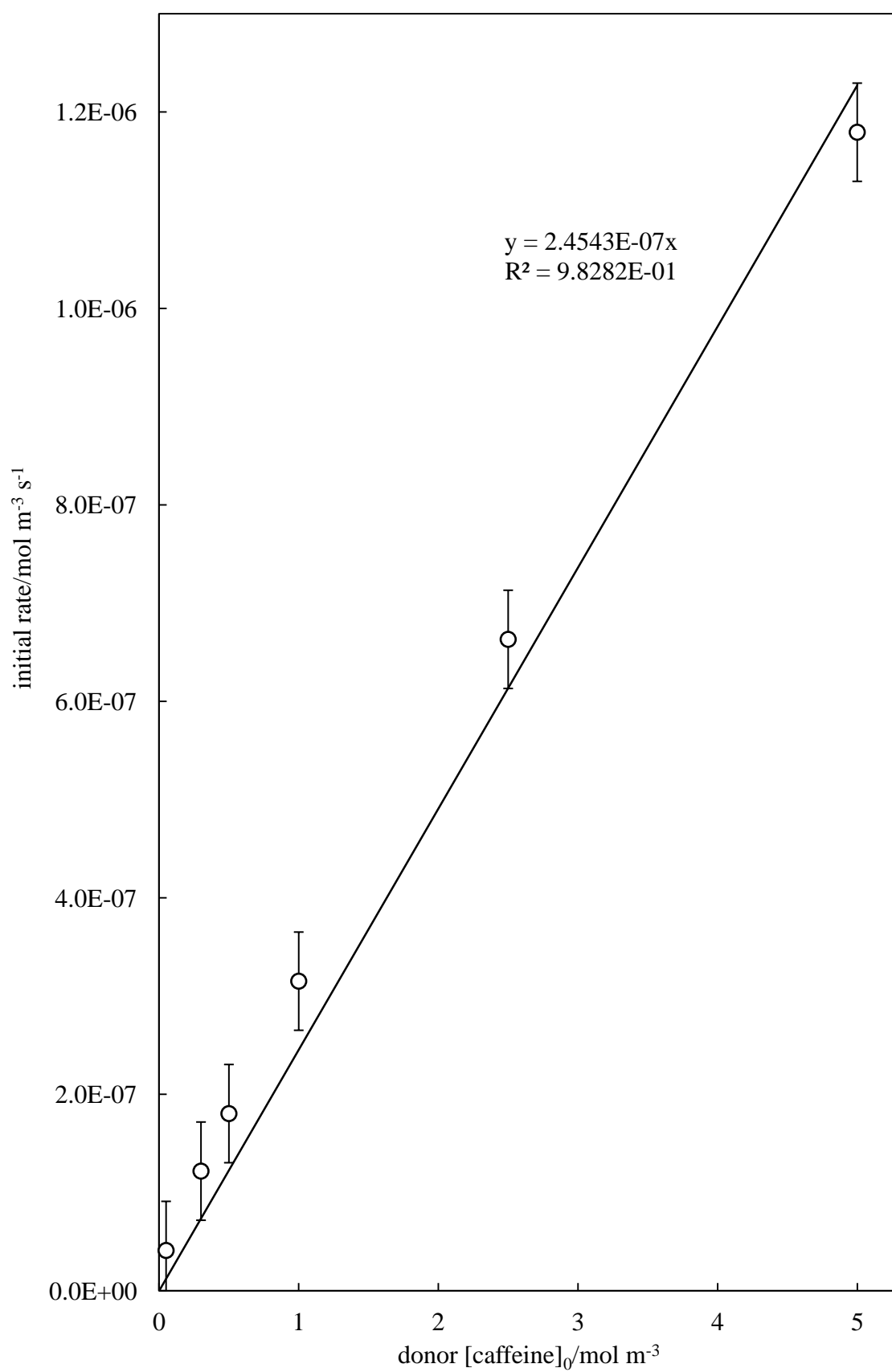
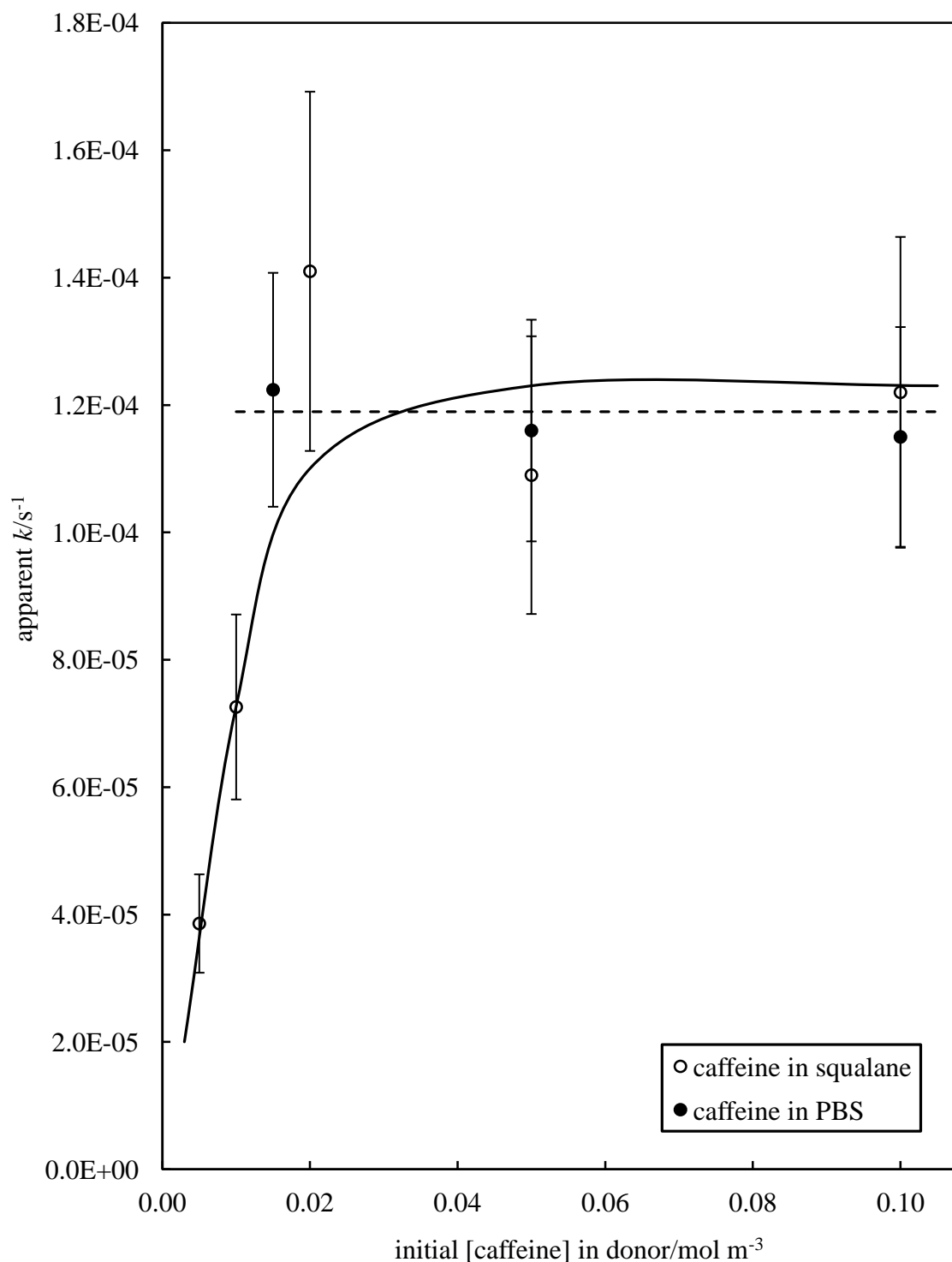


**Figure 3.7.** Derived variation of initial steady-state permeation rate versus initial donor concentration; the solid line shows the linear fit used to obtain  $k$ .



Of the eight possible combinations of permeant, donor solvent and membrane investigated experimentally, seven of the systems are observed to follow the theoretical model for the permeation conditions employed here. However, the system of caffeine permeating through a cellulose membrane from a squalane donor solution shows anomalous behaviour. In particular, the measured plots of  $C_{\text{rec}}$  versus time are observed to deviate from exponential behaviour and the permeation rate coefficient  $k$  is not independent of the initial donor phase concentration. Figure 3.8 shows that  $k$ , as predicted, is independent of initial concentration for caffeine permeating through cellulose from a PBS donor solvent but unexpectedly dependent for squalane as the donor solvent. The caffeine/cellulose/squalane system was therefore examined in further detail to determine which of the theoretical model assumptions may not be valid for this case. It is first noted that the permeant caffeine has a very high partition coefficient from the squalane donor solvent to the cellulose membrane ( $K_{\text{cellulose-squalane}} = 250$ ) and hence the permeation is predicted to be very rapid. Furthermore, squalane as the donor solvent is approximately 26 times more viscous than PBS ( $20.8 \text{ mPa s}$  compared with  $0.76 \text{ mPa s}$ )<sup>2</sup> which is expected to slow mass transport within the donor phase. Hence, it was hypothesised that the rate-limiting step of the overall permeation process may be switched from diffusion across the membrane (assumed in the theoretical model) to mass transport within the squalane donor phase.

**Figure 3.8.** Variation of apparent  $k$  value with initial caffeine concentration in the donor compartment for the permeation of caffeine through cellulose from either PBS or squalane at a constant donor stirring speed (using a magnetic stirrer) of 4200 rpm. The horizontal dashed line corresponds to the “true”  $k$  value for caffeine in PBS, i.e. corresponding to membrane permeation being rate limiting for which  $k$  is independent of the initial concentration.



This hypothesis, was tested by investigating how the donor phase stirring speed affected the permeation of caffeine through a cellulose membrane from a squalane donor solution as shown in Figures 3.9 and 3.10. If membrane diffusion is rate-limiting, the permeation rate coefficient  $k$  is expected to be unaffected by the donor compartment stirring speed, whereas increased stirring will increase the permeation rate if mass transport within the donor phase is rate limiting. Figure 3.9 shows illustrative traces of  $C_{\text{rec}}$  versus time for two different stirring speeds in the squalane donor compartment. It can be seen that the curves deviate from exponential behaviour and that increased stirring speed increases the permeation rate. Figure 3.10 shows that  $k$ , derived from  $C_{\text{rec}}$  versus time plots, is independent of stirring speed for caffeine permeating through cellulose from a PBS donor solution but strongly dependent when permeating from a squalane donor solution. For an illustrative purpose, one permeation rate run was performed with decane as the donor solvent because decane has a viscosity (0.78 mPa s)<sup>3</sup> much lower than squalane (20.8 mPa s) and similar to that of PBS (0.76 mPa s). If it is assumed that the affinity of the caffeine for decane and squalane are similar, then the  $k$  value observed for decane is expected to be similar to that predicted for squalane if mass transport in the donor phase were not rate-limiting. As seen in Figure 3.10, the decane value and the highest stirring speed squalane measurement are reasonably similar. The conclusion here is that the anomalous behaviour of the caffeine/cellulose/squalane system is due to a switch in rate-limiting step to mass transport in the donor phase under the standard permeation conditions used here. For this system, rate-limiting membrane diffusion is only approached at the highest donor stirring speed used and  $k$  under these conditions is approximately  $1 \times 10^{-3} \text{ s}^{-1}$ . Apparent  $k$  values measured at lower stirring speeds should not be analysed in terms of the theoretical model used here.

**Figure 3.9.** Variation of  $C_{\text{rec}}$  versus time for the permeation of caffeine through cellulose membranes from identical squalane donor solutions for two different stirring speeds of the donor compartment. The dashed lines indicate the “best-fit” exponential curves.

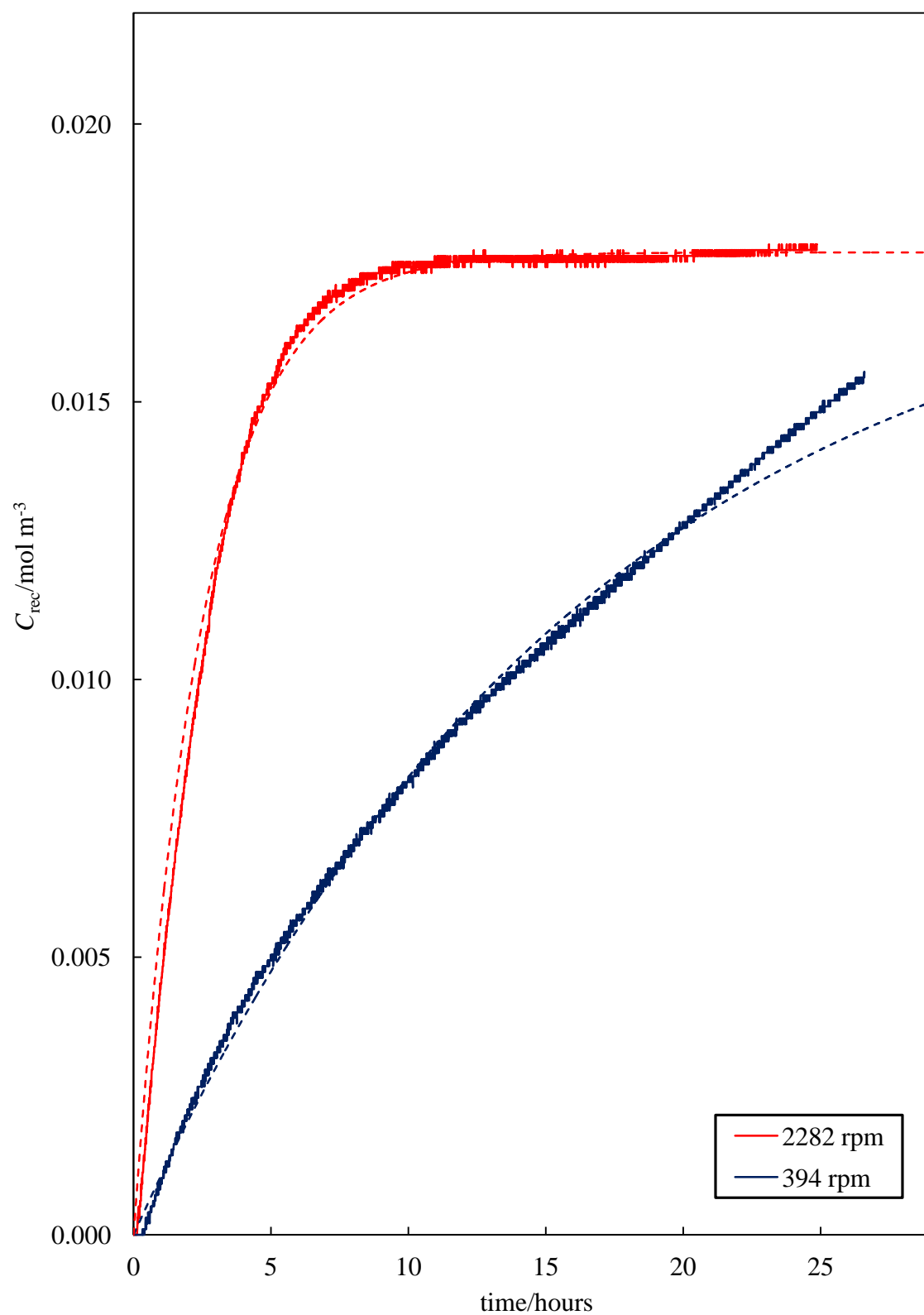
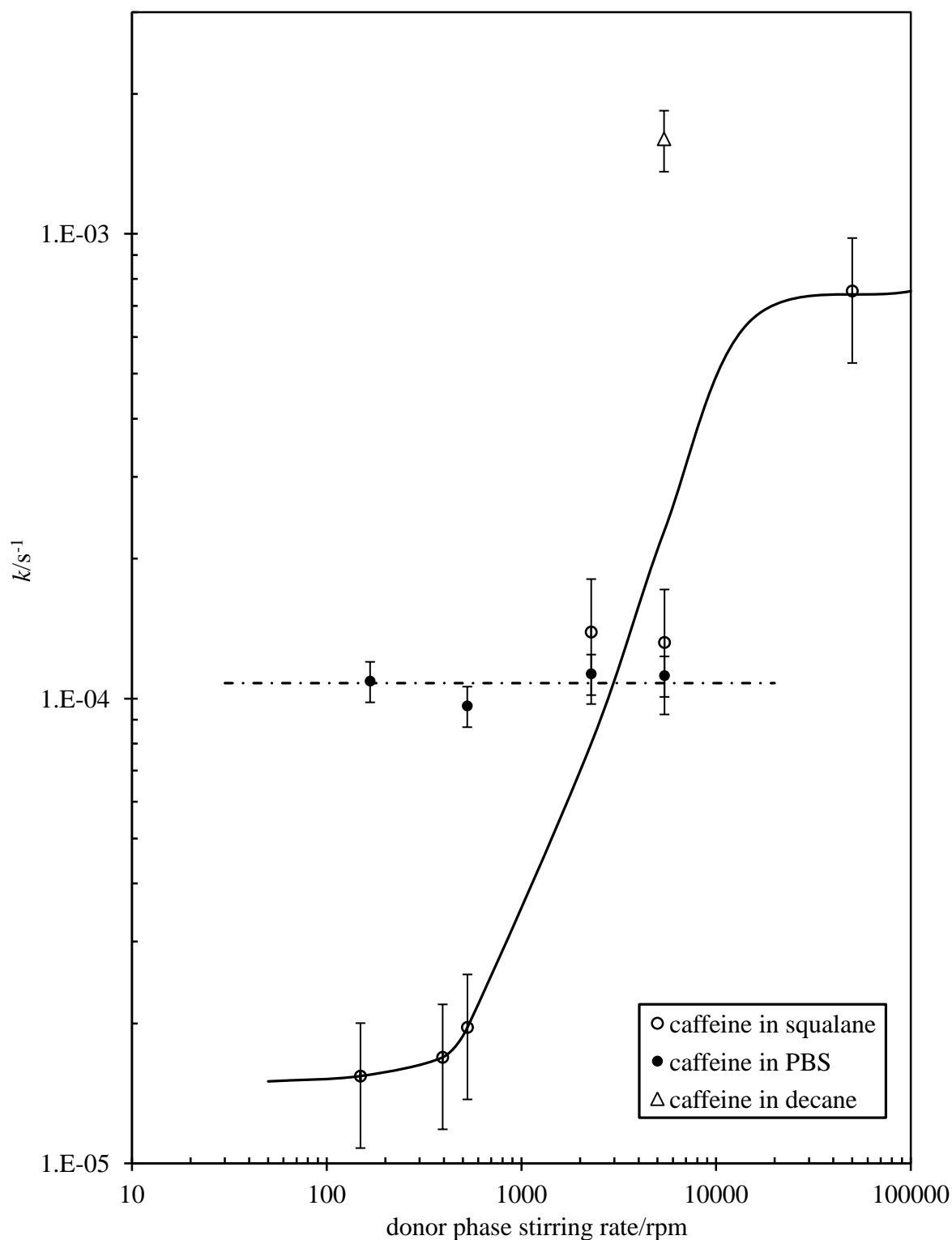


**Figure 3.10.** Variation of the apparent  $k$  value with donor stirring speed for the permeation of caffeine through cellulose membranes from either PBS or squalane donor solutions. A single value for decane as the donor phase solvent is also shown for illustrative purposes. The solid line is a guide for the eye. The horizontal dashed line corresponds to the stirring speed-independent  $k$  value for the PBS donor solution.



Following exclusion of the low donor stirring speed data for the caffeine/cellulose/squalane system, the experimental values of  $k$  and  $C_{\text{rec},\infty}$  for all systems were compared with values calculated according to equations 3.9 and 3.10 of the theoretical model. As discussed earlier and summarised in Table 3.2, all partition coefficients were measured or derived from measured values with proper consideration of solution non-ideality effects appropriate to the concentration ranges used in the membrane permeation studies. The diffusion coefficients  $D$  for the different permeant and membrane combinations were not measured directly; they were obtained by fitting measured and calculated  $k$  values using the solver function in Microsoft EXCEL. In this fitting procedure, it was assumed that  $D$  was not affected by the donor solvent used, i.e.  $D$  depended only on the nature of the permeant and the membrane. Hence, the eight different permeant/solvent/membrane systems yield four values of  $D$  which are summarised previously in Table 3.2. Numerous authors report the permeation of testosterone and caffeine across PDMS and cellulose membranes in terms of the permeability coefficient  $k_p$ , where,

$$k_p = \frac{K_{\text{mem-don}} D}{X} \quad (3.16)$$

Hence, some limited comparison of the  $D$  values described in this study with literature can be made as follows.  $D$  for testosterone in PDMS at 32°C estimated here ( $9.3 \times 10^{-12} \text{ m}^2 \text{ s}^{-1}$ ) is in agreement with the value from reference 4 of  $9.4 \times 10^{-12} \text{ m}^2 \text{ s}^{-1}$  and consistent with estimated limits of greater than  $5 \times 10^{-12} \text{ m}^2 \text{ s}^{-1}$  at 37°C (derived, using equation 3.16, from permeability coefficient values given in references 5 and 6 combined with a limiting value of the membrane-donor partition coefficient from this work). The value of  $D$  for caffeine in PDMS at 32°C estimated here ( $1.6 \times 10^{-12} \text{ m}^2 \text{ s}^{-1}$ ) is reasonably consistent with values of 6 and  $7 \times 10^{-12} \text{ m}^2 \text{ s}^{-1}$  at 37°C, derived, using equation 3.16, from permeability coefficient values from references 5 and 7 respectively, combined with a value of the membrane-donor partition coefficient from this work.

The comparison of the theoretical model with the experimentally determined extents and rate coefficients of all eight permeant/solvent/membrane systems is shown, as plots of calculated versus measured values of  $C_{\text{rec},\infty}$  (Figure 3.11) and  $k$  (Figure 3.12) respectively. Based on exponential fits to plots of  $C_{\text{rec}}$  versus time, the measured values



of  $C_{\text{rec},\infty}$  and  $k$  are reasonably accurate with estimated uncertainties of the order of 10% or less. Uncertainties in the calculated values of  $C_{\text{rec},\infty}$  and  $k$  are mainly determined by the relatively high uncertainties in the measured partition coefficients of Figures 3.2, 3.3 and 3.4 but also include uncertainties in the ancillary parameters such as the donor and receiver compartment volumes and the membrane thickness and area. The overall uncertainties in the calculated  $C_{\text{rec},\infty}$  and  $k$  values are estimated to be of the order of approximately 50%. Within these uncertainties, a single, fitted value of  $D$  for each permeant/membrane combination successfully captures the effects of changing the donor solvent from PBS to squalane. It can be seen from Figures 3.11 and 3.12 that the theoretical model simultaneously describes both the equilibrium ( $C_{\text{rec},\infty}$ ) and kinetic ( $k$ ) aspects of the permeation behaviour of the eight diverse experimental systems.

Of the eight permeant/solvent/membrane systems, it can be seen that one (caffeine permeating through PDMS from a PBS donor) is very slow, one (caffeine permeating through cellulose from a squalane donor) is very fast and all other systems show similar “medium” rates. The key factor determining the observed differences in  $k$  over nearly 4 orders of magnitude are the relative values of the sum of the partition coefficients ( $K_{\text{mem-don}} + K_{\text{mem-rec}}$ ) as described and predicted in the theoretical model previously. The differences in diffusion coefficient  $D$  between the different systems are of secondary importance in affecting  $k$ .

**Figure 3.11.** Comparison of measured and calculated values of the equilibrium fraction of permeant extracted to the receiver compartment  $C_{\text{rec},\infty}$  for all the different combinations of permeant, donor solution solvent and membrane. The dashed line indicates perfect agreement between theory and experiment.

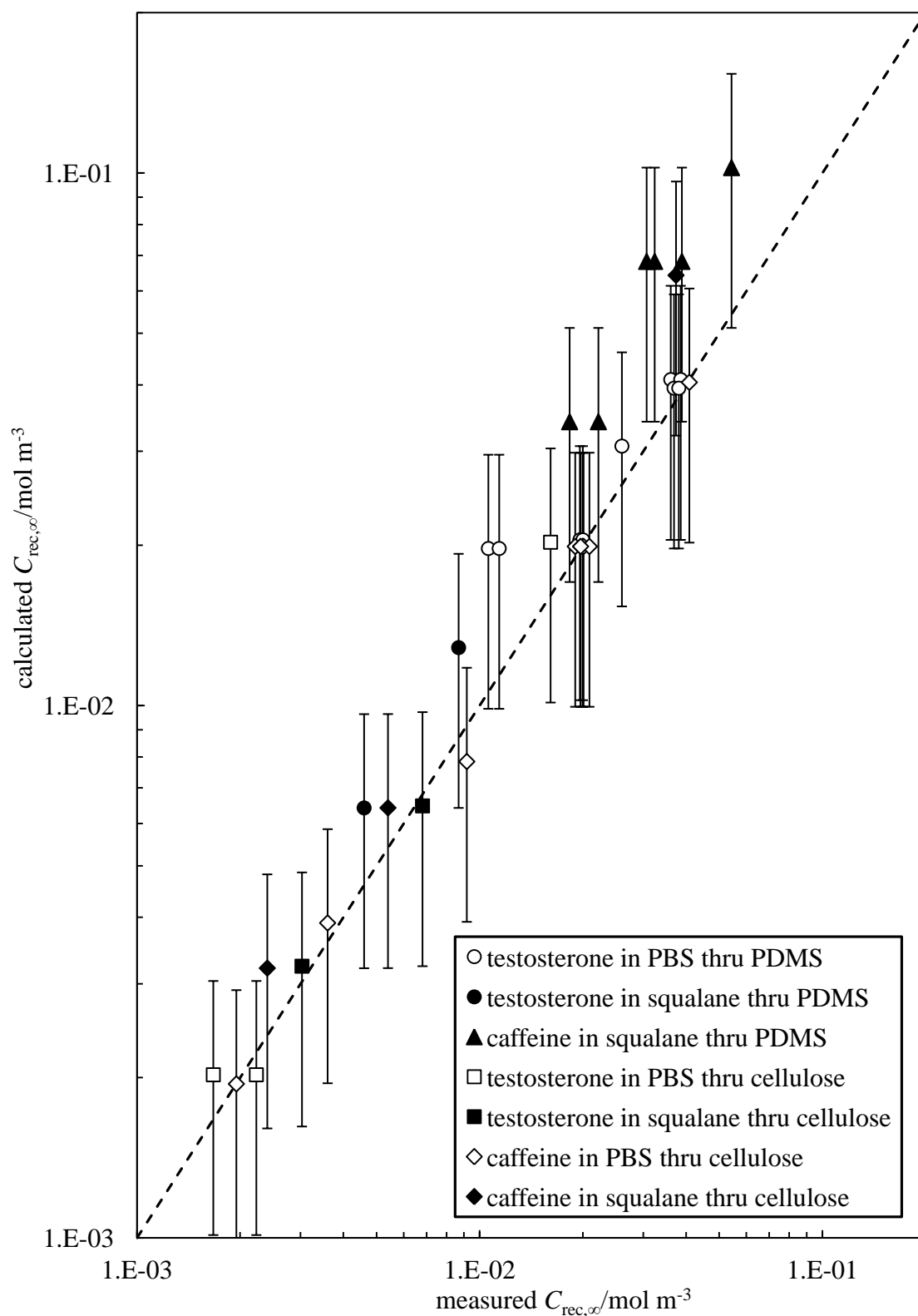
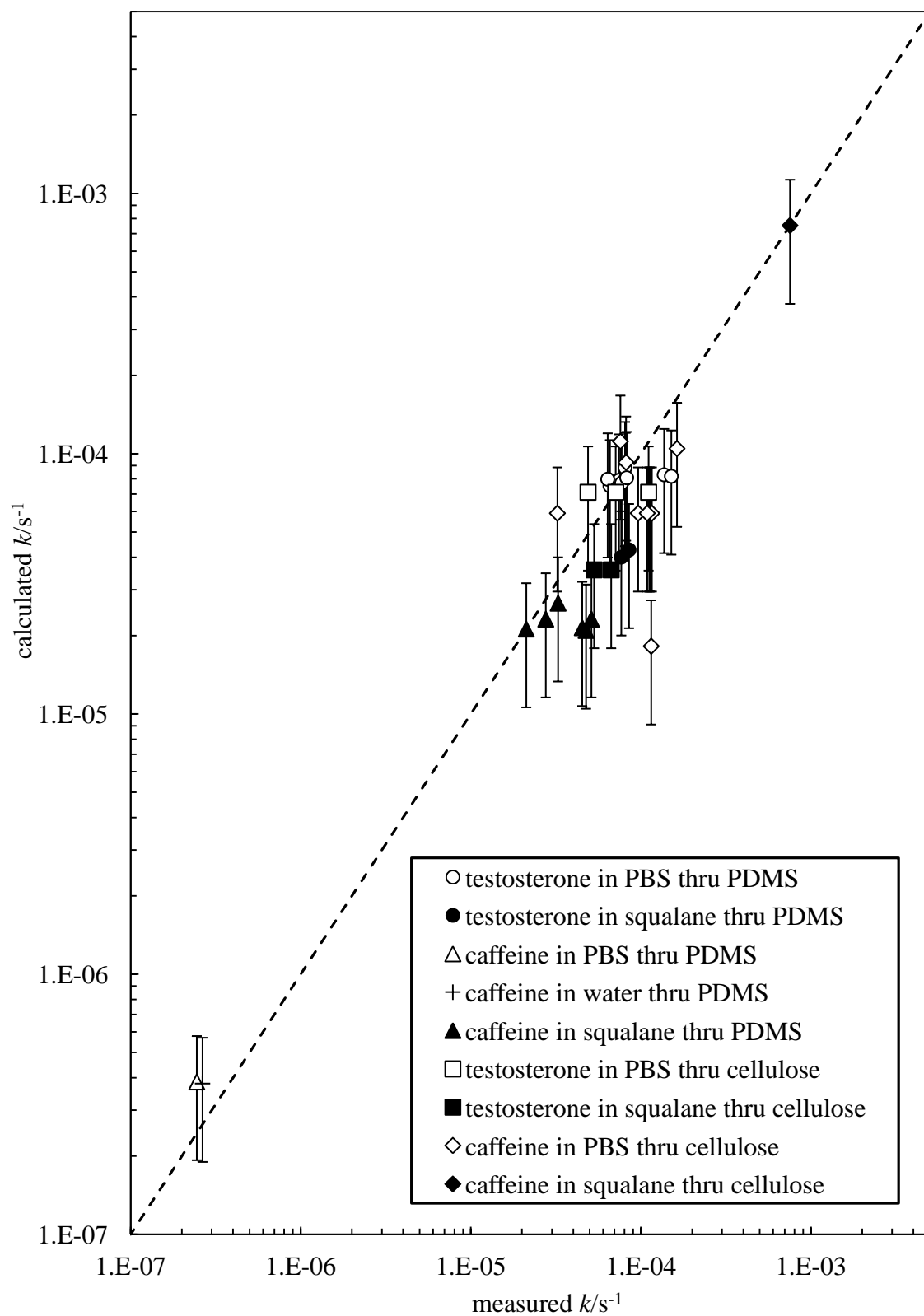


**Figure 3.12.** Comparison of measured and calculated values of the 1<sup>st</sup>-order permeation rate coefficient  $k$  for all the different combinations of permeant, donor solution solvent and membrane. The dashed line indicates perfect agreement between theory and experiment.



### 3.2.5 *Deviations from the model assumptions*

The strategy adopted here of quantitatively analysing experimental permeation data in terms of a theoretical model based on clearly established underpinning assumptions, provides a clear and systematic means of determining the origins of the many different possible ways in which the donor solvent can affect permeation. For systems for which the model assumptions are valid, the model shows that donor solvent effects on the extent and rate of membrane permeation are primarily controlled by how the three partition coefficients  $K_{\text{don-rec}}$ ,  $K_{\text{mem-don}}$  and  $K_{\text{mem-rec}}$  change with donor solvent. The extent of permeation is determined by the relative volumes of the donor and receiver compartments and the value of  $K_{\text{don-rec}}$ . For equal donor and receiver volumes, the permeation rate coefficient is proportional to the sum ( $K_{\text{mem-don}} + K_{\text{mem-rec}}$ ) and hence the magnitude of the donor solvent effect on rate is strongly affected by the natures of both the membrane and the permeant as seen in Table 3.1.

For the experimental permeation cell used here (with stirring in both donor and receiver compartments), most of the permeation systems investigated follow the behaviour predicted by the model, i.e. the set of model assumptions are valid in most of the systems. Observed deviations from the model enable full and systematic discussion of all the additional possible ways in which the donor solvent can affect permeation, i.e. those effects not simply related to partition coefficient changes. The additional possible effects which arise from solvent changes, rendering one or more of the model assumptions invalid are therefore discussed under sub-headings which link to the key model assumptions.

#### 3.2.5.1 The rate-limiting step changes from membrane diffusion

The first model assumption is that permeant diffusion across the membrane is rate-limiting and that all other mass transport and partitioning steps are relatively fast; this key assumption justifies the use of pseudo-equilibrium equations for the various partitioning processes. The model predicts the important “signature” features expected for permeation with rate-limiting membrane diffusion which are: (i) plots of  $C_{\text{rec}}$  versus time are exponential; (ii) the permeation rate coefficient  $k$  is independent of the initial permeant concentration and (iii) the permeation rate coefficient is independent of stirring speed (for stirring rates above a lower threshold). Figures 3.8, 3.9 and 3.10

show how the caffeine/squalane/cellulose system deviates from the model in these three aspects and is thereby revealed as having undergone a change in rate limiting step. In general, for the membrane thicknesses and membrane diffusion coefficients seen here, membrane diffusion is expected to remain rate-limiting when (i) donor and receiver compartments are stirred; (ii) the donor solvent viscosity is not too large and (iii) the membrane partition coefficients are such that very fast permeation is not obtained. The switch in rate-limiting step observed here for the caffeine/cellulose system when changing the donor solvent from PBS to squalane, is a result of the high viscosity of squalane relative to PBS plus the fact that the sum of the partition coefficients ( $K_{\text{mem-don}} + K_{\text{mem-rec}}$ ) favours very fast permeation for squalane as the donor solvent.

It is noted here that rate-limiting membrane diffusion is not desirable in particular applications which require slow or sustained drug release profiles. There is an extensive literature describing a wide range of different types of donor compartment formulations in which the drug or other active species is encapsulated using, for example, polymers within the donor vehicle.<sup>8-10</sup> Even for these formulations, it remains important to establish unambiguously that membrane diffusion is not rate-limiting under the particular experimental conditions used in order to correctly interpret permeation measurements.

#### 3.2.5.2 The lag time is not negligibly small relative to the overall permeation time scale

The model predictions assume that the permeant concentration gradient across the membrane is linear, corresponding to “steady-state” diffusion, which is valid at times longer than the lag time. Hence, for the plots of  $C_{\text{rec}}$  versus time to exhibit the predicted exponential shape, it is required that the lag time  $L$  is negligibly small relative to the timescale of the overall permeation run. As seen in Table 3.2, the values of  $L$  estimated using equation 3.15 and the fitted values of  $D$  for the different systems range from 24 – 683 s. Given that  $L$  is generally small relative to the permeation time scale of 5 – 50 hours, deviations from the exponential shape in the overall plots of  $C_{\text{rec}}$  versus time are generally small as seen, for example, in Figure 3.5. However, the small deviations are observable by “zooming in” on the short time behaviour, particularly for the caffeine/PDMS systems where  $L$  is estimated to be relatively large. Figure 3.13 shows

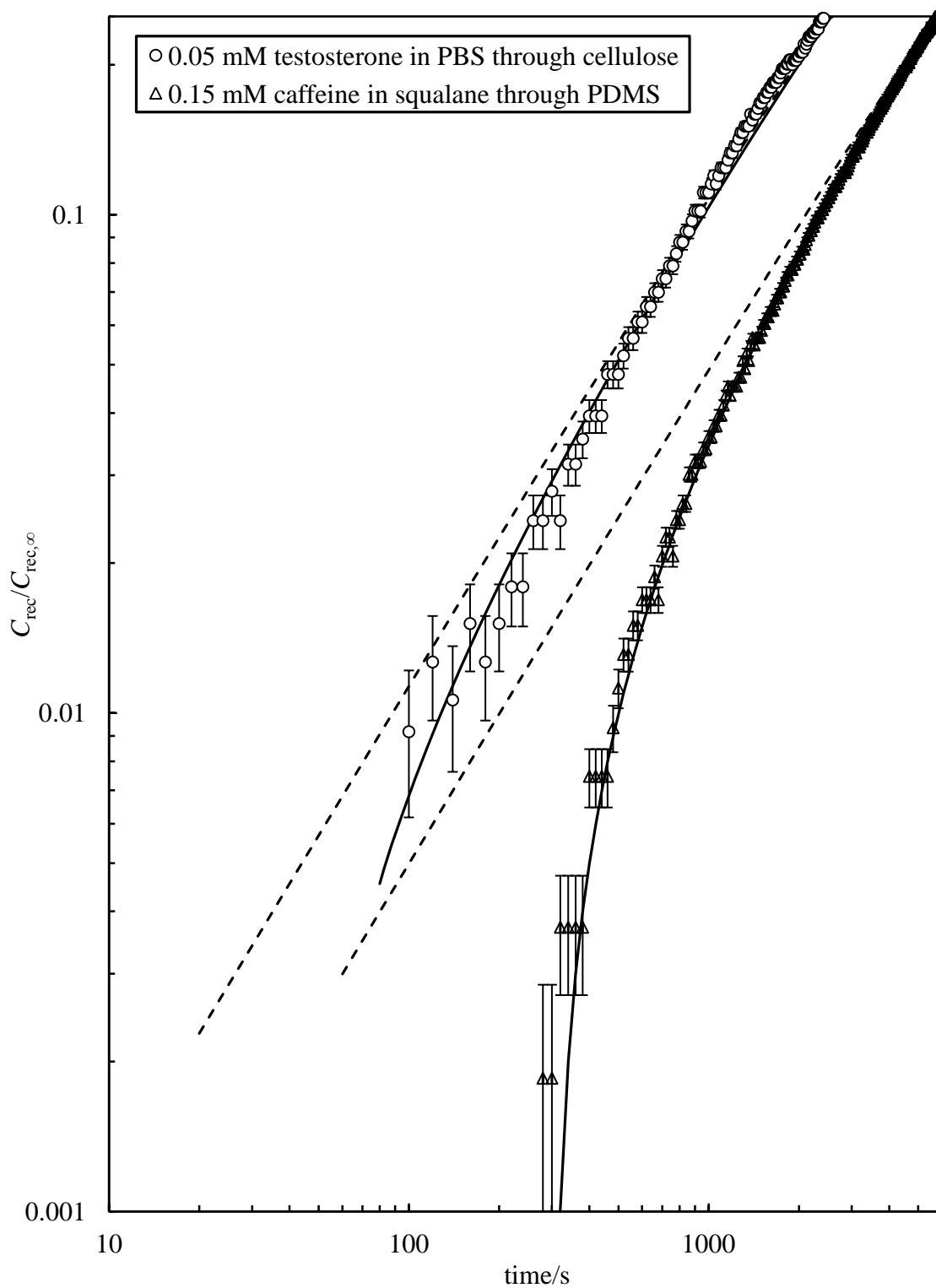
two examples of the short time behaviour of plots of  $C_{\text{rec}}/C_{\text{rec},\infty}$  versus time. The testosterone/PBS/cellulose system (with estimated  $L$  of 24 s) is compared with the caffeine/squalane/PDMS system (with estimated  $L$  of 683 s). For each plot, the dashed straight line indicates exponential behaviour seen for times  $\gg L$ . The solid lines correspond to fitted curves which are reasonably well described using equation 3.17 with floated values of  $L$ .

$$C_{\text{rec}} \approx C_{\text{rec},\infty} + (C_{\text{rec},0} - C_{\text{rec},\infty})\exp(-k\{t - L\}) \quad (3.17)$$

Qualitatively, it can be seen that the deviations from exponential behaviour are much greater for caffeine/squalane/PDMS systems than for testosterone/PBS/cellulose systems. Semi-quantitatively, fitting the curves of Figure 3.13 to equation 3.17 yields approximate values of  $L$  of 40 and 300 s respectively. Quantitative agreement with the  $L$  values from Table 3.2 (24 and 683 s respectively) is rather poor; this is probably due to the experimental uncertainty in the start time of the permeation runs which is estimated to be of the order of 2 minutes or so. In principle, measurement of the lag time provides a method to obtain an independent estimate of the diffusion coefficient  $D$ . As shown by the comparison of the different estimates of the lag time, this is unreliable for the experimental procedure used here.

Deviations from the predicted model behaviour due to lag time effects are expected for systems with thick membranes and low values of the diffusion coefficient (see equation 3.15). In general, the effect is not dependent on the donor solvent. However, it is important to be aware of whether or not permeation runs are occurring under steady or non-steady state conditions in order to avoid incorrect interpretation of experimental permeation kinetic data.

**Figure 3.13.** Illustrative plots of the short-time behaviour of  $C_{\text{rec}}/C_{\text{rec},\infty}$  versus time for testosterone in PBS through cellulose (estimated  $L = 24$  s) and caffeine in squalane through PDMS (estimated  $L = 683$  s). For each plot the dashed line indicates exponential behaviour corresponding to  $L = 0$ . The solid lines are fits to equation 3.17 with the floated value of  $L = 40$  and  $300$  s respectively, as described previously.



### 3.2.5.3 Membrane diffusion does not follow Fick's laws and the membrane is not uniform throughout

In the derivation of the model equations, it is assumed that pseudo-equilibrium partitioning of the permeant occurs from the solvents to the membrane and that the membrane properties are uniform throughout its depth. For partitioning to occur, the membrane must be liquid-like rather than crystalline which will be the case for a synthetic polymer membrane at a temperature above its glass transition temperature. This is valid for PDMS but is almost certainly not the case for dry cellulose. However, as noted earlier, the cellulose membrane used here is pre-soaked in PBS and maintained in contact with a PBS receiving phase during permeation. The dry cellulose membrane swells to almost double its thickness following equilibration with PBS and so the actual membrane used consists of approximately 50% cellulose and 50% water. This water swollen membrane is likely to be liquid-like and thus the assumption made here is expected to be valid. The PDMS membrane properties are thought to be uniform throughout its depth. For the cellulose, it is noted that contact with PBS causes swelling in thickness but not in area and hence the membrane must possess anisotropic properties. However, there is no evidence that the membrane properties vary throughout the depth of the membrane (i.e. along the same axis as the direction of membrane permeation) and hence it is thought the assumptions made here are also valid.

The model derived here will not be valid for composite membranes containing both liquid-like and solid regions for which the membrane properties will not be uniform throughout the membrane depth. This will be the case for synthetic membranes which have a degree of crystallinity, composite membranes containing solid filler particles or for natural membranes such as the stratum corneum of human skin which is a composite containing regions of lipids and corneocytes.<sup>11</sup> For such membranes, there will be additional considerations relating to, for example, the “tortuosity” of the permeants pathway through the membrane. However, factors such as the tortuosity are not expected to be affected by the choice of donor solvent unless the solvent alters the membrane structure, e.g. the degree of crystallinity (see section 3.2.5.4 below).



#### 3.2.5.4 Donor and/or receiver solvents may permeate or affect the membrane

It is assumed in the model that only the permeant species permeates through the membrane and that its diffusion coefficient in the membrane is independent of its concentration within the membrane. Changing the donor solvent can affect permeation by rendering these assumptions invalid in several ways. Firstly, if the nature of the donor solvent is such that the permeant partitioning from the donor phase to the membrane is high, a high permeant concentration in the donor compartment would give a locally high permeant concentration in the membrane which could affect the diffusion coefficient and cause it to depend on the localised (membrane depth dependent) permeant concentration. Such behaviour would result in non-exponential permeation plots. For the experimental systems measured here, this effect cannot be rigorously excluded but the lack of deviation from exponential curves due to this cause and the overall agreement between theory and experiment seen in Figures 3.11 and 3.12 suggest that the effect, if present, is reasonably small.

Secondly, different donor solvents may swell the membrane to different extents and thereby affect the partitioning and diffusion coefficient of the permeant in the membrane. This effect has been reported in many literature studies of solvent effects in permeation<sup>12-17</sup> but is not present for the experimental systems studied here. As noted earlier, PDMS membranes show no significant swelling in either PBS or squalane solvents. The cellulose membranes are swollen in thickness (but not area) by PBS and not swollen by squalane. Given that the cellulose membranes were pre-soaked in PBS and remained in contact with the PBS receiver solution during the permeation runs, the nature of the membrane was not affected by switching the donor solvent. For the cellulose membranes, the final values of all partition and diffusion coefficients listed in Table 3.2 refer to the PBS-saturated membrane rather than “dry” cellulose. Further evidence for the lack of this type of solvent effect arises from the observation that a single value of  $D$  successfully accounts for both PBS and squalane as donor solvent for all the membrane/permeant combinations. A scenario whereby the donor solvent is shown to cause significant swelling of the membrane has been investigated and is described later in section 3.3.

The third type of solvent effect which may invalidate this model assumption occurs when the donor and receiver solvents are mutually miscible to a significant extent and

can permeate the membrane during a permeation run. In this case, the solvent compositions of both the donor and receiver compartment will change during a permeation run. Such time-dependent solvent compositions will cause time-dependent changes in the partition coefficients which, in turn, will cause deviations from the predicted exponential behaviour. This possibility can be excluded for the experimental systems measured here since aqueous PBS and squalane are not miscible to any significant extent at 32°C. A scenario whereby two mutually miscible donor and receiver solvents are used during the membrane permeation studies has been investigated and thus, this effect is observed. The results from these additional studies are described later in section 3.4.

#### 3.2.5.5 Non-ideal behaviour of the permeant solutions

As noted above, the model derivation assumes that all partition coefficients (expressed as the ratio of equilibrium concentrations equal to the apparent value of  $K$ ) are single-valued and independent of concentration. In fact, only the thermodynamic partition coefficient equal to the ratio of activities is a true constant; non-ideal solution behaviour can cause the apparent partition coefficient to be a function of permeant concentration, and hence time, during a membrane permeation run. Because solution non-ideality depends on the balance of solvent-solvent, solvent-solute and solute-solute interactions, it should always be considered as a possible contribution to an observed, overall donor solvent effect in permeation. All solutions behave ideally in the limit of infinite dilution and hence activity coefficients are likely to progressively deviate from unity with increasing concentration which, in turn, may cause changes in the apparent  $K$  values at higher concentrations. If the concentration change during a permeation experiment causes a significant change in the apparent  $K$  value, then this alteration in  $K$  during the run is predicted to lead to deviations from the exponential form of the  $C_{\text{rec}}$  versus time plot. If the apparent  $K$  value is constant over the concentration range of the permeation run but was measured at a different concentration, then exponential behaviour is predicted but the measured apparent  $K$  value may not equal the value appropriate for the analysis of the specific permeation run. To avoid both types of potential error, it is recommended to measure the apparent  $K$  value as a function of concentration. Overlaying the concentration ranges of the permeation runs then enables proper selection of the apparent  $K$  value which is appropriate to the permeation run(s).

The application of this approach to the experimental systems studied here is shown in Figures 3.2, 3.3 and 3.4. It can be seen there that the practice of estimating an apparent  $K$  value from the ratio of permeant solubilities in the two solvents is not recommended; the resultant apparent  $K$  value refers to the maximum accessible concentrations where non-ideality effects will, in general, be largest.

For the systems studied here, Figures 3.2, 3.3 and 3.4 show that approximately constant apparent  $K$  values, which are appropriate to the concentration ranges of the permeation runs, can be selected for most systems. The exception is caffeine partitioning between PBS and a cellulose membrane where non-ideality effects are large over the relevant concentration range. In this case, the data of Figure 3.4 were used to obtain different apparent  $K$  values which were approximately valid for the average concentration range of the different individual permeation runs with different initial permeant concentrations.

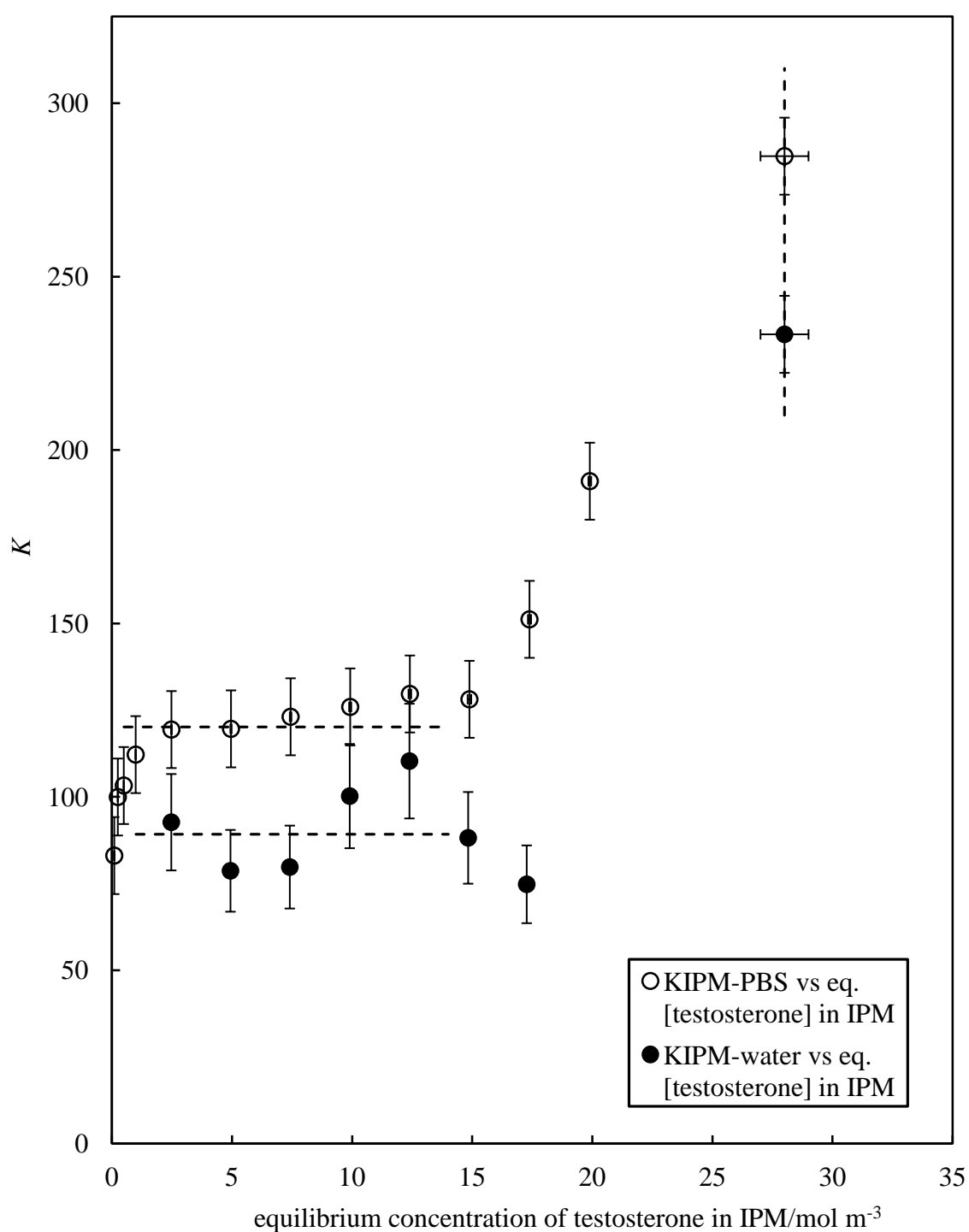
### **3.3 Membrane permeation studies influenced by undesired solvent-membrane interactions**

As discussed previously, one solvent effect which may lead to the invalidation of the underlying assumptions of the theoretical model, arises from a chemical incompatibility between the donor solvent and the membrane. Presented below is a study whereby the chosen donor solvent (IPM) is absorbed by the chosen membrane (PDMS) within the time-scale of a permeation run, causing a substantial increase in the membranes thickness, length, width and therefore a significant variation in the membranes chemical composition. The permeation of testosterone through PDMS membranes from aqueous (PBS and water) and oil (IPM) donor solutions has been investigated and the elucidation of this solvent effect is next described.

The solubility of testosterone in IPM was determined using UV-visible spectrophotometry and was found to be 28 mM at 32°C. As expected, this solubility is far greater than that in PBS and water (0.098 mM and 0.12 mM respectively at 32°C). The partition coefficients,  $K_{\text{IPM-PBS}}$  and  $K_{\text{IPM-water}}$ , for testosterone, were measured over a range of concentrations producing the results illustrated in Figure 3.14. Within the estimated uncertainties, the values of these partition coefficients are shown to be independent of overall testosterone concentration for solutions within the range of 1–15

mM, suggesting that possible non-ideality effects are negligibly small over this concentration range. However, Figure 3.14 also illustrates that outside of this concentration range, large deviations in the values of these partition coefficients are observed. As expected, these deviations increase with increasing testosterone concentration, until the values for the partition coefficients, corresponding to the ratios of the solubilities of testosterone in the respective solvents, is reached. Figure 3.14 again illustrates the importance of this vigorous analysis to determine the relevant partition coefficient values depending upon the concentration of the permeant used in the permeation runs. For the permeation investigations presented here, all testosterone concentrations were maintained within a 1–15 mM range, such that a single value of the relevant partition coefficients can be assigned. The concentration-independent average values of the respective partition coefficients, indicated by the horizontal lines in Figure 3.14 were used in the analysis of the membrane permeation results.

**Figure 3.14.** Variation of measured testosterone partition coefficients at 32°C between IPM and PBS (open circles) or IPM and water (filled circles) with equilibrium testosterone concentration in the IPM phase. For each data series, the respective horizontal dashed line indicates the testosterone concentration range used in the permeation experiments and the corresponding average value of  $K$  over the experimental concentration range. The vertical dashed line indicates the solubility of testosterone in IPM for which  $K$  is taken to be the ratio of the solvent solubilities.



A summary of all relevant partition coefficients for the analysis of permeation runs involving an IPM donor solution is given in Table 3.3. The value for testosterone's  $K_{\text{PDMS-IPM}}$  partition coefficient could not be measured using the described depletion method but is derived from testosterone's  $K_{\text{PDMS-PBS}}$  and  $K_{\text{IPM-PBS}}$  concentration-independent partition coefficients as shown in equation 3.18. The ideality of testosterone's  $K_{\text{PDMS-PBS}}$  partition coefficient is illustrated previously in Figure 3.3.

$$K_{\text{PDMS-IPM}} = \frac{C_{\text{PDMS}}}{C_{\text{IPM}}} = \frac{C_{\text{PDMS}}}{C_{\text{PBS}}} \frac{C_{\text{PBS}}}{C_{\text{IPM}}} = \frac{K_{\text{PDMS-PBS}}}{K_{\text{IPM-PBS}}} \quad (3.18)$$

**Table 3.3.** Equilibrium partition coefficients for testosterone measured at 32°C used to obtain the calculated values of  $C_{\text{rec},\infty}$  and  $k$  for membrane permeation studies involving an IPM donor solution.

Parameter	Value	Comment
$K_{\text{IPM-PBS}}$	124±5	Measured
$K_{\text{IPM-water}}$	92±15	Measured
$K_{\text{PDMS-water}}$	3.7±1	Measured
$K_{\text{PDMS-PBS}}$	5±2	Measured
$K_{\text{PDMS-IPM}}$	0.04±0.01	Derived from measured $K$ values
$K_{\text{PBS-water}}$	0.74±0.15	Derived from measured $K$ values

Figure 3.14 and Table 3.3 illustrate that testosterone has a greater affinity for dissolution within IPM than within PBS by a magnitude of approximately 125. Similarly, testosterone is shown to favour dissolution within a hydrophobic PDMS membrane over that of PBS by a magnitude of 5, and hence, has an affinity for dissolution within a PDMS membrane over IPM by a magnitude of 0.04 (i.e. 1/25).

With reference to equation 3.12 (repeated below), which is used to accurately predict the rate coefficient of membrane permeation of a solute from a solution, it is noted that when the system geometrical parameters, initial donor solution concentrations and permeant diffusion coefficients remain constant, the rate of transport of testosterone across a PDMS membrane from a PBS donor solution, is expected to be approximately double that from an IPM donor solution, in accordance with the relevant system partition coefficients. This is illustrated in Table 3.4.

$$\frac{kXV_{\text{rec}}}{AD} = K_{\text{mem-don}} + K_{\text{mem-rec}} \quad (3.12)$$

**Table 3.4.** Dimensionless permeation rate coefficients calculated using the respective permeant partition coefficients for testosterone in PBS and IPM donor solutions, permeating through a PDMS membrane into a PBS receiver phase at 32°C.

Donor solution	$K_{\text{mem-don}}$	$K_{\text{mem-rec}}$	Dimensionless permeation rate coefficient ( $kXV_{\text{rec}}/AD$ )
Testosterone in PBS	5	5	10
Testosterone in IPM	0.04	5	5.04

An example of the permeation curves obtained for testosterone permeating through PDMS membranes from IPM and PBS donor solutions is given in Figure 3.15. When comparing these two permeation curves, it is important to note that the initial concentration of testosterone in the two permeation experiments is not equal. This difference in permeant concentration is compulsory, as membrane permeation of hydrophobic testosterone, from oil donor solutions of IPM, into aqueous receiving solutions of PBS is disfavoured, as denoted by the equilibrium partition coefficient  $K_{\text{don-rec}}$ , where  $K_{\text{IPM-PBS}} = 124$ . Hence, if donor solutions of IPM with testosterone concentrations equal to those in the PBS donor solutions (which are restricted by the relatively low solubility of testosterone in PBS) were used, then the concentration of testosterone detected in the receiving phase would be at least 124 times smaller than these already low initial donor concentrations. In fact, the observed concentrations of testosterone in the receiving phase of this experimental investigation would be more than 124 times smaller than the initial IPM donor concentration because a small amount of testosterone will, in addition, partition to the hydrophobic membrane volume. Thus, permeant detection with the UV-visible spectrophotometer would become poor and high in error.

However, as predicted and illustrated previously in Figure 3.5, the value of the 1<sup>st</sup>-order permeation rate coefficient  $k$  is independent of the initial permeant concentration in the donor compartment. Thus, with reference to equation 3.12, it remains to be expected that the permeation of testosterone from a PBS donor solution should be more

rapid than that from an IPM donor solution, irrespective of this initial permeant concentration difference.

Figure 3.15 shows measured plots of  $C_{\text{rec}}$  versus time for the permeation of testosterone through PDMS membranes from both IPM and PBS donor solutions. It is noted here that both systems are described exceedingly well by exponential curves, as illustrated by the precision of data fitting. As denoted by the half lives of these exponential curves, it is apparent that the permeation of testosterone through PDMS from IPM donor solutions is significantly faster than that from PBS donor solutions. Hence, this observation contradicts the predictions made previously. Figure 3.16 shows plots of measured vs. calculated values of  $C_{\text{rec},\infty}$  and  $k$  for the permeation of testosterone through PDMS membranes from IPM, PBS and water donor solutions. The calculated data, produced from equations 3.9 and 3.10, is derived from the corresponding partition coefficient values listed in Table 3.3. Given that it has been concluded that the permeant membrane diffusion coefficient is independent of donor solvent type, these calculations utilize testosterone's diffusion coefficient through PDMS membranes ( $D = 9.3 \times 10^{-12} \text{ m}^2 \text{ s}^{-1}$ ) as listed previously in Table 3.2. The measured data is extracted from the raw experimental data via the use of the Microsoft EXCEL solver function, as formerly described.



**Figure 3.15.** Measured variation of receiver compartment concentration  $C_{\text{rec}}$  with time for testosterone in donor solutions of IPM (blue solid line) and PBS (red solid line) permeating through PDMS membranes at 32°C. The initial donor concentrations of testosterone are shown in the key. The dashed lines correspond to the best-fit to the exponential function described by equation 3.8.

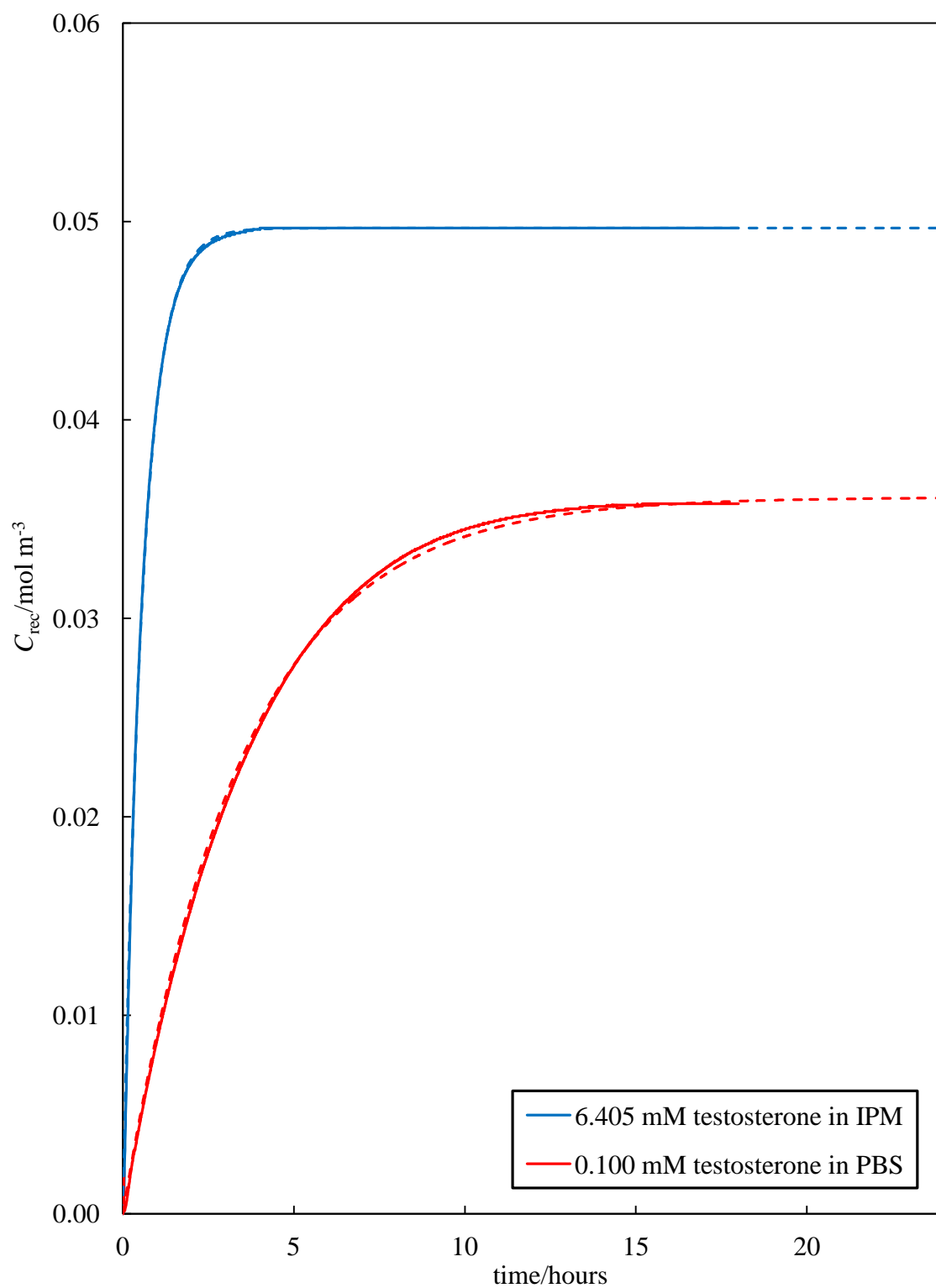
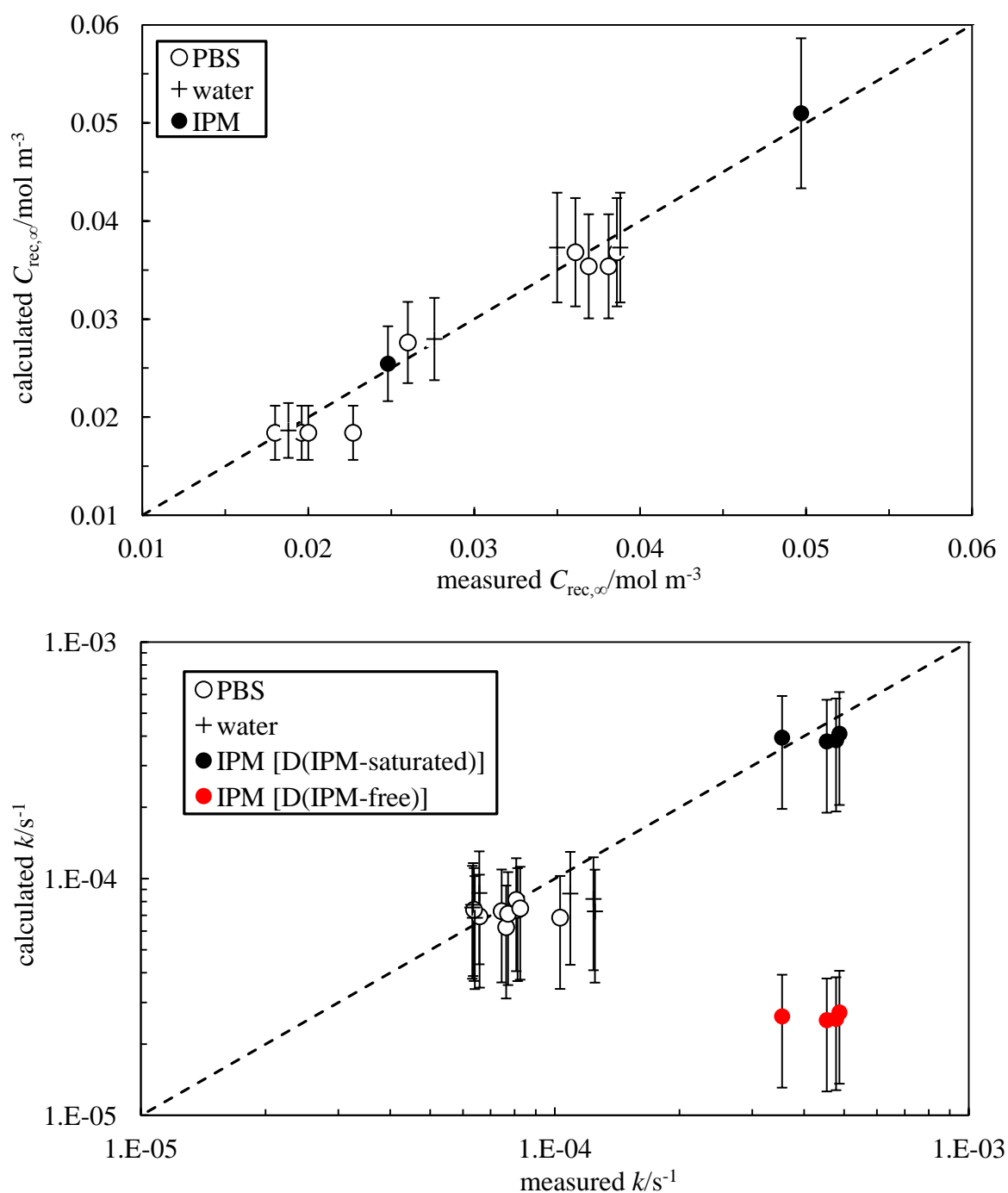


**Figure 3.16.** Comparison of measured and calculated values of the equilibrium fraction of permeant extracted to the receiver compartment  $C_{\text{rec},\infty}$  (upper plot) and the 1<sup>st</sup>-order permeation rate constant  $k$  (lower plot) for testosterone permeating through PDMS membranes from PBS, water and IPM donor solutions. In the lower plot, calculated data for testosterone in IPM donor solutions incorporating both the diffusion coefficient  $D$  for IPM-free PDMS membranes [ $D(\text{IPM-free}) = 9.3 \times 10^{-12} \text{ m}^2 \text{ s}^{-1}$ ] (red filled circles) and IPM-saturated PDMS membranes [ $D(\text{IPM-saturated}) = 1.4 \times 10^{-10} \text{ m}^2 \text{ s}^{-1}$ ] (black filled circles), is shown.



Inspection of Figure 3.16 reveals that the calculated values of  $k$  for testosterone permeating through PDMS membranes from IPM donor solutions, are approximately 10 times lower than the experimentally measured values when calculated using the permeant membrane diffusion coefficient from the previous study (i.e.  $D = 9.3 \times 10^{-12} \text{ m}^2 \text{ s}^{-1}$ ). The calculated values of  $k$  for PBS and water donor solutions and the calculated values of  $C_{\text{rec},\infty}$  for IPM, PBS and water donor solutions, accurately describe the experimental observations. In experiments where the PDMS membrane was soaked in IPM, it was observed that the membrane swelled causing an increase in length, width and depth, each by approximately 20% in 1 day. It is concluded therefore, that the calculated and measured data for all permeation experiments of testosterone from PBS, water and IPM donor solutions, through PDMS membranes, cannot be fitted using a single value of testosterone's membrane diffusion coefficient  $D$ . Hence, different values of  $D$  are required for donor solutions in the absence of IPM [ $D(\text{IPM-free}) = 9.3 \times 10^{-12} \text{ m}^2 \text{ s}^{-1}$ ] (i.e. the value described in Table 3.2) and donor solutions of IPM [ $D(\text{IPM-saturated}) = 1.4 \times 10^{-10} \text{ m}^2 \text{ s}^{-1}$ ]. The value of  $D$  for the IPM-saturated PDMS membranes is selected by allowing it to float when optimising the exponential fit using Microsoft EXCEL's solver function. This effect is thought to be caused by the penetration/swelling of the PDMS membrane by the IPM solvent, leading to an increased permeation rate as observed in other studies.<sup>12</sup> Using the final parameter set listed in Table 3.3 and the two values of testosterone's diffusion coefficient for IPM-free and IPM-saturated PDMS membranes, the correlation between measured and calculated values of  $C_{\text{rec},\infty}$  and  $k$  show good agreement. The calculated data for IPM donor solutions, incorporating this refined value of the diffusion coefficient for testosterone in IPM-saturated PDMS membranes is also plotted on Figure 3.16 for a comparative purpose.

Figure 3.16 again illustrates that the theoretical model successfully captures the influence of the donor solvent on the extent and rate of membrane permeation. In addition to fitting the relevant data by incorporating a second value of  $D$  for IPM-saturated PDMS membranes, it is also appropriate to consider variations in the values of testosterone's  $K_{\text{mem-don}}$  and  $K_{\text{mem-rec}}$  partition coefficients, as the chemical composition of the PDMS membranes is shown to vary in the presence of IPM. This effect has been investigated showing that by allowing these partition coefficient values to appropriately adjust within a reasonable range, for testosterone partitioning to IPM-

saturated PDMS membranes, does allow for the fitting of the theoretical model to be improved slightly. However, as discussed previously, time dependent changes in these partition coefficient values would give rise to a loss of exponentiality. Given that the permeation data is described exceedingly well by exponential curves, as predicted and shown by the dashed lines in Figure 3.15, it is concluded that this effect is minor.

### **3.4 Membrane permeation studies influenced by mutually miscible, dissimilar donor and receiver solvents**

As discussed previously, another solvent effect which may lead to the invalidation of the underlying assumptions of the theoretical model arises from a mutual miscibility between different donor and receiver solvents. In the derivation and application of the theoretical model, it is assumed that only the permeant species under analysis permeates the membrane. If a chosen donor solvent is dissimilar to the chosen receiver solvent, and the two solvents are miscible with each other, a series of events can occur leading to the invalidation of this assumption. If the donor and receiver solvents are capable of permeating the membrane within the same timescale as the permeant under analysis, and this mixture of solvents is susceptible to absorbing UV/visible light at the same corresponding wavelength as the permeant, then this will in-turn create errors in the analytical technique employed here. Furthermore, this time-dependent mixing of dissimilar donor and receiver solvents will result in a time-dependent set of  $K_{\text{mem-don}}$ ,  $K_{\text{mem-rec}}$  and  $K_{\text{don-rec}}$  permeant partition coefficients, such that they eventually equilibrate when both the donor and receiver solutions have equal chemical composition and hence,  $K_{\text{mem-don}} = K_{\text{mem-rec}}$  and  $K_{\text{don-rec}} = 1$ . Presented below is a permeation study whereby the chosen donor solvent (PG) is mutually miscible with the chosen receiver solvent (PBS), illustrating the key observations of such events and the corresponding resolutions.

In a similar method to that demonstrated previously, the experimental data for testosterone and caffeine permeating through PDMS membranes from PG donor solutions, is analysed via comparison to the calculated data predicted using equations 3.9 and 3.10 of the theoretically derived model.

The solubility of the permeants in PG is investigated prior to the analysis of the relevant system partition coefficients. The solubilities of testosterone and caffeine in

PG at 32°C were found to be 248.62 mM and 11.69 mM respectively. Upon further analysis, it is noted here that testosterone's solubility in PG is far greater than that of both caffeine and testosterone in any other solvent used in the permeation studies presented here, as illustrated in Table 3.4.

**Table 3.4.** A summary of all caffeine and testosterone solubilities within the different solvents used in this research at 32°C.

Permeant	Solvent	Solubility at 32°C/mM
Testosterone	Water	0.12
Testosterone	PBS	0.098
Testosterone	Squalane	0.81
Testosterone	PG	248.62
Testosterone	IPM	28.00
Caffeine	Water	140.19
Caffeine	PBS	122.25
Caffeine	Squalane	0.48
Caffeine	PG	11.69

As described previously, calculation of the theoretical data via use of the derived model, requires knowledge of the relevant  $K_{\text{mem-don}}$  and  $K_{\text{mem-rec}}$  permeant partition coefficients. In the scenario described here, this respectively corresponds to testosterone and caffeine's  $K_{\text{PDMS-PG}}$  and  $K_{\text{PDMS-PBS}}$  partition coefficients. The value for testosterone and caffeine's  $K_{\text{PDMS-PG}}$  partition coefficients could not be measured using the described depletion method, due to testosterone's excessively large affinity to PG and caffeine's low affinity to the PDMS membrane. These values are therefore derived from the respective  $K_{\text{PG-squalane}}$  (see Figure 3.17) and  $K_{\text{PDMS-squalane}}$  concentration-independent partition coefficients, as shown in equation 3.19. The ideality of testosterone and caffeine's  $K_{\text{PDMS-squalane}}$  partition coefficients are illustrated previously in Figure 3.3.

$$K_{\text{PDMS-PG}} = \frac{C_{\text{PDMS}}}{C_{\text{PG}}} = \frac{C_{\text{PDMS}}}{C_{\text{squalane}}} \frac{C_{\text{squalane}}}{C_{\text{PG}}} = \frac{K_{\text{PDMS-squalane}}}{K_{\text{PG-squalane}}} \quad (3.19)$$

Figure 3.17 illustrates the measured values of testosterone and caffeine's  $K_{\text{PG-squalane}}$  partition coefficients at 32°C. The values of these partition coefficients are shown to be concentration-independent across the range of concentrations used within the membrane permeation runs (illustrated by the horizontal dashed lines).

A summary of all relevant partition coefficient values required for the analysis of testosterone and caffeine permeating through a PDMS membrane from donor solutions of PG is given below in Table 3.5.

**Table 3.5.** Equilibrium permeant partition coefficients used to obtain the theoretical calculated data for the permeation of testosterone and caffeine from PG donor solutions through PDMS membranes at 32°C.

Permeant	Parameter	Value	Comment
Testosterone	$K_{\text{PDMS-PBS}}$	$5 \pm 2$	Measured
Testosterone	$K_{\text{PG-squalane}}$	$165 \pm 8$	Measured
Testosterone	$K_{\text{PDMS-squalane}}$	$0.8 \pm 0.2$	Derived from measured $K$ values
Testosterone	$K_{\text{PDMS-PG}}$	$4.9 \pm 1 \times 10^{-3}$	Derived from measured $K$ values
Caffeine	$K_{\text{PDMS-PBS}}$	$0.14 \pm 0.04$	Measured
Caffeine	$K_{\text{PG-squalane}}$	$94 \pm 9$	Measured
Caffeine	$K_{\text{PDMS-squalane}}$	$15 \pm 5$	Measured
Caffeine	$K_{\text{PDMS-PG}}$	$0.16 \pm 0.04$	Derived from measured $K$ values

**Figure 3.17.** Variation of the measured  $K_{\text{PG-squalane}}$  partition coefficients at 32°C with equilibrium permeant concentration in PG for testosterone (filled diamonds) and caffeine (open triangles). The horizontal dashed lines indicate the permeant concentration range used in the respective membrane permeation experiments and the corresponding average value of  $K_{\text{PG-squalane}}$  over this experimental permeant concentration range. The vertical dashed lines indicate the solubility values of the permeant for which  $K_{\text{PG-squalane}}$  was taken to be the ratio of solvent solubilities.

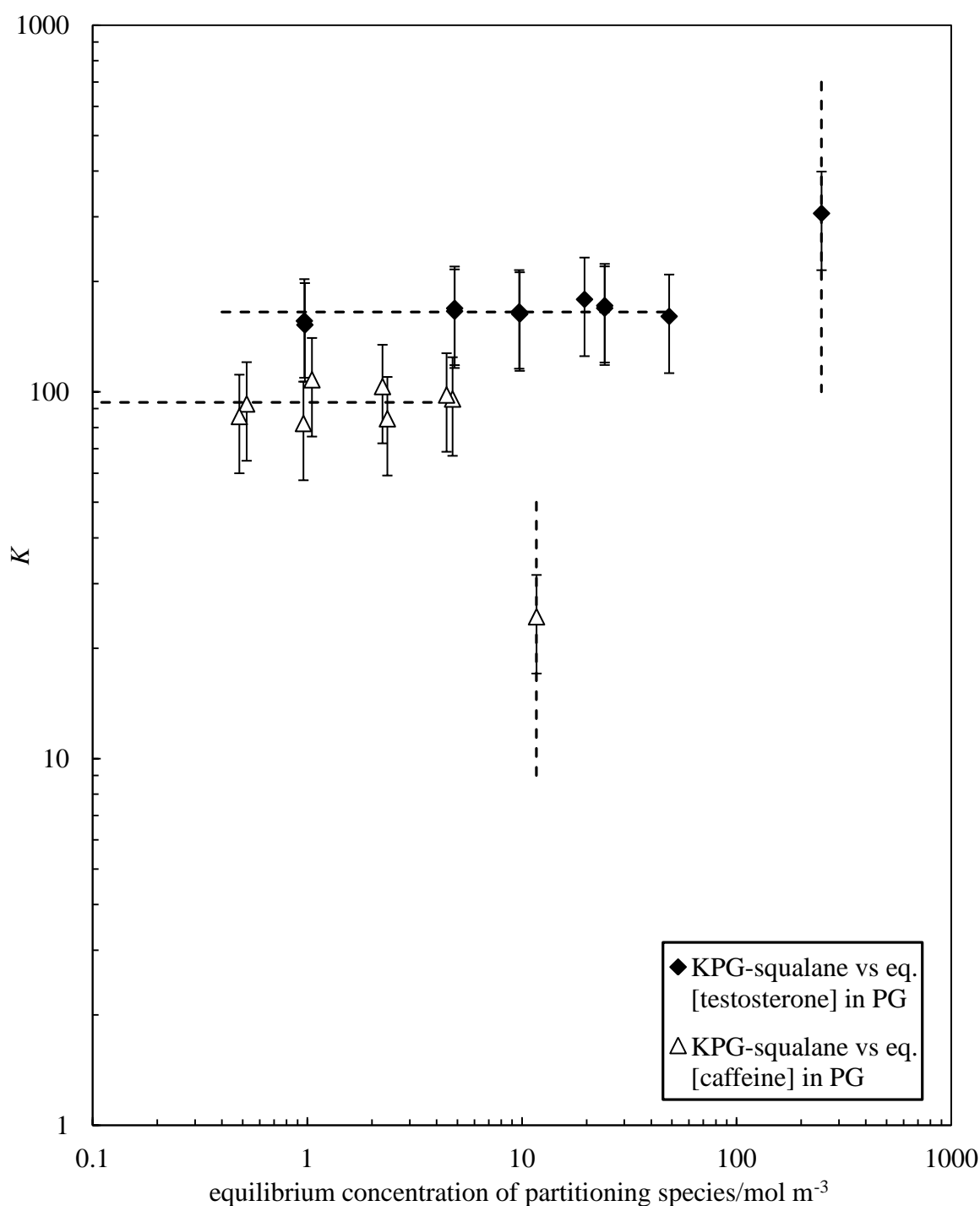
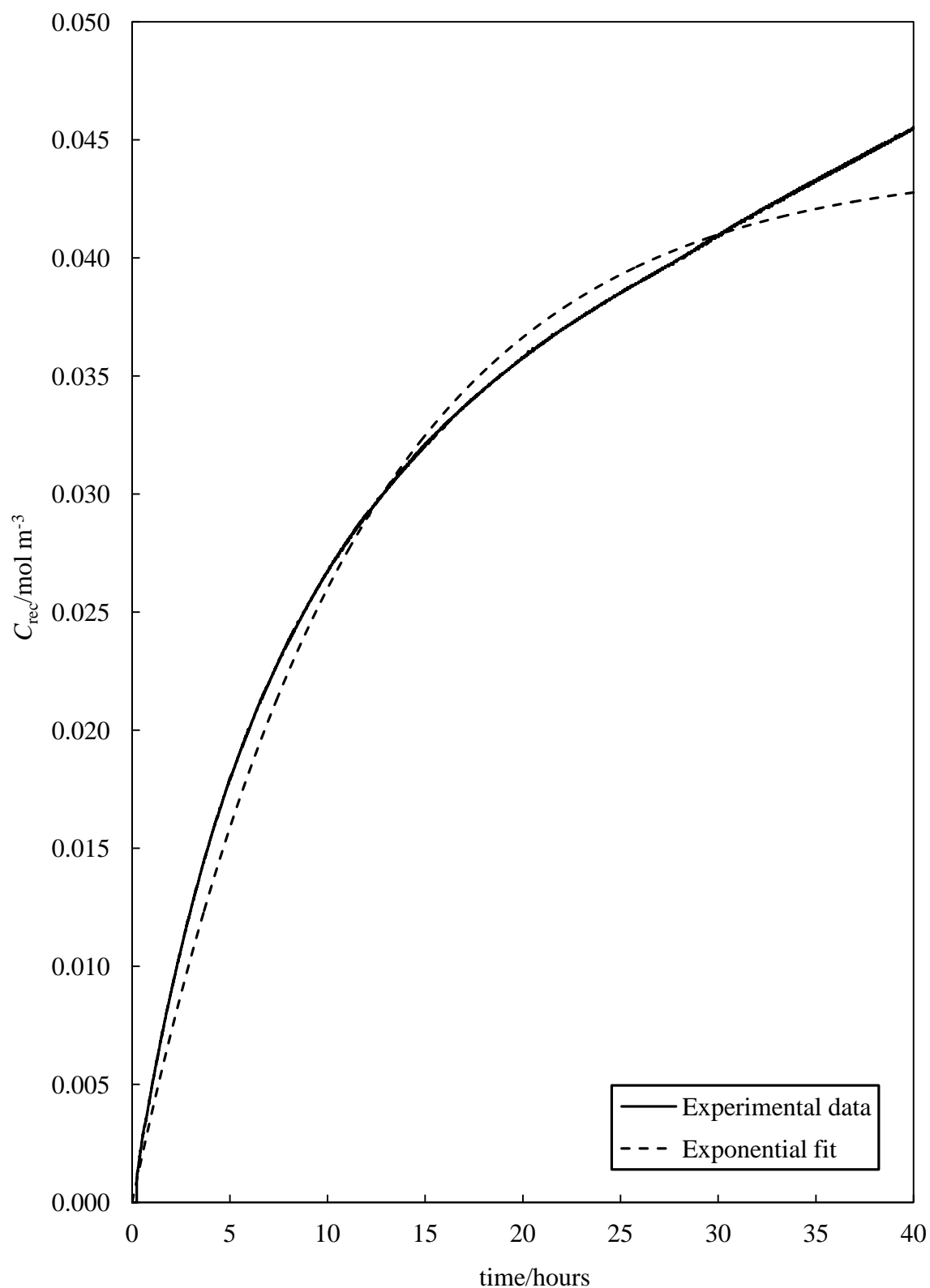


Figure 3.18 illustrates an example of the results obtained for the permeation of testosterone from a PG donor solution through a PDMS membrane and into a PBS receiver solution. The solid line indicates the experimental raw data obtained from this study and the dashed line corresponds to the best fit of an exponential curve to the raw data, which is predicted in accordance with equation 3.8. The loss of predicted exponentiality of the experimental raw data is eminent and is caused by several factors. Given that the PG donor solvent and PBS receiver solvent are miscible, and as formerly discussed, if these solvents are capable of permeating the PDMS membrane within the same time scale as the permeant under analysis, then this will yield a set of time-dependent values of  $K_{\text{mem-don}}$  and  $K_{\text{mem-rec}}$  corresponding to the extent of donor/receiver solvent mixing in both donor and receiver phases. It is also noted that the experimental raw data does not reach an equilibrium  $C_{\text{rec},\infty}$  value within the 40 hour timescale. This is in accordance with the solubility of testosterone in the receiver phase gradually increasing as the concentration of PG in this phase, having permeated the PDMS membrane, increases also.



**Figure 3.18.** Variation of  $C_{\text{rec}}$  versus time for the permeation of testosterone through a PDMS membrane from an initial donor solution of PG of testosterone concentration 35 mM, into an initial receiver solution of PBS, at 32°C. The dashed line indicates the “best-fit” exponential curve predicted by the theoretical model (equation 3.8).



In order to study systems incorporating donor solutions of PG, the issue of simultaneous permeant and solvent permeation through the membrane, arising from a mutual miscibility between the donor and receiver solvents, must be overcome. One method which may be employed to resolve this difficulty, is to select a receiver solvent which is known to be sufficiently immiscible with the donor solvent. In the scenario presented here, a squalane receiver solvent may be used as it is highly immiscible with PG at 32°C. Alternatively, the same solvent used for the donor phase may also be used for the receiver phase, such that there is no concentration gradient of solvent across the membrane and thus no net diffusion of the donor and receiver phases through the membrane. Such experimental conditions yield time-independent values of the  $K_{\text{mem-don}}$  and  $K_{\text{mem-rec}}$  permeant partition coefficients and compel the value of  $K_{\text{don-rec}}$  such that  $K_{\text{don-rec}} = 1$  at all times during the membrane permeation run.

Figure 3.19 illustrates the results obtained from membrane permeation studies of testosterone and caffeine in donor solutions of PG, permeating through PDMS membranes into receiver solutions also consisting of PG. With reference to Table 3.5, these experimental conditions therefore yield the values  $K_{\text{mem-don}}$  and  $K_{\text{mem-rec}} = K_{\text{PDMS-PG}} = 4.9 \times 10^{-3}$  and 0.16 for testosterone and caffeine respectively. In consideration of equation 3.12 of the theoretical model described previously, it is therefore predicted that the rate of caffeine permeation from PG donor solutions through PDMS membranes into PG receiver solutions, should be similar to that of caffeine in PBS donor solutions permeating PDMS membranes into PBS receiver solutions. Conversely, the rate of testosterone permeation from PG donor solutions through PDMS membranes into PG receiver solutions is predicted to be slower further still, as illustrated in Table 3.6.

**Table 3.6.** Dimensionless permeation rate coefficients calculated using equation 3.12 and the respective permeant partition coefficients for testosterone and caffeine permeating through PDMS membranes at 32°C.

System	$K_{\text{mem-don}}$	$K_{\text{mem-rec}}$	Dimensionless permeation rate coefficient ( $kXV_{\text{rec}}/AD$ )
Caffeine in PBS donor, through PDMS, into PBS receiver	0.14	0.14	0.28
Caffeine in PG donor, through PDMS, into PG receiver	0.16	0.16	0.32
Testosterone in PG donor, through PDMS, into PG receiver	$4.9 \times 10^{-3}$	$4.9 \times 10^{-3}$	$9.8 \times 10^{-3}$

In accordance with the predictions made here, Figure 3.19 illustrates that the permeation rates of both testosterone and caffeine from PG donor solutions through PDMS membranes into PG receiver solutions, are so slow that the full exponential curves are not observed over the 20 hour timescale of the experimental runs. Like that discussed previously for the permeation of caffeine in PBS donor solutions through PDMS membranes into PBS receiver solutions, the measured plots illustrated in Figure 3.19 correspond to the permeation of only a small fraction of the total permeant present and are approximately linear. The gradients of these individual lines correspond to the initial steady-state permeation rates of the respective systems, which, according to the theoretical model, are predicted to scale with initial donor phase concentration, with the constant of proportionality equal to the permeation rate coefficient  $k$ . The linear scaling of initial steady-state permeation rate with initial permeant concentration is shown in Figure 3.20 and hence, the gradients of these linear plots are equal to the 1<sup>st</sup>-order permeation rate coefficients  $k$ .

**Figure 3.19.** Measured initial rate of change of receiver compartment permeant concentration  $C_{\text{rec}}$  with time for testosterone (upper plot) and caffeine (lower plot) permeating through PDMS membranes from PG donor solutions into PG receiver solutions at 32°C. The initial donor compartment concentrations of the permeants (in descending order) are shown in the keys.

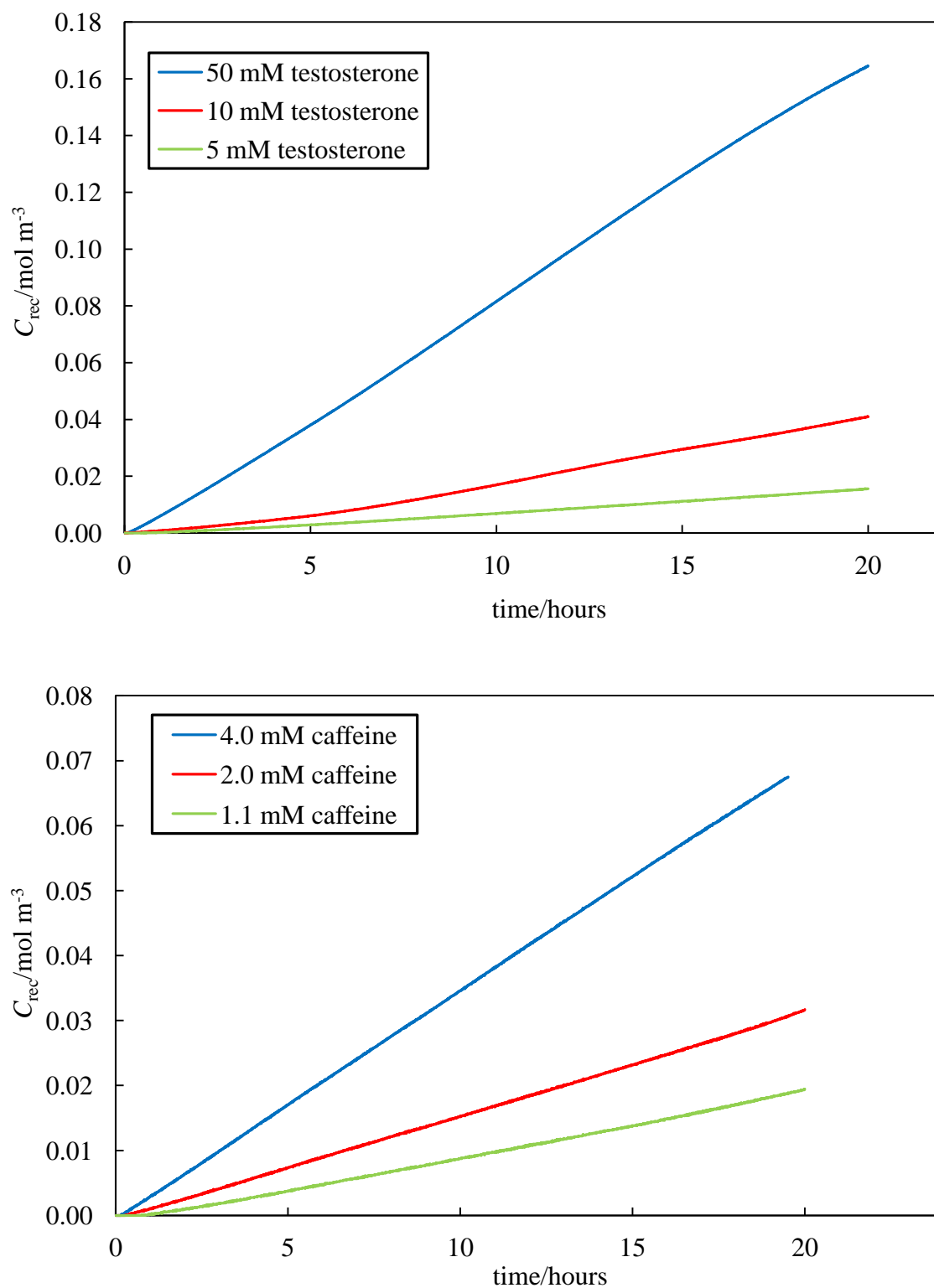
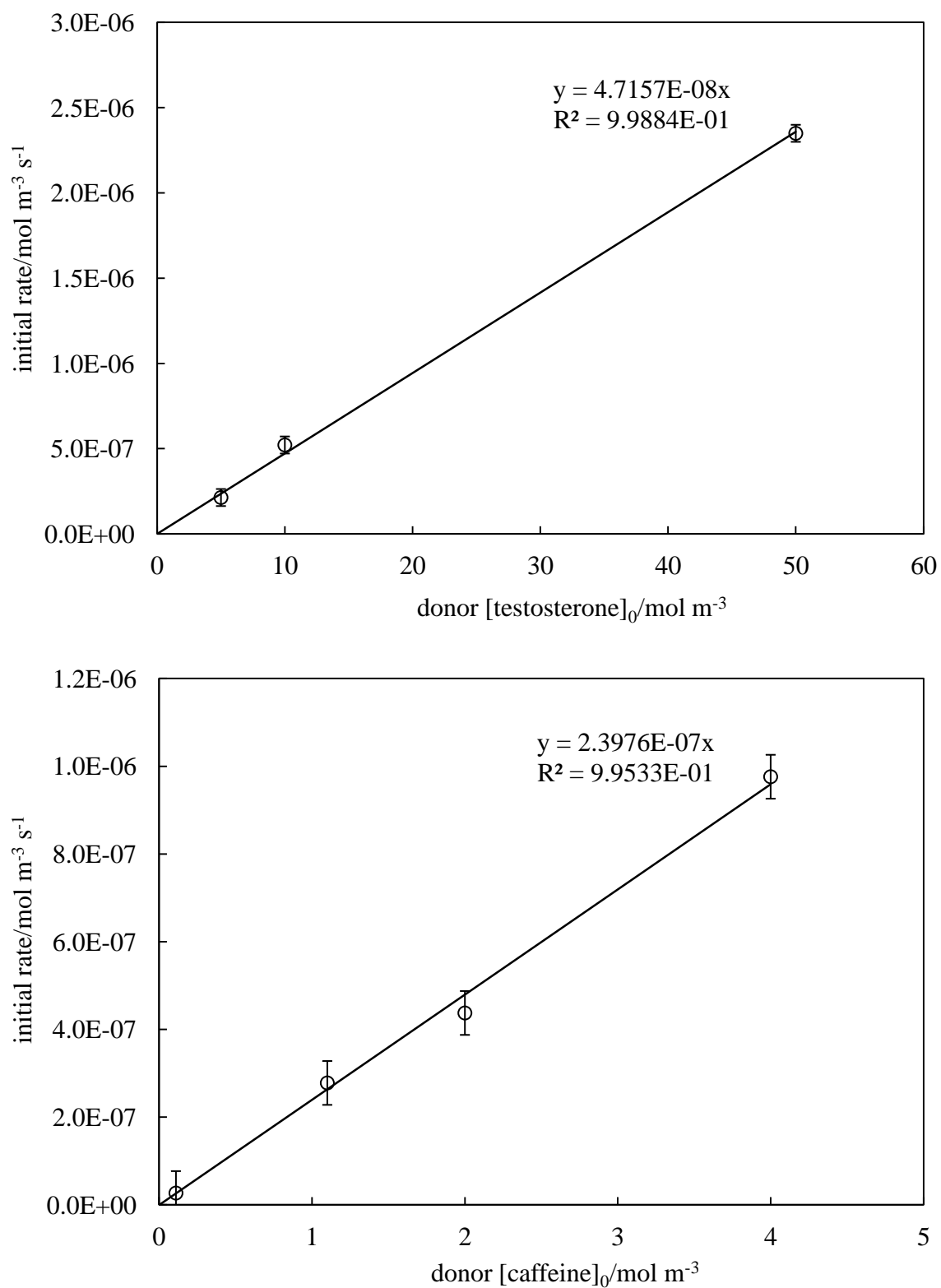


**Figure 3.20.** Derived variation of initial steady-state permeation rates for testosterone (upper plot) and caffeine (lower plot) permeating through PDMS membranes from PG donor solutions into PG receiver solutions versus initial donor concentration. The solid lines show the linear fits used to obtain the respective values of  $k$ .



Investigations into the chemical compatibility between solutions of PG and the PDMS membrane illustrate that no significant swelling of the membrane is present after 72 hours submersion. Therefore, it follows that calculations of the theoretical values of the 1<sup>st</sup>-order permeation rate coefficients  $k$  incorporate the use of the membrane diffusion coefficients for testosterone and caffeine through non-swollen, chemically unaffected PDMS membranes, which were originally listed in Table 3.2 (i.e.  $D = 9.3 \times 10^{-12} \text{ m}^2 \text{ s}^{-1}$  and  $1.6 \times 10^{-12} \text{ m}^2 \text{ s}^{-1}$  for testosterone and caffeine respectively). This is supported by the fact that the permeant membrane diffusion coefficient is dependant only on (i) the size and shape of the permeating species, which are constant irrespective of the donor and receiver solvents used, and (ii) the viscosity of the membrane, which is assumed to be constant and equal to the viscosity of the membranes used in all previously discussed studies absent of IPM, given that no swelling of the PDMS membrane is observed during submersion within a solution of PG.

The comparison of the measured and theoretical 1<sup>st</sup>-order permeation rate coefficients for testosterone and caffeine in PG donor solutions permeating through PDMS membranes into PG receiver solutions, is shown as plots of calculated versus measured values of  $k$  in Figure 3.21. For comparative purposes, the data for all permeant/solvent/membrane systems described in this chapter is also plotted in this Figure. The evaluation of measured and theoretical values of  $C_{\text{rec},\infty}$  for the systems incorporating a PG donor solution are absent due to experimental impracticalities illustrated by the exceedingly slow rate of membrane permeation in Figure 3.19. Figure 3.21 shows that the rate of caffeine permeation from PG donor solutions through PDMS membranes into PG receiver solutions, is very similar to the rate of caffeine permeation from PBS donor solutions through PDMS membranes into PBS receiver solutions, as predicted in Table 3.6. Furthermore, in accordance with these predictions, the rate of membrane permeation of testosterone from PG donor solutions through PDMS into PG receiver solutions, is shown to be the slowest of all permeant/solvent/membrane systems investigated here.

**Figure 3.21.** Comparison of measured and calculated values of the 1<sup>st</sup>-order permeation rate coefficients  $k$  for testosterone and caffeine permeating through PDMS membranes from PG donor solutions into a PG receiver solvent (red markers). For a comparative purpose, the data from all other permeation runs of varied combinations of permeant, donor solution solvent and membrane, all incorporating a PBS receiver phase, are also illustrated (black markers). The dashed line indicates perfect agreement between theory and experiment.

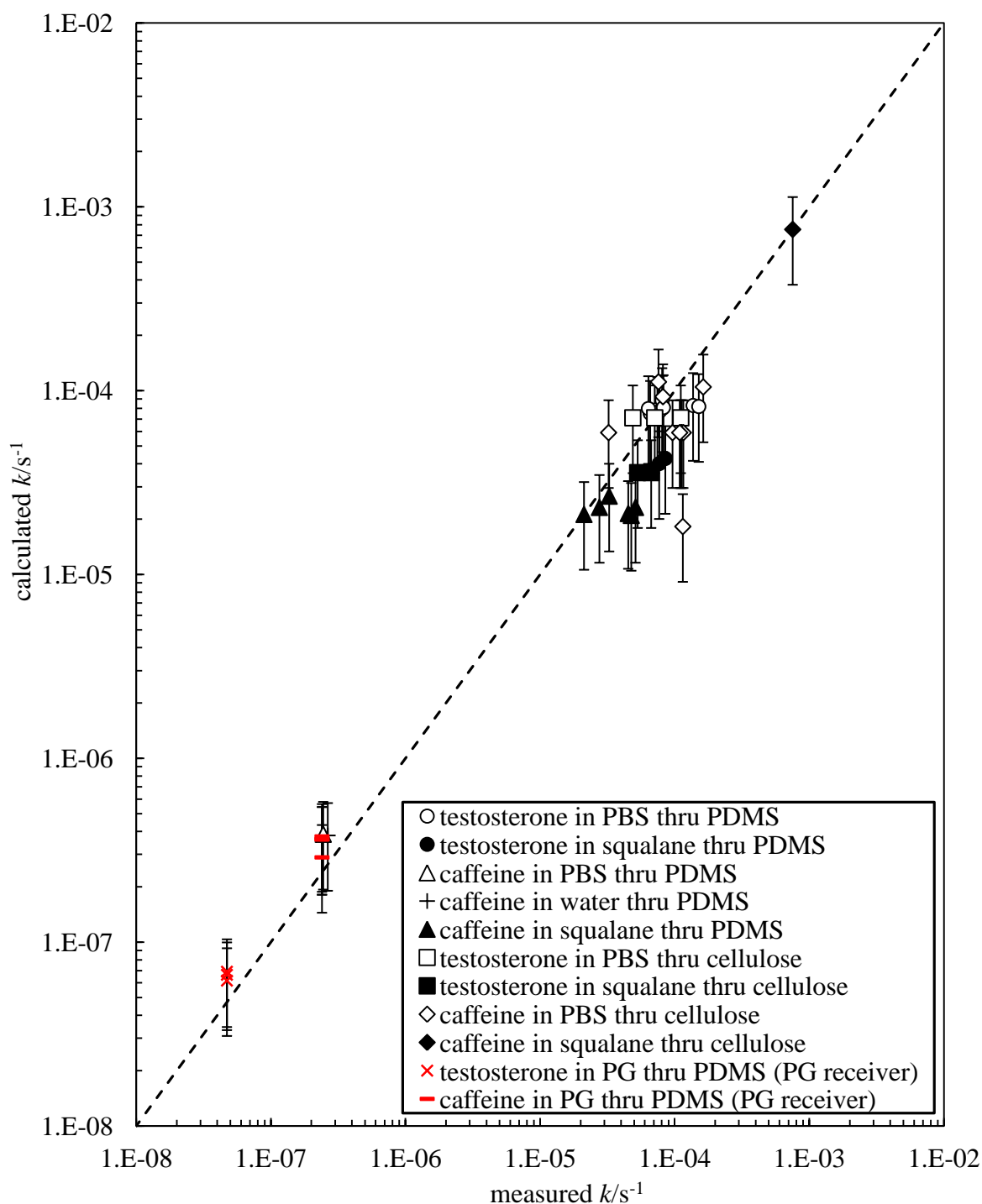


Figure 3.21 again illustrates that the theoretical model successfully captures the effects of changing the donor solvent, permeant and membrane, but also successfully accounts for variations in the chosen receiver solvent by application of the relevant  $K_{\text{mem-don}}$  and  $K_{\text{mem-rec}}$  permeant partition coefficients. Such variations in the chosen receiver solvent may often be required to overcome undesired simultaneous solvent/permeant membrane permeation, as illustrated here, in order to understand the permeation characteristics of a specific experimental system. The theoretical model is illustrated to accurately account for such variations across nearly 5 orders of magnitude by incorporating multiple independently measured parameters and a single, systematically fitted value of  $D$  for each permeant/membrane combination irrespective of the solvents used.

Preliminary investigations into the transport of permeants from PG donor solutions through cellulose membranes, illustrate that the undesired issue of simultaneous solvent/permeant membrane permeation is more problematic than in the scenario described above for permeation through PDMS membranes. As expected, solutions of polar PG and aqueous PBS more readily permeate through hydrophilic cellulose membranes which are already swollen with PBS, than through dry hydrophobic PDMS membranes. Consequently, permeation studies from PG donor solutions through cellulose membranes into PBS receiver solutions are highly impractical due to the arisen difficulties. In an attempt to substitute the PBS receiver phase for a PG receiver phase, like that described above, investigations into the chemical compatibility between solutions of PG and the cellulose membrane, illustrated that no significant swelling of the membrane is present after 72 hours submersion. This is dissimilar to previous studies concerning the use of PBS solvents whereby cellulose membranes were shown to almost double their thickness upon contact with PBS. Hence, in resolving the issue of simultaneous solvent/permeant membrane permeation by using PG as both donor and receiver solvents, a second problem is introduced as fitting of the theoretical and experimental data requires the introduction of additional membrane diffusion coefficients, corresponding to the permeation of testosterone and caffeine through unswollen cellulose membranes in the absence of PBS. For the purpose of the studies presented here, results concerning the permeation of testosterone and caffeine from donor solutions of PG through cellulose membranes are excluded, as such data



are hereby unnecessary to illustrate the accuracy of the derived theoretical model and understanding behind membrane permeation.

The different characteristics of membrane permeating systems incorporating PBS and PG receiver phases, cannot be directly compared with one another as they are each influenced by different experimental conditions, and hence, different  $K_{\text{mem-rec}}$  permeant partition coefficients. However, given that the theoretical model is rigorously shown to accurately predict both the extent and rate of membrane permeation for all possible combinations of permeant, membrane, donor solution and receiver solution investigated here, a prediction of the characteristics for testosterone and caffeine permeating through PDMS and cellulose membranes from PG donor solutions into PBS receiver solutions can be correctly drawn, irrespective of the experimental challenges otherwise faced. Table 3.7 illustrates an example of such predictions, whereby the permeation of testosterone from PG donor solutions through PDMS membranes into a PBS receiver phase cannot be accurately measured due to issues concerning simultaneous solvent/permeant membrane permeation, but theoretically can be precisely analysed and compared using the derived model.

**Table 3.7.** Comparison of the theoretical fractions of permeant extracted (calculated using equation 3.11) and the theoretical dimensionless permeation rate coefficients (calculated using equation 3.12). The respective permeant partition coefficients for testosterone permeating through PDMS membranes into a PBS receiver phase from various donor solution solvents at 32°C are also given.

<b>System</b>	$K_{\text{mem-don}}$	$K_{\text{mem-rec}}$	<b>Fraction of permeant extracted</b>	<b>Dimensionless permeation rate coefficient (<math>kXV_{\text{rec}}/AD</math>)</b>
Testosterone in PBS donor, through PDMS, into PBS receiver	5.0	5.0	0.50	10.0
Testosterone in squalane donor, through PDMS, into PBS receiver	0.8	5.0	0.14	5.8
Testosterone in PG donor, through PDMS, into PBS receiver	$4.9 \times 10^{-3}$	5.0	$9.79 \times 10^{-4}$	5.0

Table 3.7 illustrates that the rate of testosterone permeation from a PG donor solution through a PDMS membrane into a PBS receiver solution, is in fact similar to the rate of permeation from a squalane donor solution through a PDMS membrane into a PBS receiver solution, which becomes apparent with reference to the approximate half-life of the fitted exponential curve illustrated previously in Figure 3.18. However, as expected, the fraction of permeant extracted from a PG donor solution is considerably less than that from an equivalent squalane or PBS donor solution due to the high affinity of testosterone towards dissolution within the PG.

It may therefore seem puzzling that PG is often used as a component in pharmaceutical topical formulations to enhance both (i) the penetration of active permeants through the skin and (ii) the solubility of permeants within the formulation composition. The release of permeants, such as testosterone, from PG through synthetic PDMS membranes is highly disfavoured in comparison to that from other oil

topical vehicles, such as squalane, as assigned by the described partition coefficients and solvent strengths. However, the enhancement of penetration through the skin is thought to arise from the penetration of PG into the skin, decreasing the skin's barrier resistance<sup>18-19</sup> and hence, with respect to the model proposed here, varies the permeant diffusion coefficient within the skin like that observed previously for testosterone permeating through IPM-saturated PDMS membranes.

### **3.5 Theoretical modelling of membrane permeation from donor solutions into open, variable-volume receiver solutions**

As described in Chapter 2.2.4, the experimental permeation rate apparatus can be configured such that the receiving solution flows from a batch of pure solvent, past the underside of the permeation membrane, through the UV/visible spectrophotometer for permeant concentration analysis and then to an (open) waste volume. This experimental approach may be used to simulate, for example, with the use of a biological skin membrane, the dermal transport of a permeant across the skin and into the human body, whereby the volume of the receiver phase (i.e. the blood stream) is significantly larger than the volume of the applied donor phase. With respect to the analysis of the derived theory for membrane permeation through uniform synthetic membranes, it follows that the theoretical model presented here should account for the experimental observations made irrespective of the experimental setup and receiver compartment configuration. Hence, in the subsequent study, the derived model is systematically adapted to predict the extent and rate of membrane permeation observed for transport into an open receiver configuration. These systematic model adaptations ensure that the same portrayed mechanism of membrane permeation, assumptions and underlying principles, described previously in the model derivation, are obeyed at all times.

The investigations on membrane permeation into an open receiver phase configuration were conducted through the analysis of testosterone permeating from an IPM donor solution, through a hydrophobic PDMS membrane, into an aqueous PBS open receiver phase. At the time of experimental practice, the issue of membrane swelling by the oil donor solvent causing a variation in the permeant membrane diffusion coefficient was not fully recognised and hence was not avoided. However, no problems are introduced by this unawareness as the gathered data are appropriately

theoretically fitted via use of the previously described permeant membrane diffusion coefficient for testosterone permeating through IPM-saturated PDMS membranes (i.e.  $D(\text{IPM-saturated}) = 1.4 \times 10^{-10} \text{ m}^2 \text{ s}^{-1}$ ).

### 3.5.1 *Adapting the theoretical model to account for membrane permeation into open, variable-volume receiver solutions*

For the situation in which the receiver solution flows past the underside of the permeation membrane to a (open) waste volume, first consider the case in which the donor compartment permeant concentration ( $C_{\text{don}}$ ) is not significantly depleted over the experimental time scale (i.e.  $C_{\text{don}}$  is approximately constant). At times scales larger than the previously described lag time  $L$  (i.e. when the linear membrane permeant concentration gradient is established), it is shown below that  $C_{\text{don}}$  decreases exponentially with half-life  $t_{1/2}$ . Hence, the half-life  $t_{1/2}$  provides a characteristic time required to achieve a significant change in  $C_{\text{don}}$ . Therefore, for time-scales greater than  $L$  but less than  $t_{1/2}/10$ , it follows that the permeation is “steady state” but  $C_{\text{don}}$  has changed by less than 5%. As shown later,  $t_{1/2}$  is approximately 20 hours for the system studied here, and hence measurements of  $C_{\text{rec}}$  on time scales of between a few minutes (ensuring both the calculated lag time of approximately 18 seconds (calculated using equation 3.15) and the experimental error concerned with the initiation of the experiment, are both overcome) and around 100 minutes (calculated using  $t_{1/2}/10$ ) correspond to steady-state permeation at constant values of  $C_{\text{don}}$ . Therefore, under these conditions the permeant concentration in the flowing receiving solution ( $C_{\text{rec}}$ ) is time-independent.

To adequately simplify the model derivation for the transport of a permeant across a membrane into an open receiver phase, the fraction of the total permeant which is located within the membrane is neglected. In consideration of the experimental conditions used here, the membrane’s volume is approximately 0.2% of the total volume and the permeant (testosterone) partition coefficient to the membrane from the PBS receiver phase  $K_{\text{PDMS/PBS}} = 5$ . Hence, the fraction of the total permeant located within the membrane is insignificant (approximately 1%). In justifiably neglecting the permeant concentration within the membrane, mass balance requires that the number of moles of permeant diffusing across the membrane per second is equal to the number of

moles of permeant transported per second in the flowing receiver solution. Hence in maintaining accordance with Fick's first law, it follows that:

$$\left(\frac{AD}{X}\right)(C_{\text{mem,d}} - C_{\text{mem,r}}) = C_{\text{rec}} F = \left(\frac{AD}{X}\right)(K_{\text{mem-don}} C_{\text{don}} - K_{\text{mem-rec}} C_{\text{rec}}) \quad (3.20)$$

where  $F$  is the volumetric flow rate of the receiver compartment solution. Rearrangement of equation 3.20 then yields an expression given by equation 3.21 for how the measured concentration  $C_{\text{rec}}$  depends on the volumetric flow rate of the receiver compartment for short-time runs in which  $C_{\text{don}}$  remains approximately constant.

$$C_{\text{rec}} = \left( \frac{ADK_{\text{mem-don}} C_{\text{don}} / (XF)}{1 + ADK_{\text{mem-rec}} / (XF)} \right) \quad (3.21)$$

In further development of the theoretical model for the transport of a permeant across a membrane and into an open receiver phase configuration, an expression is subsequently derived to predict how  $C_{\text{rec}}$  varies with time, over time scales greater than  $t_{1/2}$  and at a constant receiver phase flow rate  $F$ . In such studies, the permeant concentration within the donor phase solvent  $C_{\text{don}}$  will decrease from its initial value to approach zero. The rate of change of donor compartment concentration, again maintaining reference to the specified model assumptions and Fick's first law, is given by

$$\frac{dC_{\text{don}}}{dt} = -\left(\frac{AD}{XV_{\text{don}}}\right)(K_{\text{mem-don}} C_{\text{don}} - K_{\text{mem-rec}} C_{\text{rec}}) \quad (3.22)$$

Substituting for  $C_{\text{rec}}$  according to equation 3.21 gives

$$\frac{dC_{\text{don}}}{dt} = -\left(\frac{ADK_{\text{mem-don}}}{XV_{\text{don}}} + \frac{ADK_{\text{mem-rec}} K_{\text{mem-don}} AD / (XF)}{XV_{\text{don}} (1 + ADK_{\text{mem-rec}} / (XF))}\right) C_{\text{don}} = -k_o C_{\text{don}} \quad (3.23)$$

where  $k_o$  is the 1<sup>st</sup>-order permeation rate coefficient corresponding to the open, variable-volume receiver compartment configuration. Integration of equation 3.23 gives

$$C_{\text{don}} = C_{\text{don},0} \exp(-k_o t) \quad (3.24)$$

Substitution for  $C_{\text{don}}$  according to equation 3.21 then gives the final expression for  $C_{\text{rec}}$  as a function of time.

$$C_{\text{rec}} = C_{\text{rec},0} \exp(-k_o t) \quad (3.25)$$

where  $k_o$  is defined according to equation 3.23 and  $C_{\text{rec},0}$  is given by

$$C_{\text{rec},0} = \left\{ \frac{ADK_{\text{mem-don}}/(XF)}{1 + (ADK_{\text{mem-rec}}/(XF))} \right\} C_{\text{don},0} \quad (3.26)$$

Inspection of equations 3.25 and 3.26 illustrates that, in an open, variable-volume receiver compartment configuration, the permeant concentration in the receiver compartment is expected to decrease, obeying the trends of an exponential curve characterised by two parameters ( $C_{\text{rec},0}$  and  $k_o$ ). In contrast to the closed-loop receiver configuration, these parameters are predicted to depend on the flow rate used in the receiver compartment.

### 3.5.2 Comparing the theoretical model with experimental results for membrane permeation into an open, variable-volume receiver configuration

Permeation runs using an open, variable-volume receiver configuration were conducted using a stirred donor compartment containing solutions of testosterone in IPM permeating through PDMS membranes into an open receiver phase consisting of aqueous PBS. These conditions were selected as an oil donor solution enabled a relatively high number of moles of testosterone to be used and produced receiver compartment concentrations high enough to be reliably measured. With these incorporated experimental conditions, calculation of the theoretical initial concentration of the permeant in the receiver phase ( $C_{\text{rec},0}$ ) and the rate coefficient of membrane permeation ( $k_o$ ), utilises the values of the variables;  $K_{\text{mem-don}} = K_{\text{PDMS-IPM}} = 0.04 \pm 0.01$ ,  $K_{\text{mem-rec}} = K_{\text{PDMS-PBS}} = 5 \pm 1$  and  $D(\text{IPM-saturated}) = 1.4 \times 10^{-10} \text{ m}^2 \text{ s}^{-1}$ .

Figure 3.22 shows comparison plots of  $C_{\text{rec}}$  versus time for open (with a fixed receiver phase flow rate of  $1 \text{ ml min}^{-1}$ ) and closed-loop receiver configurations for donor compartments containing solutions of testosterone in IPM. In the open configuration, the testosterone concentration in the receiver phase decreases

exponentially to zero as predicted by equation 3.25 whereas, as discussed previously, in the closed-loop receiver configuration, the concentration of the permeant in the receiver phase increases exponentially from zero to the final, equilibrium value  $C_{\text{rec},\infty}$  according to equation 3.8. Under the conditions used here, the permeation rate coefficient  $k_o$  for the open configuration is much slower than for the closed loop configuration ( $k$ ) as illustrated by the half-lives of the two exponential curves. A further key difference between the two experimental receiver phase configurations is the observed fraction of permeant extracted from the donor compartment. The maximum fraction of total testosterone extracted from the donor compartment to the receiver compartment for the closed-loop receiver configuration used here is approximately 1% (with a receiver compartment volume of 3.98 ml), whereas in the open receiver configuration, virtually 100% of the testosterone is extracted since the receiver solution flow is continued until all of the initial testosterone is depleted from the donor solution. For the run shown in Figure 3.22, the final total volume of receiver solution was 4800 ml pumped over 80 hours. In the context of medical applications, this open receiver configuration is likely to be more representative of the situation in which a drug permeates from the small donor volume of a skin patch application for example, into the much larger volume of the human blood stream.

Unlike the closed-loop configuration, in the open configuration the testosterone concentration in the receiver compartment is predicted to depend on the volumetric flow rate of the receiver solution (see equation 3.21). This prediction was tested as shown in Figure 3.23 by measuring the steady-state values of  $C_{\text{rec}}$  as a function of flow rate for a fixed value of testosterone concentration (5.8 mM) in IPM in the donor compartment. It can be seen that the measured data agree well with the predictions of equation 3.21 using the same consistent set of input parameters used previously to fit all membrane permeation runs. The loss of a smooth exponential curve in the experimental data, as illustrated in Figure 3.22, is caused by minor fluctuations in the receiver phase flow rate across the 80 hours experimental time period.

Figures 3.22 and 3.23 help illustrate that the single, unified theoretical model described here correctly predicts the observed behaviour in both open and closed-loop receiver compartment configurations of the permeation cell.

**Figure 3.22.** Upper plot: measured and calculated (smooth line) values of  $C_{\text{rec}}$  versus time for a donor compartment containing 5.8 mM testosterone in IPM permeating to an open receiver phase with  $1 \text{ ml min}^{-1}$  volumetric flow rate. Lower plot: measured (solid line) and calculated (dashed line) values of  $C_{\text{rec}}$  versus time for a donor compartment containing 6.4 mM testosterone in IPM permeating to a closed-loop receiver phase.

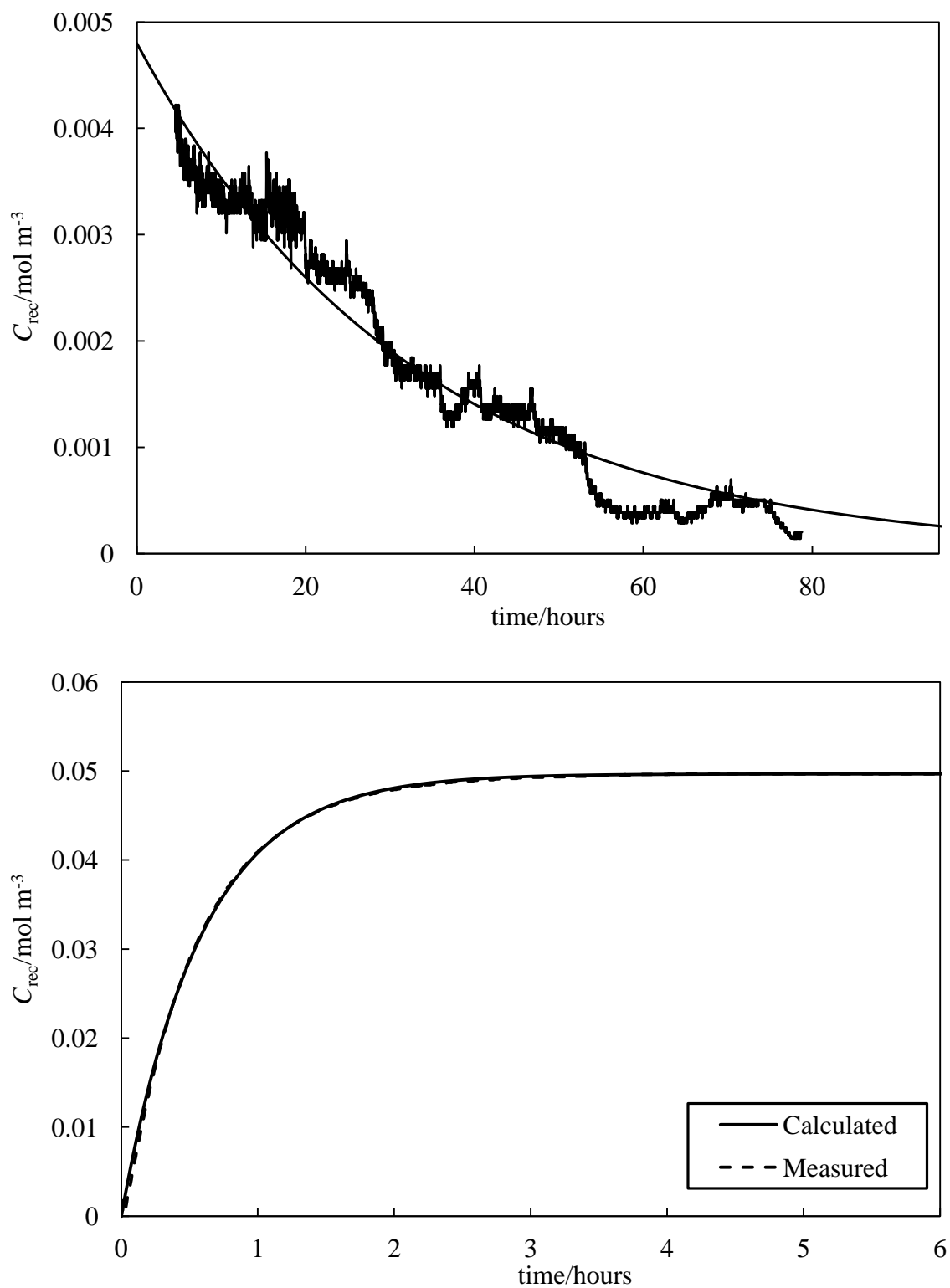
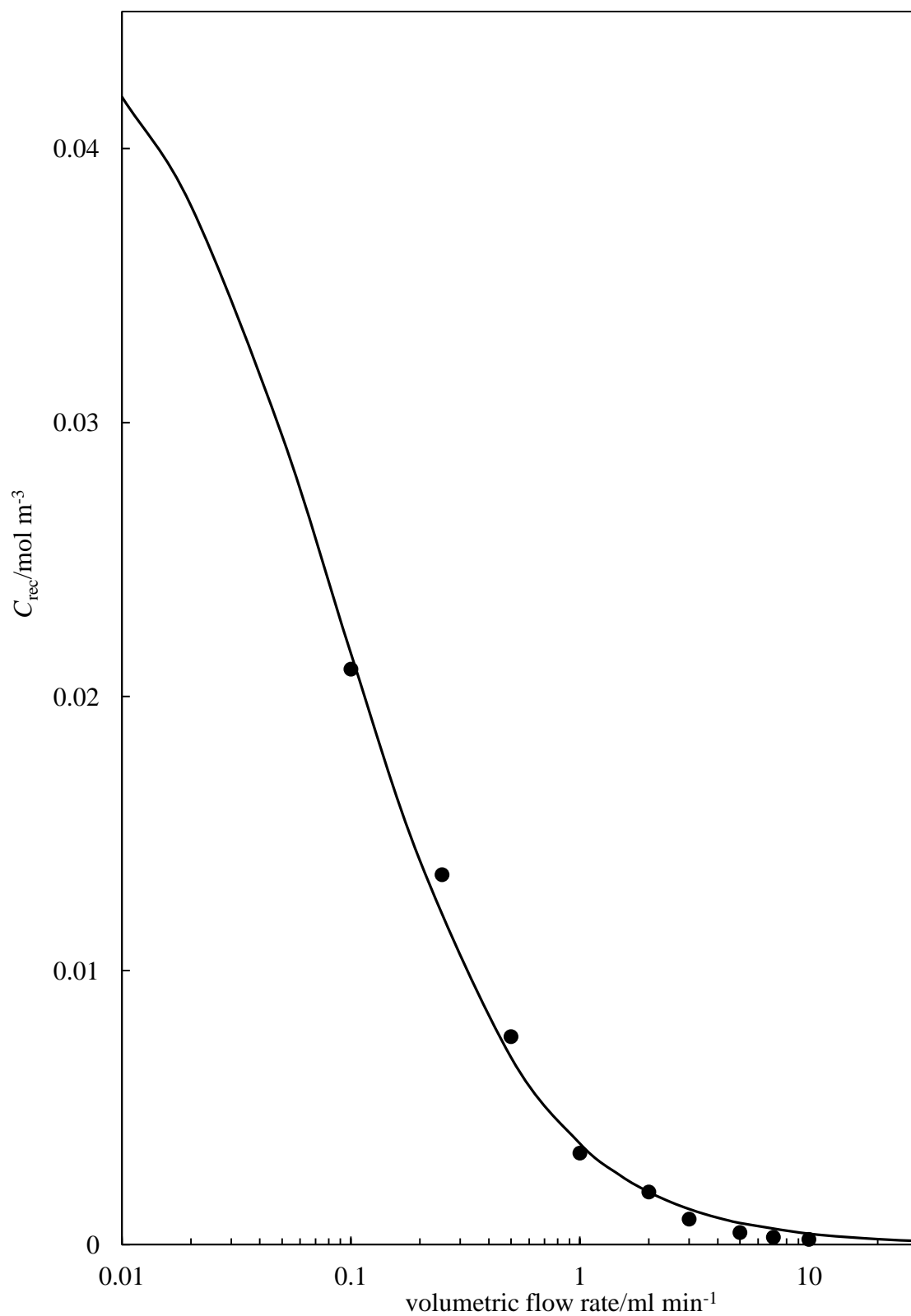




**Figure 3.23.** Comparison of measured (filled circles) and calculated (solid line) steady-state values of  $C_{\text{rec}}$  measured for different open receiver compartment flow rates for a donor compartment containing a constant concentration of testosterone in IPM (5.8 mM).



### 3.6 Conclusions

The establishment of a framework has been presented, by which donor solvent effects and all their different possible origins can be resolved and understood. Based on well established and rigorous physico-chemical principles, an explicit set of equations have been developed to describe the equilibrium and kinetic behaviour of permeating systems for which a set of five key assumptions are valid. For such systems, the model predicts the key features of permeating systems obeying these assumptions and how their validity or otherwise can be experimentally tested. For systems which obey the model assumptions and conditions of constant permeation cell geometry and permeant diffusion coefficients within the membrane, the effects of changing the donor solvent on the extent and rate of membrane permeation are entirely determined by two equilibrium partition coefficients:  $K_{\text{mem-don}}$  and  $K_{\text{mem-rec}}$ .

Additional possible donor solvent effects can arise when changing the donor solvent renders one or more of the key model assumptions invalid. Hence, in addition to altering permeation through changes in the  $K_{\text{mem-don}}$  and  $K_{\text{mem-rec}}$  permeant partition coefficients, changing the donor solvent can:

1. Alter the permeation rate-limiting step from membrane diffusion.
2. Change whether or not the membrane diffusion occurs under steady-state conditions.
3. Alter the membrane structure or uniformity.
4. Cause time-dependent changes in the solvent composition of the membrane or the donor and receiver phases.
5. Affect the extent of non-ideal permeant solution behaviour.

Using the comparison of model predictions and experimental data for numerous permeation systems which differ widely in the hydrophobicity/hydrophilicity of the permeant, donor solvent, receiver solvent and membrane, it is shown possible to identify and quantify effects including a change in the rate-determining step of permeation, non-ideal solution behaviour of the permeant solutions, deviations due to non-steady-state conditions, deviations due to changing permeant membrane diffusion coefficients and undesired solvent permeation through the membranes.

The derived model successfully accounts for the experimentally observed rates and extents of permeant membrane permeation into both closed-loop and variable-volume (open) receiver compartment configurations, using a single set of independently measured input parameters and a single, systematically fitted value of the permeants membrane diffusion coefficient.

Overall, the main outcome of the results presented in this chapter is the development of a rigorous theoretical and experimental framework whereby donor solvent effects in permeation can be determined and their origins fully elucidated.

### 3.7 References

1. S.H. Yalkowsky and Y. He, *Handbook of Aqueous Solubility Data*, CRC Press, Boca Raton, 2003.
2. A. Kumagai and S. Takahashi, *Int. J. Thermophys.*, **16**, 773, (1995).
3. *Thermodynamics Research Centre API44 Hydrocarbon Project. Selected values of properties of hydrocarbons and related compounds*, Texas A&M University, Thermodynamics Research Centre, 1978.
4. B.P. Binks, P.D.I. Fletcher, A.J. Johnson and R.P. Elliott, *Langmuir*, **28**, 2510, (2012).
5. G.M. Khan, Y. Frum, O. Sarheed, G.M. Eccleston and V.M. Meidan, *Int. J. Pharm.*, **303**, 81, (2005).
6. Y. Frum, G.M. Eccleston and V.M. Meidan, *Eur. J. Pharm. Biopharm.*, **67**, 434, (2007).
7. M. Dias, A. Farinha, E. Faustino, J. Hadgraft, J. Pais and C. Toscano, *Int. J. Pharm.*, **182**, 41, (1999).
8. J.C. Moreau, B. Leclerc, J. Mazan, G. Couarraze, G. Torres and H. Porte, *J. Mater. Sci. Mater. Med.*, **2**, 243, (1991).
9. J. Siepmann, F. Lecomte and R. Bodmeier, *J. Controlled Release*, **60**, 379, (1999).
10. G. Piel, M. Piette, V. Barillaro, D. Castagne, B. Evrard and L. Delattre, *Int. J. Pharm.*, **312**, 75, (2006).
11. See, for example J. Hadgraft, *Eur. J. Pharm. Biopharm.*, **58**, 291, (2004).
12. M.-L. Leichtnam, H. Rolland, P. Wuthrich and R.H. Guy, *J. Controlled Release*, **113**, 57, (2006).
13. W.J. McAuley, K.T. Mader, J. Tetteh, M.E. Lane and J. Hadgraft, *Eur. J. Pharm. Sci.*, **38**, 378, (2009).
14. W.J. McAuley, M.D. Lad, K.T. Mader, P. Santos, J. Tetteh, S.G. Kazarian, J. Hadgraft and M.E. Lane, *Eur. J. Pharm. Biopharm.*, **74**, 413, (2010).
15. G. Oliveira, A.E. Beezer, J. Hadgraft and M.E. Lane, *Int. J. Pharm.*, **393**, 61, (2010).
16. W.J. McAuley, G. Oliveira, D. Mohammed, A.E. Beezer, J. Hadgraft and M.E. Lane, *Int.J. Pharm.*, **396**, 134, (2010).

17. R.M. Watkinson, R.H. Guy, G. Oliveira, J. Hadgraft and M.E. Lane, *Skin Pharmacol. Physiol.*, **24**, 22, (2011).
18. A.C. Williams and B.W. Barry, *Adv. Drug Deliv. Rev.*, **56**, 603, (2004).
19. P. Santos, A.C. Watkinson, J. Hadgraft and M.E. Lane, *Int. J. Pharm.*, **439**, 260, (2012).

## CHAPTER 4

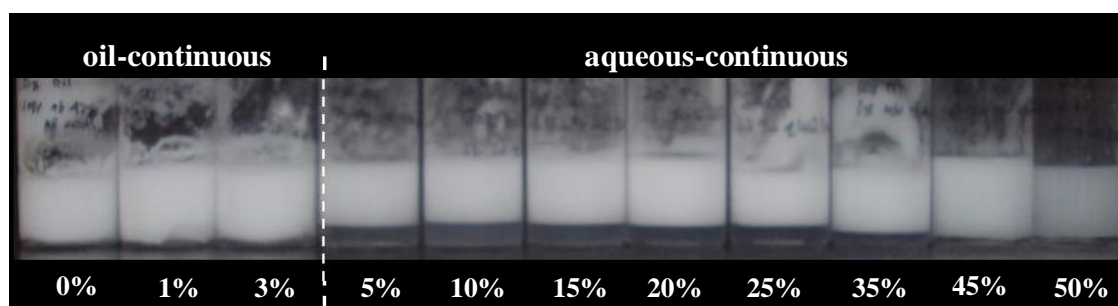
### PREPARATION AND PROPERTIES OF WATERLESS, PARTICLE-STABILISED EMULSIONS

#### 4.1 Introduction

Some pharmaceutical emulsions, often incorporating paraffin oil, are administered as creams to the surface of the skin and can contain high concentrations of a diol such as propane-1,2-diol. It is believed that such diols improve the solubility of the active ingredient within the emulsion (as illustrated in Chapter 3) and facilitate the transport of the active ingredient across the skin structure.<sup>1-3</sup> The addition of various diols to emulsions of paraffin liquid and water, stabilised by non-ionic surfactants, has been shown to promote a transitional phase inversion of the emulsion from water-in-oil to oil-in-water by increasing the hydrophilicity of the system.<sup>4</sup> It is thereby suggested that the diol acts as a cosurfactant and adsorbs at the oil-water interface, which consequently causes the headgroup region of the surfactant to swell.

The influence of propane-1,2-diol on the preparation of particle-stabilised emulsions of paraffin liquid and water has also been investigated.<sup>5</sup> In this study Binks *et al.* produce a series of emulsions which contain 50 vol.% paraffin liquid and an increasing concentration of propane-1,2-diol as a replacement for water in the emulsion polar phase. Figure 4.1 illustrates this emulsion series and identifies the preparation of a stable emulsion composed solely of paraffin liquid, propane-1,2-diol and fumed silica particles possessing 42% SiOH (i.e. no water).

**Figure 4.1.** Appearance and type of emulsions 1 month after preparation from equal volumes of paraffin liquid and aqueous propane-1,2-diol containing 1 wt.% silica particles possessing 42% SiOH, as a function of diol volume with respect to the total volume of emulsion. Taken from reference 5.



In this chapter, the observation made in reference 5 on the preparation of waterless emulsions is investigated further by studying the influence of oil type, polar liquid type and particle hydrophobicity on the preparation of waterless, particle-stabilised emulsions. The contents of this chapter are included in a recent patent.<sup>6</sup>

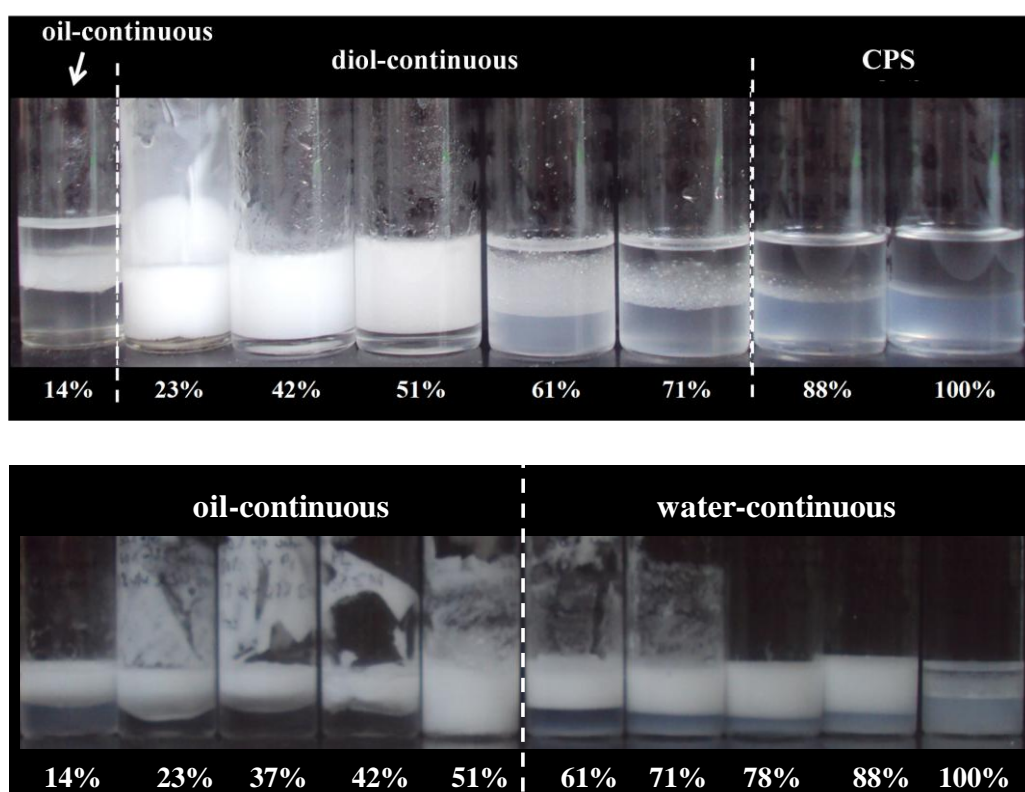
#### 4.2 Preparation and properties of waterless, particle-stabilised emulsions incorporating paraffin liquid oil and various diol polar phases

Few reports exist on the preparation of stable emulsions of oil and non-aqueous polar liquids in the absence of water. Those that do exist, describe the preparation of non-aqueous emulsions which are stabilised by surfactants<sup>7-9</sup> or amphiphilic block and statistical copolymers.<sup>10</sup> However, the surfactants and copolymers required to stabilise these emulsions are quite exotic and therefore rather expensive. Furthermore, Hamill and Petersen<sup>7</sup> illustrate that non-aqueous emulsions do not emulsify in accordance with predictions based on the HLB of a given suitable surfactant and hence, the preparation of a desired emulsion type is not intuitive.

In development of the observation made in Figure 4.1, Binks *et al.* investigated the preparation of emulsions of 50 vol.% paraffin liquid, 50 vol.% propane-1,2-diol and 1 wt.% fumed silica particles of varied hydrophobicity (i.e. surface % SiOH).<sup>5</sup> Figure 4.2 (upper) illustrates this series of emulsions 6 months after preparation and for comparative purposes, the equivalent paraffin liquid/water emulsion series is also shown (lower). As expected, it is possible to transitionally phase invert the prepared waterless emulsions from oil-in-diol to diol-in-oil through alteration of the particle

contact angle  $\theta$  at the oil/diol interface. For the emulsion series illustrated in the top image of Figure 4.2, the expected change from  $\theta < 90^\circ$  (corresponding to oil-in-diol emulsions) to  $\theta > 90^\circ$  (corresponding to diol-in-oil emulsions) occurs between emulsions stabilised by fumed silica particles possessing between 23 and 14% SiOH on their surfaces.

**Figure 4.2.** Appearance and type of emulsions 6 months after preparation from 50 vol.% paraffin liquid and 50 vol.% propane-1,2-diol (upper), and 50 vol.% paraffin liquid and 50 vol.% water (lower) as a function of particle hydrophobicity. Both emulsion series contain 1 wt.% silica particles of given % SiOH content. CPS refers to complete phase separation. Images reproduced from reference 5.



With reference to Figure 4.2, the particle hydrophobicity required to induce a transitional phase inversion of an emulsion of paraffin liquid and propane-1,2-diol (14–23% SiOH) is significantly greater than that of the equivalent emulsion of paraffin liquid and water (51–61% SiOH). Given that the transitional phase inversion of particle-stabilised emulsions occurs when the particle contact angle  $\theta$  with the oil-polar liquid interface is  $90^\circ$ , it is now of interest to understand the origin of the different



emulsion inversion points for emulsions incorporating different combinations of oil and polar liquid.

#### 4.2.1 *A theoretical method for predicting the particle hydrophobicity required to induce transitional phase inversion of particle-stabilised emulsions*

Since determination of the contact angle  $\theta$  that a small particle makes with the oil-polar liquid interface is challenging, several advances have been recently made, which include a gel trapping technique,<sup>11</sup> a film calliper method<sup>12</sup> and the use of ellipsometry.<sup>13</sup> However, none of these methods are ideally suited to polydisperse particles and partially fused aggregates like that of fumed silica. Instead, a theoretical model<sup>14</sup> can be used to calculate the contact angle  $\theta$  as a function of % SiOH on the particle surfaces.

For a solid particle (s) located at the oil (o)-polar liquid (l) interface, the three interfacial tensions are related to the contact angle  $\theta$  (measured in the polar liquid phase) by the Young equation, such that:

$$\cos\theta = \frac{\gamma_{so}-\gamma_{sl}}{\gamma_{ol}} \quad (4.1)$$

Although the interfacial tension between oil and the polar liquid,  $\gamma_{ol}$ , can be measured accurately, there are no direct methods for measuring the interfacial tensions between the solid particle and the polar liquid,  $\gamma_{sl}$ , and the solid particle and the oil,  $\gamma_{so}$ . It would be useful to use equation 4.1 to predict values for the contact angle if it were possible to estimate these two interfacial tensions from some other source of data. This requires the use of combining rules that allow any interfacial tension to be predicted from surface tension components and the determination of such components from solid surfaces. A common approach<sup>15,16</sup> is that of expressing any surface tension  $\gamma$  as a sum of components due to dispersion forces ( $\gamma^d$ ) and polar forces ( $\gamma^p$ ), such that:

$$\gamma = \gamma^d + \gamma^p \quad (4.2)$$

The interfacial tension between two phases is then expressed in terms of these two components for each phase and become

$$\gamma_{sl} = \gamma_{sa} + \gamma_{al} - 2\sqrt{\gamma_s^d \gamma_l^d} - 2\sqrt{\gamma_s^p \gamma_l^p} \quad (4.3)$$

$$\gamma_{so} = \gamma_{sa} + \gamma_{oa} - 2\sqrt{\gamma_s^d \gamma_o^d} - 2\sqrt{\gamma_s^p \gamma_o^p} \quad (4.4)$$

$$\gamma_{ol} = \gamma_{oa} + \gamma_{al} - 2\sqrt{\gamma_o^d \gamma_l^d} - 2\sqrt{\gamma_o^p \gamma_l^p} \quad (4.5)$$

for the solid-polar liquid, solid-oil and oil-polar liquid interfaces, respectively, where ‘a’ represents air. Although it has been suggested that the polar component could be better described in terms of acid-base interactions,<sup>17</sup> it has also been established that when such components are used to predict the contact angle  $\theta$ ,<sup>14,18</sup> the values are very close to those obtained by the simple Owens and Wendt method<sup>16</sup> described above. Each input parameter of equations 4.3 to 4.5 can then be measured either directly (for liquid-air surface tensions or liquid-liquid interfacial tensions) or indirectly (for dispersion and polar components of the solid surface energy,  $\gamma_{sa}$ ), like that illustrated by Binks and Clint,<sup>19</sup> and hence the values of  $\gamma_{sl}$ ,  $\gamma_{so}$  and  $\gamma_{ol}$  can be implemented into equation 4.1 to determine the contact angle, particle detachment energy and thus stability of any desired emulsion system.

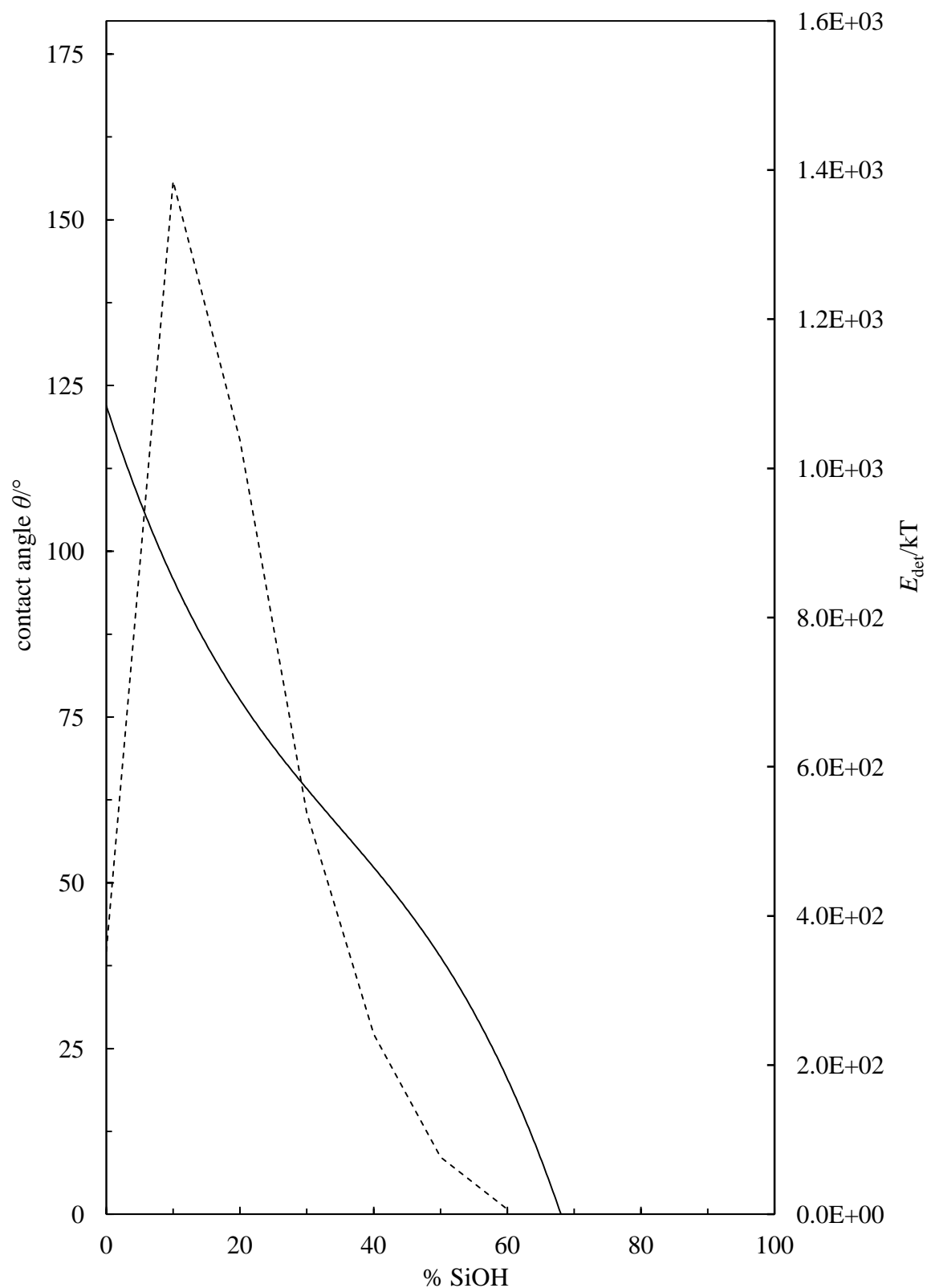
To give an example of the application of this theoretical method, Figure 4.3 shows the calculated contact angle  $\theta$  of a fumed silica particle at the oil-polar phase interface (left-hand ordinate), plotted as a function of the % SiOH on the particle surface.<sup>5</sup> The data referred to correspond to a series of emulsions which contain 50 vol.% paraffin liquid, 25 vol.% propane-1,2-diol, 25 vol.% water and 1 wt.% fumed silica particles. The measurement and derivation of the required parameters for the application of the discussed theoretical model are described within reference 5. However, to summarise, the calculated contact angle  $\theta$  decreases as expected with an increase in particle hydrophilicity and equals 90° for particles possessing 13% SiOH corresponding to the predicted point of transitional phase inversion for this emulsion system. The energy of detachment of a single particle,  $E_{det}$ , calculated using equation 1.14 of Chapter 1, is also plotted in Figure 4.3 (right-hand ordinate). A distinct maximum in the energy of detachment of a single particle occurs at 13% SiOH implying maximum emulsion stability at this condition.

The application of this theoretical method for predicting the contact angle  $\theta$  of a particle at an oil-polar phase liquid interface, and the stability of the resulting emulsions, has been established and is reputable.<sup>5,18,20</sup> The model therefore allows for

the accurate prediction of the required % SiOH on such modified silica particles to produce a 90° contact angle, corresponding to the point of emulsion transitional phase inversion.

The inversion of waterless emulsions, shown in Figure 4.2, has consequently produced a series of investigations into the preparation of other emulsion systems containing various different oils, polar liquids and solid particles. The first aspect investigated was the preparation of emulsions containing a paraffin liquid oil phase and a varied diol phase. The diols chosen for this investigation were butane-1,2-diol and pentane-1,5-diol.

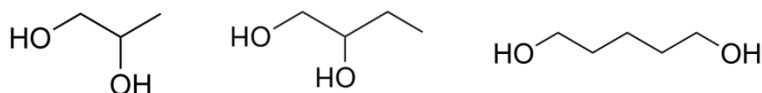
**Figure 4.3.** Calculated oil-polar phase contact angle (filled line, left-hand ordinate) and particle detachment energy (dashed line, right-hand ordinate) of silica nanoparticles in paraffin liquid and 50 vol.% propylene glycol in water systems, as a function of % SiOH on particle surfaces. Particle radius = 10 nm. Data reproduced from reference 5.



#### 4.2.2 *Waterless, particle-stabilised emulsions of paraffin liquid and either butane-1,2-diol or pentane-1,5-diol*

The polar liquids chosen in mixtures with paraffin liquid were butane-1,2-diol and pentane-1,5-diol. Their structures are given in Figure 4.4 along with that of propane-1,2-diol for a comparison.

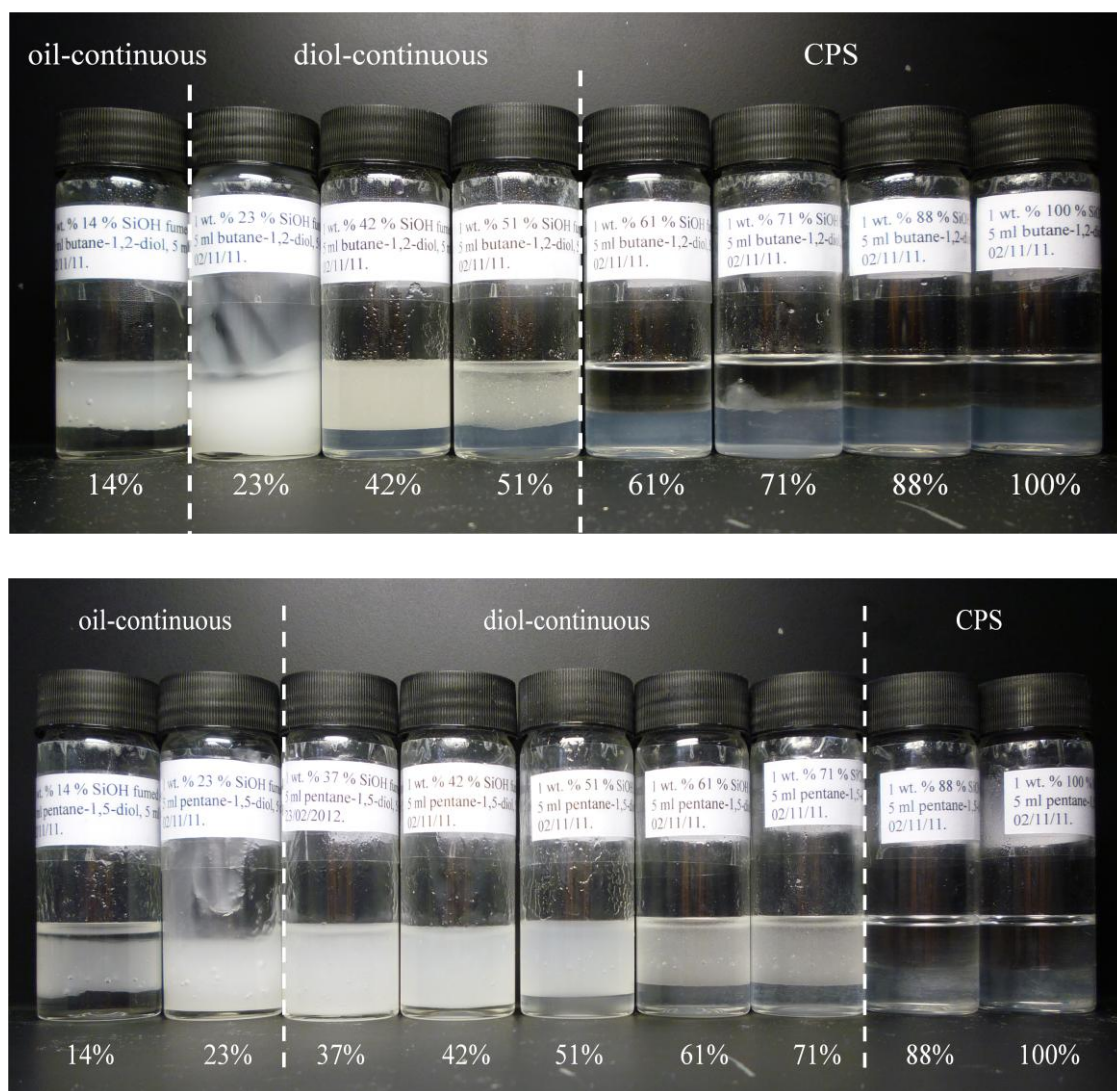
**Figure 4.4.** Structures of propane-1,2-diol ( $C_3H_8O_2$ ) (left), butane-1,2-diol ( $C_4H_{10}O_2$ ) (middle) and pentane-1,5-diol ( $C_5H_{12}O_2$ ) (right).



For a direct comparison with Figure 4.2, all emulsions discussed subsequently were prepared from 50 vol.% paraffin liquid, 50 vol.% respective diol and 1 wt.% fumed silica particles of varied hydrophobicity. Figure 4.5 illustrates the prepared waterless emulsions of paraffin liquid and butane-1,2-diol (upper), and paraffin liquid and pentane-1,5-diol (lower) 1 month after emulsification. The condition for transitional phase inversion, via application of the drop test method, optical microscopy and measurement of the emulsion conductivities, is also indicated for each emulsion system.

Figure 4.5 reinforces the fact that stable waterless emulsions of paraffin liquid and a diol can be prepared in the presence of hydrophobic fumed silica particles. It is noted here that emulsions of paraffin liquid and butane-1,2-diol completely phase separate within 1 month when prepared using silica particles possessing > 51% SiOH. By comparison, this transition to complete phase separation occurs above 71% SiOH for propane-1,2-diol containing emulsions. Furthermore, emulsions of paraffin liquid and pentane-1,5-diol are shown to be considerably more stable towards complete phase separation than systems incorporating butane-1,2-diol, when stabilised by silica particles up to 71% SiOH. For emulsions of both series, prepared using silica particles of wettability near to that required to induce transitional phase inversion, the resulting stable emulsions show a high stability towards creaming, sedimentation and coalescence over time scales in excess of 6 months.

**Figure 4.5.** Appearance and type of emulsions 1 month after preparation from 50 vol.% paraffin liquid and 50 vol.% butane-1,2-diol (upper), and 50 vol.% paraffin liquid and 50 vol.% pentane-1,5-diol (lower) as a function of particle hydrophobicity. Both emulsion series contain 1 wt.% silica particles of with % SiOH given. CPS refers to complete phase separation.



Emulsions of paraffin liquid and butane-1,2-diol or pentane-1,5-diol are shown to transitionally phase invert when prepared using silica particles of grades between 14-23% and 23-37% SiOH respectively. This point of transitional phase inversion is similar to that of emulsions incorporating propane-1,2-diol (14-23% SiOH), but occurs at lower % SiOH (i.e. more hydrophobic) than that required to invert the equivalent paraffin liquid and water emulsion (51-61% SiOH). With reference to the theoretical method described in section 4.2.1, the % SiOH required to induce transitional phase inversion of the systems illustrated here can be accurately predicted through

measurement and derivation of the three interfacial tensions  $\gamma_{so}$ ,  $\gamma_{sl}$  and  $\gamma_{ol}$ , which are then applied to equation 4.1. The determination of the required interfacial tensions for each respective system and therefore the prediction of the % SiOH at which transitional phase inversions will occur, deviates from the primary aims of this research studentship and therefore forms one aspect of the proposed future work. However, a first approximation for the influence of the chemistry of a diol on the type and stability of the waterless emulsion prepared can be made. Table 4.1 summarises the key observations from Figures 4.2 and 4.5 for the three waterless emulsion systems incorporating a paraffin liquid oil phase and various different diol polar phases. The properties of the equivalent emulsion of paraffin liquid and water are also given.

**Table 4.1.** Summary of the key observations from the prepared emulsions of paraffin liquid and pentane-1,5-diol, propane-1,2-diol or butane-1,2-diol stabilised by silica particles. The observations from the equivalent emulsion series of paraffin liquid and water are also given. CPS refers to complete phase separation.

<b>Emulsion polar liquid phase</b>	<b>% SiOH to induce transitional phase inversion</b>	<b>% SiOH for CPS</b>
Water	51-61	100
Pentane-1,5-diol	23-37	$\geq 88$
Propane-1,2-diol	14-23	$\geq 88$
Butane-1,2-diol	14-23	$\geq 61$

The contact angle  $\theta$ , corresponding to transitional phase inversion is influenced by the values of the three interfacial tensions  $\gamma_{so}$ ,  $\gamma_{sl}$  and  $\gamma_{ol}$ , as discussed. For the emulsion systems shown here, the values of  $\gamma_{so}$  are fixed for the interfacial tensions between paraffin liquid and the different grades of fumed silica particles used. However, the values of  $\gamma_{sl}$  and  $\gamma_{ol}$  vary for each system and depend on the polar liquid present. Therefore, as a first approximation, the determination of the polar liquid relative hydrophobicities will reveal information regarding the magnitude of these interfacial tensions for each emulsion system prepared.

The observations summarised in Table 4.1 suggest that butane-1,2-diol is the most hydrophobic polar liquid of the diols investigated here, as it is shown to promote transitional phase inversion of the concerned emulsion system between 14-23% SiOH, and favours complete phase separation in systems incorporating silica particles above a 61% SiOH grade. Conversely, the most hydrophilic polar liquid (i.e. water), promotes transitional phase inversion in equivalent emulsions stabilised by silica particles of a 51-61% SiOH grade, and disfavours complete phase separation of the emulsion for all particle hydrophobicities up to a 100% SiOH grade. Consequently, pentane-1,5-diol and propane-1,2-diol are intermediate in hydrophobicity to that of water and butane-1,2-diol.

With reference to the diol structures given previously, it is plausible that butane-1,2-diol is more hydrophobic than propane-1,2-diol arising from the additional methyl group on the otherwise identical chemical structure. Hence, although both diols are shown to produce a transitional phase inversion of the corresponding emulsion between silica particle grades of 14-23% SiOH, the precise difference in the point of inversion is likely to be concealed within this 9% window of % SiOH content. Furthermore, propane-1,2-diol is shown to be more capable of stabilising the concerned emulsion series against complete phase separation with silica particles up to a higher % SiOH grade, like that of water. It is also plausible that although pentane-1,5-diol consists of a longer hydrocarbon chain, the presence of two terminal hydroxyl groups and the molecules ability to rotate and form different conformers, renders the molecule comparatively more hydrophilic than propane-1,2-diol and butane-1,2-diol.

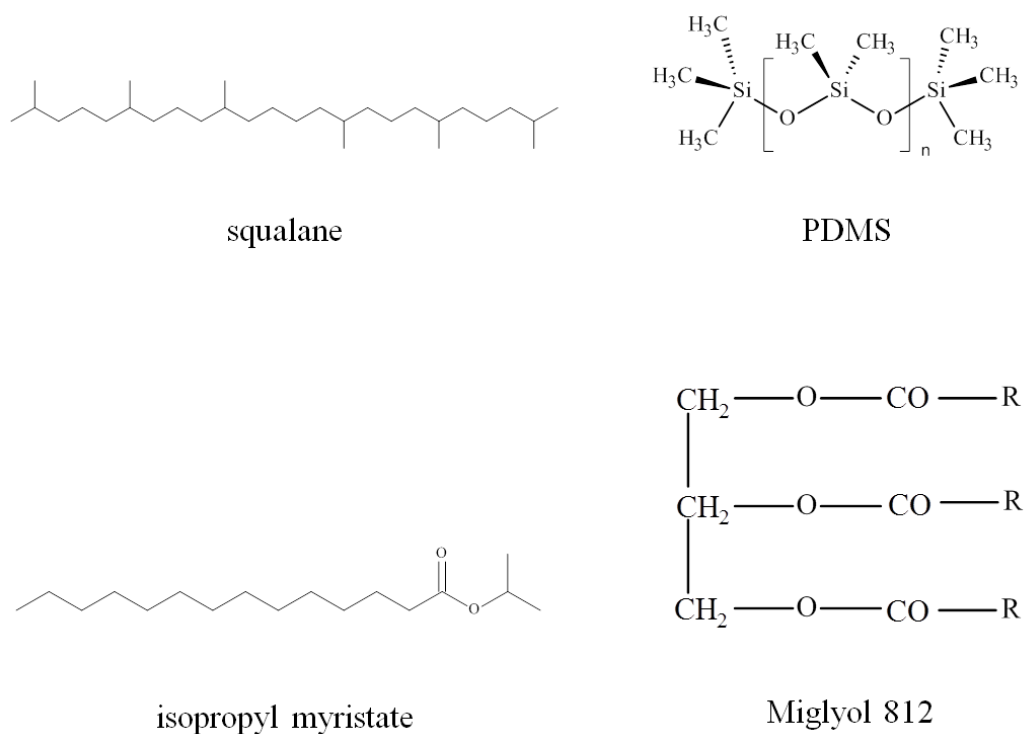
In summary, it has been shown possible to prepare stable waterless emulsions of both oil-in-diol and diol-in-oil types, incorporating paraffin liquid and various different diols. Variation of the diol has been shown to produce a significant change in the type and stability of emulsion prepared for a chosen oil and constant particle hydrophobicity, by alteration of the  $\gamma_{sl}$  and  $\gamma_{ol}$  interfacial tensions, which are secondarily related to the respective diol hydrophobicity. To further investigate the preparation of waterless particle-stabilised emulsions, the next study examines the preparation and properties of waterless emulsions which contain a selected diol polar phase (propane-1,2-diol) and various different oil phases.



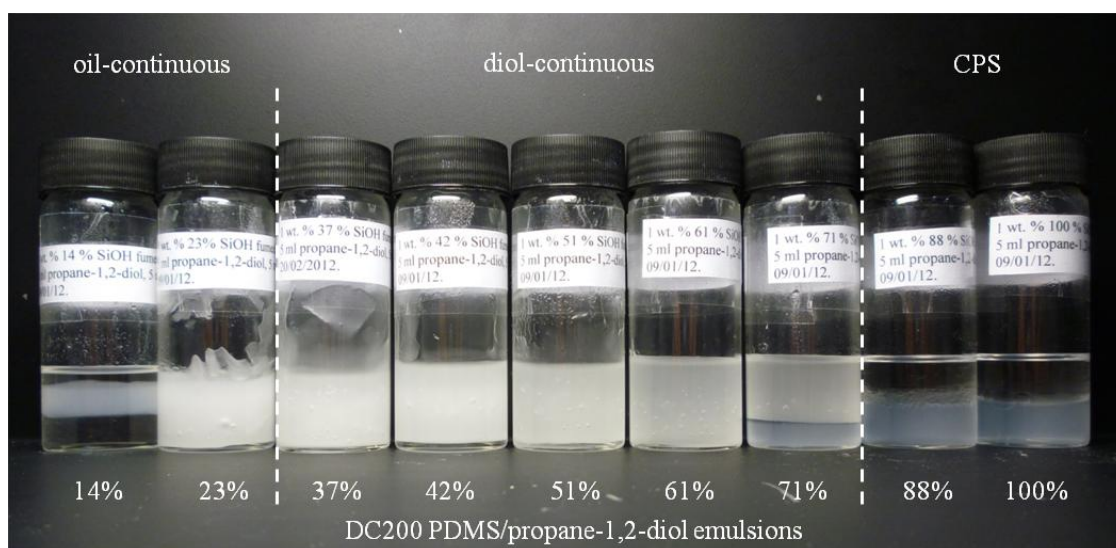
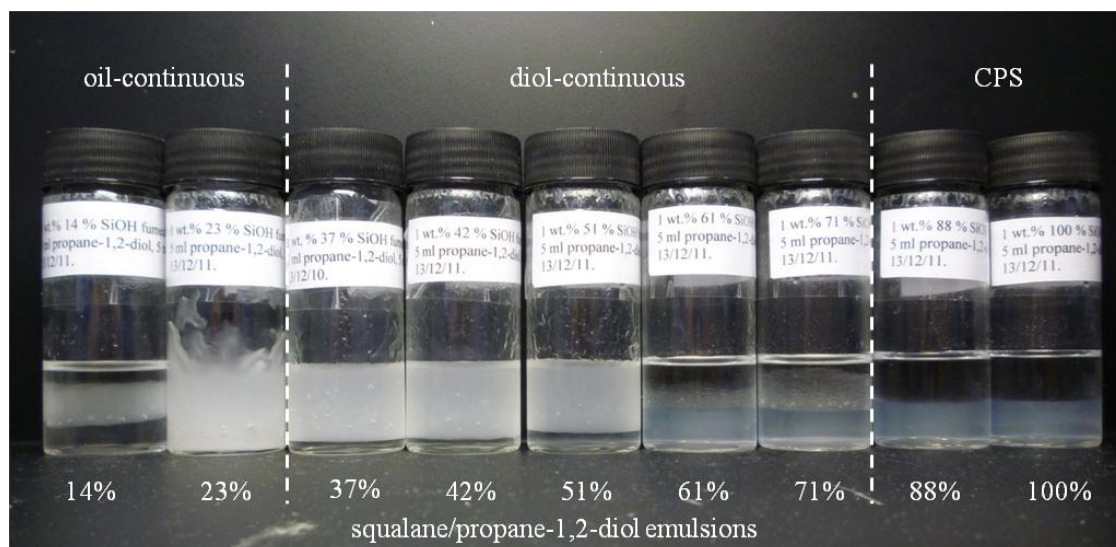
### 4.3 Preparation and properties of waterless, particle-stabilised emulsions incorporating propane-1,2-diol polar phases and various oil phases

The investigation into the preparation of waterless, particle-stabilised emulsions containing a diol polar phase (propane-1,2-diol) and various different oil phases was conducted. A range of different oil phases, including an alkane oil (squalane), an ester oil (isopropyl myristate), a silicone oil (DC 200 PDMS) and an oil composed of a mixture of triglycerides<sup>21</sup> (Miglyol 812), was used. To enable a direct comparison with the emulsions described previously, all systems presented here incorporated 50 vol.% oil phase, 50 vol.% polar liquid phase and 1 wt.% fumed silica particles of a varied hydrophobicity. Figure 4.6 shows the chemical structure of four of the oils used. Miglyol 812 is composed of 55% triglycerides of C<sub>8</sub> and 45% triglycerides of C<sub>10</sub>. For comparison, the emulsion system previously discussed containing paraffin liquid and propane-1,2-diol is often referred to, whereby the paraffin liquid is composed of a mixture of heavier alkanes of C<sub>12</sub>-C<sub>20</sub>. Figure 4.7 shows photographs of the different emulsion systems 1 month after preparation and Table 4.2 summarises the findings.

**Figure 4.6.** Structures of squalane (C<sub>30</sub>H<sub>62</sub>), DC200 PDMS (C<sub>2</sub>H<sub>6</sub>OSi)<sub>n</sub>, isopropyl myristate (C<sub>17</sub>H<sub>34</sub>O<sub>2</sub>) and Miglyol 812 (where R = C<sub>8</sub> or C<sub>10</sub>).



**Figure 4.7.** Appearance and type of emulsions 1 month after preparation from 50 vol.% propane-1,2-diol and 50 vol.% squalane, DC200 PDMS, Miglyol 812 or isopropyl myristate as a function of particle hydrophobicity (given as % SiOH). All emulsions contain 1 wt.% fumed silica particles. CPS refers to complete phase separation.



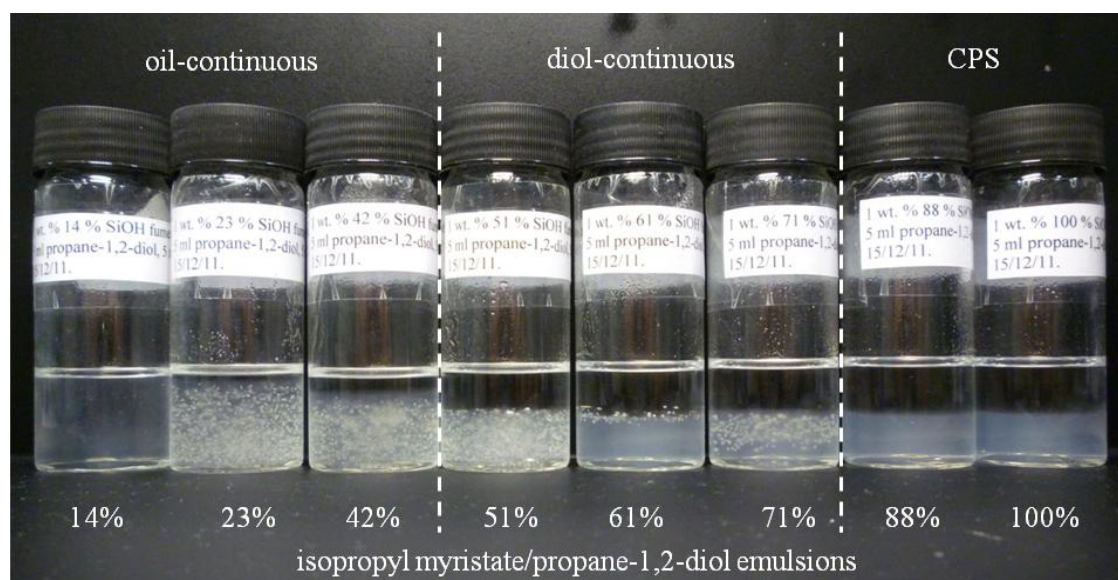
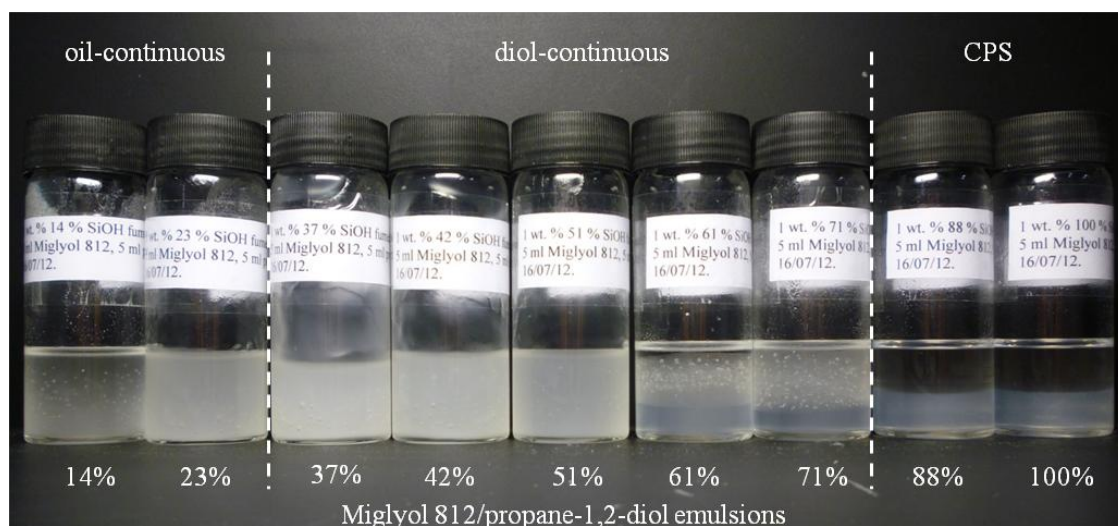


**Table 4.2.** Summary of the key observations from the prepared emulsions of propane-1,2-diol and paraffin liquid, squalane, DC200 PDMS, Miglyol 812 or isopropyl myristate.

Emulsion oil phase	% SiOH to induce transitional phase inversion	% SiOH above which CPS occurs
Paraffin liquid	12-23	88
Squalane	23-37	88
DC200 PDMS	23-37	88
Miglyol 812	23-37	88
Isopropyl myristate	42-51	88

Figure 4.7 again illustrates the formation of stable waterless emulsions which incorporate a propane-1,2-diol polar liquid phase and various different oil phases. The prepared emulsions are once more shown to transitionally phase invert through variation of the stabilising silica particle hydrophobicity, which influences the particle contact angle  $\theta$  at the oil/polar liquid interface. The analysis of the observed points of transitional phase inversion is difficult without the accurate determination of the relevant interfacial tensions for application to the theoretical method described previously. It is apparent however, that all emulsion systems summarised in Table 4.2 show a similar resistance towards complete phase separation.

Several other interesting observations are made in Figure 4.7. Firstly it is apparent that there is a significant change in the rheology of the prepared waterless emulsions around transitional phase inversion. Oil-continuous emulsions have a gel-like consistency which maintain a deformed shape and hence, do not settle to form a horizontal emulsion-air interface within 1 month after preparation. Conversely, diol-continuous emulsions of the same oil/diol/particle type composition, are more liquid-like and therefore settle within the vessel immediately after emulsification. This is particularly noticeable for emulsions of squalane or DC200 PDMS. Secondly, for waterless emulsions containing isopropyl myristate, transparent homogenous emulsions result. The presence of air bubbles incorporated during homogenisation are visible in such transparent emulsions, whilst emulsions which completely phase separate illustrate a clear boundary between the two immiscible phases due to the hydrophilic silica particles residing in the more dense, polar liquid phase. These two observations are investigated in more detail below.

#### 4.3.1 *Gelling of oil-continuous waterless emulsions around the point of transitional phase inversion*

The observed gelling of oil-continuous waterless emulsions may be due to several reasons. Firstly, an addition of excess hydrophobic silica particles, which will reside in the oil-continuous phase, could cause an increase in the overall viscosity of such emulsions. It is suggested that within liquids of low polarity, like that of squalane, such silica particles can form strong hydrogen bonds with neighbouring particles between the exposed silanol groups, resulting in the formation of structured, solid-like particle networks and hence give rise to a gel.<sup>22</sup> Such structured networks would otherwise be

absent in an equivalent diol-continuous emulsion as it is suggested that in polar liquids the excess hydrophobic particles form a hydrogen bonded solvation layer around the particle surface and therefore produce non-structured, stable dispersions.<sup>22</sup> Alternatively, the observed gelling may occur due to extensive flocculation of uncharged dispersed droplets. Flocculation of an emulsion usually leads to enhanced creaming or sedimentation because the flocs of droplets rise faster, in accordance with Stoke's law, than individual droplets due to their effective larger radius (see equation 1.15 of Chapter 1). However, exceptions can occur when flocculation can lead to a structured solid-like network of droplets throughout the emulsion and therefore produces a gelled formulation.<sup>23</sup> To investigate whether the observed gelling shown in Figure 4.7 is a result of thickening of the emulsion continuous phase or flocculation of the emulsion dispersed phase, several investigations were performed.

The gelling of an emulsion continuous phase via the addition of excess silica particles will lead to an increase in the viscosity of the overall emulsion as described by the Einstein equation,<sup>24</sup> whereby:

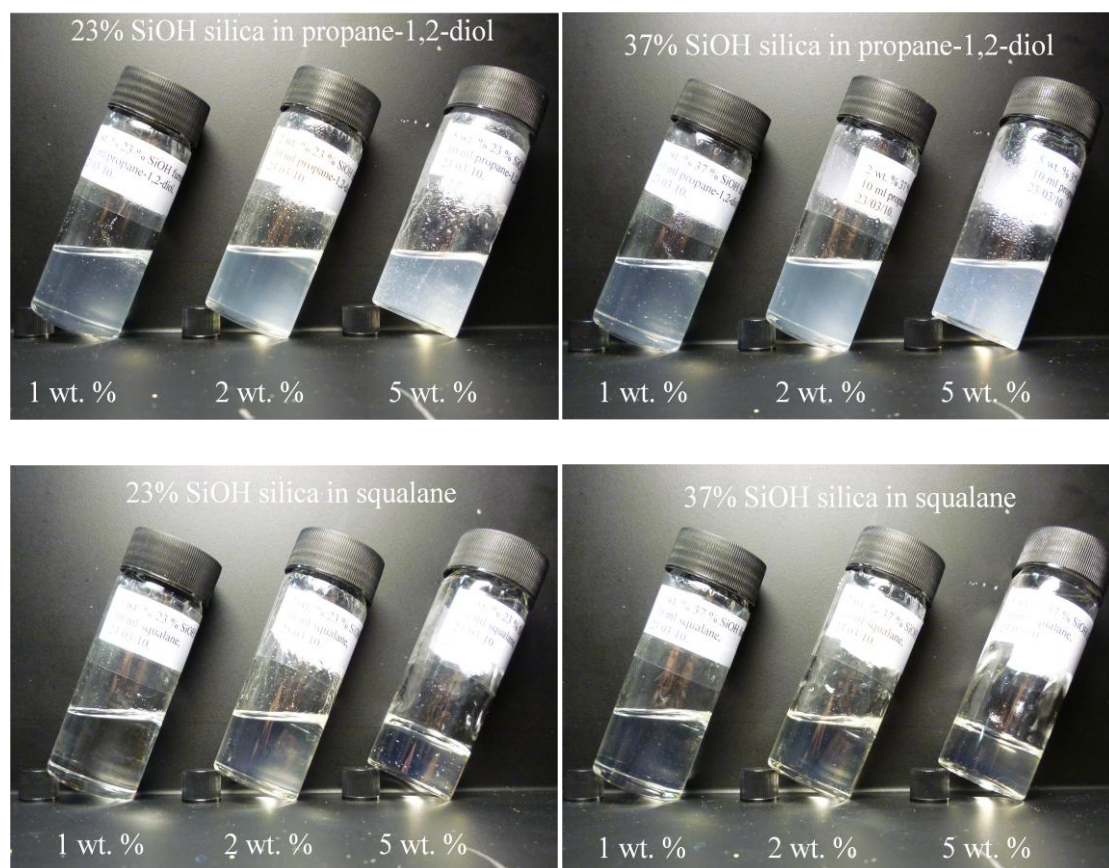
$$\eta = \eta_0 + 2.5\phi \quad (4.6)$$

where  $\eta$  represents the viscosity of the overall emulsion,  $\eta_0$  represents the viscosity of the emulsion continuous phase and  $\phi$  represents the dispersed phase volume fraction. The concentration of excess emulsifying silica particles, which are not adsorbed at the oil/diol interface and therefore reside in the emulsion continuous phase can be calculated.<sup>25</sup> However, given that all emulsions prepared here contain 5 ml oil, 5 ml polar liquid and 1 wt.% silica particles with respect to the overall mass of the emulsion, the maximum possible concentration of particles in the emulsion continuous phase is approximately 2 wt.%, assuming no particles are adsorbed at the oil/diol interface. To investigate the extent of gelling of both the oil and polar liquid emulsion phases with increasing concentration of silica particles, an increasing mass of particles was dispersed within a chosen oil (squalane) and a chosen diol (propane-1,2-diol). Particles responsible for stabilising both diol-in-oil emulsions (23% SiOH) and oil-in-diol emulsions (37% SiOH) were investigated. Figure 4.8 clearly illustrates that no gelling of the propane-1,2-diol polar phase occurs with increasing silica particle concentration up to an overestimated excess of 5 wt.%. This therefore corresponds to the formation of a hydrogen bonded solvation layer around the particles dispersed within the polar



diol phase.<sup>22</sup> Conversely, significant gelling of the squalane oil phase is observed for silica particle concentrations of 5 wt.%. Once more, this corresponds to the observations made by Kahn *et al.* presuming the formation of hydrogen bonds between neighbouring silica particles dispersed within a non-polar liquid.<sup>22</sup> However, in the context of the observations made in Figure 4.7, the dispersion of silica particles in Figure 4.8 which simulates the highest possible concentration of particles in the emulsion continuous phase (2 wt.% silica particles with respect to the mass of the oil phase, as discussed previously) does not form a gelled consistency which conclusively shows that the predominant cause of the observed gelling of oil-continuous emulsions is not via thickening of the emulsion continuous phase.

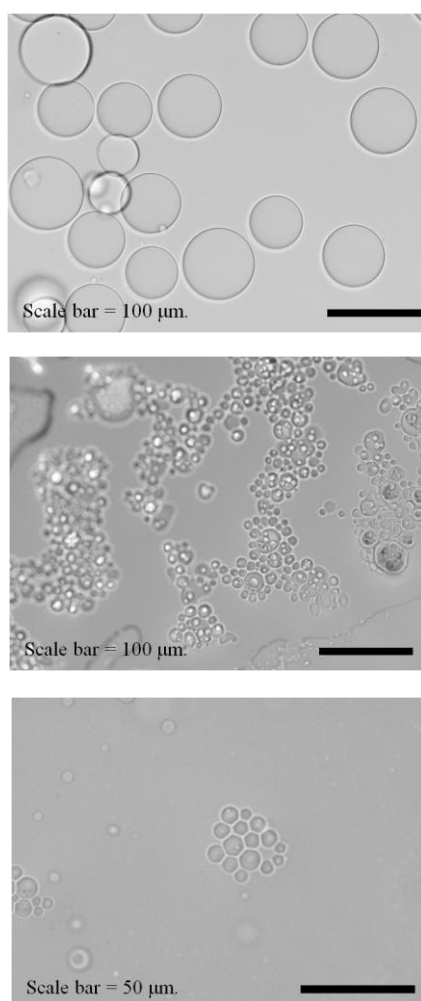
**Figure 4.8.** Appearance of squalane and propane-1,2-diol solutions with increasing concentrations of fumed silica particles of a 23% or 37% SiOH grade dispersed within (given). All photographs were taken 24 hours after sample preparation.



To investigate the presence of dispersed droplet flocculation leading to the gelling of the prepared oil-continuous emulsions, optical micrographs of dilute emulsions of squalane and propane-1,2-diol stabilised by silica particles of a 23% SiOH grade

(forming gelled diol-in-oil emulsions) and a 37% SiOH grade (forming non-gelled oil-in-diol emulsions) were captured and are shown in Figure 4.9. The absence of droplet flocculation is apparent for non-gelled diol-continuous emulsions stabilised by silica particles of a 37% SiOH grade. However, the optical micrographs of dilute gelled diol-in-oil emulsions of paraffin liquid and propane-1,2-diol stabilised by silica particles of a 23% SiOH grade, illustrate significant droplet flocculation. The gelling of the waterless emulsions upon transitional phase inversion is therefore concluded to be caused by the flocculation of dispersed emulsion droplets creating a structured, solid-like network throughout the emulsion formulations.

**Figure 4.9.** Optical micrographs of dilute emulsions of paraffin liquid and propane-1,2-diol stabilised by 1 wt.% silica particles. A non-gelled oil-in-diol emulsion incorporating silica particles of a 37% SiOH grade (upper) and a gelled diol-in-oil emulsion incorporating silica particles of a 23% SiOH grade (centre and lower) are shown.



#### 4.3.2 Preparation and properties of transparent waterless, particle-stabilised emulsions incorporating paraffin liquid oil and various polyol polar phases

The transparency of the prepared waterless emulsions of isopropyl myristate and propane-1,2-diol shown in Figure 4.7 was investigated. It has been shown that the preparation of transparent emulsions can be achieved by matching the refractive indices of the immiscible liquids.<sup>26</sup> The refractive index of isopropyl myristate and propane-1,2-diol were measured at 25°C using an Abbé refractometer and found to be very similar (1.434 and 1.432 respectively), confirming the cause of this observation. In further development of the work presented here, the preparation of equivalent waterless emulsions containing various different polyols as the polar liquid phase was conducted. To simultaneously investigate the preparation of transparent emulsions and the preparation of waterless emulsions incorporating a range of polar liquid phases other than diols a selection of polyols were used. The polyols were selected such that some had a similar refractive index to the chosen oil phase (paraffin liquid), and others had a different one. The polyols chosen for this investigation were propan-1-ol, glycerol and polyethylene glycol (PEG 300) whose structures are given in Figure 4.10.

**Figure 4.10.** Structures of propan-1-ol ( $C_3H_8O$ ) (left), glycerol ( $C_3H_8O_3$ ) (middle) and PEG 300 ( $C_{2n}H_{4n+2}O_{n+1}$ ) (right).

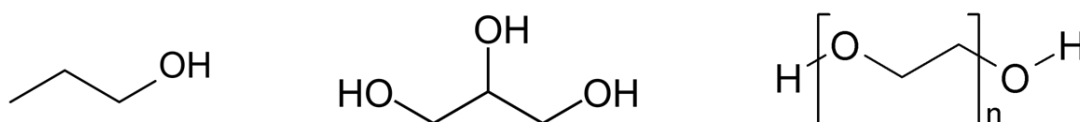


Table 4.3 lists the measured refractive indices of the liquids incorporated in the waterless emulsion systems presented here.



**Table 4.3.** Measured refractive indices at 25°C of various liquids.

<b>Liquid</b>	<b>Refractive index</b>
Paraffin liquid	1.475
Isopropyl myristate	1.434
Miglyol 812	1.450
Propane-1,2-diol	1.432
Glycerol	1.473
PEG 300	1.464
Propan-1-ol	1.386

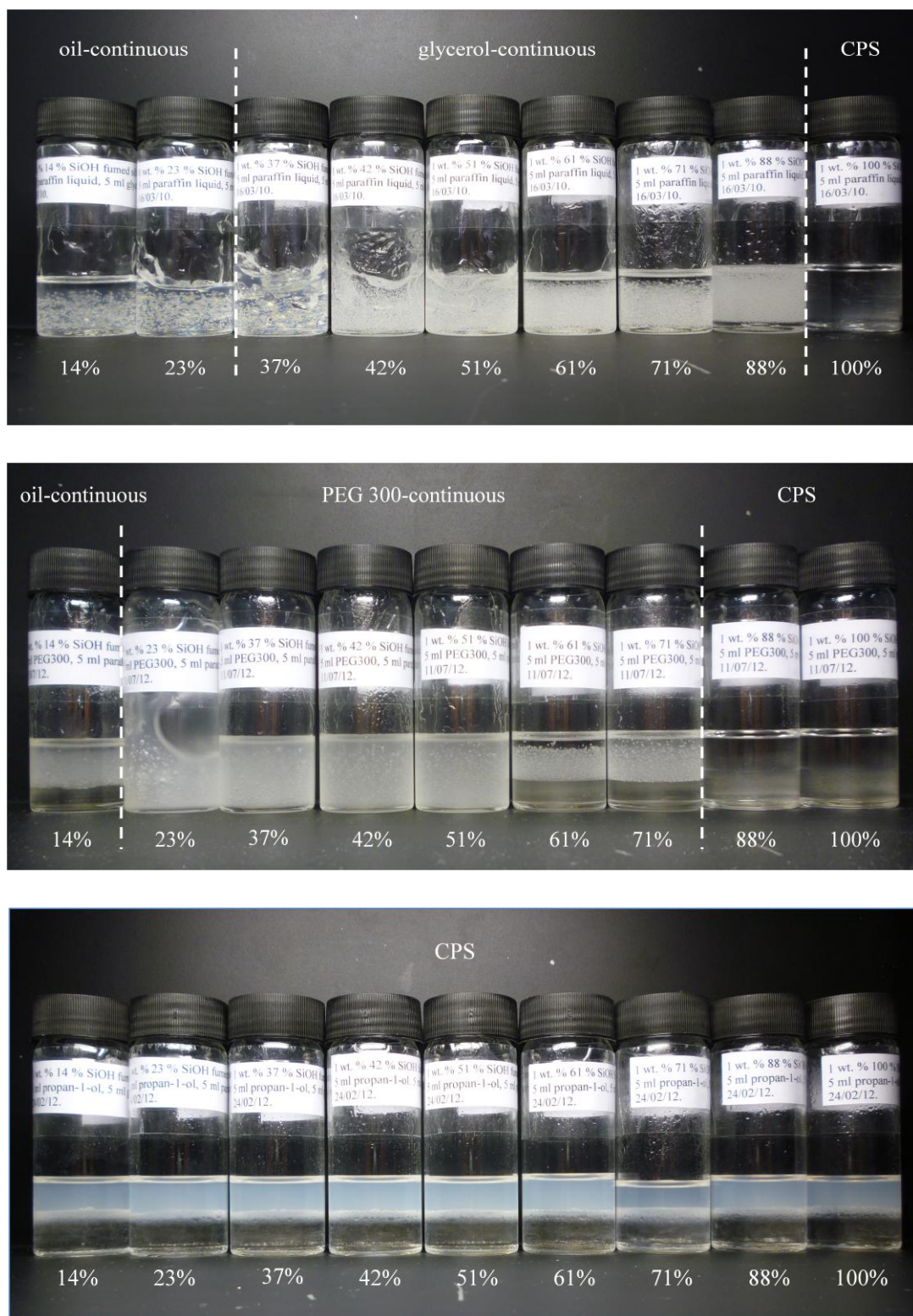
The data presented in Table 4.3 helps to illustrate the magnitude in which the refractive indices of the emulsion components must be matched to produce a transparent waterless emulsion. With reference to this data, it is clear why emulsions of isopropyl myristate and propane-1,2-diol produce transparent emulsions due to the refractive index similarity of 1.434 and 1.432 respectively. Conversely, emulsions of paraffin liquid (refractive index = 1.475) and propane-1,2-diol (refractive index = 1.432) produce an opaque white formulation due to their relatively large difference in refractive indices. Prior to preparation of the waterless emulsions which incorporate the three polyol polar liquids illustrated in Figure 4.10, it is therefore predicted that emulsions of paraffin liquid and glycerol (refractive indices of 1.475 and 1.473 respectively) will produce transparent emulsions, whilst that of paraffin liquid and PEG 300 (refractive indices of 1.475 and 1.464 respectively) and paraffin liquid and propan-1-ol (refractive indices of 1.475 and 1.386 respectively) will produce opaque white emulsions.

Figure 4.11 illustrates the appearance of the prepared waterless emulsions incorporating these additional polyol polar liquids, 1 month after emulsification. As predicted the preparation of emulsions incorporating paraffin liquid and glycerol yields transparent formulations, in which air bubbles captured during homogenisation are observed suspended within. Furthermore, emulsions of paraffin liquid and PEG 300 produce more opaque emulsions due to the dissimilar refractive indices of the liquid phases. Conversely, emulsions of paraffin liquid and propan-1-ol are shown to be unstable towards droplet coalescence and therefore completely phase separate when

incorporating silica particles of all hydrophobicities from 14-100% SiOH. The cause of this instability is not apparent without measurements of the relevant interfacial tensions between the respective phases and then application of these values to the theoretical method described previously.

The exact meaning of the term ‘waterless emulsions’ was investigated by determination of the water content in numerous of the emulsion oil and polar liquid phases. This analysis was conducted via the use of a Karl Fischer Autotitrator, and concluded that the average water content in the emulsions was  $\leq 0.15\%$ .

**Figure 4.11.** Appearance and type of emulsions 1 month after preparation from 50 vol.% paraffin liquid and 50 vol.% glycerol (upper), PEG 300 (centre) or propan-1-ol (lower) as a function of particle hydrophobicity (given in % SiOH). All emulsions contain 1 wt.% fumed silica particles.



#### **4.4 Preparation of waterless emulsions stabilised by precipitated calcium carbonate particles**

The application of the prepared waterless emulsions to the surface of the skin is not recommended by the Food and Drug Administration (FDA) agency due to their incorporation of non-biocompatible fumed silica nanoparticles. In the short subsequent investigation, the preparation of waterless emulsions of paraffin liquid and propane-1,2-diol stabilised by biocompatible particles of precipitated calcium carbonate was studied. These emulsions were prepared via an identical experimental procedure to those previously illustrated and incorporate a 50 vol.% oil phase (paraffin liquid), 50 vol.% polar liquid phase (propane-1,2-diol) and 1 wt.% precipitated calcium carbonate particles.

Figure 4.12 illustrates the appearance of two waterless emulsions of paraffin liquid and propane-1,2-diol 1 month after emulsification, stabilised by two grades of precipitated calcium carbonate. The formation of a diol-continuous emulsion is achieved via the use of an unmodified, hydrophilic precipitated calcium carbonate (Calofort U) whilst the formation of an oil-continuous emulsion is achieved via the use of a precipitated calcium carbonate which has been hydrophobised through the addition of a stearate coating (Calofort SV). The application of such particle-stabilised emulsions to the surface of the skin will more-likely be approved by the FDA agency and therefore prove as interesting formulations with many potential aspects for use in dermal drug delivery applications.

**Figure 4.12.** Appearance and type of emulsions 1 month after preparation from 50 vol.% paraffin liquid and 50 vol.% propane-1,2-diol stabilised by 1 wt.% of hydrophobised (left) and unmodified, hydrophilic (right) precipitated calcium carbonate particles.



#### 4.5 Conclusions

In this chapter, the preparation of waterless, particle-stabilised emulsions of various different oil types and non-aqueous polar liquids has been illustrated. A first approximation for the analysis of the observations made during the preparation of these emulsions has been conducted by reference to the predicted liquid phase relative hydrophobicities. A thorough analysis of the observations made here is achievable through the accurate determination of the interfacial tensions between the respective oil, polar liquid and solid particle phases of each emulsion. These studies therefore contribute to the future work resulting from this research.

The emulsions discussed in this chapter prove to be very interesting candidates for potential vehicles in the delivery of drugs across the skin. Their incorporation of both an oil phase and a diol phase, which is reputable for enhancing the penetration of many drug molecules through skin and being a good solvents for many drugs, provides the possibility of a formulation which is capable of containing and rapidly delivering very high drug concentrations compared to that of conventional emulsions of oil and water.

#### 4.6 References

1. R.G. Strickley, *Pharm. Res.*, **21**, 201, (2004).
2. B. de Spiegeleer, E. Wattyn, G. Slegers, P. van der Meeren, K. Vlamincx and L. van Vooren, *Pharm. Dev. Technol.*, **11**, 275, (2006).
3. A. Otto, J.W. Wiechers, C.L. Kelly, J. Hadgraft and J. du Plessis, *Skin Pharmacol. Physiol.*, **21**, 326, (2008).
4. B.P. Binks, P.D.I. Fletcher, M.A. Thompson and R.P. Elliott, *Colloids Surf. A*, **390**, 67, (2011).
5. B.P. Binks, P.D.I. Fletcher, M.A. Thompson and R.P. Elliott, *Langmuir*, (2013), submitted.
6. Non-aqueous solid stabilized emulsions, *US Pat.*, 61/767,880, 2013. (Inventors: B.P. Binks, R.P. Elliott, P.D.I. Fletcher, A.J. Johnson and M.A. Thompson).
7. R.D. Hamill and R.V. Petersen, *J. Pharm. Sci.*, **55**, 1268, (1966).
8. R.D. Hamill and R.V. Petersen, *J. Pharm. Sci.*, **55**, 1274, (1966).
9. A. Imhof and D.J. Pine, *J. Colloid Interface Sci.*, **192**, 368, (1997).
10. M. Klapper, S. Nenov, R. Haschick, K. Müller and K. Müllen, *Acc. Chem. Res.*, **41**, 1190, (2008).
11. V.N. Paunov, *Langmuir*, **19**, 7970, (2003).
12. T.S. Horozov, D.A. Braz, P.D.I. Fletcher, B.P. Binks and J.H. Clint, *Langmuir*, **24**, 1678, (2008).
13. A. Stocco, W. Drenckhan, E. Rio, D. Langevin and B.P. Binks, *Soft Matter*, **5**, 2215, (2009).
14. B.P. Binks and J.H. Clint, *Langmuir*, **18**, 1270, (2002).
15. F.M. Fowkes, *J. Phys. Chem.*, **67**, 2538, (1963).
16. D.K. Owens and R.C. Wendt, *J. Appl. Polym. Sci.*, **13**, 1741, (1969).

17. C.J. van Oss, R.J. Good and M.K. Chaudhury, *Langmuir*, **4**, 884, (1988).
18. B.P. Binks, A.F.K. Dyab and P.D.I. Fletcher, *Phys. Chem. Chem. Phys.*, **9**, 6391, (2007).
19. B.P. Binks and J.H. Clint, *Langmuir*, **18**, 1270, (2002).
20. B.P. Binks, P.D.I. Fletcher, B.L. Holt, P. Beaussoubre and K. Wong, *Phys. Chem. Chem. Phys.*, **12**, 11954, (2010).
21. S.R. Howe and L. Borodinsky, *Food Addit. Contam.*, **15**, 370, (1998).
22. S.A. Kahn, S.R. Raghavan and H.J. Walls, *Langmuir*, **16**, 7920, (2000).
23. *Modern Aspects of Emulsion Science*, (ed. B.P. Binks), Royal Society of Chemistry, Cambridge, 1998.
24. E.W.J. Mardles, *Nature*, **145**, 970, (1940).
25. B.P. Binks, P.D.I. Fletcher, B.L. Holt, J. Parker, P. Beaussoubre and K. Wong, *Phys. Chem. Chem. Phys.*, **12**, 11967, (2010).
26. W.F. Whitmore and R.E. Linehan, *Ind. Eng. Chem.*, **21**, 878, (1929).

## CHAPTER 5

### MEMBRANE PERMEATION FROM DONOR PARTICLE DISPERSIONS AND PARTICLE-STABILISED EMULSIONS

#### 5.1 Introduction

The establishment of a framework is presented in Chapter 3, by which the influence of the donor solvent on the rate and extent of membrane permeation of a permeant, and all of the different possible origins of such influences are resolved and understood. Based on well established and rigorous physico-chemical principles, an explicit set of equations are presented to describe both the equilibrium and kinetic behaviour of membrane permeating systems incorporating a solvent donor phase, for which a set of five key assumptions are valid. For such systems, the model predicts the key features of permeating systems obeying these assumptions and how their validity or otherwise can be experimentally tested. For systems which obey the model assumptions and conditions of constant permeation cell geometry and permeant diffusion coefficients within the membrane, the effects of changing the donor solvent on the extent and rate of membrane permeation are shown to be entirely determined by the two equilibrium permeant partition coefficients  $K_{\text{mem-don}}$  and  $K_{\text{mem-rec}}$ .

In cosmetic and pharmaceutical applications, the permeating species (i.e. the active drug) may be contacted with the donor-side of the membrane (i.e. the skin) in a variety of formulation types including, *inter alia*, solutions in either aqueous or oil solvents (as described in Chapter 3) or dissolved within multiphase, colloiddally microstructured systems, such as particle dispersions or emulsions which may be of either an oil-in-water (o/w) or water-in-oil (w/o) type. Emulsions provide the pharmaceutical industry with various advantages including, amongst other things, a degree of control over drug release, an increase in drug solubility within the formulation, improved aesthetics for topical application and a reduction in formulation costs via the replacement of a fraction of the more expensive oil solvent with water.<sup>1</sup>

In this chapter, the membrane permeation of a permeant from donor particle dispersions and particle-stabilised emulsions, is investigated in accordance with the unified theoretical model for membrane permeation which is derived in Chapter 3. The unified model is systematically adapted to account for the additional partitioning of the



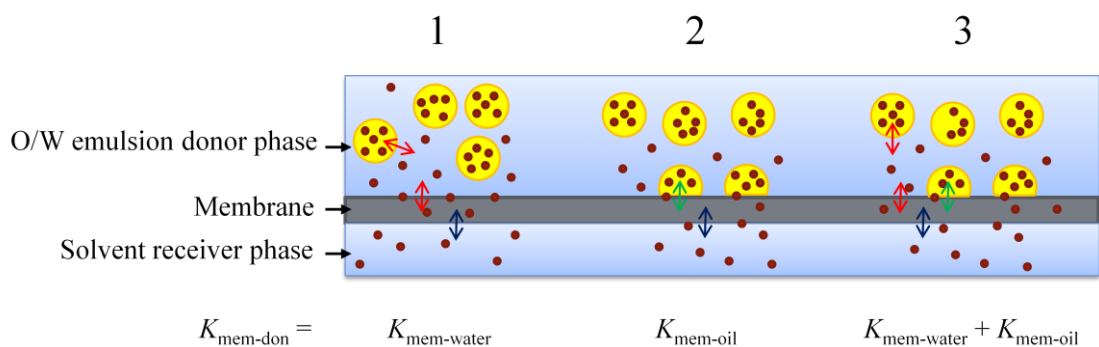
permeant between the dispersed and continuous phases of such donor formulations, whilst maintaining the set of key assumptions and underlying principles of diffusion described in Chapter 3. In a similar manner to that presented previously, the predictions made using the adapted theoretical model are then compared directly with the experimental results for the extents and rates of membrane permeation from such donor formulations, which are gathered via the use of the developed recirculating, closed-loop receiver phase experimental method described in Chapter 2. The release of permeants from both conventional oil-water and waterless (see Chapter 4) emulsions of both oil-in-polar liquid and polar liquid-in-oil types are investigated.

## 5.2 Adapting the unified theoretical model to account for donor particle dispersions and particle-stabilised emulsions

The unified theoretical model derived in Chapter 3 is relevant to the situation whereby the permeant is initially dissolved within a solution which is contacting the donor-side of the synthetic isotropic membrane. In such circumstances, both the extent and rate of permeant membrane permeation are shown to be dependent on the relative values of the  $K_{\text{mem-don}}$  and  $K_{\text{mem-rec}}$  permeant partition coefficients, which are determined by the combination of the solvent, permeant and membrane under analysis. For situations involving a donor particle dispersion or particle-stabilised emulsion, the determination of the  $K_{\text{mem-don}}$  permeant partition coefficient and the concentration of the permeant in direct contact with the membrane, is made more complex by the presence of additional phases in the donor medium, of which the permeant can partition to. Furthermore, in the presence of particle-stabilised emulsions, determination of the value for the  $K_{\text{mem-don}}$  permeant partition coefficient will ultimately depend on the emulsion phase (i.e. dispersed or continuous) which is directly contacting the membrane surface, and hence, will depend on the mechanism of permeant delivery from particle-stabilised emulsions. The envisaged possible mechanisms of permeant delivery from particle-stabilised emulsions are illustrated in Figure 5.1. The first feasible mechanism occurs via the permeant firstly partitioning between the emulsion dispersed and continuous phases and then partitioning directly from the emulsion continuous phase into the outermost layer of the membrane. Upon partitioning to the donor-side outer layer of the membrane, the permeant will then obey the same mechanism of rate-limiting diffusion across the membrane as described in

Chapter 3. In consideration of this mechanism of permeant release from a particle-stabilised emulsion, the value of the  $K_{\text{mem-don}}$  permeant partition coefficient is therefore denoted by the permeant partition coefficient between the membrane and the emulsion continuous phase,  $K_{\text{mem-cont}}$ . Alternatively, the second plausible mechanism of permeant delivery from a particle-stabilised emulsion, is via the adhesion of the dispersed emulsion droplets to the surface of the membrane followed subsequently by partitioning of the permeant from within the dispersed emulsion phase directly to the membrane donor-side outer layer. Here, the value of the  $K_{\text{mem-don}}$  permeant partition coefficient would therefore be equal to the value of the permeant partition coefficient between the membrane and the emulsion dispersed droplet phase,  $K_{\text{mem-drop}}$ . Finally, the third feasible mechanism of permeant delivery from donor particle-stabilised emulsions, entails both of the above mechanisms whereby permeant transfer to the membrane occurs from both the emulsion continuous and dispersed phases. Hence, the value of the  $K_{\text{mem-don}}$  permeant partition coefficient would be equal to the sum of the values of the  $K_{\text{mem-cont}}$  and  $K_{\text{mem-drop}}$  permeant partition coefficients. Figure 5.1 shows a schematic representation of these three feasible mechanisms from an oil-in-water emulsion and the respective equivalent values of the  $K_{\text{mem-don}}$  permeant partition coefficient.

**Figure 5.1.** A schematic representation of the possible mechanisms of permeant release from an oil-in-water donor particle-stabilised emulsion, through a synthetic membrane and into a single solvent receiver phase.



For the derivation of the theoretical model described subsequently, it is assumed that upon application of a particle-stabilised emulsion to the donor-side of the membrane, transport of the permeant to the donor-side outer layer of the membrane occurs exclusively via transfer from the continuous phase of the donor formulation (i.e.

mechanism 1). The event of dispersed emulsion droplet adhesion to the membrane requires an energetically unfavourable detachment of a large amount of emulsifying particles from the oil/polar liquid interface. As described in Chapter 1, this detachment energy,  $E_{\text{det}}$ , equates to several thousand kT for a single nanoparticle residing at the interface of such particle-stabilised emulsions and hence, the emulsion droplets show a high resistance towards such droplet adhesion. This resistance to particle detachment from the fluid-fluid interface is demonstrated by Weitz *et al.*<sup>2</sup> where it was shown that upon reducing the volume of the dispersed emulsion drops, the particles still remain attached at the interface but form a “buckled” shell as the interfacial area reduces, hence justifying this assumption plausible. The validity of this assumption is later examined.

In order to maintain the key assumptions described in Chapter 3 during the derivation of the theoretical model, it is consequently assumed that the partitioning of the permeant between the dispersed and continuous phases of both particle dispersions and particle-stabilised emulsions, is non-rate-limiting with regards to the overall membrane permeation process. Therefore, diffusion of the permeant across the membrane remains to be considered as the overall rate-limiting step of membrane permeation. The validity of this assumption is also later examined.

### 5.2.1 *Derivation of the adapted theoretical model to account for donor particle dispersions and particle-stabilised emulsions*

In order to compare the theoretical and experimental membrane permeation data, the derivation of an equation to describe how the concentration of the permeant in the receiving phase ( $C_{\text{rec}}$ ) varies as a function of time  $t$ , like that described in Chapter 3, is required. For the application of particle dispersions or particle-stabilised emulsions to the donor-side of the membrane, and with regards to the assumed mechanism of permeant delivery from the continuous phase of these formulations, the first step in this derivation is to derive a relationship between the concentration of the permeant in the overall volume of the donor formulation ( $C_{\text{don}}$ ) and the concentration present in the continuous phase of the donor compartment ( $C_{\text{cont}}$ ). Hence, the distribution of the permeant between the emulsion dispersed droplets and the continuous phase needs to be accounted for in the presence of a particle-stabilised emulsion, in addition to the significant adsorption of the permeant from the continuous phase solution onto the

surfaces of the particles used to stabilise the emulsions or which are otherwise present alone in the particle dispersions. Given that it is assumed that all partitioning processes are fast relative to permeant diffusion across the membrane, the relationship between  $C_{\text{cont}}$  and the concentration of the permeant in the dispersed emulsion droplet phase ( $C_{\text{drop}}$ ) is given by the appropriate equilibrium partition coefficient expression

$$K_{\text{drop-cont}} = \frac{C_{\text{drop}}}{C_{\text{cont}}} \quad (5.1)$$

To account for the adsorption of the permeant from the continuous phase to the emulsifying or dispersed particles, it is assumed that the adsorption follows a Langmuir adsorption isotherm according to the Langmuir equation

$$\frac{\Gamma}{\Gamma_{\text{max}}} = \frac{GC_{\text{cont}}}{1 + GC_{\text{cont}}} \quad (5.2)$$

where  $\Gamma$  is the amount of permeant adsorbed per unit mass of the particles, hence,  $\Gamma/\Gamma_{\text{max}}$  is the fractional permeant coverage of the particle surface and  $G$  is a system dependant constant. Furthermore, the number of moles of adsorbed permeant ( $n_{\text{ads}}$ ) is equal to  $\Gamma m_p$ , where  $m_p$  is the mass of particles in the donor formulation and therefore

$$\frac{n_{\text{ads}}}{V_{\text{donor}}} = \frac{m_p \Gamma_{\text{max}} GC_{\text{cont}}}{(1 + GC_{\text{cont}}) V_{\text{donor}}} \quad (5.3)$$

To help simplify the subsequent expressions,  $\Gamma_{\text{max}} G$  is denoted as the constant  $H$  and it is assumed that the permeant adsorption onto the particles is weak such that  $GC_{\text{cont}} \ll 1$ . This assumption is justified later in this chapter, and hence, equation 5.3 simplifies to

$$\frac{n_{\text{ads}}}{V_{\text{donor}}} = \frac{m_p H C_{\text{cont}}}{V_{\text{donor}}} \quad (5.4)$$

Therefore, the overall concentration of the permeant in the donor compartment ( $C_{\text{don}}$ ) for a donor particle-stabilised emulsion is the sum of the contributions from the permeant present in the dispersed emulsion drops, the emulsion continuous phase, and that adsorbed on the emulsifying particle surfaces according to

$$C_{\text{don}} = (\phi_{\text{drop}} K_{\text{drop-cont}}) C_{\text{cont}} + (1 - \phi_{\text{drop}}) C_{\text{cont}} + \left( \frac{m_p H}{V_{\text{don}}} \right) C_{\text{cont}} \quad (5.5)$$

where  $\phi_{\text{drop}}$  is the volume fraction of dispersed emulsion drops in the donor formulation (i.e.  $\phi_{\text{drop}} = 0$  for particle dispersions). Rearranging this equation gives an expression for  $C_{\text{cont}}$  in terms of  $C_{\text{don}}$ , the relevant volume fractions, the particle concentration and other parameters, such that

$$C_{\text{cont}} = \frac{C_{\text{don}}}{\{1 + (\phi_{\text{drop}} K_{\text{drop-cont}}) - \phi_{\text{drop}} + (m_p H / V_{\text{don}})\}} \quad (5.6)$$

Having derived an equation to describe the relationship between the concentration of the permeant in the entire donor formulation ( $C_{\text{don}}$ ) and the permeant concentration present in the continuous phase of the donor compartment ( $C_{\text{cont}}$ ), the same mathematical derivation to that illustrated in Chapter 3 is followed. The subsequent derivation therefore describes how the concentration of the permeant in the receiving phase ( $C_{\text{rec}}$ ) is expected to vary as a function of time, when a particle dispersion or particle-stabilised emulsion is applied to the donor-side of the membrane and hence, incorporates the additional parameters of equation 5.6 to that presented in Chapter 3.

As described in Chapter 3, the total number of moles of permeant in the system ( $n_t$ ) is equal to

$$n_t = C_{\text{don}} V_{\text{don}} + C_{\text{rec}} V_{\text{rec}} + C_{\text{mem}} V_{\text{mem}} \quad (5.7)$$

Again, under steady-state conditions, there is a linear permeant concentration gradient across the membrane that varies from  $C_{\text{mem,d}}$  at the donor-side surface to  $C_{\text{mem,r}}$  at the receiver side surface and hence,  $C_{\text{mem}} = (C_{\text{mem,d}} + C_{\text{mem,r}}) / 2$ . The permeant concentrations in the membrane on the donor and receiver sides ( $C_{\text{mem,d}}$  and  $C_{\text{mem,r}}$  respectively) are related to the concentrations  $C_{\text{cont}}$  and  $C_{\text{rec}}$  by the relevant partition coefficients according to

$$C_{\text{mem,d}} = K_{\text{mem-cont}} C_{\text{cont}} \quad (5.8)$$

$$C_{\text{mem,r}} = K_{\text{mem-rec}} C_{\text{rec}} \quad (5.9)$$

and hence, rearrangement of equation 5.7 gives

$$C_{\text{don}} = \frac{(n_t - C_{\text{rec}} V_{\text{rec}} - K_{\text{mem-cont}} C_{\text{cont}} V_{\text{mem}} / 2 - K_{\text{mem-rec}} C_{\text{rec}} V_{\text{mem}} / 2)}{V_{\text{don}}} \quad (5.10)$$

which is equivalent to that of equation 3.5 of Chapter 3, but accounts for the concentration of the permeant in the continuous phase of the donor formulation instead of the overall donor solution. Hence, equation 5.10 can be substituted into equation 5.6 which is expressed in the form  $C_{\text{cont}} = C_{\text{don}}/B$ , where  $B$  is defined by the denominator of equation 5.6. Hence, the relationship between  $C_{\text{cont}}$  and  $C_{\text{rec}}$  is given by

$$C_{\text{cont}} = \frac{n_t / BV_{\text{don}}}{(1 + (K_{\text{mem-cont}} V_{\text{mem}} / 2BV_{\text{don}}))} - \frac{(V_{\text{rec}} / BV_{\text{don}} + K_{\text{mem-rec}} V_{\text{mem}} / 2BV_{\text{don}})C_{\text{rec}}}{(1 + (K_{\text{mem-cont}} V_{\text{mem}} / 2BV_{\text{don}}))} \quad (5.11)$$

Under steady-state permeation conditions, i.e. following the lag time when the steady-state, linear concentration gradient of permeant across the membrane is established, the permeant concentration gradient across the membrane ( $dC_{\text{mem}}/dx$ ) is

$$\frac{dC_{\text{mem}}}{dx} = \frac{(C_{\text{mem,d}} - C_{\text{mem,r}})}{X} \quad (5.12)$$

where  $C_{\text{mem}}$  is the permeant concentration at depth  $x$  in the membrane,  $C_{\text{mem,d}}$  is the concentration at the donor-side surface,  $C_{\text{mem,r}}$  is the receiver-side surface concentration, and  $X$  is the total membrane thickness as described in Chapter 3. The rate of change of permeant concentration in the receiver compartment ( $dC_{\text{rec}}/dt$ ) is related to the concentration gradient across the membrane according to Fick's first law, such that

$$\frac{dC_{\text{rec}}}{dt} = \left( \frac{AD}{XV_{\text{rec}}} \right) (C_{\text{mem,d}} - C_{\text{mem,r}}) \quad (5.13)$$

where  $A$  is the surface area of the membrane and  $D$  is the diffusion coefficient of the permeant in the membrane. Substituting for  $C_{\text{mem,d}}$  and  $C_{\text{mem,r}}$  followed by substitution for  $C_{\text{cont}}$  according to equation 5.11 (expressed in the form  $C_{\text{cont}} = Y - ZC_{\text{rec}}$ , where  $Y$  and  $Z$  are the first and second quotients of equation 5.11), gives

$$\frac{dC_{\text{rec}}}{dt} = \left( \frac{ADK_{\text{mem-cont}}Y}{XV_{\text{rec}}} \right) - \left\{ \frac{AD(K_{\text{mem-cont}}Z + K_{\text{mem-rec}})}{XV_{\text{rec}}} \right\} C_{\text{rec}} \quad (5.14)$$

Finally, integration of equation 5.14 gives

$$C_{\text{rec}} = C_{\text{rec},\infty} + (C_{\text{rec},0} - C_{\text{rec},\infty})\exp(-kt) \quad (5.15)$$

where the long-time, limiting value of the permeant concentration in the receiver compartment ( $C_{\text{rec},\infty}$ ) and the first-order rate coefficient  $k$  are

$$C_{\text{rec},\infty} = \left\{ \frac{K_{\text{mem-cont}} Y}{K_{\text{mem-cont}} Z + K_{\text{mem-rec}}} \right\} \quad (5.16)$$

$$k = \left\{ \frac{AD(K_{\text{mem-cont}} Z + K_{\text{mem-rec}})}{XV_{\text{rec}}} \right\} \quad (5.17)$$

For the application of a particle dispersion or particle-stabilised emulsion to the donor-side of the membrane, the concentration of the permeant in the receiver phase ( $C_{\text{rec}}$ ) is predicted to increase exponentially from  $C_{\text{rec},0}$  to  $C_{\text{rec},\infty}$ , with a first-order permeation rate coefficient  $k$ , given that the set of assumptions described in Chapter 3 are abided by throughout. It is also assumed that the additional partitioning of the permeant between the dispersed and continuous phases of such donor formulations is non-rate-limiting, such that the rate-determining step of the overall membrane permeation process remains to be diffusion of the permeant across the membrane (this step is accounted for by assumption I of Chapter 3). Furthermore, it is assumed that the mechanism of membrane permeation of a permeant from a particle-stabilised emulsion occurs exclusively via partitioning of the permeant to the membrane from the continuous phase of the donor formulation.

### 5.2.2 Predicting the extent and rate of membrane permeation from donor particle-stabilised emulsions

In Chapter 3 it was shown that upon simplifying the derived expressions for  $C_{\text{rec},\infty}$  and  $k$ , by removing factors such as the permeant concentration and the geometric parameters of the permeating system (i.e. letting  $V_{\text{don}} = V_{\text{rec}}$  and  $V_{\text{mem}} = 0$ ), the relative rates and extents of membrane permeation were shown to be dependent only on the values of the two partition coefficients  $K_{\text{mem-don}}$  and  $K_{\text{mem-rec}}$ . Hence, a quick and accurate prediction for the experimentally observed rates and extents of membrane permeation could be made for any given combination of donor solvent, permeant and

membrane. In the scenario presented here, concerning the use of particle-stabilised emulsions as the donor phase, these predictions are made more complex due to the incorporation of the additional  $Z$  parameter in equations 5.16 and 5.17. In a complex manner, the  $Z$  parameter accounts for the additional partitioning of the permeant between the dispersed and continuous phases of the donor particle-stabilised emulsion, and for the adsorption of the permeant onto the surfaces of the particles present in the respective donor formulations prior to partitioning to the membrane. However, the influence of the  $Z$  parameter on the resulting values of  $C_{\text{rec},\infty}$  and  $k$  is not apparent because  $Z$ , in-turn, depends on an incorporated  $B$  parameter, which depends further still on various other system dependent parameters i.e.  $H$ ,  $\phi_{\text{drop}}$ , etc.

The primary interest in this chapter is in understanding how the emulsion type (i.e. oil-in-water or water-in-oil) and dispersed volume fraction (i.e.  $\phi_{\text{drop}}$ ) for a given emulsion composition, influences the characteristics of permeant delivery across a membrane. For example, in considering two emulsions of identical permeant concentration and chemical composition, the primary aims are:

1. To understand how the permeant delivery across a membrane from an emulsion of 50 vol.% oil in 50 vol.% water (oil-in-water) varies compared to that of an emulsion of 50 vol.% water in 50 vol.% oil (water-in-oil) of identical permeant concentration and chemical composition.
2. To understand how the permeant release from a particle-stabilised emulsion of 25 vol.% oil dispersed in 75 vol.% water (oil-in-water) compares to that of a particle-stabilised emulsion of 75 vol.% water dispersed in 25 vol.% oil (water-in-oil) of equal permeant concentration.

With regards to predicting the extent (i.e.  $C_{\text{rec},\infty}$ ) of permeant delivery from a particle-stabilised emulsion of a given composition, the concentration of the permeant in the receiving phase of the closed-loop experimental apparatus at infinite time ( $C_{\text{rec},\infty}$ ) is predicted to be non-dependent on the emulsion type in the donor phase. The value of  $C_{\text{rec},\infty}$  is related to the equilibrium distribution of the permeant between the three phases present in any system incorporating a donor particle-stabilised emulsion (i.e. the emulsion dispersed phase, the emulsion continuous phase and the experimental apparatus receiving phase). Hence, irrespective of the type of emulsion applied to the donor side of the membrane, the permeant will partition between these three phases



until its equilibrium position is reached and hence the value of  $C_{\text{rec},\infty}$  will be equal for a given emulsion composition.

However, the influence of the emulsion type and dispersed volume fraction on the predicted first-order rate coefficient  $k$  for the membrane permeation of a permeant from a particle-stabilised emulsion is not intuitive. Consider for example, the permeation of testosterone from an oil-in-water emulsion through a hydrophobic membrane. As a first approximation, given that testosterone has an affinity for the hydrophobic membrane over the aqueous continuous phase of the emulsion (i.e.  $K_{\text{mem-cont}} \gg 1$ ), it may be initially foreseen that the testosterone more rapidly partitions from the emulsion to the membrane, compared to that from an equivalent water-in-oil emulsion ( $K_{\text{mem-cont}} \leq 1$ ). However, the additional distribution of the testosterone between the water continuous phase and the dispersed oil phase of the emulsion (where  $K_{\text{drop-cont}} \gg 1$ ) makes these predictions significantly more complex. The subsequent derivation therefore aims to illustrate the influence of the emulsion type and the dispersed volume fraction of a donor particle-stabilised emulsion on the first-order rate coefficient of membrane permeation of a permeant.

Firstly, consider the relevant equations for describing the first-order permeation rate coefficient as derived previously. In repeating equation 5.17, these are

$$k = \left\{ \frac{AD(K_{\text{mem-cont}}Z + K_{\text{mem-rec}})}{XV_{\text{rec}}} \right\} \quad (5.17)$$

where

$$Z = \left\{ \frac{V_{\text{rec}}/BV_{\text{don}} + K_{\text{mem-rec}}V_{\text{mem}}/2BV_{\text{don}}}{1 + (K_{\text{mem-cont}}V_{\text{mem}}/2BV_{\text{don}})} \right\} \quad (5.18)$$

and

$$B = \left\{ (1 + \phi_{\text{drop}}K_{\text{drop-cont}}) - \phi_{\text{drop}} + (m_p H/V_{\text{don}}) \right\} \quad (5.19)$$

Like that shown in Chapter 3, to highlight the sole influence of the donor formulation on the characteristics of membrane permeation, let  $V_{\text{don}} = V_{\text{rec}}$ ,  $V_{\text{mem}} = 0$  and  $H = 0$  (i.e. temporarily ignore the influence of permeant adsorption onto the particle surfaces). Again, the first-order permeation rate coefficient can be expressed as

the dimensionless rate coefficient ( $kXV_{\text{rec}}/AD$ ) (denoted as  $k'$ ) such that equations 5.17–5.19 simplify to

$$k' = K_{\text{mem-cont}} Z + K_{\text{mem-rec}} \quad (5.20)$$

$$Z = \left\{ \frac{1/B + K_{\text{mem-rec}}/2B}{1 + (K_{\text{mem-cont}}/2B)} \right\} \quad (5.21)$$

and

$$B = (1 + \phi_{\text{drop}} K_{\text{drop-cont}}) - \phi_{\text{drop}} \quad (5.22)$$

Substitution of equation 5.22 into 5.21 then yields

$$Z = \left\{ \frac{\left( \frac{1}{1 + \phi_{\text{drop}} K_{\text{drop-cont}} - \phi_{\text{drop}}} \right) + \left( \frac{K_{\text{mem-rec}}}{2(1 + \phi_{\text{drop}} K_{\text{drop-cont}} - \phi_{\text{drop}})} \right)}{\left( 1 + \frac{K_{\text{mem-cont}}}{2(1 + \phi_{\text{drop}} K_{\text{drop-cont}} - \phi_{\text{drop}})} \right)} \right\} \quad (5.23)$$

For an emulsion system composed of two immiscible liquids (denoted as liquid 1 and liquid 2), two different values of  $k'$  can be assigned. Let  $k'_{1-2}$  correspond to the emulsion of liquid 1 dispersed in liquid 2 and  $k'_{2-1}$  correspond to the emulsion of liquid 2 dispersed in liquid 1. With reference to this notation, the permeant partition coefficient  $K_{\text{mem-cont}}$  is systematically denoted as  $K_{\text{mem-2}}$  and  $K_{\text{mem-1}}$ , and  $K_{\text{drop-cont}}$  is denoted as  $K_{1-2}$  and  $K_{2-1}$  respectively for emulsions denoted by  $k'_{1-2}$  and  $k'_{2-1}$ . The influence of the emulsion type on the first-order permeation rate coefficient  $k$  is therefore illustrated through consideration of the ratio  $k'_{1-2}/k'_{2-1}$  such that

$$\frac{k'_{1-2}}{k'_{2-1}} = \frac{K_{\text{mem-2}} Z_{1-2} + K_{\text{mem-rec}}}{K_{\text{mem-1}} Z_{2-1} + K_{\text{mem-rec}}} \quad (5.24)$$

where

$$Z_{1-2} = \left\{ \frac{\left( \frac{1}{1 + \phi_1 K_{1-2} - \phi_1} \right) + \left( \frac{K_{\text{mem-rec}}}{2(1 + \phi_1 K_{1-2} - \phi_1)} \right)}{\left( 1 + \frac{K_{\text{mem-2}}}{2(1 + \phi_1 K_{1-2} - \phi_1)} \right)} \right\} \quad (5.25)$$

and

$$Z_{2-1} = \left\{ \frac{\left( \frac{1}{1 + \phi_2 K_{2-1} - \phi_2} \right) + \left( \frac{K_{\text{mem-rec}}}{2(1 + \phi_2 K_{2-1} - \phi_2)} \right)}{\left( 1 + \frac{K_{\text{mem-1}}}{2(1 + \phi_2 K_{2-1} - \phi_2)} \right)} \right\} \quad (5.26)$$

To simplify the above expressions, a common numerator and denominator is required and hence, it follows that

$$\phi_2 = 1 - \phi_1 \quad (5.27)$$

$$K_{2-1} = \frac{1}{K_{1-2}} \quad (5.28)$$

$$K_{\text{mem-1}} = \frac{K_{\text{mem-2}}}{K_{1-2}} \quad (5.29)$$

Finally, the substitution of equations 5.27 - 5.29 into equation 5.26 followed by the further substitution of equations 5.25 and 5.26 into equation 5.24 yields

$$\frac{k'_{1-2}}{k'_{2-1}} = \frac{K_{\text{mem-2}} \left\{ \frac{\left( \frac{1}{1 + \phi_1 K_{1-2} - \phi_1} \right) + \left( \frac{K_{\text{mem-rec}}}{2(1 + \phi_1 K_{1-2} - \phi_1)} \right)}{\left( 1 + \frac{K_{\text{mem-2}}}{2(1 + \phi_1 K_{1-2} - \phi_1)} \right)} \right\} + K_{\text{mem-rec}}}{\frac{K_{\text{mem-2}}}{K_{1-2}} \left\{ \frac{\left( \frac{1}{1 + ((1 - \phi_1)/K_{1-2}) - 1 + \phi_1} \right) + \left( \frac{K_{\text{mem-rec}}}{2(1 + ((1 - \phi_1)/K_{1-2}) - 1 + \phi_1)} \right)}{\left( 1 + \frac{(K_{\text{mem-2}}/K_{1-2})}{2(1 + ((1 - \phi_1)/K_{1-2}) - 1 + \phi_1)} \right)} \right\} + K_{\text{mem-rec}}} \quad (5.30)$$

Through the application of complex algebra, it can be shown that this fraction reduces to 1 for any given values of  $K_{\text{mem-2}}$ ,  $K_{\text{mem-rec}}$ ,  $K_{1-2}$  and  $\phi_1$ . Although this simplification is not given here, it has been tested numerically by substituting a range of values for these variable parameters and consistently illustrates a value of  $k'_{1-2}/k'_{2-1} = 1$ . It is therefore predicted that the first-order rate coefficient  $k$  of membrane permeation from particle-stabilised emulsions of identical composition is independent of emulsion type and dispersed phase volume fraction.

This prediction is based on the assumption that permeant adsorption onto the emulsion-stabilising particles is negligible (i.e.  $H = 0$ ). Given that  $H$  corresponds to the permeant adsorption onto the particles from the emulsion continuous phase, it follows that if  $H$  is significantly different for an oil-in-water and a water-in-oil emulsion, then a difference in both the measured values of  $C_{\text{rec},\infty}$  and  $k$  between the two emulsion types is expected.

For emulsions of varying composition (i.e. oil and water vol.%), the characteristics of membrane permeation are expected to change in accordance with varying the donor solvents, as described in Chapter 3. Given that this influence has been thoroughly explained previously, it is not investigated in this chapter.

The predictions made here are valid for systems incorporating a constant value of the permeant diffusion coefficient through the membrane  $D$ . In the results discussed subsequently, the permeation of both caffeine and testosterone through a PDMS membrane from both the developed waterless particle-stabilised emulsions (see Chapter 4) and conventional oil-water particle-stabilised emulsions are investigated. The waterless emulsion system examined is that composed of a polar propane-1,2-diol (PG) phase and a squalane oil phase, of which both emulsion components have been shown in Chapter 3 to not modify the value of the permeant diffusion coefficient within a PDMS membrane. The membrane permeation of a permeant from this waterless emulsion series is therefore expected to obey the predictions outlined here. The conventional oil-water particle-stabilised emulsion system investigated is composed of a water polar phase and an isopropyl myristate (IPM) oil phase, whereby the IPM solvent has been shown to modify the diffusion coefficient of testosterone within the PDMS membrane and hence produce deviations from the theoretical predictions made here. Prior to these analyses, the determination of the different adsorption coefficients  $H$ , for the adsorption of testosterone and caffeine, from the relevant solvents to the surface of the different particles used to stabilise the respective emulsions was investigated. These analyses were completed by studying the membrane permeation of each permeant from donor particle dispersions in the respective solvents.

### 5.3 Measuring the membrane permeation of permeants from donor particle dispersions

The comparison of the adapted theoretical model and the experimental results was conducted by first investigating the membrane permeation of permeants from donor particle dispersions in order to determine the relevant adsorption coefficients ( $H$ ). Given that  $H$  corresponds to the adsorption of the permeant onto the surface of the particles from the emulsion continuous phase, particle dispersions within several different solvents were investigated corresponding to the different emulsions studied. The chosen solvents were PG and squalane, which are the respective continuous phases of the oil-in-polar liquid and polar liquid-in-oil waterless emulsions investigated, and water and IPM, which are the respective continuous phases of the conventional oil-in-water and water-in-oil emulsions investigated. The release of testosterone and caffeine from donor particle dispersions through a PDMS membrane was examined. For each solvent, the coefficient of permeant adsorption ( $H$ ) was determined by monitoring the release of a permeant from a series of solutions of equal initial permeant concentration but varied dispersed particle concentrations. The wettability of the silica particles dispersed within the solvents, described by the particle surface % SiOH, was determined by the particle wettability required to stabilise the corresponding emulsion whereby that solvent formed the emulsion continuous phase. The different emulsion types investigated and the respective silica particle % SiOH required are summarised in Table 5.1.

**Table 5.1.** A summary of the wettability of the different silica particles used to stabilise the different emulsions investigated in the membrane permeation studies, through reference to the % SiOH present on the surface of the silica particles. The corresponding adsorption coefficient notation is given for each emulsion.

Donor emulsion	Required silica particle % SiOH	Corresponding $H$ notation
Squalane-in-PG	42% SiOH	$H_{PG}$
PG-in-squalane	23% SiOH	$H_{squalane}$
IPM-in-water	75% SiOH	$H_{water}$
Water-in-IPM	61% SiOH	$H_{IPM}$

Figures 5.2 and 5.3 show examples of the experimental results obtained from the permeation of testosterone from silica particle dispersions in solvents of water and IPM respectively. All dispersions in water have an initial testosterone concentration of 0.1 mM with varying dispersed particle concentrations. All dispersions in IPM have an initial testosterone concentration of 12.8 mM with varying dispersed particle concentrations. It can be seen that increasing the dispersed silica particle concentration causes both  $C_{\text{rec},\infty}$  and  $k$  to decrease in both water and IPM solvent systems. This is qualitatively consistent with the predictions of equations 5.15-5.17 based on the concept that testosterone adsorption onto the silica nanoparticles decreases the concentration available in the solvent continuous phase, which thereby decreases both  $C_{\text{rec},\infty}$  and  $k$ . The adsorption coefficients ( $H$ ) for each permeant adsorbing onto the relevant silica particles from the continuous solvent phases, were extracted from these studies via the use of Microsoft EXCEL's solver function. In calculating the theoretical values of  $C_{\text{rec},\infty}$  and  $k$  using equations 5.16 and 5.17, by application of the input parameters described in Chapter 3 and repeated below in Table 5.2, the lack of fit of experimental data to that of calculated data, due to an effective reduction in permeant concentration through adsorption onto the particles, is accounted for by allowing the value of  $H$  to float until the expected correlation between experimental results and theoretical results is re-established. In these calculations, all geometrical parameters such as the volume of the donor phase ( $V_{\text{don}}$ ), the volume of the receiver phase ( $V_{\text{rec}}$ ) and the area of the membrane over which permeation occurs ( $A$ ), remain constant and equal to the values described in Chapters 2 and 3.

**Table 5.2.** System dependent parameter values used in the calculation of  $C_{\text{rec},\infty}$  and  $k$  for the permeation of testosterone and caffeine in donor particle dispersions in solvents of PG, squalane, water and IPM through PDMS membranes at 32°C.

<b>Donor phase</b>	<b><math>K_{\text{mem-cont}}</math></b>	<b><math>K_{\text{mem-rec}}</math></b>	<b><math>D / \text{m}^2 \text{s}^{-1}</math></b>
Testosterone in PG + silica particles (42% SiOH)	$4.9 \times 10^{-3}$	$4.9 \times 10^{-3}$	$9.3 \times 10^{-12}$
Testosterone in squalane + silica particles (23% SiOH)	0.8	5	$9.3 \times 10^{-12}$
Testosterone in water + silica particles (75% SiOH)	3.7	5	$9.3 \times 10^{-12}$
Testosterone in IPM + silica particles (61% SiOH)	0.04	5	$1.4 \times 10^{-10}$
Caffeine in PG + silica particles (42% SiOH)	0.16	0.16	$1.6 \times 10^{-12}$
Caffeine in squalane + particles (23% SiOH)	15	0.14	$1.6 \times 10^{-12}$

**Figure 5.2.** Effect of silica nanoparticle concentration of a 75% SiOH grade, on the permeation of testosterone from donor compartments containing particle dispersions in water with an initial concentration of testosterone of 0.1 mM. The key shows the nanoparticle concentration in the donor compartment in ascending order in units of mg mL<sup>-1</sup>.

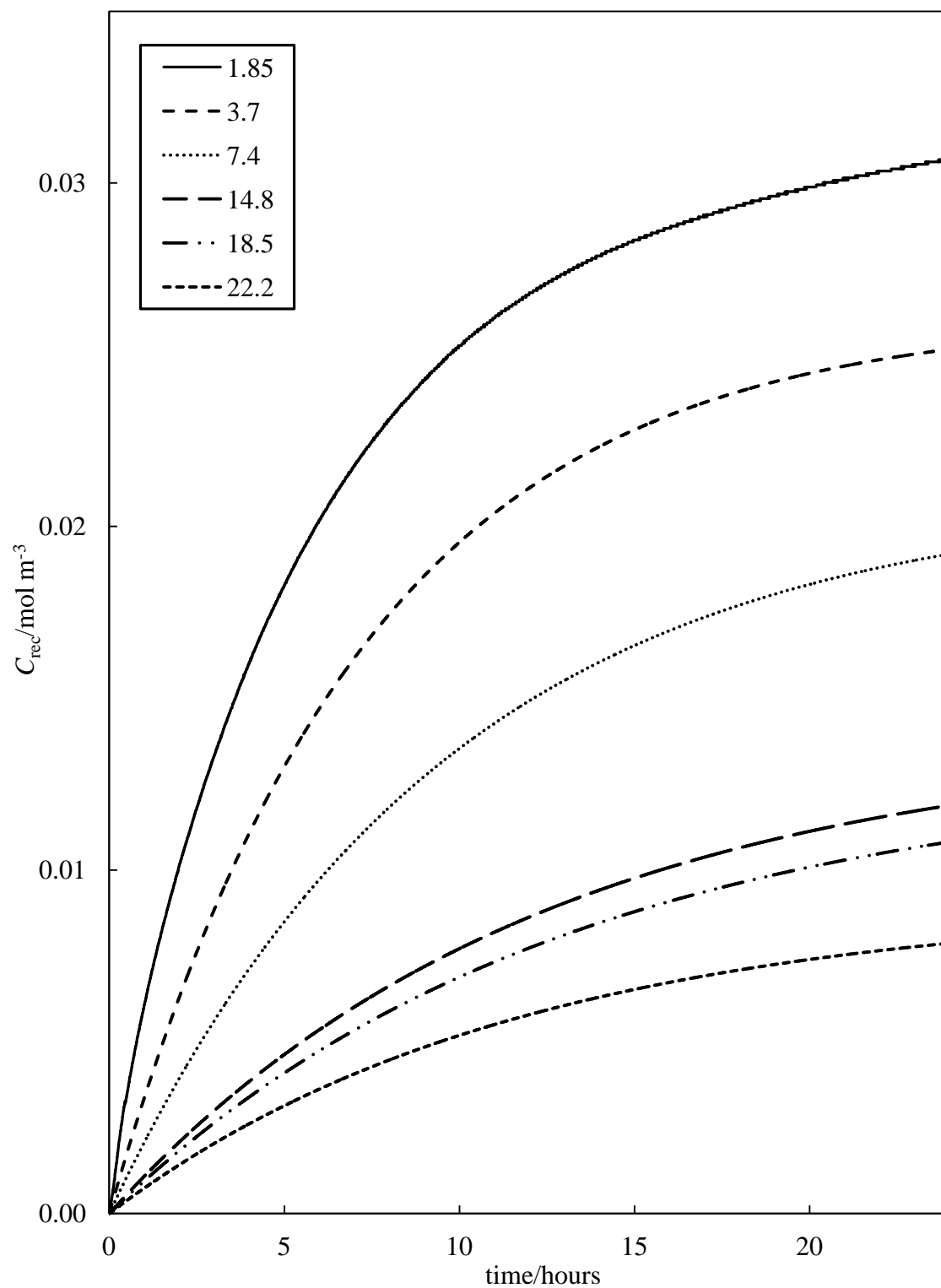




**Figure 5.3.** Effect of silica nanoparticle concentration of a 61% SiOH grade on the permeation of testosterone from donor compartments containing particle dispersions in IPM with an initial concentration of testosterone of 12.8 mM. The key shows the nanoparticle concentration in the donor compartment in ascending order in units of mg mL<sup>-1</sup>.

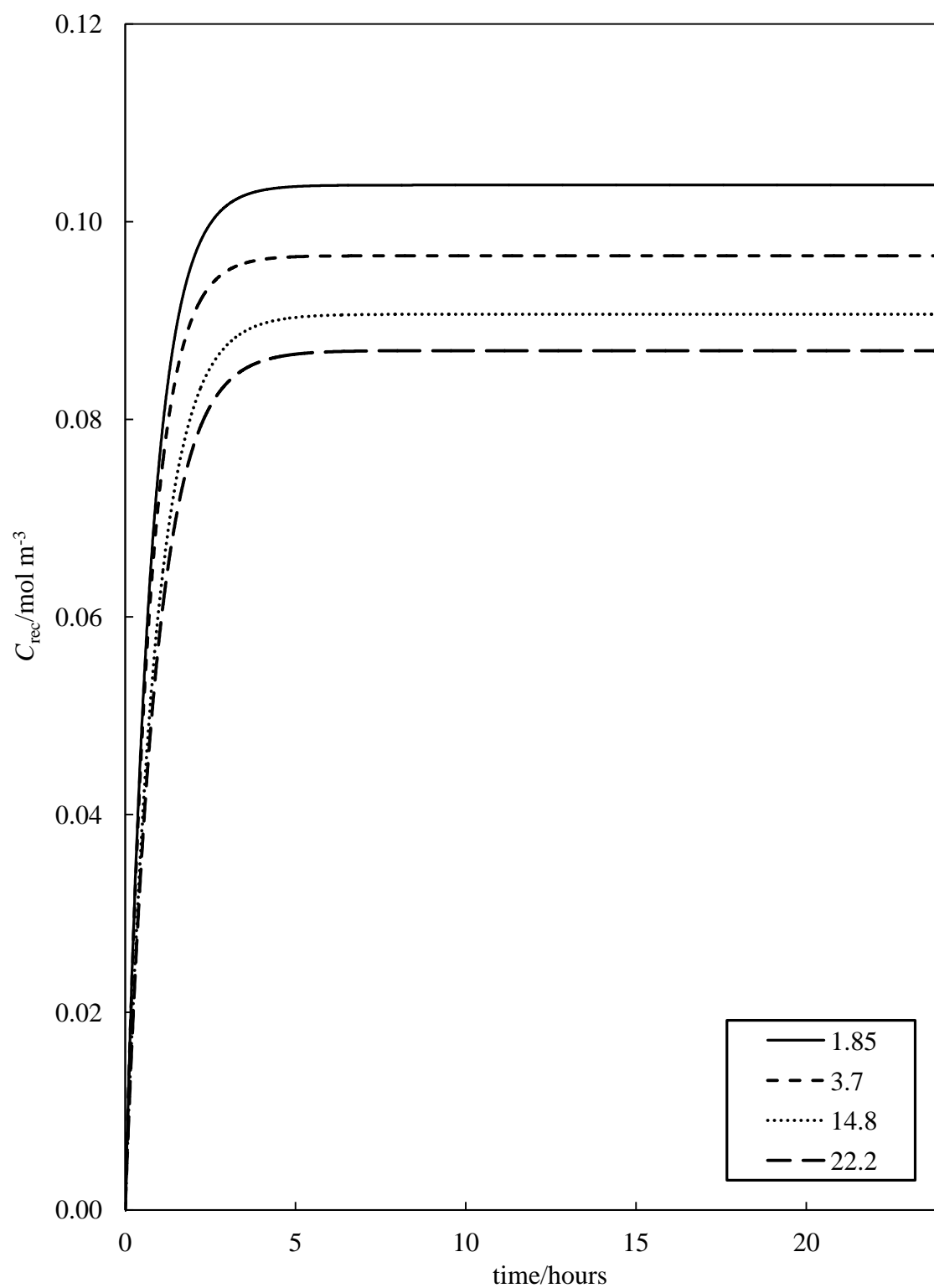


Table 5.3 illustrates the concluded set of permeant adsorption coefficients determined in this manner, for the adsorption of testosterone and caffeine onto silica particles of the respective % SiOH grades from the relevant solvents. The extent at which the particle concentration influences the values of  $C_{\text{rec},\infty}$  and  $k$  is dependent on the solvent been analysed. For example, water is a poor solvent for hydrophobic testosterone, hence adsorption onto the silica particles is more potent than in IPM which is a much better solvent for testosterone. This change in the extent of influence in the variation of  $C_{\text{rec},\infty}$  and  $k$  is reflected by the numerical values of  $H$  given in table 5.3.

**Table 5.3.** Summary of the experimentally determined  $H$  coefficients for the adsorption of testosterone and caffeine from various solvents onto the surface of silica nanoparticles of the relevant % SiOH grades.

Permeant	Solvent	% SiOH on silica particles	$H$ value / $\text{g}^{-1} \text{m}^3$
Testosterone	PG	42	$H_{\text{PG}} = 7.8 \times 10^{-5}$
Testosterone	Squalane	23	$H_{\text{squalane}} = 2.8 \times 10^{-4}$
Testosterone	Water	75	$H_{\text{water}} = 2.6 \times 10^{-4}$
Testosterone	IPM	61	$H_{\text{IPM}} = 9.0 \times 10^{-6}$
Caffeine	PG	42	$H_{\text{PG}} = 1.6 \times 10^{-4}$
Caffeine	Squalane	23	$H_{\text{squalane}} = 1.2 \times 10^{-3}$

The assumption made previously that the permeant adsorption to the silica nanoparticles is weak (i.e.  $GC_{\text{cont}} \ll 1$ ) is next examined. Consider, for example, the adsorption of testosterone onto the surface of the silica particles from solvents of water and IPM as shown in Figures 5.2 and 5.3. As described previously, the value of the adsorption parameter  $H$ , is equal to  $G\Gamma_{\text{max}}$ . The value of  $\Gamma_{\text{max}}$ , corresponding to close-packed, monolayer coverage of the silica nanoparticle surface, is estimated from crystallographic data for the dimensions of a testosterone molecule<sup>3</sup> to be approximately  $2.4 \text{ molecules nm}^{-2}$ . Given that the specific surface area of the silica nanoparticles used is  $200 \text{ m}^2 \text{ g}^{-1}$ ,  $\Gamma_{\text{max}}$  corresponds to  $8.0 \times 10^{-4} \text{ mol g}^{-1}$  and hence,  $G_{\text{water}}$  and  $G_{\text{IPM}} = 0.33$  and  $0.011 \text{ mol}^{-1} \text{ m}^3$ , respectively. In the context of this example, for the nanoparticle dispersion permeation experiments, the water and IPM donor

compartments contained 0.1 and 12.8 mol m<sup>-3</sup> total permeant concentrations (were 1 mol m<sup>-3</sup> = 1 mM), and hence,  $G_{\text{water}}C_{\text{cont}} < 0.03$  and  $G_{\text{IPM}}C_{\text{cont}} < 0.14$ . It is therefore concluded that the assumption of weak permeant adsorption to the particle surfaces, giving the linear behaviour of equation 5.4, is approximately valid for all particle dispersions investigated here.

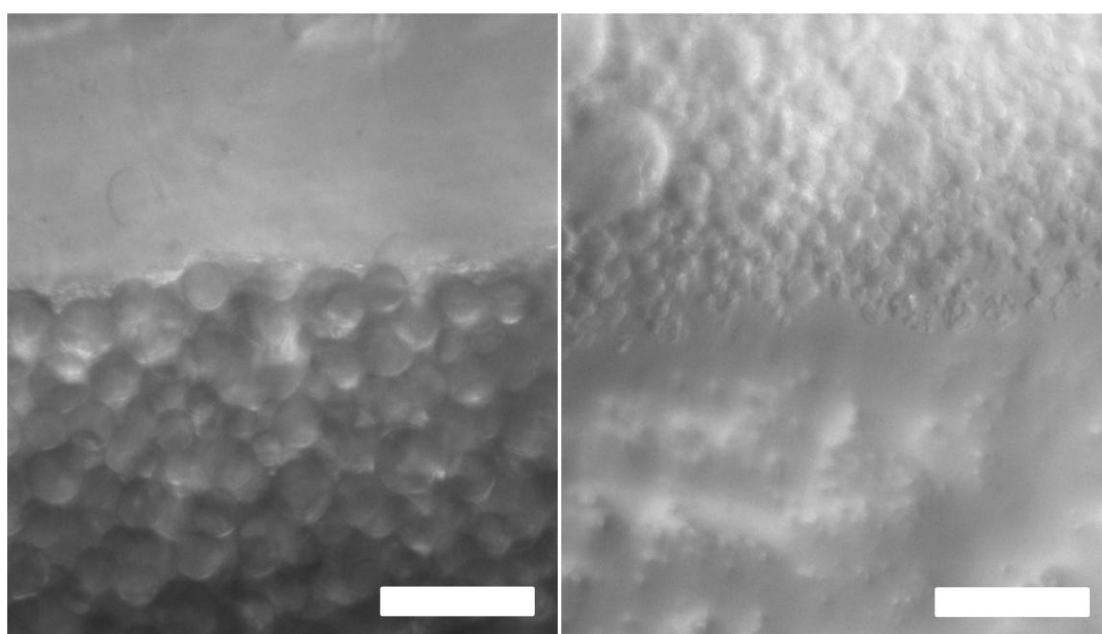
#### 5.4 Measuring the membrane permeation of permeants from donor particle-stabilised emulsions

Prior to the analysis of permeant release from particle-stabilised emulsions, the assumed mechanism of permeant delivery to the membrane exclusively from the emulsion continuous phase is firstly examined. The permeant release from particle-stabilised emulsions of PG and squalane is then analysed as these systems are predicted to obey the theoretical predictions as discussed previously. The transport of a permeant from the conventional oil-water emulsions incorporating an IPM solvent are then discussed whereby deviations from the theoretical model are predicted and accounted for through a variation of the permeant diffusion coefficient within the membrane.

##### 5.4.1 *Justifying the mechanism of permeant release from donor particle-stabilised emulsions*

In the theoretical model of membrane permeation discussed here, it is assumed that the emulsion drops do not adhere to the membrane such that permeant transfer to the membrane from a donor particle-stabilised emulsion occurs exclusively from the emulsion continuous phase. This assumption was checked by recording optical micrographs of both IPM-in-water and water-in-IPM emulsion drops at the interface of the PDMS membrane. As shown in Figure 5.4, even when the observation cell is oriented such that gravity or buoyancy forces (through emulsion creaming or sedimentation respectively) favour drop-membrane contact, the drops closest to the membrane surface do not adhere to the membrane. It is shown that upon contact with the membrane, the dispersed emulsion drops remain spherical and are observed to be mobile when viewed “live”. An absence of droplet adhesion to the membrane was again observed when viewing the PG-in-squalane and squalane-in-PG waterless emulsions at the PDMS membrane surface.

**Figure 5.4.** Optical micrographs showing an IPM-in-water emulsion stabilised by 75% SiOH silica particles at the PDMS membrane surface (left) and a water-in-IPM emulsion stabilised by 61% SiOH silica particles at the PDMS membrane surface (right). The IPM-in-water emulsion drops are in buoyant contact with the PDMS membrane as the membrane is oriented above the emulsion such that creaming of the less dense emulsion oil drops forces them onto the membrane. The water-in-IPM emulsion drops are sedimented onto the PDMS membrane which is oriented beneath the emulsion, under the force of gravity as they are denser than the oil continuous phase. Scale bars = 50  $\mu\text{m}$ .



#### 5.4.2 *Membrane permeation from waterless particle-stabilised emulsions of squalane and PG*

As described by equation 5.30 of the theoretical model, the first-order permeation rate coefficient  $k$ , is predicted to be independent of the emulsion type and dispersed volume fraction for emulsions of identical chemical composition, given that permeant adsorption onto the stabilising particles is negligible (i.e.  $H = 0$ ) and that the solvents present do not change the value of the permeant diffusion coefficient within the membrane ( $D$ ). For particle-stabilised waterless emulsions of PG and squalane, both solvents have been shown in Chapter 3 to not affect the values of the diffusion coefficients of testosterone and caffeine in a PDMS membrane. The theoretical predictions made previously, are therefore expected to be valid for the experimental

results gathered from these emulsion systems. In this study, the membrane permeation of various concentrations of testosterone and caffeine from emulsions of 50 vol.% PG, 50 vol.% squalane and 1 wt.% silica particles of the required % SiOH, from both squalane-in-PG emulsions and PG-in-squalane emulsions were investigated. Figures 5.5 and 5.6 show some of the experimental results for the permeation of testosterone and caffeine through PDMS membranes from these donor emulsions.

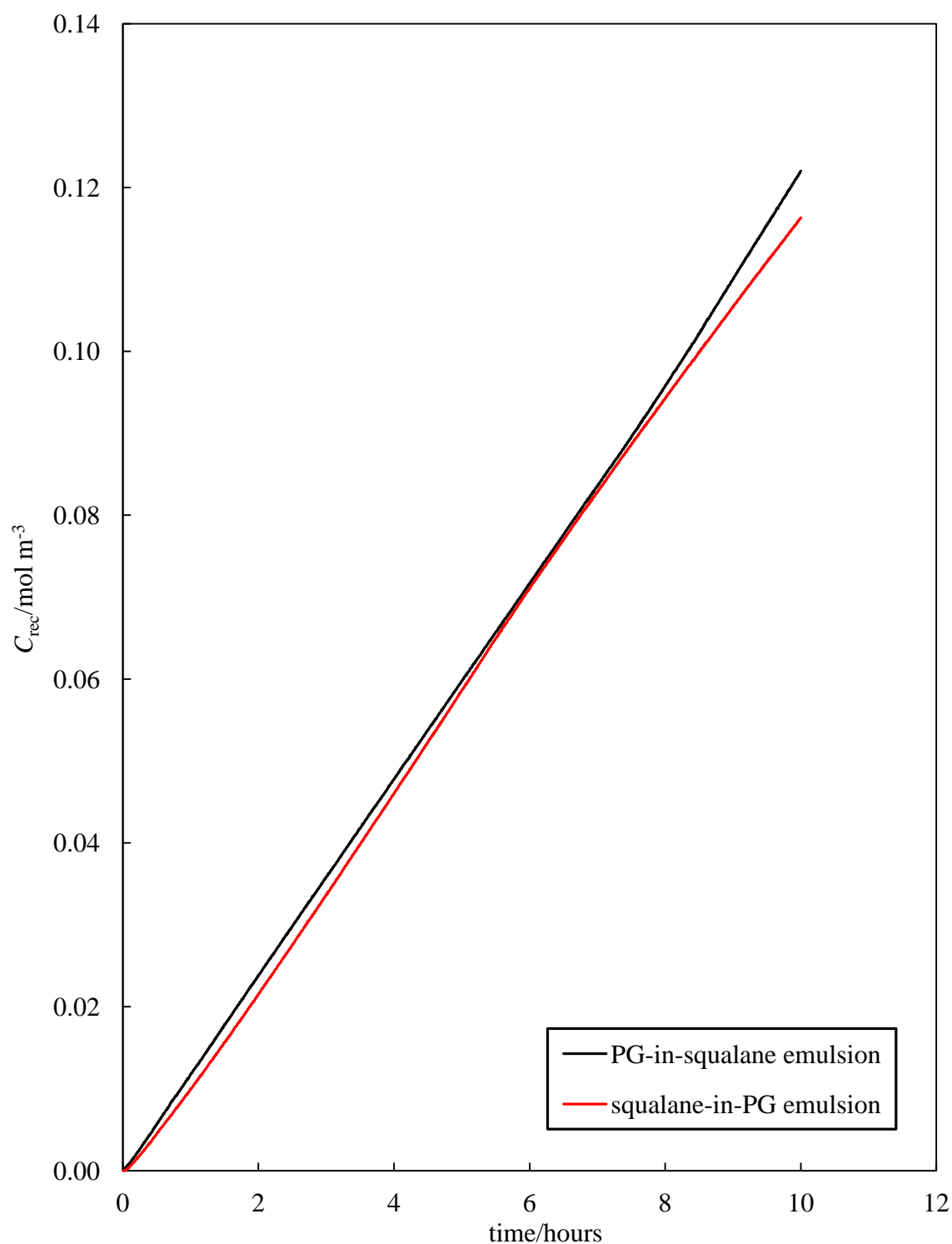
Figure 5.5 illustrates the raw experimental data from the permeation of testosterone with an initial concentration of 25 mM in the donor phase from both squalane-in-PG and PG-in-squalane emulsions, through a PDMS membrane into a PG receiver phase. In accordance with the theory and the relevant partition coefficients described in Chapter 3 and given in Table 5.4, the observed permeation rate is very slow. Consequently, the extent of permeation (i.e.  $C_{\text{rec},\infty}$ ) is not determined. However, it is clear that the rate of membrane permeation is independent of the emulsion type applied in the donor phase for a given emulsion composition. As described in Chapter 3, the gradients of these plots correspond to the initial steady-state permeation rates, which scale with initial donor phase concentration whereby the constant of proportionality is equal to the permeation rate coefficient  $k$ . Studies from equivalent emulsions of various other initial testosterone concentrations therefore yielded accurate values of  $k$ .

Figure 5.6 illustrates the raw experimental data from the permeation of caffeine with an initial concentration of 2 mM in the donor phase from both squalane-in-PG and PG-in-squalane emulsions, through a PDMS membrane into a PG receiver phase. Again, as predicted by the theoretical model, the rate of permeation across a PDMS membrane is shown to be independent of the donor emulsion type.

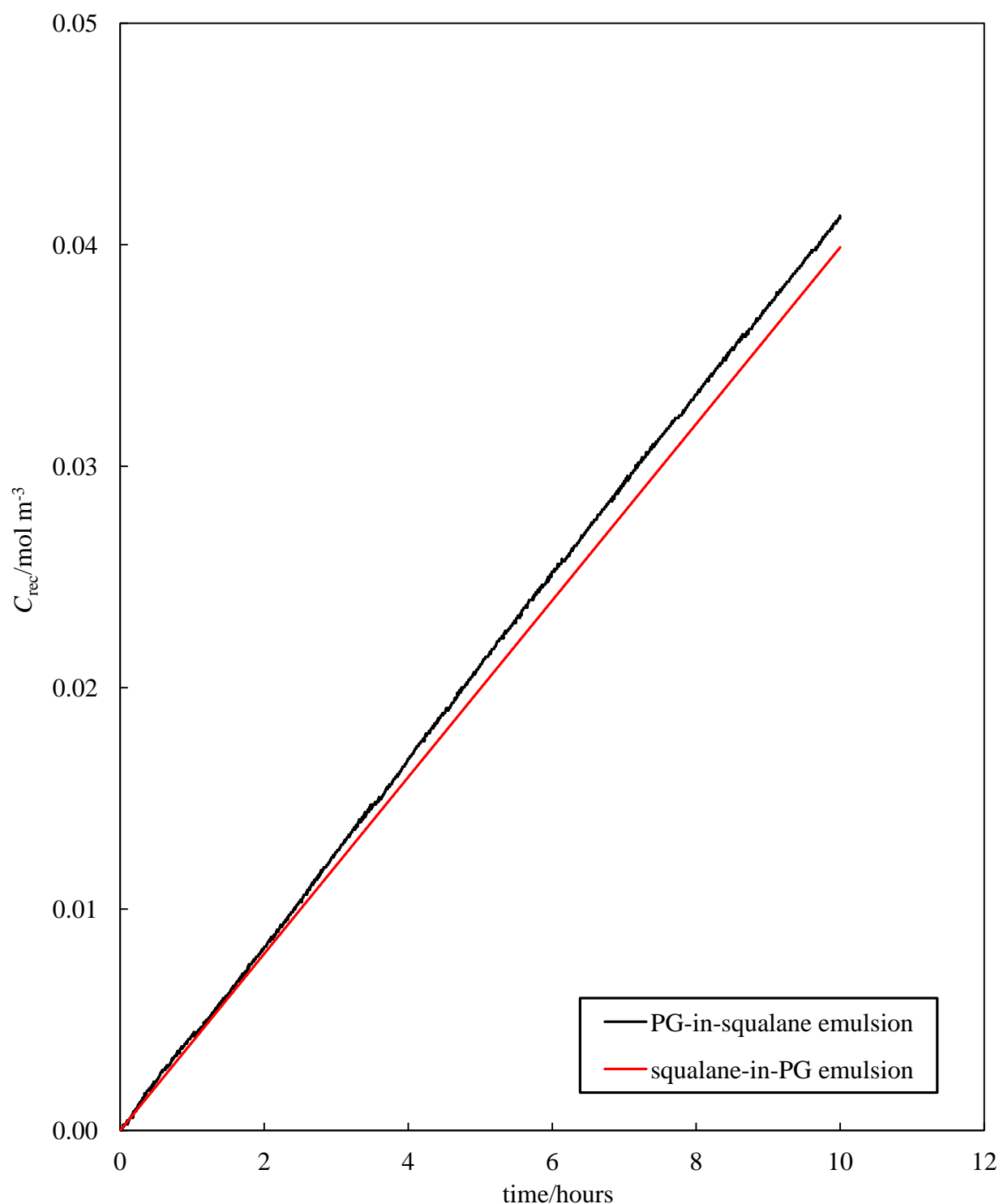
**Table 5.4.** Summary of the relevant equilibrium partition coefficients used to calculate the theoretical values of  $C_{\text{rec},\infty}$  and  $k$  for the permeation of testosterone and caffeine from squalane-in-PG and PG-in-squalane donor emulsions, through a PDMS membrane and into a PG receiver phase at 32°C.

<b>Donor phase</b>	<b><math>K_{\text{drop-cont}}</math></b>	<b><math>K_{\text{mem-cont}}</math></b>	<b><math>K_{\text{mem-rec}}</math></b>
Testosterone in squalane-in-PG emulsion	$6.1 \times 10^{-3}$	$4.9 \times 10^{-3}$	$4.9 \times 10^{-3}$
Testosterone in PG-in-squalane emulsion	165	0.8	$4.9 \times 10^{-3}$
Caffeine in squalane-in-PG emulsion	$1.1 \times 10^{-2}$	0.16	0.16
Caffeine in PG-in-squalane emulsion	94	15	0.16

**Figure 5.5.** Variation of  $C_{\text{rec}}$  with time for the permeation of testosterone through a PDMS membrane from donor particle-stabilised emulsions of PG-in-squalane (stabilised by silica particles of a 23% SiOH grade) and squalane-in-PG (stabilised by silica particles of a 42% SiOH grade) of initial testosterone concentrations of 25 mM, into a PG receiver phase. Both emulsions contain 50 vol.% squalane, 50 vol.% PG and 1 wt.% silica particles.



**Figure 5.6.** Variation of  $C_{\text{rec}}$  with time for the permeation of caffeine through a PDMS membrane from donor particle-stabilised emulsions of PG-in-squalane (stabilised by silica particles of a 23% SiOH grade) and squalane-in-PG (stabilised by silica particles of a 42% SiOH grade) of initial caffeine concentrations of 2 mM, into a PG receiver phase. Both emulsions contain 50 vol.% squalane, 50 vol.% PG and 1 wt.% silica particles.





The stability of the emulsions applied to the donor phase during a permeation run was monitored. Table 5.5 illustrates the emulsion mean drop diameters and standard deviations before and after each membrane permeation experiment. It is conclusive that the applied particle-stabilised waterless emulsions do not undergo a significant instability during the permeation experiments.

**Table 5.5.** Mean and standard deviation (SD) of drop diameter distributions of the donor emulsions before and after membrane permeation experiments.

Donor phase	Before		After	
	Mean/ $\mu\text{m}$	SD/ $\mu\text{m}$	Mean/ $\mu\text{m}$	SD/ $\mu\text{m}$
Testosterone in squalane-in-PG emulsion	48.5	3.5	49.3	3.8
Testosterone in PG-in-squalane emulsion	9.8	1.4	10.0	1.2
Caffeine in squalane-in-PG emulsion	46.4	5.1	48.7	4.9
Caffeine in PG-in-squalane emulsion	10.1	2.3	9.9	1.6

The initial permeation plots shown in Figures 5.5 and 5.6 conclusively illustrate that the rate of membrane permeation from particle-stabilised emulsions is independent of the donor emulsion type. The minor differences in the observed permeation rates shown in these figures correspond to the difference in the coefficients of permeant adsorption to the particle surfaces ( $H$ ), which is neglected in the theoretical model (i.e. assumed that  $H = 0$ ). However, the minor differences in the measured permeation rates correlate with the measured  $H$  adsorption coefficients given in Table 5.3 previously. In other words, the permeation of testosterone from a PG-in-squalane emulsion is expected to be marginally faster than from an equivalent squalane-in-PG emulsion given that  $H_{\text{squalane}} = 2.8 \times 10^{-4} \text{ g}^{-1} \text{ m}^3$  and  $H_{\text{PG}} = 7.8 \times 10^{-5} \text{ g}^{-1} \text{ m}^3$  for testosterone. Likewise, the permeation of caffeine from a PG-in-squalane emulsion is expected to be marginally faster than from an equivalent squalane-in-PG emulsion given that  $H_{\text{squalane}} = 1.2 \times 10^{-3} \text{ g}^{-1} \text{ m}^3$  and  $H_{\text{PG}} = 1.6 \times 10^{-4} \text{ g}^{-1} \text{ m}^3$  for caffeine.

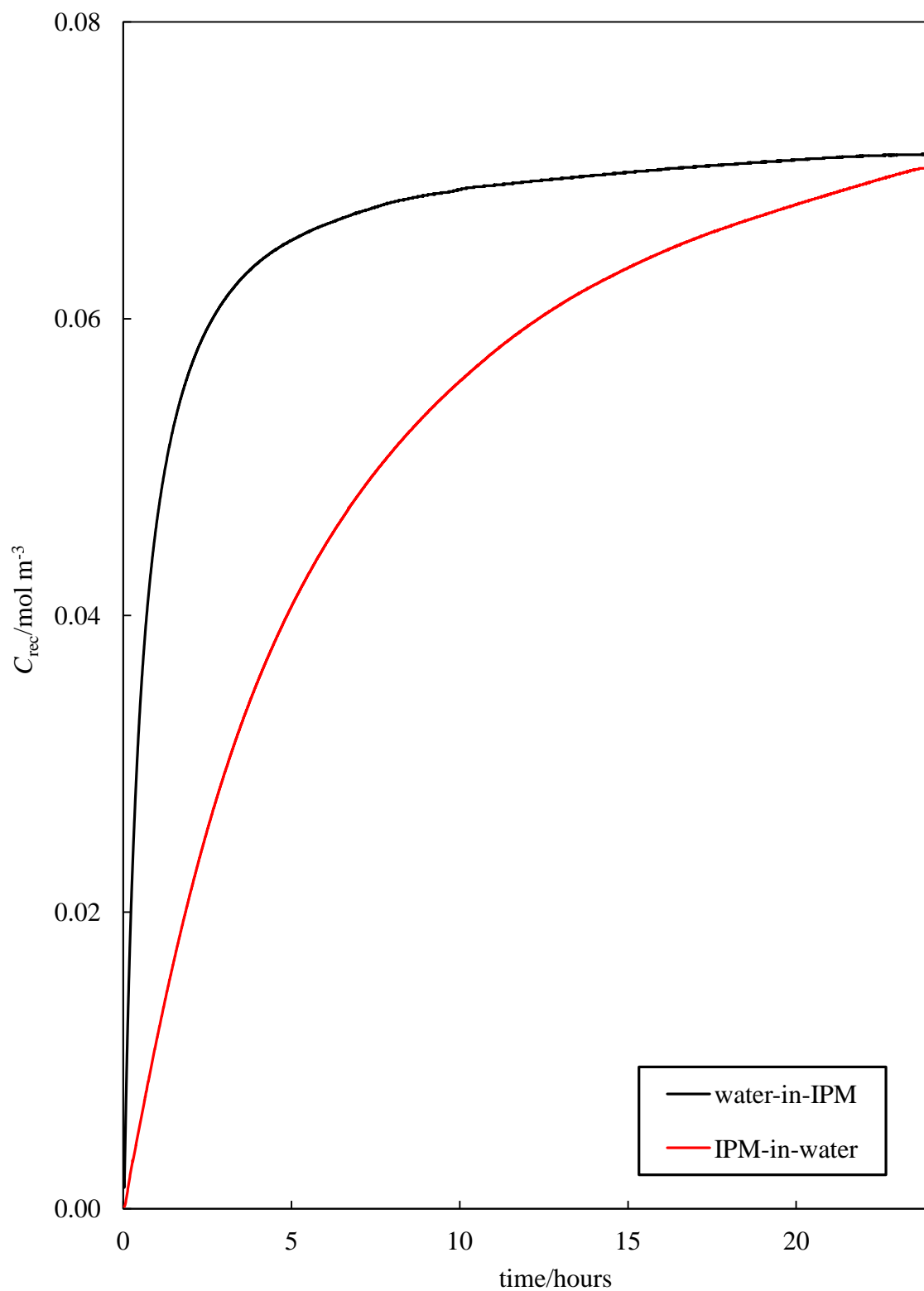
#### 5.4.3 *Membrane permeation of testosterone from a conventional oil-water emulsion of IPM and water*

The results discussed subsequently refer to the membrane permeation of testosterone from a conventional oil-water particle-stabilised emulsion through a PDMS membrane and into a PBS receiver phase.

As previously illustrated, the membrane permeation of a permeant from a particle-stabilised emulsion obeys the derived theoretical model when permeant adsorption to the stabilising particles is negligibly small, and when the emulsion solvents do not interact with the membrane, which would otherwise result in changing the permeant diffusion coefficient within the membrane ( $D$ ). In the emulsion system presented here, the incorporated IPM solvent has been shown in Chapter 3 to adjust the permeant diffusion coefficient of testosterone within the PDMS membrane. It is therefore predicted that when an IPM-continuous emulsion is applied in the donor phase, the transfer of testosterone across the PDMS membrane will be very different to that of an equivalent water-continuous emulsion, whereby the dispersed oil drops do not contact the membrane, given that the assumed mechanism of exclusive permeant release from the emulsion continuous phase is correct.

Figure 5.7 shows the permeation of testosterone across a PDMS membrane into a PBS receiver phase from emulsions of IPM-in-water and water-in-IPM of identical chemical composition.

**Figure 5.7.** Comparison of plots of  $C_{\text{rec}}$  versus time for testosterone permeating from donor compartments containing IPM-in-water and water-in-IPM emulsions through a PDMS membrane into a PBS receiver phase. Both emulsions contain 50 vol.% IPM, 50 vol.% water, 1 wt.% silica particles and an initial testosterone concentration in the donor compartment of 6.41 mM.



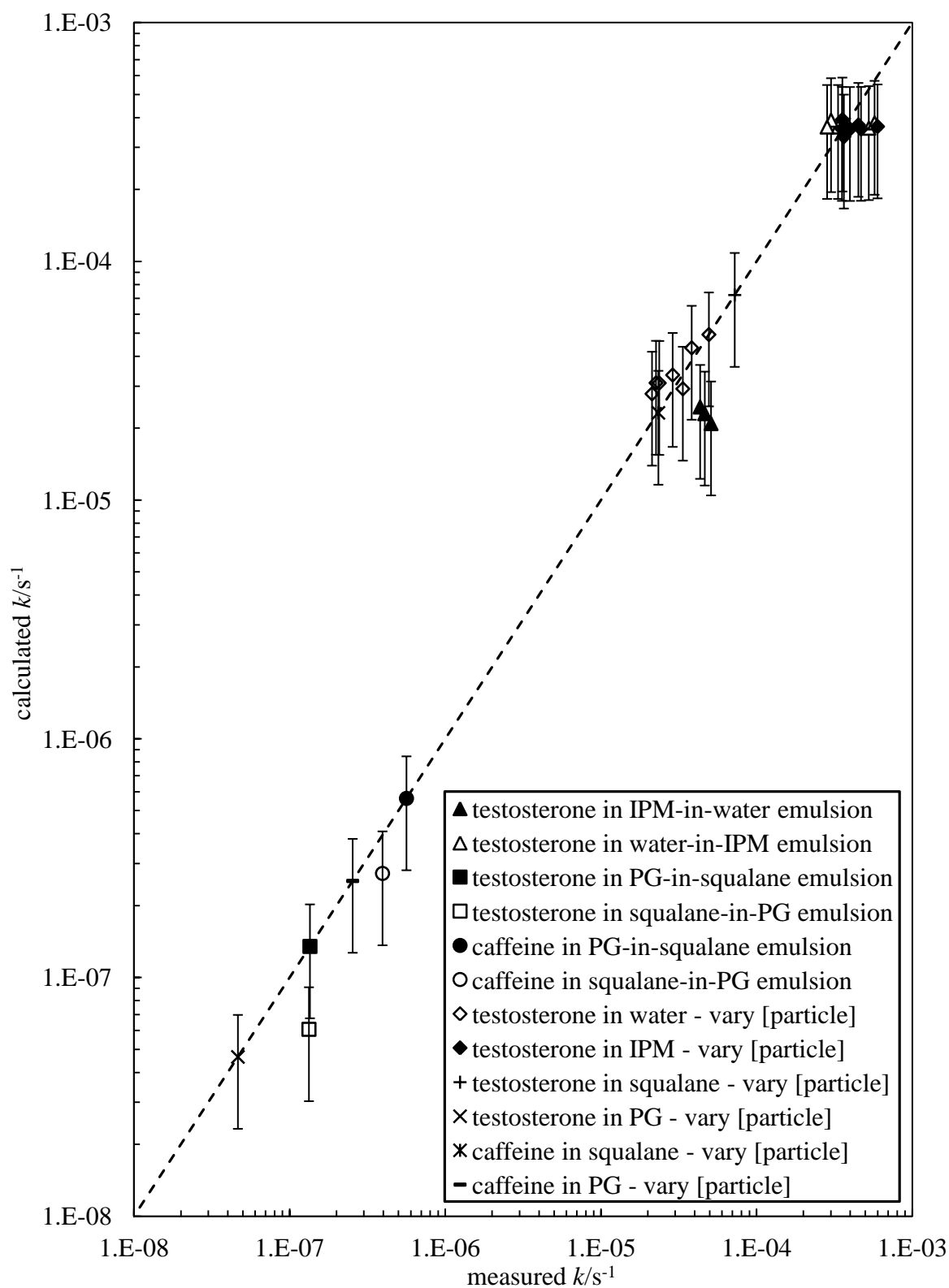
It is clear that if one of the emulsion solvents is capable of adjusting the permeant diffusion coefficient within the membrane, then the rate of membrane permeation is highly dependent on the emulsion type. However, by application of the relevant parameters into the theoretical model (i.e.  $D(\text{IPM-free}) = 9.3 \times 10^{-12} \text{ m}^2 \text{ s}^{-1}$  and  $D(\text{IPM-saturated}) = 1.4 \times 10^{-10} \text{ m}^2 \text{ s}^{-1}$  for testosterone in IPM-in-water and water-in-IPM donor emulsions respectively), it can be shown that the model still accounts for these observations. Comparison plots of the measured versus the calculated first-order permeation rate coefficients (calculated using the system dependent parameters listed in Table 5.6) are given in Figure 5.8. The data from the previous waterless emulsion systems and particle dispersions is also plotted here to demonstrate the validity of the model.

The correlation between the measured and calculated values of  $k$  shown in Figure 5.8 justifies the mechanism of exclusive permeant release from the emulsion continuous phase. The correct calculations of the experimentally measured first-order rate coefficients through application of the values of  $D$  for IPM-free systems when IPM is the dispersed phase of the emulsion, suggests that the dispersed IPM droplets in an IPM-in-water emulsion do not adhere to the membrane. Furthermore, given that the full exponential curves in the permeation experiments are obtained, the accurate values of  $C_{\text{rec},\infty}$  can be extracted from the experimental data. As predicted, the values of  $C_{\text{rec},\infty}$  are not dependent on the emulsion type applied to the donor phase as shown in Figure 5.7, because as discussed, the value of  $C_{\text{rec},\infty}$  represents the equilibrium distribution of the permeant between the solvent phases present, which is identical for two emulsions of the same chemical composition but opposing type.

**Table 5.6.** Summary of the relevant equilibrium partition coefficients and permeant diffusion coefficients used to calculate the theoretical values of the first-order permeation rate coefficient  $k$ , for the permeation of testosterone from IPM-in-water and water-in-IPM donor emulsions, through a PDMS membrane and into a PBS receiver phase at 32°C.

Donor phase	$K_{\text{drop-cont}}$	$K_{\text{mem-cont}}$	$K_{\text{mem-rec}}$	$D / \text{m}^2 \text{ s}^{-1}$
Testosterone in IPM-in-water emulsion	92	3.7	5	$9.3 \times 10^{-12}$
Testosterone in water-in-IPM emulsion	$1.1 \times 10^{-2}$	0.04	5	$1.4 \times 10^{-10}$

**Figure 5.8.** Comparison of measured and calculated values of  $k$  for permeation runs incorporating testosterone and caffeine in various different particle-stabilised emulsions and particle dispersions, through PDMS membranes and into a PG or PBS receiver phase at 32°C.



## 5.5 Conclusions

The theoretical model described here successfully accounts for the rates and extents of permeation of testosterone and caffeine through PDMS membranes from donor compartments containing either particle dispersions or particle-stabilised oil-in-polar liquid or polar liquid-in-oil emulsions. The key features of the permeation behaviour in the systems are that

- I. the rate-limiting step of the permeation is permeant diffusion across the membrane; all permeant partitioning and adsorption processes are relatively fast such that they are maintained in local equilibrium and
- II. the particle-stabilised emulsions drops do not adhere to the PDMS membrane, which means that permeant transfer from the drops to the membrane only occurs through partitioning into the emulsion continuous phase.

As predicted from the derived theoretical model, both the extent and rate of membrane permeation of a permeant from a particle-stabilised donor emulsion, are independent of the emulsion type and dispersed phase volume fraction for a given emulsion composition, given that permeant adsorption to the stabilising particles is absent and the emulsion solvents do not modify the permeants diffusion coefficient within the membrane. Therefore, a difference in the rate of permeant delivery from chemically identical emulsions of opposing types can be achieved if desired, through control of these parameters accordingly. For example, although PG has been shown to not modify the diffusion coefficients of testosterone and caffeine in a PDMS membrane, it is common knowledge that it does modify the diffusion coefficients of many permeants in human skin, and so such emulsion formulations of identical composition may offer slow or rapid drug delivery rates across the skin as desired, depending on the emulsion type.

The permeation characteristics from the waterless emulsions which were developed in Chapter 4 have been analysed and are shown to obey the theoretical model of membrane permeation derived here. These formulations are very interesting candidates in the field of drug delivery and formulation design because they are capable of dissolving very high concentrations of hydrophobic permeants compared to equivalent conventional oil-water emulsions. In applications where a large dosage of a

hydrophobic drug is required in the form of an emulsion rather than a solution, these formulations may therefore be ideal.

Lastly, a comment on whether the model described here may be applicable to a wider range of systems other than particle dispersions and particle-stabilised emulsions, and in particular, whether the model is applicable to donor compartments containing emulsions stabilised by surfactants rather than particles. It is likely that partitioning processes within the donor compartment surfactant-stabilised emulsion remain fast relative to the rate-limiting membrane diffusion step. This expectation is consistent with the observation that the drop size in surfactant-stabilised donor emulsions has virtually no effect on the membrane permeation rate.<sup>4</sup> However, other aspects may cause the permeation behaviour to differ. Firstly, surfactant-stabilised oil-in-water emulsion drops are likely to adhere to a hydrophobic membrane such that the membrane is in direct contact with the oil of the emulsion drops rather than exclusively with the aqueous continuous phase of the emulsion. This effect would cause deviations from the predictions of the model presented here. Secondly, surfactant monomers and micelle or microemulsion aggregates present in the surfactant-stabilised emulsions could potentially interact with the membrane and affect the rate of permeant diffusion. Hence, although the model presented here provides a useful framework to account for many different types of donor compartment mixtures, caution must be exercised to ensure that the model assumptions remain valid for each type.

## 5.6 References

1. C.A. Langley and D. Belcher, *FASTtrack Pharmaceutical Compounding and Dispensing*, Pharmaceutical Press, 2007.
2. S.S. Datta, H.C. Shum and D.A. Weitz, *Langmuir*, **26**, 18612, (2010).
3. A.L. Thakkar, N.D. Jones, H.A. Rose, L.G. Tensmeyer and N.A. Hall, *Acta Cryst.*, **B26**, 1184, (1970).
4. P. Izquierdo, J.W. Wiechers, E. Escribano, M.J. Garcia-Celma, T.F. Tadros, J. Esquena, J.C. Dederen and C. Solans, *Skin Pharmacol. Physiol.*, **20**, 263, (2007).



## CHAPTER 6

### SUMMARY OF CONCLUSIONS AND FUTURE WORK

#### 6.1 Conclusions

A highly reproducible method for accurately monitoring the transport of a species from a donor compartment, through a membrane and to a receiver compartment has been developed. The experimental apparatus can be adapted to include either a closed-loop, recirculating receiving phase with a constant volume or an open, variable volume receiving phase which simulates more accurately, for example, the conditions of drug delivery to the human body where the volume of the donor formulation applied to the membrane (i.e. the skin) is significantly smaller than the receiving phase (i.e. the blood stream).

The developed experimental method was then used to monitor the release of a permeant from various donor formulations through isotropic synthetic membranes. The membrane permeation from more simplistic single phase donor solvents was initially investigated with an aim to understand how changing the donor compartment solvent can affect both the rate and extent of membrane permeation of a chosen permeant. To elucidate and understand (i) all possible origins of the observed donor solvent effects, (ii) how to resolve which donor solvent effect or effects may be operating in a particular system and (iii) how the donor solvent effects depend on the nature of both the permeating species and the membrane, the membrane permeation from every possible combination of oil or aqueous donor solvent, hydrophobic or hydrophilic membrane and hydrophobic or hydrophilic permeant was investigated. An explicit set of equations were developed based on rate-limiting diffusion across the membrane which accurately describe the experimentally observed equilibrium and kinetic behaviour of permeating systems for which five key assumptions are valid. For such systems the model predicts the key features of permeating systems obeying these assumptions and how their validity or otherwise can be experimentally tested. It has been shown that for systems which obey the model assumptions and conditions of constant permeation cell geometry and permeant diffusion coefficient within the membrane, the effect of changing the donor solvent on the rate and extent of membrane

permeation are entirely determined by the two permeant partition coefficients:  $K_{\text{mem-don}}$  and  $K_{\text{mem-rec}}$ .

Additional donor solvent effects are shown to arise when changing the donor solvent renders one or more of the key model assumptions invalid. Therefore, in addition to changing the  $K_{\text{mem-don}}$  and  $K_{\text{mem-rec}}$  permeant partition coefficients, changing the donor solvent can also:

1. Alter the permeation rate-limiting step from membrane diffusion.
2. Change whether or not the membrane diffusion occurs under steady-state conditions.
3. Alter the membrane structure and uniformity.
4. Cause time-dependent changes in the solvent composition of the membrane or the donor and receiver phases.
5. Affect the extent of non-ideal permeant solution behaviour.

The derived model successfully accounts for the experimentally observed rates and extents of membrane permeation into both a closed-loop, recirculating receiver phase and an open, variable volume receiver phase configuration of the experimental apparatus.

The development of a new type of topical formulation was then discussed through the preparation of waterless particle-stabilised emulsions. The preparation of various different waterless emulsions has been demonstrated incorporating numerous different oil and polyol immiscible liquid phases. The preparation of highly stable oil-in-polar liquid and polar liquid-in-oil emulsions is demonstrated and explained through reference to the predicted particle contact angle  $\theta$  at the liquid-liquid interface based on the hydrophobic/hydrophilic moieties of the incorporated liquid phases. The properties of the prepared emulsions were discussed and causes of the observed characteristics, such as emulsion transparency through matching of the immiscible liquid refractive indices, and emulsion gelling through aggregation of the dispersed emulsion droplets, was revealed. The exact meaning of the term ‘waterless emulsions’ was investigated via the determination of the water content in the different oil and polar liquid emulsion phases. For all emulsions prepared here, the water content of the prepared emulsions was  $\leq 0.15\%$ .

The transport of a permeant from more complex multiphase donor formulations, such as particle dispersions and particle-stabilised emulsions, through isotropic membranes was then investigated using the closed-loop recirculating receiver phase configuration of the experimental technique previously developed. The theoretical model was systematically adjusted to account for the additional partitioning of the permeant between the various phases present in these more complex donor formulations, but maintains the same underlying principles of the theoretical model derived previously for a single solvent donor phase. Here, it was again found that the derived model successfully accounts for the experimentally observed rates and extents of membrane permeation from such donor formulations. The key features of the permeation behaviour in these systems are that (i) the rate-limiting step of membrane permeation from these multiphase donor formulations, is permeant diffusion across the membrane (i.e. all permeant partitioning and adsorption processes within the donor phase are relatively fast such that they are maintained within local equilibrium) and (ii) the particle-stabilised emulsion drops do not adhere to the membrane, such that permeant transfer from the dispersed emulsion drops to the membrane occurs exclusively through partitioning into the emulsion continuous phase.

Finally, both the rate and extent of membrane permeation of a permeant from a donor particle-stabilised emulsion has been shown both theoretically and experimentally to be independent of the a emulsion type and dispersed phase volume fraction for a given emulsion composition, given that permeant adsorption to the stabilising particles is negligible and that the emulsion solvents do not modify the permeants diffusion coefficient within the membrane.

## **6.2 Future work**

The research presented here is predominantly concerned with the membrane permeation of a species through isotropic synthetic membranes. One of the topics of great interest for future work is the field of membrane permeation through anisotropic membranes such as skin. The influence of the membrane wettability on the rate and extent of membrane permeation has been discussed in detail in Chapter 3 whereby studies through both hydrophobic and hydrophilic membranes were conducted. The skin however, is a composite of both hydrophilic and hydrophobic regions and is anisotropic in that the properties of permeation depend on the direction of which the

permeant is diffusing. It is therefore predicted that a theoretical model based on rate-limiting membrane permeation through the membrane, can again be produced but must account for this additional tortuous pathway of diffusion and this choice of pathway depending on the partitioning of the permeants to the different hydrophobic and hydrophilic regions of the skin.

The comparison of membrane permeation results from surfactant-stabilised emulsions to that of particle-stabilised emulsions will also prove interesting for future research. Given that surfactant molecules are in a constant dynamic equilibrium between adsorption and desorption at the emulsion liquid-liquid interface, unlike solid particles which are bound to the interface, it is possible that surfactant-stabilised emulsions give rise to a different mechanism of permeant delivery. It has been conclusively shown that when a particle-stabilised emulsion is applied to the donor side of a membrane, dispersed droplet adhesion onto the membrane does not occur. This is not necessarily true for surfactant-stabilised emulsions and therefore the mechanism of permeant delivery may be different and produce radically different permeation characteristics. Several claims suggest that particle-stabilised emulsions offer an enhanced efficacy over that surfactant-stabilised emulsions,<sup>1-2</sup> however little evidence of the cause for these claims nor a thorough understanding of the mechanisms of drug delivery have yet been given.

A further development in the understanding of the points of transitional phase inversion of the waterless emulsion formulations, illustrated in Chapter 4, should be conducted through application of the theoretical model described in section 4.2.1. The application of this model requires the measurement of all respective interfacial tensions between the different incorporated liquids and will ultimately explain the observed points of transitional phase inversion through reference to the three-phase contact angle  $\theta$  of the particles at the liquid-liquid interfaces.

### 6.3 References

1. J. Frelichowska, M.A. Bolzinger, J. Pelletier, J.P. Valour and Y. Chevalier, *Int. J. Pharm.*, **371**, 56, (2009).
2. J. Frelichowska, M. A. Bolzinger J. P. Valour, H. Mouaziz, J. Pelletier and Y. Chevalier, *Int. J. Pharm.*, **368**, 7, (2009).

## APPENDIX

This section contains Figures which were used in the construction of Chapters 2-5.

**Figure A1.1.** Calibration plot of spectrophotometric absorbance at 251 nm versus concentrations of testosterone dissolved in PBS at 32°C with a 1 cm path length.

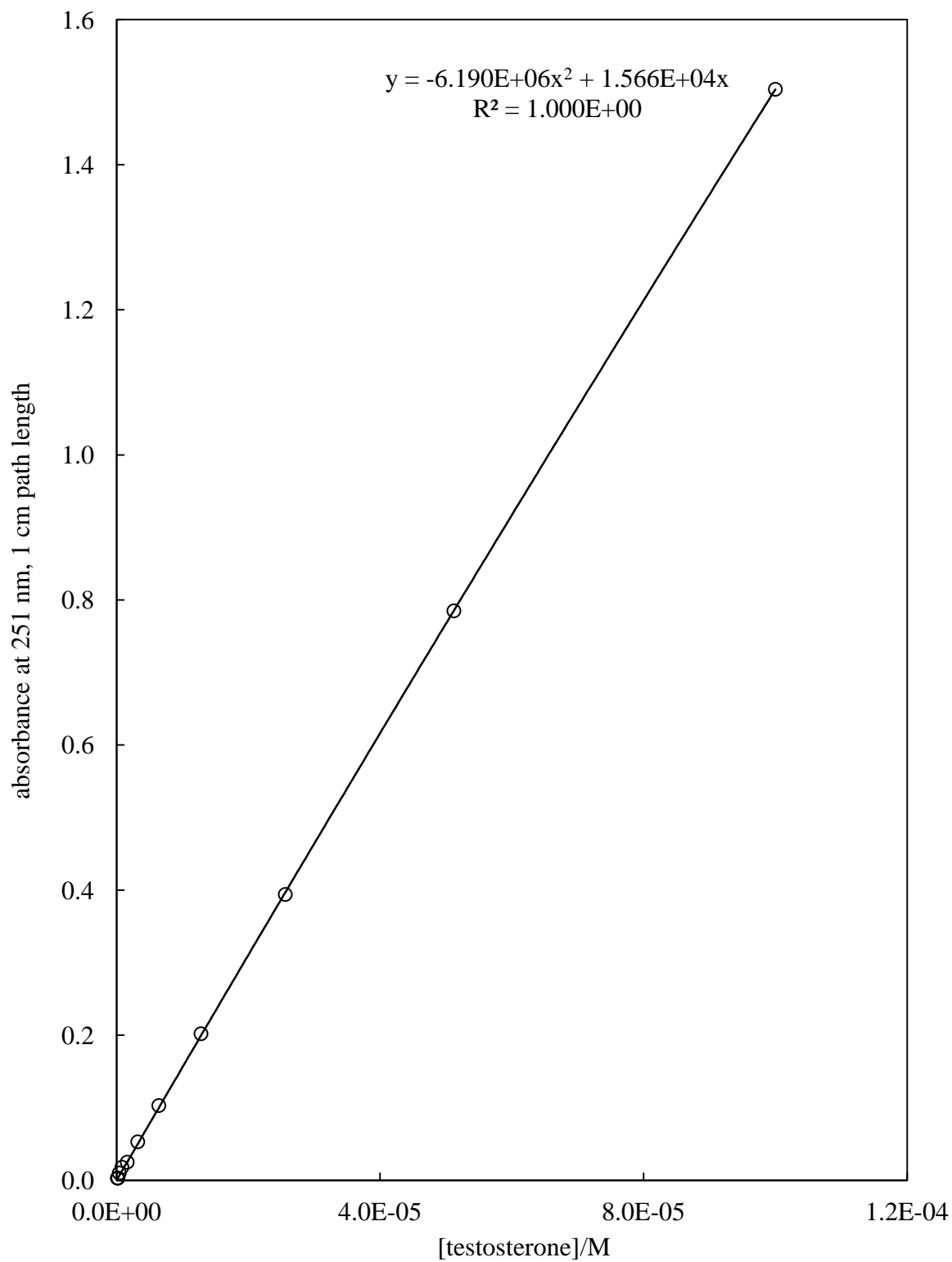


**Figure A1.2.** Calibration plot of spectrophotometric absorbance at 248 nm versus concentrations of testosterone dissolved in water at 32°C with a 1 cm path length.

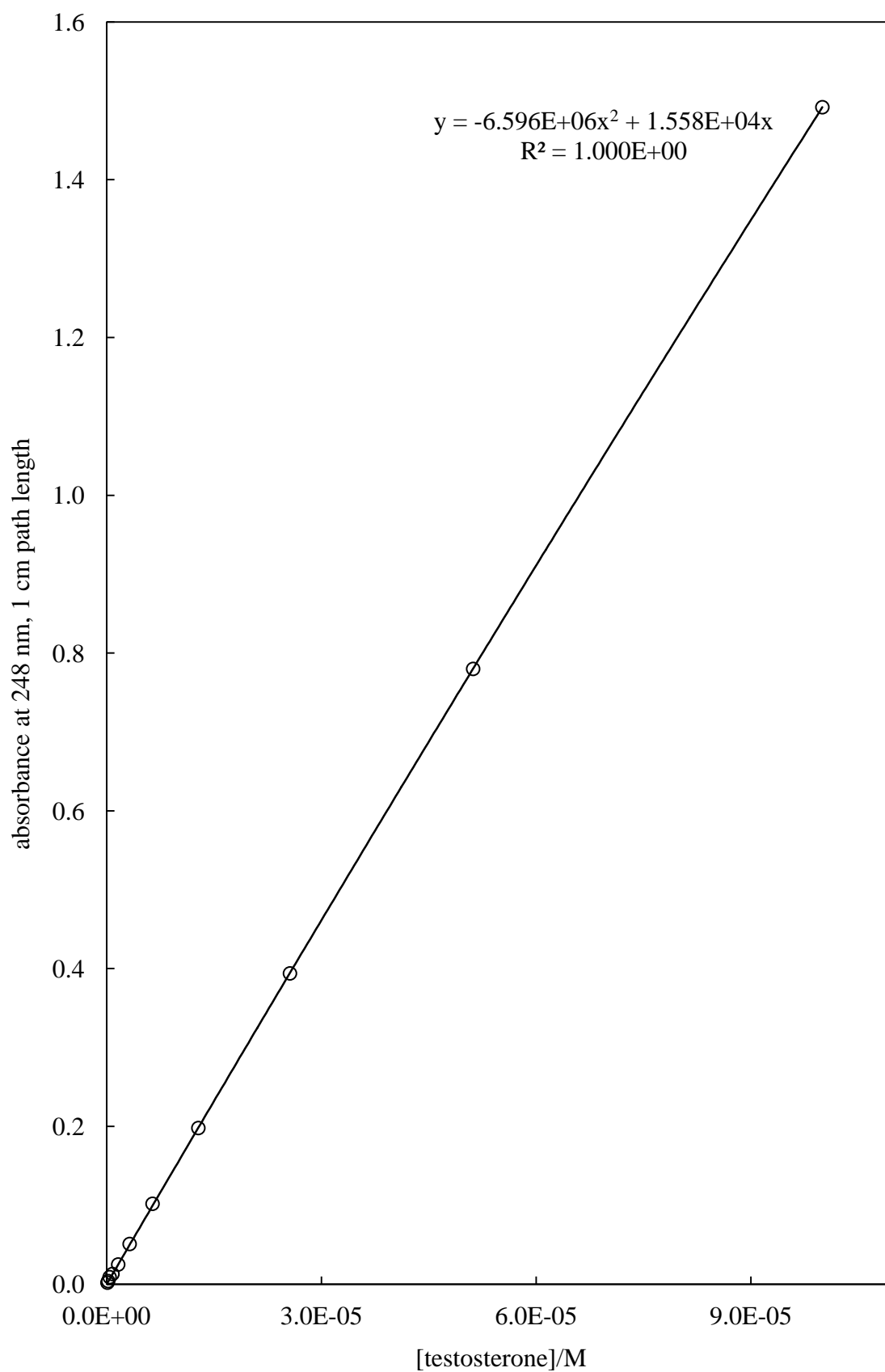


**Figure A1.3.** Calibration plot of spectrophotometric absorbance at 233 nm versus concentrations of testosterone dissolved in squalane at 32°C with a 1 cm path length.

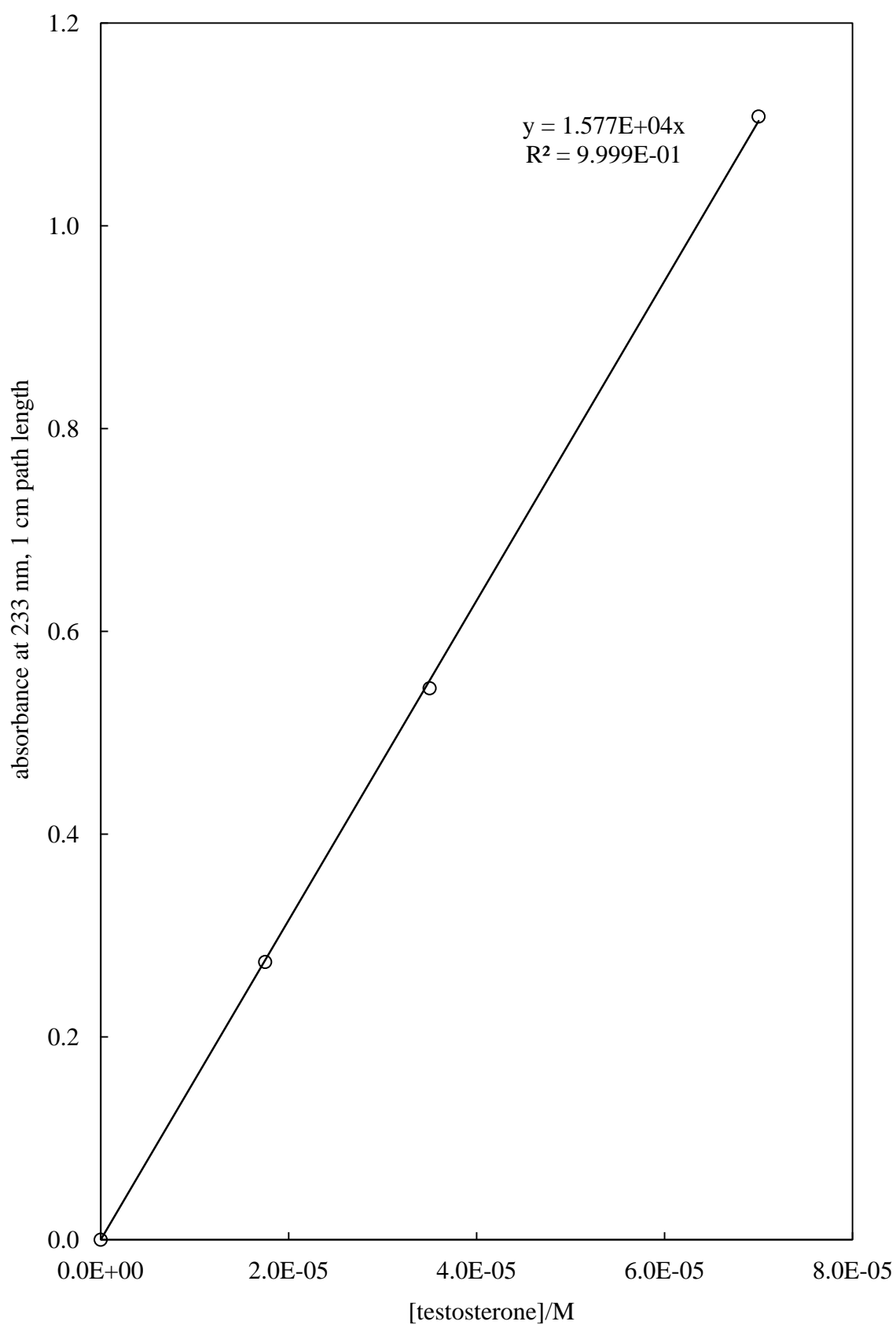




**Figure A1.4.** Calibration plot of spectrophotometric absorbance at 243 nm versus concentrations of testosterone dissolved in PG at 32°C with a 1 cm path length.

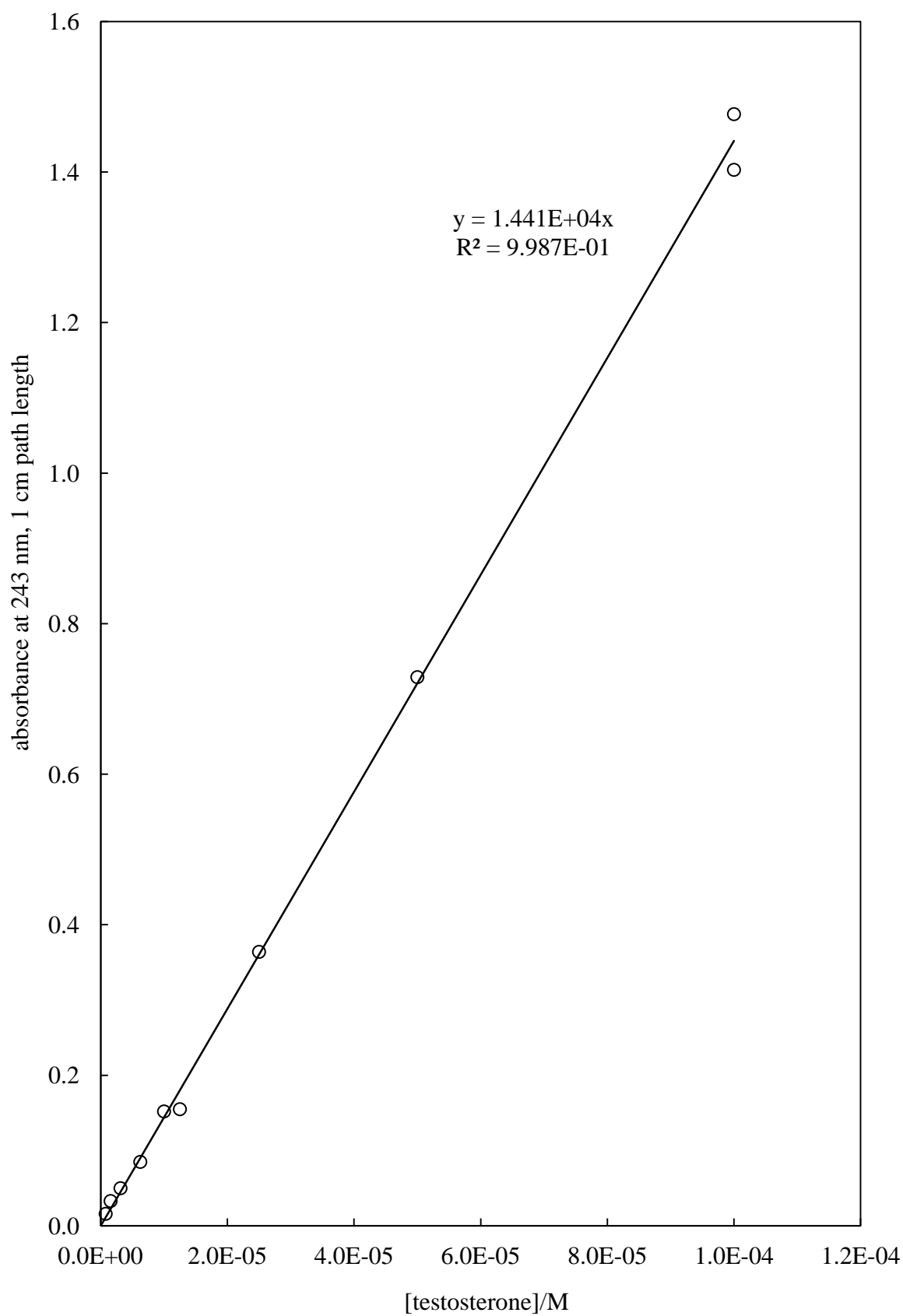


**Figure A1.5.** Calibration plot of spectrophotometric absorbance at 255 nm versus concentrations of testosterone dissolved in IPM at 32°C with a 1 cm path length.

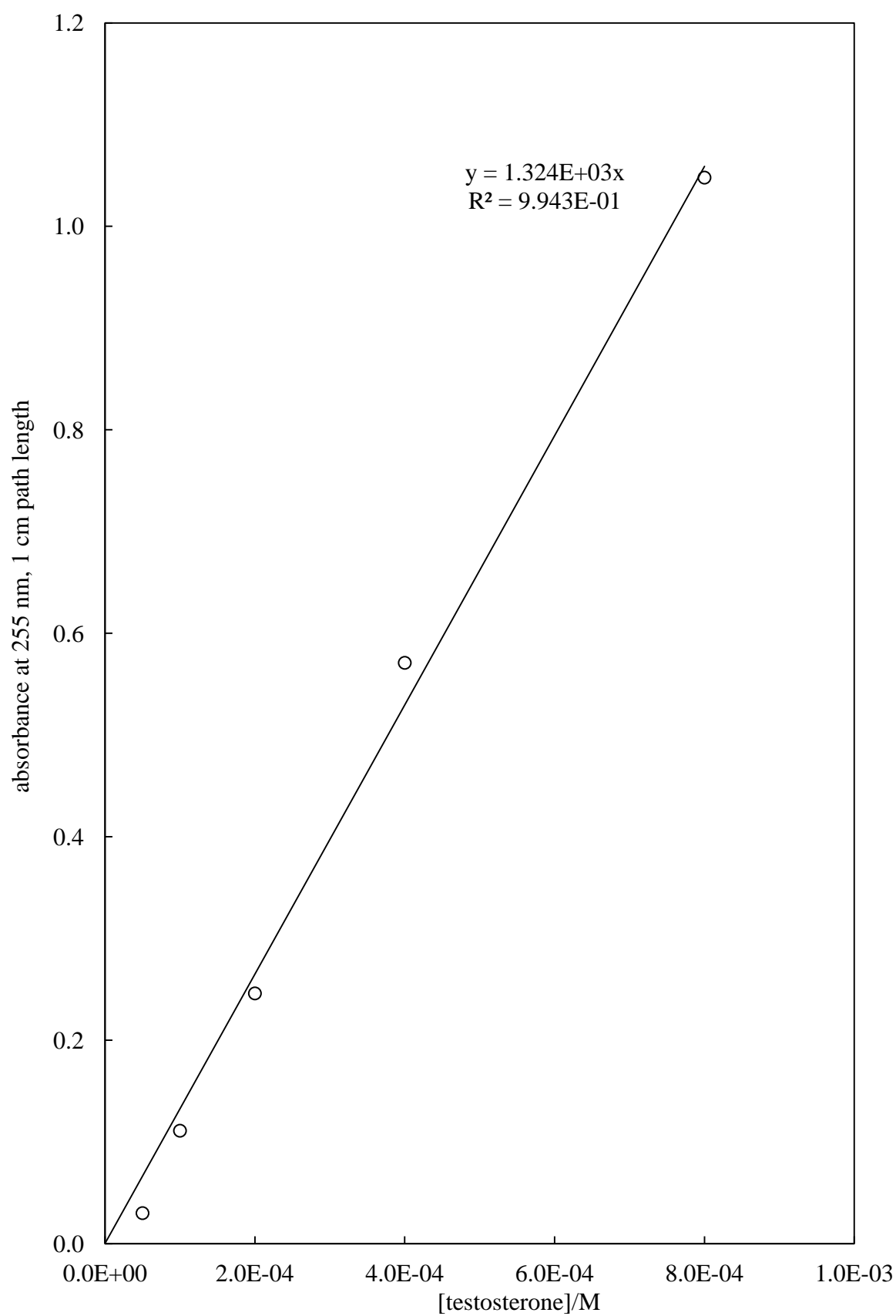


**Figure A1.6.** Calibration plot of spectrophotometric absorbance at 273 nm versus concentrations of caffeine dissolved in PBS at 32°C with a 1 cm path length.

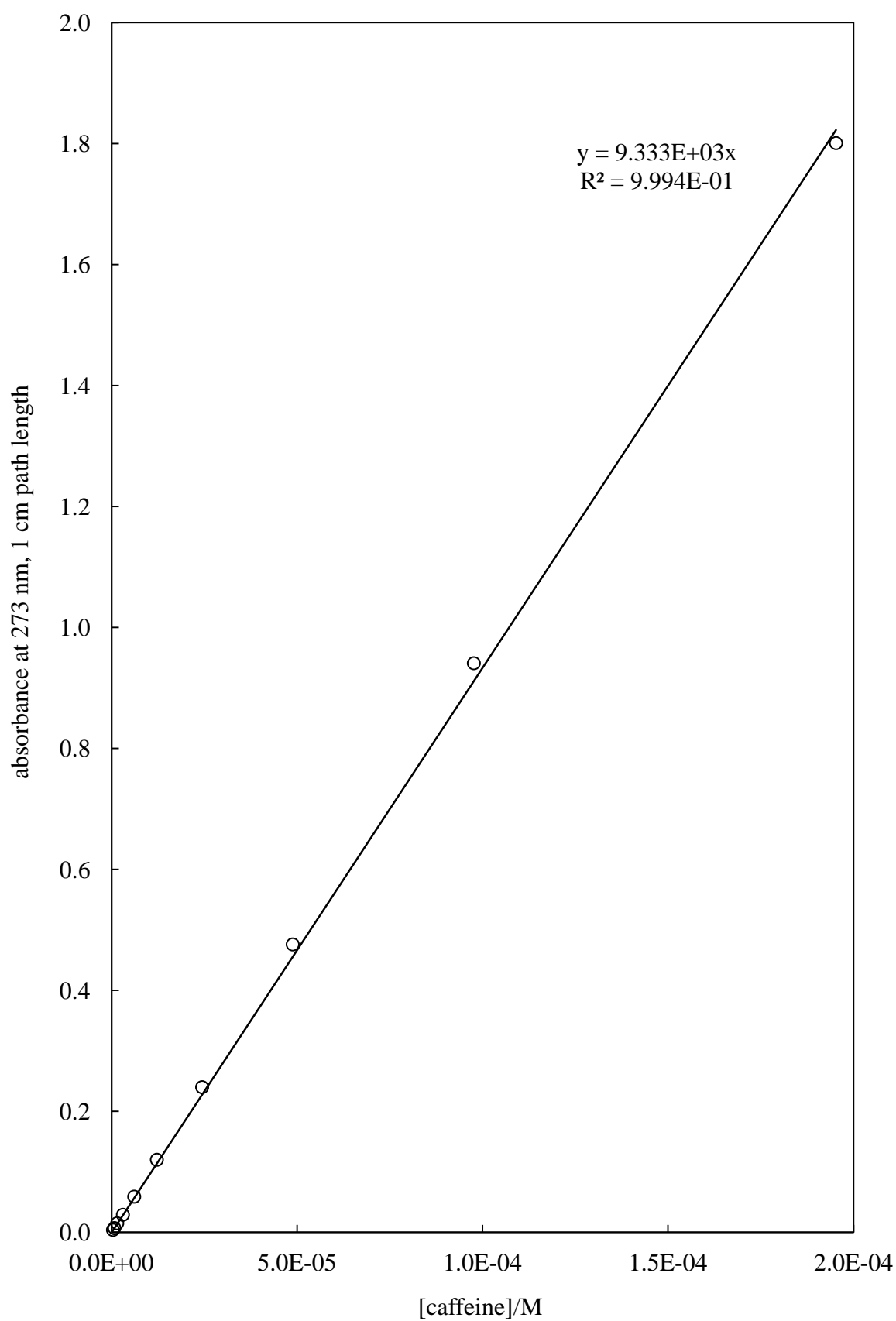


**Figure A1.7.** Calibration plot of spectrophotometric absorbance at 273 nm versus concentrations of caffeine dissolved in water at 32°C with a 1 cm path length.

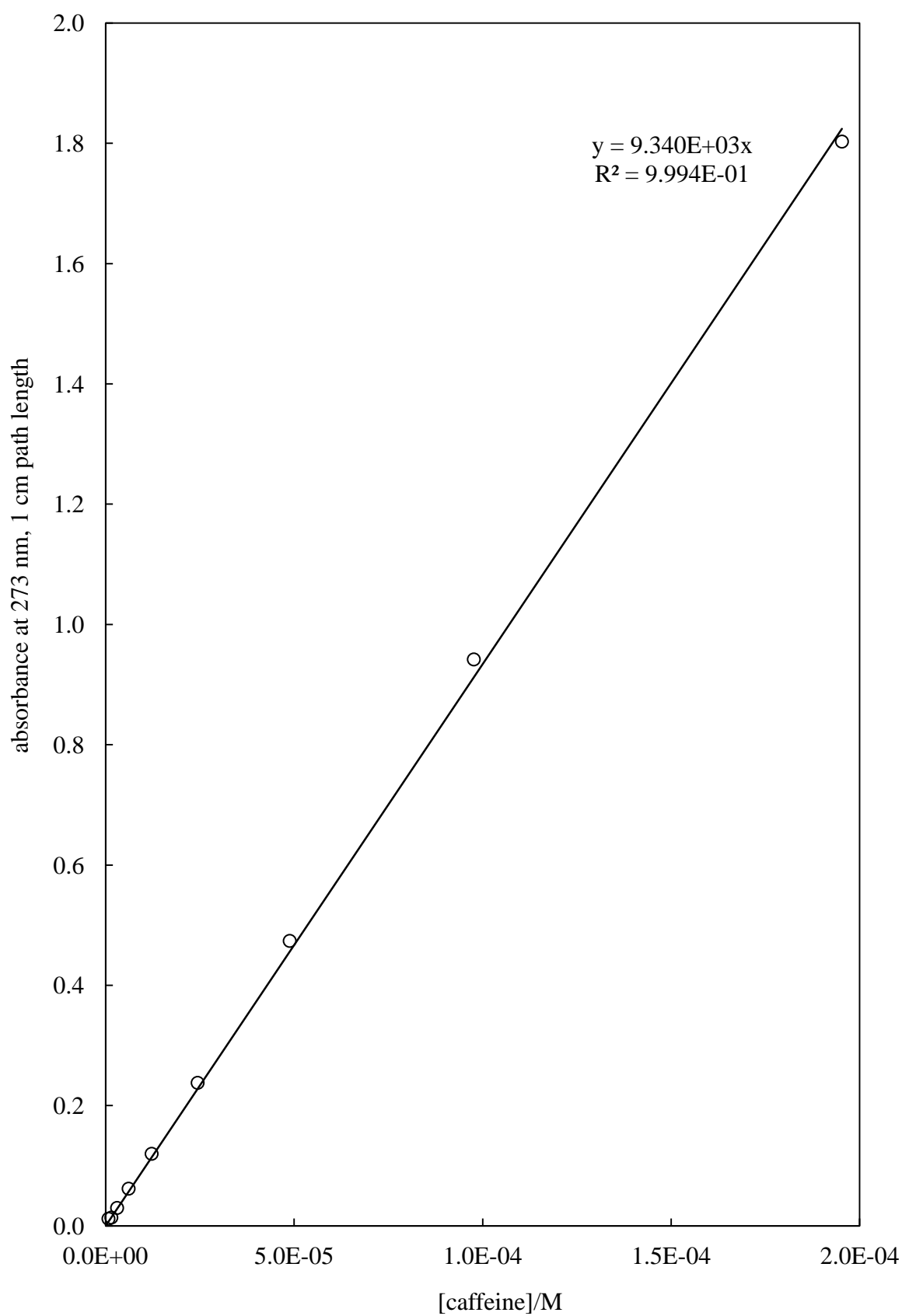


**Figure A1.8.** Calibration plot of spectrophotometric absorbance at 277 nm versus concentrations of caffeine dissolved in squalane at 32°C with a 1 cm path length.

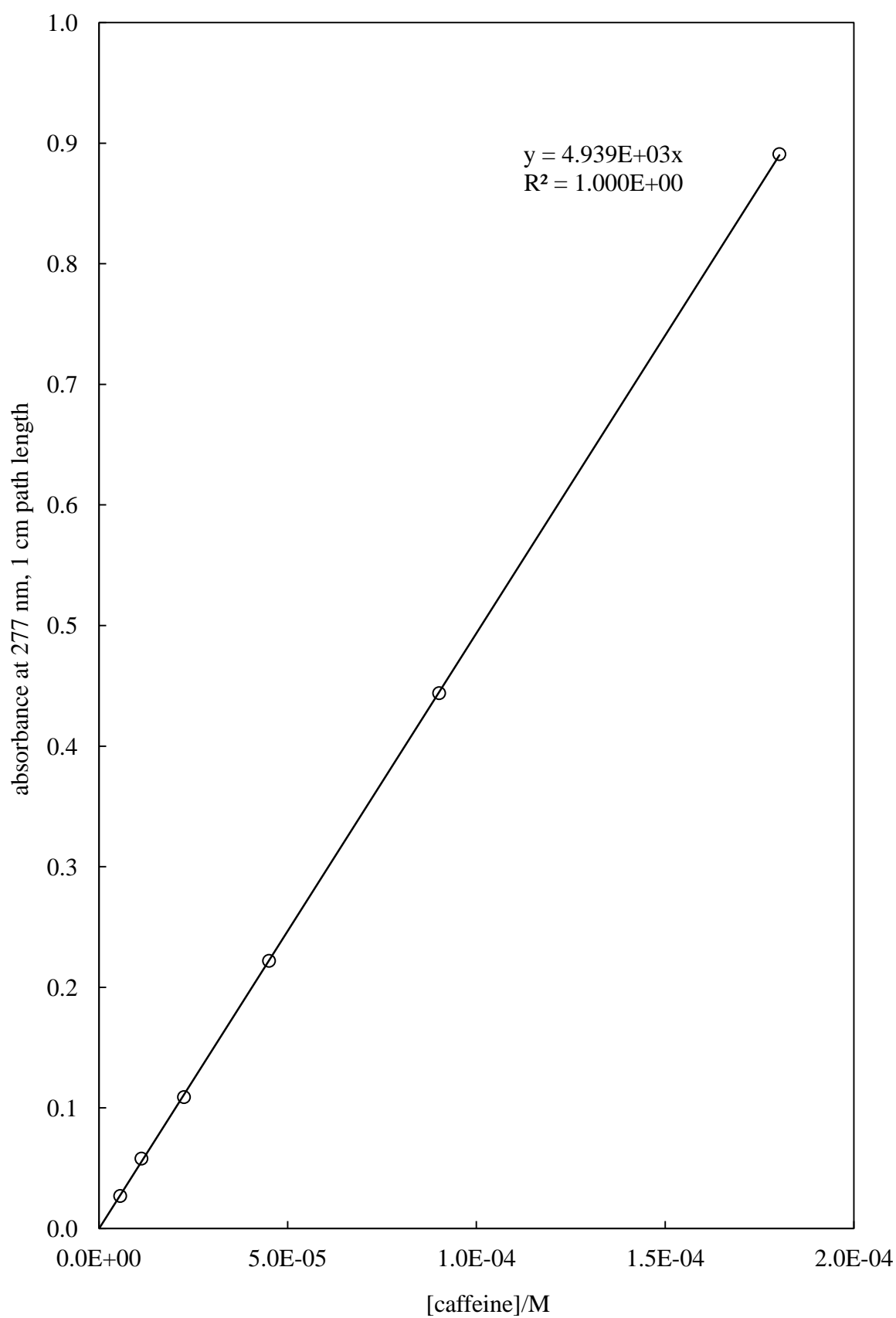


**Figure A1.9.** Calibration plot of spectrophotometric absorbance at 273 nm versus concentrations of caffeine dissolved in PG at 32°C with a 1 cm path length.

